Technische Universität München

Fakultät für Chemie
Lehrstuhl für Physikalische Chemie

Pristine and Induced Linear and Nonlinear Chiroptical Activity in Films and at Surfaces

Alexander Björn von Weber

Vollständiger Abdruck der von der promotionsführenden Einrichtung der Fakultät für Chemie der Technischen Universität München zur Erlangung des akademischen Grades eines **Doktors der Naturwissenschaften** genehmigten Dissertation.

Vorsitzender	Priv.-Doz. Dr. Friedrich Esch
Prüfer der Dissertation	1. Prof. Dr. Ulrich K. Heiz
	2. Prof. Dr. Klaus Köhler

Die Dissertation wurde am 23.04.2019 an der Technischen Universität München eingereicht und durch die promotionsführende Einrichtung der Fakultät für Chemie am 21.05.2019 angenommen.

Acknowledgments

This work would not have been possible if not for the people dear to me, colleagues, friends, and family. I am extremely grateful for the support and help they gave me.

First, Ueli Heiz who supervised me and who always had an open ear for my questions and concerns. I am also sincerely grateful to my mentor Aras Kartouzian. He gave me complete freedom in my work and how to pursue the bigger goals. On the other hand, he was always there when I needed help in the laboratory and his ideas. All the discussions we had about experimental challenges or scientific observations were most valuable to me.

I am also very thankful to my predecessor, Tobias Lünskens, who taught me everything about laser spectroscopy and showed me all the tips and tricks about the setup. Later on, Matthias Jakob joined the group and together we moved the setup to the new building. He was not only a great colleague, but a true friend and the setup would not be as it is without him. I am extremely grateful to Farinaz Mortaheb for her lovely support not only in the laboratory but also through the rough times with her cheerful nature.

I am very thankful to Ventsislav Valev and David Hooper who welcomed me with open arms in their laboratory at the University of Bath and willingly spend so much effort for our collaboration. I also want to thank our other collaborators José Lorenzo Alonso-Gòmez and Ani Ozcelik from the Universidade de Vigo who entrusted us to study their samples.

The electronic and mechanical workshops gave me also great support and always took their time to teach me valuable knowledge apart from my scientific topic.

I also want to thank Lara Milakovic, Toni Murnauer, Feng Wang, Thorben Eggert, Radka Kittova, Maximilian Hohmann, Melda Akay, Philip Stanley, Erika Keil and Eva Kratzer who contributed to this work in the course of their research internship, bachelor's or master's theses in the laboratory.

Last but not least, I cannot express my gratitude to my parents Maya and Stefan and my grandparents Brigitte and Heinz for the support and love they gave me. They were always there when needed and they taught me the value of education. Thank you so much!

Abstract

The demand for enantiopure drugs is rapidly increasing and so does the interest in asymmetric heterogeneous catalysts. But only a few catalysts are known so far and their mechanism not understood. In this work, an approach is presented on how the asymmetrization of such heterogeneous catalysts can be studied by means of chiroptical spectroscopy.

For this purpose, the nonlinear chiroptical spectroscopy method second-harmonic generation circular dichroism (SHG-CD) was implemented in the ultra-high vacuum (UHV) setup. In the first step, the characteristics of the technique were studied using the example of enantiopure molecular films. The inherently high sensitivity of SHG-CD was demonstrated in an in situ study on the optical activity (OA) of submonolayer 1,1'-Bi-2-naphthol (BINOL) films. This sensitivity was proven again in a study on device-compatible chiroptical surfaces of a single monolayer of upstanding chiral allenes to which conventional CD spectrometer are blind. It was also shown how isotropy affects the measured OA on the example of crystallization in BINOL films and, therefore, holds structural information, too.

In the next step, the adsorption of chiral molecules on a silver surface was studied by means of SHG-CD under controlled and essential UHV conditions. The interaction between the chiral modifier and the metal surface was explained based on the response of the silver surface plasmon in the form of a red or blue shift and a simultaneous broadening. Further, an asymmetrization of the metal was observed through an induced OA of its plasmon, which represents a proof-of-principle for the suggested approach. In a similar manner the interaction between molecules and coinage metal clusters, as so-called model catalysts, was studied.

The phenomena of induced OA was also explored in thin organic films. It was proven that well-known concepts from the liquid phase can be applied in the solid state as well to explain the two present an independent mechanism of induced OA. The applied modular approach of a “transparent” chiral modifier and an absorbing dye allows a highly tunable and custom OA. Paired with the simple and straightforward fabrication by spin-coating, this makes it a promising approach for optically active films for the application, for example, as filters.

Zusammenfassung

Die Nachfrage nach reinen Enantiomeren in Medikamenten steigt rapide an sowie das Interesse an asymmetrischen heterogenen Katalysatoren. Allerdings sind bis jetzt nur wenige solche Katalysatoren bekannt und ihre Funktionsweise ist noch nicht verstanden. In dieser Arbeit wird ein Ansatz vorgestellt, mit dem eine Asymmetrisierung eines heterogenen Katalysators mittels chiroptischer Spektroskopie untersucht werden kann.

Zu diesem Zweck wurde der experimentelle Ultrahochvakuum-Aufbau (UHV) um die nichtlineare, chiroptische Spektroskopiemethode der „second-harmonic generation circular dichroism“ (SHG-CD) erweitert. In einem ersten Schritt wurden ihre Eigenschaften anhand molekularer Filme untersucht. Die inhärent hohe Sensitivität von SHG-CD wurde in einer in situ Studie über die optische Aktivität (OA) von Submonolagen 1,1’-Bi-2-naphthol (BINOL) demonstriert. Die Sensitivität wurde abermals in einer Arbeit über die chiroptischen Eigenschaften von robusten, stehenden Monolagen von Allenen, für die konventionelle CD-Spektrometer blind sind, bestätigt. Außerdem wurde an dem Beispiel von Kristallisation in BINOL-Filmen gezeigt, wie Isotropie die gemessene OA beeinflusst und diese somit auch strukturelle Informationen beinhaltet.

In einem nächsten Schritt wurde die Adsorption von chiralen Molekülen auf einer Silberoberfläche mittels SHG-CD unter kontrollierten UHV-Bedingungen untersucht. Die Wechselwirkung zwischen dem chiralen Modifikator und der Metalloberfläche wurde auf Basis der Reaktion des Silberoberflächenplamons in Form einer Rot- oder Blauverschiebung und seiner gleichzeitigen Verbreiterung beschrieben. Außerdem wurde eine Asymmetrisierung des Metalls durch eine induzierte OA seines Plasmons gemessen, was ein Grundsatzbeweis für den vorgeschlagen Ansatz darstellt. In gleicher Weise wurde auch die Wechselwirkung zwischen Molekülen und Münzmetallclustern als sogenannte Modekatalysatoren untersucht.

Das Phänomen der induzierten OA wurde ebenfalls in dünnen, organischen Filmen untersucht. Es wurde gezeigt, dass bekannte Konzepte aus der flüssigen Phase auch im Festkörper angewandt werden können, um die zwei gegenwärtigen und unabhängigen Mechanismen der induzierten OA zu erklären. Der eingesetzte modulare Ansatz eines transparenten, chiralen Modifikators und eines absorbierenden Farbstoffes erlaubt eine hohe abstimmbare und maßgeschneiderte OA. Dies macht es zusammen mit der einfachen und direkten Herstellung mittels Rotationsbeschichtung zu einem vielversprechenden Ansatz für optisch aktive Filme beispielsweise zum Einsatz als Filter.

Contents

1 Introduction

Chirality is a geometrical property that is defined as being distinguishable from its mirror image. That sounds abstract but it basically means that a chiral object like a right hand cannot be superposed onto the left hand. Therefore, the left and right hand are seen as opposite forms and called enantiomers. The importance of chirality for us manifests itself in the predominance for a single enantiomer in most biomaterials. Practically all natural products, such as amino and nucleic acids, proteins, lipids, hormones, vitamins, antibiotics and sugars exist in just one enantiomeric form in mother nature. The origin of this apparent disequilibrium is still under heavy debate and theories are reaching from parity-violating weak forces at the smallest scale via, among others, extraterrestrial causes till a pure accidental chain of events.[1–7] Regardless of the origin, the concept of chirality plays a key role in the field of biology. For example, the two enantiomers of carvone smell differently to us because our olfactory receptors are capable of distinguishing them.[8] But the two opposite enantiomers can also show more severe differences in their effect on our body. This can be up to a point where one enantiomer is considered the healing substance of a medicine, whereas the presence of the opposite enantiomer causes devastatingly deleterious side-effects, for example, in the case of thalidomide.[9,10] Thus, the research on compounds in their enantiopure form was rapidly increasing. However, the number of spectroscopy methods which can distinguish between opposite enantiomers is limited because they share most physical properties like their mass. Among the capable techniques, circular dichroism (CD) is the preferred one and probes the chiroptical properties. It describes a difference in absorption between left and right circularly polarized light.[11] This is also called optical activity (OA) and strongly relates to the chiral character of the molecule and its structure. Simultaneously with the fundamental interest, the demand for enantiomerically pure compounds for medical purposes further increased.[12,13]

There exist two general approaches for the synthesis of enantiopure compounds. The first is the synthesis of the racemate (an equal mixture of both enantiomers) and a subsequent separation with, for example, chiral chromatography. In the background of our limited resources, this is unfavorable but unfortunately common. The second approach is an asymmetric synthesis with enhanced production of one enantiomer which yields an enantiomeric excess (ee). Based on the observed ee of natural synthesis, it was concluded that catalytic processes are involved.[14] Thus, great efforts were made in the field of asymmetric catalysis where until recently the research concentrated on homogeneous catalysts and which are already used in industrial applications.[15,16] For obvious reasons, the heterogeneous counterpart possesses intrinsic advantages, but only a few examples are known by now.[17] There are two basic approaches for the design of an asymmetric heterogeneous catalyst. The first is

the immobilization of a homogeneous one by anchoring it to a surface.[18] The second approach is the asymmetrization of a common achiral heterogeneous catalyst. This asymmetrization can be done by functionalization with a chiral modifier, for example, an enantiomerically pure molecule.[19–22] A sketch of this approach with the example of metal clusters as heterogeneous model catalysts is given in Figure 1. So far, a resulting asymmetric catalytic activity was presented for the hydrogenation of 2-butanone by immobilized platinum nanoparticles[23] and for the enantioselective hydrogenation of β-keto esters by single crystal catalysts under controlled ultra-high vacuum (UHV) conditions.[24,25] The role of the asymmetrization and its mechanism is generally not known but possible processes have been categorized[26,27] and numerous examples presented.[28–31]

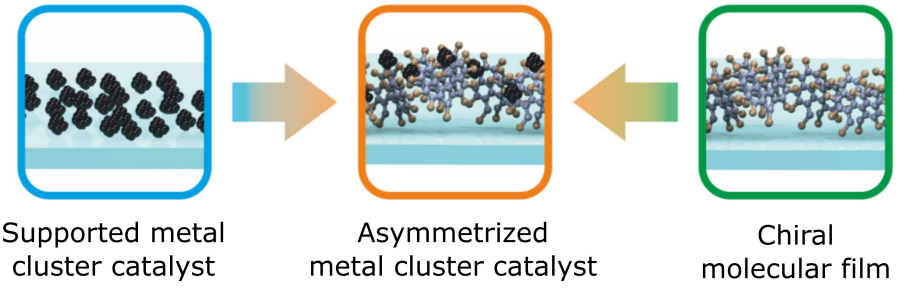

Figure 1 Diagram of approach for asymmetrization of clusters as heterogeneous model catalyst.

However, no optical method was used so far to study the chirality of such systems and in particular the transfer of chirality from the chiral modifier to the pristine achiral catalyst. This is especially surprising because the well-known effect of induced CD (ICD) yields this exact information. ICD is the induced OA in the pristine optically inactive response of the achiral compound brought by the interaction with the chiral modifier.[32–34] Among others, it holds information about the nature of their interaction and their absolute conformation.[35–37]

Yet, the study of ICD in the above-mentioned examples by means of linear CD is challenging because the low amount of chiral modifier and sometimes the catalyst itself lies often below the sensitivity of standard CD spectrometers. Alternatively, it is proposed to measure the OA with the nonlinear technique second-harmonic generation circular dichroism (SHG-CD). The measured OA is expressed by a difference in intensity of second harmonic (SH) light generated by the left and right circularly polarized light and is inherently surface sensitive.[38]

Finally, the core of this work is to demonstrate how an asymmetrization of a heterogeneous model catalyst can be studied in situ by means of the chiroptical technique SHG-CD. It is believed that the novel approach would help to further understand asymmetric heterogeneous catalysts and by that push the field forward.

2 Theory

2.1 Pristine & Induced Circular Dichroism

Absorption

The chiroptical properties of, for example, a chiral molecule express themselves in a different interaction with left and right circularly polarized light for the opposite enantiomers. The quantum mechanical description of this interaction is far from trivial. Therefore, the phenomena will be explained on a more abstract level here, but which is still explicit enough to interpret the experimental results.

When light impinges on a molecule its nuclei and electrons are forced to follow the oscillating electric (and magnetic) field of the electromagnetic wave. The frequency of the light in the visible (VIS) and ultraviolet (UV) range is too high for the nuclei to follow so that the system can be described solely by the movement of the electrons. If the energy of the light equals the difference between two energy states of the molecule, it may be absorbed as a photon and its energy will promote the molecule from an initial state i into a higher electronic excited final state f. The electrons are redistributing during this process and moving within the molecule. The motion can be expressed by transition moments, such as the electric dipole transition moment $\underline{\mu}_{if}$ and the magnetic dipole transition moment $\underline{m}_{if}$. The former describes a linear displacement of electrons and the latter a rotation of electron charge during the excitation. Now, an absorption band of an experimental measure integrated over its wavelength region is equal to the square of the connected electric dipole transition moment. It is also called "dipole strength" D_{if} and is defined as follows.[11,39]

$$D_{if} = \underline{\mu}_{if} \cdot \underline{\mu}_{fi} = \frac{6909\ h\ c}{8\ \pi^3\ N_0} \int_{\lambda_1}^{\lambda_2} \frac{\varepsilon}{\lambda}\, d\lambda \tag{1}$$

With h as the Planck constant, c as the speed of light, N_0 as the Avogadro constant and ε as the molar attenuation coefficient. The molar attenuation coefficient is linearly connected to the absorption A, which is actually measured by the spectrometer, by $A = \varepsilon\ c\ l$ with c being the molar concentration and l the pathlength. The electric dipole approximation is generally used because all other transition moments are by orders of magnitude smaller, and, therefore, are negligible for the description of the absorption.

It concludes that absorption spectra in the VIS and UV range hold information about the electronic structure of a molecule. Because the electronic structure is identical for both enantiomers of a chiral compound, UV-VIS spectroscopy cannot distinguish between them.

Circular Dichroism

Now to explain CD, imagine a chiral molecule with a helical geometric structure. A transition between two electronic states by interaction with circularly polarized light may include a rotation of electron charge along the helical axis. This ring current is described by the magnetic dipole moment. This excitation is more likely for the circular polarization (CP) which matches the rotational direction of the geometry of the molecules. Thus, the probabilities of an excitation, and absorption of the photon, are now depending on the CP of the light and the geometrical structure of the molecule in its initial state. It becomes also clear that this effect reverses for the opposite enantiomer because its rotational direction of its helical axis is reversed. Finally, the CD is defined as the difference between the molar attenuation coefficients of left and right circularly polarized light.

$$\mathrm{CD} \equiv \varepsilon_L - \varepsilon_R \tag{2}$$

A simplified diagram that explains CD and connects the energy diagram with the measured absorption and CD spectra (for both enantiomers) is given in Figure 2.

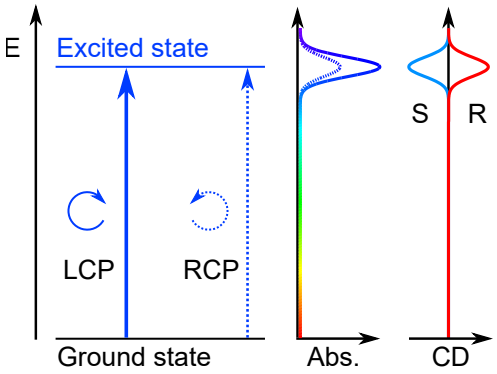

Figure 2 Simplified energy diagram and corresponding absorption spectrum for fictive R enantiomer and CD spectra for both enantiomers.

In a similar manner as for the dipole strength, Moscowitz proposed a property called “rotational strength” R_{if} which connects experimental measure and theory.[11,39]

$$R_{if} = \mathrm{Im}\{\underline{\mu}_{if} \cdot \underline{m}_{fi}\} = \mu_{if}\, m_{if}\, \cos\left(\underline{\mu},\, \underline{m}\right) = \frac{6909\ \mathrm{h\ c}}{32\ \pi^3\ N_0} \int_{\lambda_1}^{\lambda_2} \frac{\Delta\varepsilon}{\lambda}\, \mathrm{d}\lambda \tag{3}$$

It is apparent that CD is an effect based on the interaction between the electronic and magnetic transition dipole moment. Therefore, it is, in contrast to the absorption, not explainable in the electric dipole approximation and contributions from the magnetic dipole are essential.

Often a CD spectrometer would give the CD signal in quantities of an angle of ellipticity ψ, although they are actually measuring the difference in absorption between both CPs. Fortunately, the inter-

conversion is with $\psi = 33\ \Delta A$ simple. But it becomes also clear that this measured CD signal is depending on the concentration and the pathlength, as does the absorption A.

Therefore, Kuhn introduced in 1930 an anisotropy factor, which is also called g value, that is independent of the amount of probed molecules and given at one wavelength (left expression) and for a complete band (right expression).[39,40]

$$g = \frac{\Delta\varepsilon}{\varepsilon} \qquad\qquad g = 4\frac{R}{D} \tag{4}$$

In conclusion, CD can distinguish between opposite enantiomers and shows a characteristic mirror image behavior for them. If calibrated, CD can also yield an ee in a sample and can test the purity of, for example, drugs. As discussed, the OA depends also on the geometrical structure of the initial electronic state which is commonly the ground state. Hence, it is possible to derive the absolute configuration of a molecule and even the secondary structure of macromolecules, such as proteins, from CD data.

Induced Circular Dichroism

"Induced CD (ICD) is an effect [which results from] the molecular interactions between chiral (host) and achiral (guest) compounds [and] give rise to an ICD in the pristine nonoptically active response of the achiral counterpart. This expresses itself in a CD signal within the absorption bands of the achiral substance.[32–34]

Generally, all ICD mechanisms can be classified into two different categories, namely, direct ICD (DICD),[36,37] in which the structure of the guest molecule remains untouched, and indirect ICD (IICD). The former (DICD) follows the original definition of ICD, in which the chiral host and achiral guest are in vicinity of each other, yielding an ICD in the absorption of the achiral guest.[41,42] In this case, the induced OA can arise from two mechanisms. One is known as coupled oscillator effect which is dominant if the electronic transition moments of the achiral chromophore and the chiral counterpart are close in energy. The other is called one-electron effect, in which the chiral compound possesses a strong asymmetric static field, which perturbs the molecular orbitals of the achiral chromophore.[32] Every mechanism which does not fulfill these requirements falls under the second category, that is, IICD. This includes, for example, a structural perturbation of the achiral guest because of strong binding between host and guest or the induction of a chiral superstructure. In such a superstructure, the achiral guests are arranged in a chiral manner and exciton coupling between their identical chromophores would lead to bisignate CD curves because of the split Cotton effect.[35,43] Therefore, the chiral host would indirectly induce CD. The concept of ICD and the given classification are illustrated in a simplified diagram in Figure [3].[37]

Over numerous years of research, several ICD phenomena, models, and interpretations have been

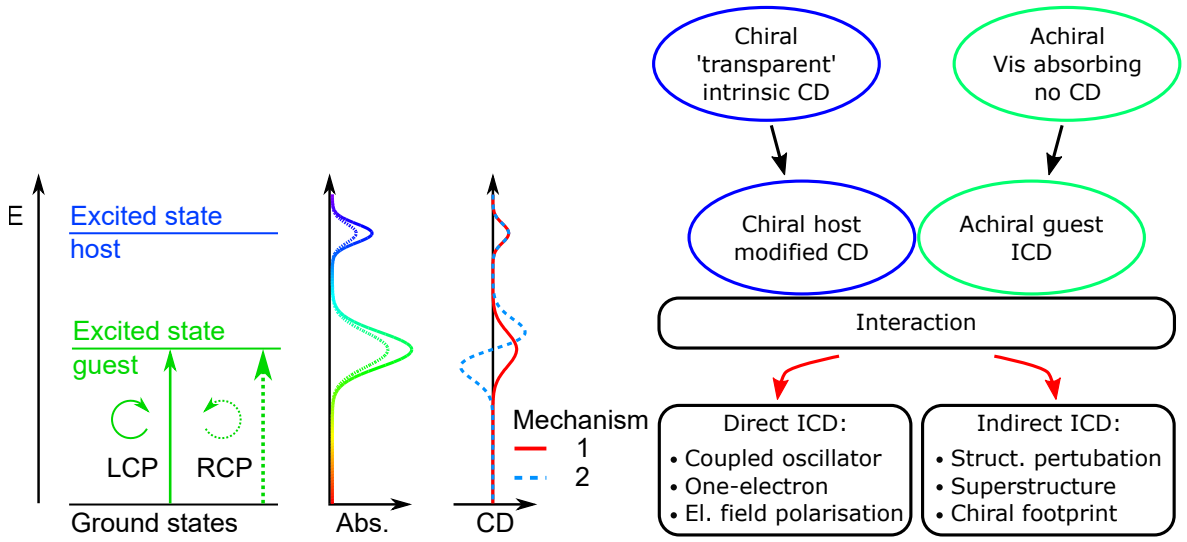

Figure 3 Left: Energy diagram and theoretical ICD spectra. Right: Diagram of the interaction between chiral and achiral compound yielding an ICD effect. (Adapted from Publication G)

provided, and a selected overview is given in the following. In particular in the field of biochemistry, the interaction between helix structures, for example, polypeptides or DNA and an achiral guest molecule leads to a variety of different ICD effects. These were used to discriminate between chemical binding modes, including intercalation or groove binding to DNA and various interaction possibilities between a dye and a polypeptide helix.[44,45] The proposed mechanisms lead to induced OA, ranging from structurally induced chirality to off- and resonant excitonic coupling.[35,44] Another frequent result is that no chemical bond between the two molecule types occurs, but rather strong electrostatic effects, hydrogen bonds, van der Waals interactions, decrease of strain energy, or even simply a dominating chiral environment are the cause for an observable ICD.[36,46,47] Also, ICD has been applied to establish the absolute configuration of a transparent chiral molecule with the aid of an achiral, chromophoric guest or to determine the orientation of the respective molecules within a host-guest complex.[36,37] ICD can hold unique information about supramolecular events.[37] Furthermore, cases have been published where DNA and drug binding sites were probed, intrinsic chirality was amplified, and ion pair structure was studied.[37,46,48]" (Publication G)

ICD effects not only occur if chiral modifier interact with molecules but also if they interact with metal surfaces and particles. Then, the ICD gives rise to an OA in the pristine optically nonactive response of the metal, such as intra- and interband transitions and its plasmon. The numerous reported ICD mechanism can be categorized in a similar manner as before. One DICD effect is, for example, brought by a chiral distribution of electron density induced by a chiral pointcharge system.[31,49,E] It is a field effect and the analog to the one-electron effect and also called electric field polarisation. A common IICD effect is the so-called chiral footprint. There, a strong binding of the chiral modifier with a highly strained adsorption motive leads to relaxation of the metal atoms in a chiral manner and

leaving the metal surface atoms in a chiral arrangement.[28,30,50,51]

In conclusion, ICD results from interaction between a chiral modifier and an achiral component. Last but not least, the form of the ICD depends on the nature and mechanism of this interaction and, therefore, holds also great information. This makes ICD such a valuable tool.

2.2 Second-Harmonic Generation Circular Dichroism

In this work, the in situ studies on the OA of films and interfaces are carried out by means of the nonlinear chiroptical technique SHG-CD. This is done because the small amount of molecules in the systems is challenging for conventional CD analysis and lies often below the sensitivity of common CD spectrometers.

SHG-CD is based on the nonlinear effect of second-harmonic generation (SHG). It describes the interaction of two photons of equal energy with a medium and a subsequent generation of a photon of double the energy. Because of the applying conservation laws, this generation is done at the expense of the two incoming photons and can be seen as transformation. The effect appear at high electric fields $E = E_0 \cos(\omega t)$, such as in the case of laser light, where the polarization P of a medium can no longer be treated linear.

$$P(t) = \varepsilon_0 \chi^{(1)} E(t) + \varepsilon_0 \chi^{(2)} E^2(t) + \ldots = P^{(1)}(t) + \underbrace{\frac{1}{2} \chi^{(2)} E_0^2 + \frac{1}{2} \chi^{(2)} E_0^2 \cos(2\omega t)}_{P^{(2)}(t)} + \ldots \quad (5)$$

The second order polarizability $P^{(2)}$ includes the SH defining term with the doubled frequency 2ω of the fundamental incoming wave. It also includes the second order susceptibility tensor $\chi^{(2)}$. The inherent surface sensitivity of SHG is mathematically expressed if one applies the expression of $P^{(2)}$ in Equation 5 on a centrosymmetric medium. The only solution is that $\chi^{(2)}$ is equal zero. Thus, the generation of SH is forbidden in most bulk media because of the predominant centrosymmetry. But this symmetry is broken at the surface or interface and SH is generated there.

SHG becomes greatly enhanced if either the fundamental ω or the SH with 2ω is in resonance with an electric dipole transition of the interacting medium. Therefore, a SH spectrum is closely connected to the extinction spectrum, which makes a comparison of both simple. Note, if in resonance with the fundamental, $\chi^{(2)}$ shows two maxima at ω and 2ω. Consequently, the connected SH spectrum also possesses two maxima at these energies, see Figure 4. Thus, the interpretation becomes ambiguous and additional information from complementary techniques are needed. If not stated differently, only the unambiguous case of resonance with the SH applies in this work.

Now, in order to study the optical activity at interfaces, Hicks and coworker developed a technique

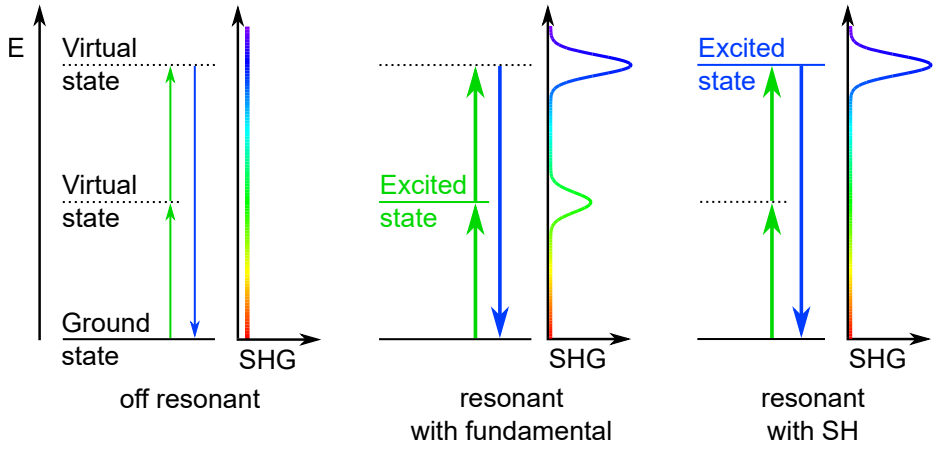

Figure 4 Simplified energy diagrams and corresponding SH spectra for all three possible cases.

that combines the inherent surface sensitive SHG with CD.[38] With this nonlinear chiroptical technique SHG-CD the SH is generated by circularly polarized light. Analog to linear CD, a difference in intensity of the SH generated by the left and right CP expresses OA and a dimensionless anisotropy factor can be defined here as well by weighting the difference with its average.

$$\text{SHG} - \text{CD} = g = \frac{I_{LCP} - I_{RCP}}{1/2\,(I_{LCP} + I_{RCP})} \tag{6}$$

With $I_{LCP/RCP}$ as SH intensity generated by the left and right CP of the fundamental light, respectively. This is graphically summarized in energy diagrams as well as theoretical SHG-CD spectra for both enantiomers in Figure 5.

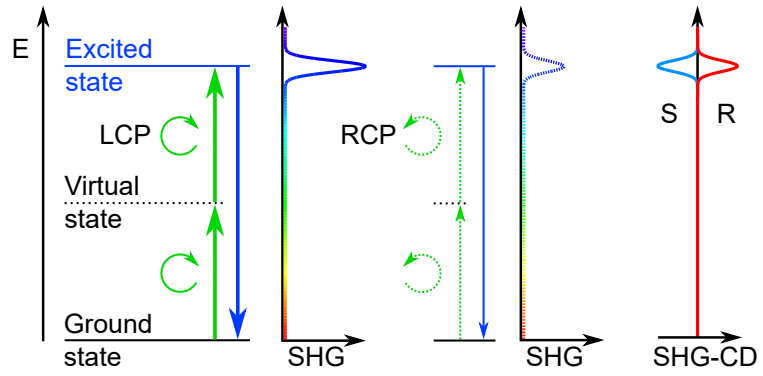

Figure 5 Simplified energy diagrams and corresponding SH spectra for left and right CP of fundamental light in case of the R enantiomer and resulting SHG-CD spectra for both enantiomers.

Early, it was demonstrated that this nonlinear anisotropy factor is up to 3 orders of magnitude larger than its linear counterpart.[38,52] In order to explain this, it has been suggested that SHG-CD can be entirely treated within the electric dipole approximation. Its rotational strength would therefore not depend on the magnetic dipole transition moment like the linear CD, see Equation 3. Because the electric dipole transition moment is much larger than the commonly small magnetic one the effect is

no longer limited by the latter.[38,52] However, other works suggested a significant contribution from the magnetic dipole to the nonlinear OA.[53–55] Therefore, the cause for the large effects in SHG-CD are still under debate.

An important difference to linear CD is that SHG-CD is directly depending on the orientation of the addressed transition moments and, therefore, molecule.[55] It was shown that flipping the molecule with respect to the propagation direction of the incoming light yields an inversion of the observed anisotropy factor.[52] Therefore, SHG-CD is sensitive to anisotropy within a sample and contributes to the observed nonlinear OA, too.

2.3 Plasmon of Coinage Metals

The optical response of the coinage metals that are studied here originate from an interaction of the light with their plasmon. The plasmon is the coherent oscillation of the conduction electrons in a bulk metal and is also called volume plasmon (VP). Within the classical Drude model, the electrons are considered free charges which are moving through a lattice of positive ions which represent the atoms. An oscillation resonance of the VP, which is called the plasma frequency ω_{VP}, can be derived.[56]

$$\omega_{VP} = \sqrt{\frac{n\, e^2}{\varepsilon_0\, m^*}} \tag{7}$$

With e as the elementary charge and ε_0 as the permittivity of free-space. The effective mass m^* includes additional forces on the electrons and can be used as correction factor in case the system deviates from the free electron approximation. Most important, the VP is depending on the square root of the density of electrons. Unfortunately, in contrast to alkali metals, coinage metals are more complex and not explained well by this model. In case of silver, the vicinity of the interband transition from the 4d to the 5s band has a significant influence on the conduction electrons and they cannot longer treated as free. As a result the plasmon energy lies at approx. 3.81 eV[57] instead of 9.2 eV, as predicted from the Drude model. But it is believed that the model is sufficient to qualitatively interpret the experimental findings here.

A plasmon also exist at a surface or interface between a metal and a dielectric medium. This so called surface plasmon (SP) is in contrast to the VP described by an electromagnetic surface wave which propagates along the metal surface. Unfortunately, SP cannot be excited by light in free space without further ado. This is because the dispersion relation lies right from the one of light.[58,59] Therefore, the wave vector of the light along the propagation of the SP in the surface plane has to be increased. This coupling is done by either an attenuated total reflection (ATR) or a grating. Additionally, a large surface roughness can be seen as superposition of many gratings and, therefore, yield the same

effect.[59] The frequencies and wavelengths of the SP and VP are connected as follows.[58,59]

$$\omega_{SP} = \underbrace{\sqrt{\frac{n\,e^2}{\varepsilon_0\,m^*}}}_{\omega_{VP}} \frac{1}{\sqrt{1+\varepsilon_d}} \qquad \lambda_{SP} = \underbrace{\sqrt{\frac{\varepsilon_0\,m^*}{n\,e^2}}}_{\lambda_{VP}} \sqrt{1+\varepsilon_d} \tag{8}$$

Therefore, the SP lies at lower energies than the VP and depends on the dielectric permittivity ε_d of the dielectric medium which is in contact to the metal surface. Thus, an increasing dielectric function, for example due to adsorbates, leads to a decreasing energy of the SP and a red shift. Also, adsorbates may localize conduction electrons of the metal in their bond to the surface and with that decrease the electron density. This would decrease the energy of both VP and SP and would cause a red shift for both.

After a successful excitation of a plasmon, various damping mechanism can lead to a relaxation and reduce its lifetime and with that increase the width of the plasmon peak. They can be categorized in non-radiative damping, such as surface roughness scattering, free-electron, intra- and interaband or interface damping, and radiation damping where a photon is generated. As mentioned, a rough surface may act as coupling aid in the excitation of the SP by light. On the other hand, it also enhances the scattering of the SP and leads to the damping of it. Thus, scattering damping is more dominant than radiation scattering on rough surfaces.[59] The free-electron damping or internal damping describes the absorption of the electromagnetic wave of the SP by a electron-hole pair close to the Fermi level. A subsequent relaxation via a coupling with phonons leads to a heating of the metal. During the intra- and interband damping, the SP is absorbed in order to excite an energetically lower lying electron.

In the case of nanoparticles with sizes comparable and smaller than the wavelength of light, the plasmon resonance is referred to as localized surface plasmon (LSP). It is additionally depending on the size[60,61] and shape[62,63] of the particles. In case of silver particles, a general blue shift of the LSP was observed with decreasing particle size. Edges may cause field enhancement effects close to them. A deviation of a spherical shape may shift the plasmon as well or leads even to a splitting of the plasmon resonance.[63] In case of nanoparticles, adsorbates yield an additional damping mechanism called chemical interface damping due to their high surface to volume ratio. It describes the scattering of LSP at surface states of adsorbates which leads to a dephasing.[64,65]

3 Experimental

3.1 In situ Second-Harmonic Generation Circular Dichroism

“Apart from the SHG-CD technique, the setup was described in various studies before. Here we focus on the necessary upgrades and challenges related to SHG-CD [, which were carried out in the course of this thesis,] accompanied by a brief description of the whole setup. The experimental setup presented in this work is a combination of a UHV system that allows for precise and reproducible sample preparation with a minimum of contamination as well as a laser spectroscopy setup for linear absorption (surface cavity ring down; s-CRD)[66,67] and nonlinear SHG studies.[61,68] A schematic view of the setup is given in Figure [6].

The UHV part of the setup can be divided into three parts. The first part is a UHV analysis chamber with a base pressure of $1 \cdot 10^{10}$ mbar and armed with a 4-axes manipulator (x, y, z, and Θ). [The

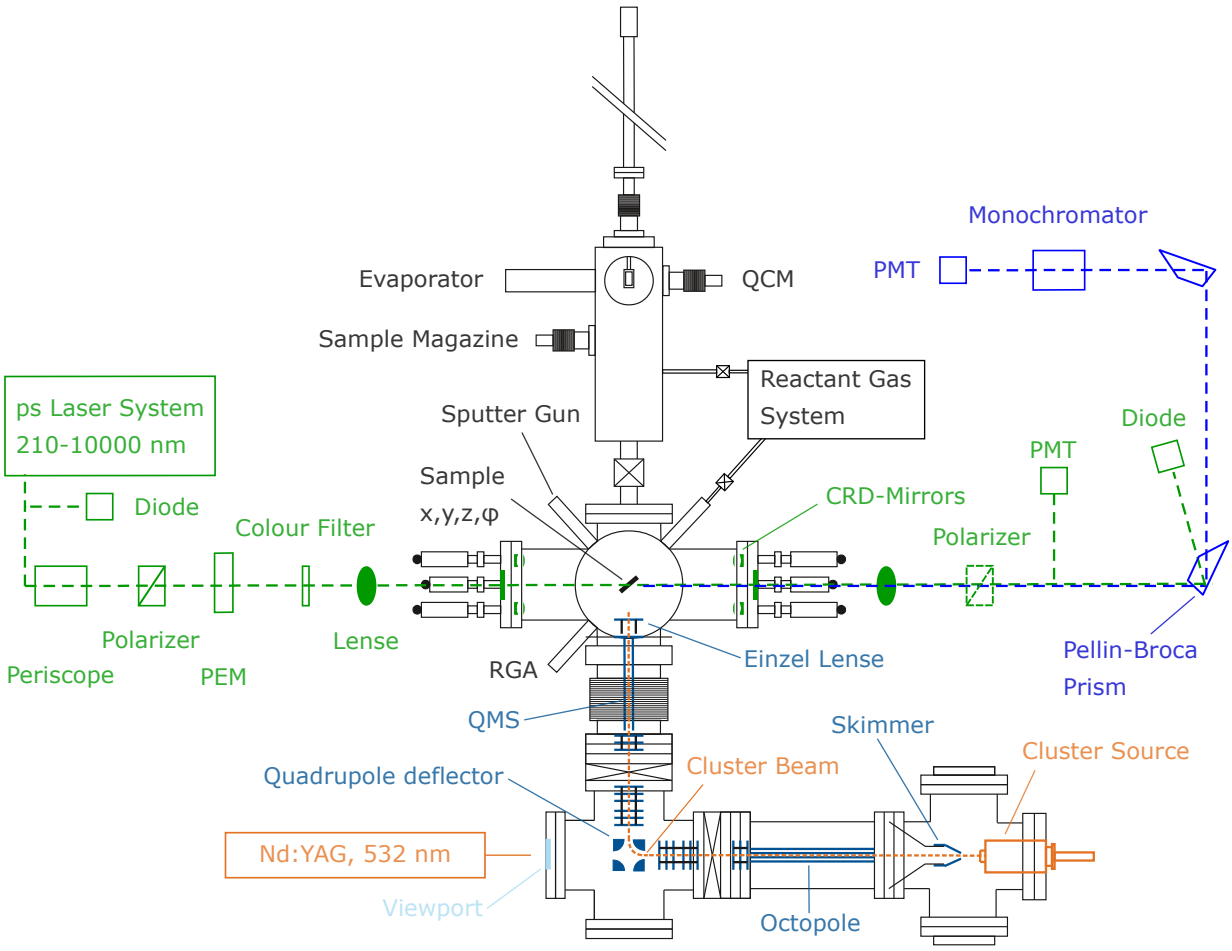

Figure 6 Experimental setup which combines optical spectroscopy methods SHG-CD and sCRD with a UHV setup including a laser ablation cluster source for in situ studies. (Adapted from Publication A)

manipulator and consequently the sample can be heated through resistive heating enabling, for example, thermal desorption or cooled by means of liquid nitrogen. The latter is of great importance to suppress self-ordering effects within the sample during the course of the experiment, see publication D.[68–70] Additionally, it is equipped with a sputter gun and an electron shower that emits slow electrons (with a kinetic energy < 15 eV) to neutralize a nonconductive substrate during sputtering. The analysis chamber further hosts a sputter gun for UHV surface cleaning. Second, a [newly designed] transfer chamber is connected to the analysis chamber through a UHV gate valve enabling sample transfer without breaking the UHV. The transfer chamber is equipped with a fast entry lock and a sample magazine. It also hosts a molecular evaporator to prepare films while the coverage is monitored by a quartz crystal microbalance (QCM; SL-A1E40 from INFICON). Third, a laser ablation cluster source is connected to the analysis chamber.[71]

The optical part of the setup can be divided into two parts. First is the light source in front of the UHV chamber where monochromatic, coherent light of well-defined polarization is generated and second, the analysis part behind the chamber and sample. The light source consists of an optical parametric amplifier laser system covering the spectral range between 210 nm and 10000 nm with a pulse duration of about 30 ps (PG401 from EKSPLA). The polarization of the laser output is purified by a Glan-Laser calcite polarizer before getting to a photoelastic modulator (PEM; II/FS42A from Hinds Instruments) where its polarization is actively set. Because the timing when the laser pulse is traversing the PEM defines the outcoming polarization, special care has to be taken with regard to the trigger of the laser. The delay between the oscillation of the PEM and one laser shot is handled by a self-made trigger box. A detailed description of the operation mode of the box (Figure [10]) and the calibration for both circular polarizations (CPs) and p-polarized light is given [below] (Figure [11, 12]). After the PEM, a 400 nm long pass filter (FELH0400 from Thorlabs) is used to remove residual SH, that may accompany the output of the laser system, before focusing the laser beam on the sample inside the UHV-chamber through a fused silica lens with a focal length of 300 mm. [The exact beam path inside the analysis chamber depends on the used geometrical mode and will be discussed in detail below.] The diameter of the laser spot size at the sample can be varied between 0.5 mm and 4 mm by moving the sample away from the focal point or towards it. The SH generated at the sample and the fundamental light propagate out of the chamber and are recollimated through a second fused silica lens with a 300 [mm] focal length. Afterwards, the fundamental and SH beams are separated by a combination of two rotatable Pellin-Broca prisms and a monochromator (MC; Omni-λ150 from LOT). For a 90° deflection of the SH beam at each prism, the angles of the prisms have to be adjusted to the wavelength and are controlled by step motors. The correlation between wavelength and motor positions is calibrated upfront and described in the SI, see Figure [9]. A photo diode detects the light intensity of the fundamental light after the first prism for power correction purposes as described later.

[Depending on the used geometrical mode, the intensity can be alternatively detected by a second diode placed right after the laser system and in front of the sample.] Finally, the pure SH light is detected by a photomultiplier tube (PMT; H9305-03 from Hamamatsu) and the resulting analog current is taken as signal, see Figure [15]. A [new self-written] central LabVIEW program controls the laser, the trigger box, PEM, step motors, MC and oscilloscope and is depicted in Figure [14]. This enables full automation and makes it possible to scan over a large wavelength range, while switching between different polarizations for each wavelength or, alternatively, monitor the time evolution in SH at a specific wavelength. [...]

To study the nonlinear optical activity of [a sample], wavelength scans between 225 nm and 340 nm of the SH (equivalent to 450 nm to 680 nm of the fundamental light) with both CPs and p-polarized fundamental light were recorded [...]. [A minimum of] 100 laser shots per wavelength and polarization were averaged. At selected wavelengths the SH was recorded for at least 10 k shots for each CP." (Publication A)

Spectroscopic Geometries

The setup enables two different geometrical modi for the fundamental light to interact with the sample insight the analysis chamber. They are called transmission and reflection geometry and their choice depends on the properties of the studied sample.

The transmission geometry is applicable for samples with a high transmission. Such samples are, for example, glass substrates with a thin molecular film or clusters with a low coverage on them. In this mode, the fundamental beam hits the sample on the "backside", transmits through the glass body and interacts with the, for example, film at the "frontside" where SH is generated, see Figure 7. The angle of incidence Θ is usually set to 70°. Such a steep angle is chosen in order to maximize the SH intensity as the intensity is increasing with angle.[72] On the other hand, the angle is well below the threshold where the beam is cut off by the body of the manipulator. The sample or substrate holder is as plate with 18 mm x 18 mm dimensioned centered hole, through which the beam passes. The sample is fixated with four clamps and the holder possesses a nose on one side which is compatible with the load and lock mechanism of the transfer stick in the transfer chamber, see Figure 7.

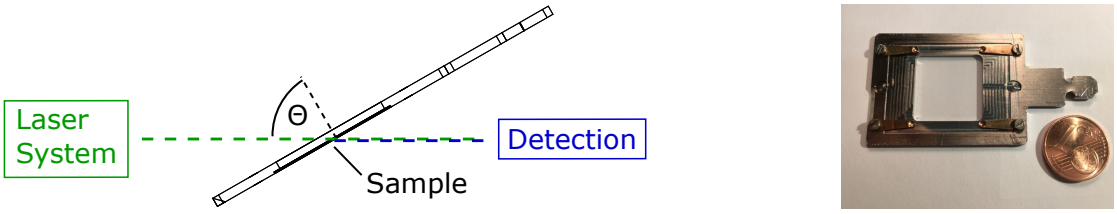

Figure 7 Left: Beam path for SHG experiments in transmission geometry. Right: Substrate holder for transmission geometry with BK7 glass substrate. (Reproduced from Publication D)

For obvious reasons, the transmission geometry is limited to highly transparent samples. Therefore, a second mode, called reflection geometry, was developed especially for opaque samples. Here, an additional holder which holds two mirrors is slid into the manipulator and placed opposite to the sample. The fundamental is now reflected by the first silver mirror (protected silver from Thorlabs; PFSQ05-03-P01) onto the sample, see Figure 8. The angle of incidence is 30° here and limited by the dimensions of the existing manipulator. At the sample the fundamental is reflected and SH generated. Note that the samples surface has to be highly reflective. Otherwise dominant scattering will make the detection of the SH impossible. A second mirror (aluminum from Thorlabs; PFSQ05-03-F01) is reflecting the fundamental and SH on the original direction and identical beam path as in case of the transmission mode. Therefore, the same procedure and same settings (calibration of prisms) can be used. The mirror holder is designed to be inserted and extracted easily from the manipulator, see Figure 8. This enables a simple switching between both modi and maintaining of the holder.

In order to allow sputtering of the samples surface and deposition of clusters onto within this mode, the sample holder has to be flipped and still fitting into the manipulator. Therefore, a flat design consisting of a base and a lid was chosen, see Figure 8. The sample, for example, a 10 mm x 10 mm silver plate is fixed between base and lid which are simply screwed together.

The following procedure was developed to ensure that the beam path is indeed identical with the one of the transmission mode. First, the laser is set to an arbitrary wavelength (here 500 nm). The light intensity is reduced by means of a neutral-density filter and the PMT is blocked throughout the whole procedure. The manipulator is raised till the light beam passes through the analysis chamber unhampered. The prisms and MC are set to pass SH of 500 nm through. Then, the sample is driven into the beam path and the angle Θ is adjusted by rotation of the manipulator till the beam passes centered through the MC again.

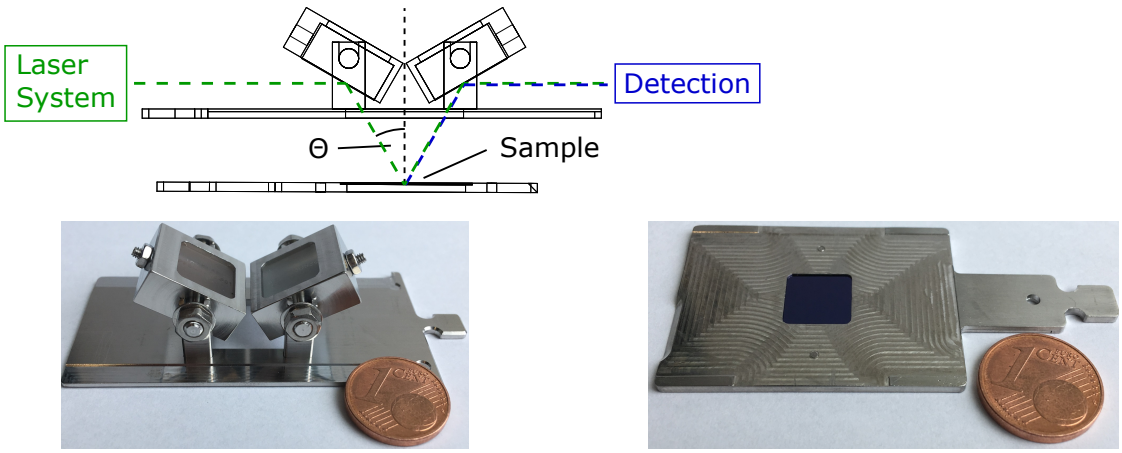

Figure 8 Top: Beam path for SHG experiments in reflection geometry. Bottom: Mirror & substrate holder with Si waver for reflection geometry.

Calibration of Prisms

"In order to split the fundamental light from the generated second harmonic (SH) light, a pair of Pellin-Broca prisms is used. To keep the deflection angle of the SH light at 90°, the angle of each prism respectively to the light beam has to be adjusted for each wavelength. This was realized by installing them on rotatable plates moved by stepper motors. The motor positions were manually adjusted for selected wavelengths over the wanted scan region using the built-in SH unit of the laser. [The light intensity was reduced by means of a neutral-density filter and the PMT was blocked throughout the whole procedure.] It was made sure that the deflection was 90° [at both prisms] and the transmission through the [MC] and the focus onto the [PMT] was centered. The motor positions plotted over the wavelength including a polynomial fit are shown in Figure [9]." (Publication A)

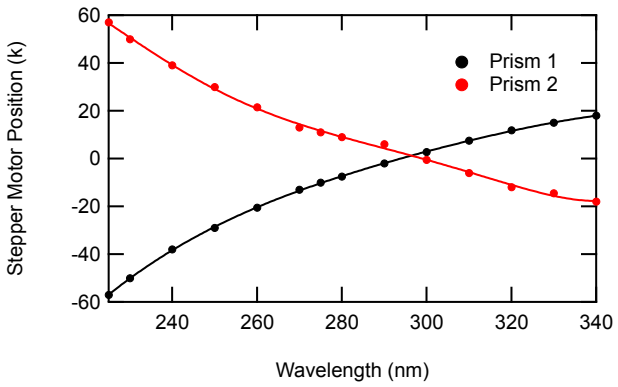

Figure 9 Stepper motor positions for angle adjustment of the two Pellin-Broca prisms for separation of the SH from the fundamental over the SH wavelength. (Reproduced from Publication A)

Calibration of Polarization

"A PEM was used to convert the p-polarized light of the laser into both circular polarizations. A PEM has the advantage over a quarter wave plate that it can be used in a wide wavelength range suitable for automated scans. The PEM is a fused silica which oscillates in one axis leading to an oscillating refractive index along this axis. This results in a retardation between the electric field vectors of light parallel and perpendicular to this optical axis when it is transmitting. In order to convert [p-polarized] light into left or right circularly polarized light, this retardation has to be $\pm 90°$. Since the PEM is oscillates with its eigenfrequency of about 42 kHz and the laser is operating at a frequency of 20 Hz, special care taken in terms of the timing between both. Therefore, a self-made trigger box was used, which takes the output signal of the eigenfrequency of the PEM and generates a trigger signal for the laser with a defined delay or phase between both. The reference output signal of the PEM with 42 kHz is connected to the trigger box. The box itself possesses an internal frequency generator operating at 20 Hz, the frequency of the laser system. After each pulse of the internal generator, the box waits

for the next flank of the reference signal of the PEM. Then, a TTL signal is sent to the output of the box after a defined delay. This output signal is used as external trigger for the laser system. A sketch of the chronology of the pulses is given in Figure [10].

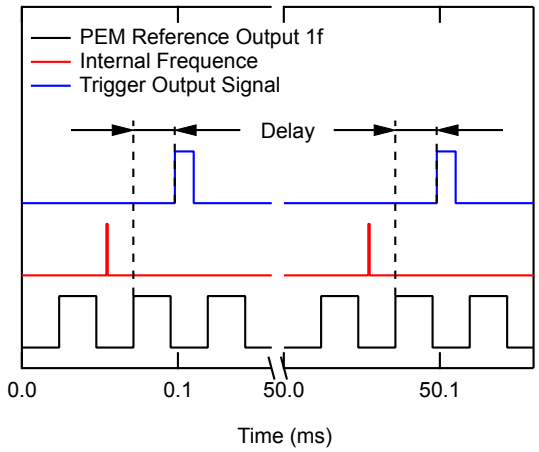

Figure 10 Sketch of the pulses of self-made trigger box to synchronize PEM and laser system. (Reproduced from Publication A)

To find the delay times at which the polarization will be converted into a circular one, a second polarizer was installed after the PEM in 90° to the first one before the PEM. This is depicted at left of Figure [11]. While the delay time was altered, the intensity of the transmitting light was recorded with the diode for different wavelengths, see Figure [11]. The intensity oscillates and shows two maxima at around 5 µs and 17 µs and two minima at 11 µs and 23 µs and is the same for all wavelengths.
At the minimum, the polarization of the initial p polarized light stays untouched by the PEM and does not transmit through the second polarizer. At the maximum, the light is converted into one of the circular polarizations (CPs) and transmits the second polarizer while converted back into linear polarized light. The intensity difference between the wavelengths depends on the wavelength-dependent power of the laser and sensitivity of the diode.
Theoretically the intensity can be expressed as

$$I = I_0 \{1 - \cos [A_0 \cos (\omega t + t_0)]\} \tag{9}$$

with I_0 as initial intensity, A_0 as amplitude of the sinusoidal retardation and ω as the eigenfrequency of the PEM.[73] A fit of the curve at 600 nm presented as a solid black line in Figure [11] depicts the delay times of 5.14(2) µs for one CP, 11.09(2) µs for p polarized and 17.03(2) µs for the other CP. The Eigenfrequency was determined at 42.1(1) kHz and is in good agreement with the measured one Eigenfrequency of the PEM controller.
For the final assignment of the circular polarizations, a similar SHG-CD experiment using a λ/4 plate on a R BINOL film was conducted. The plate was installed after the PEM. The delay time was set to

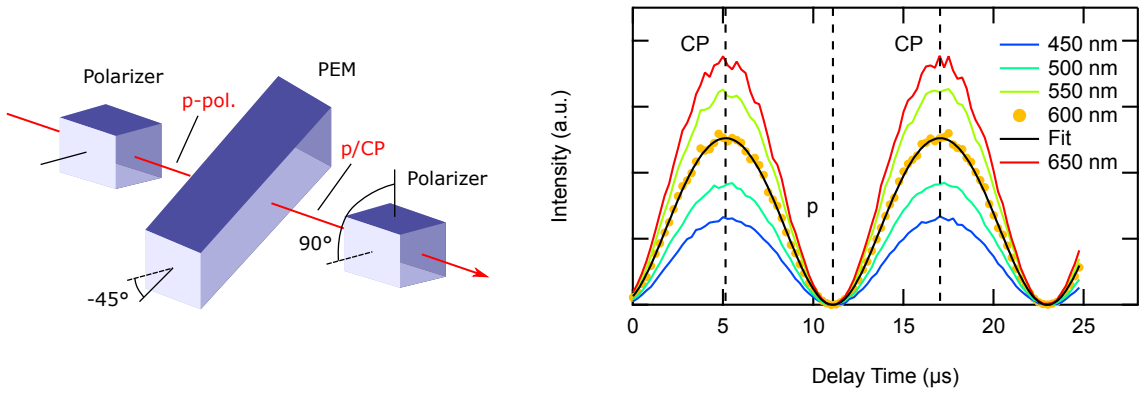

Figure 11 Left: Sequence of optical elements used for the calibration of the delay times between PEM and laser which define the polarization. Right: Intensity of transmitted light through PEM and analyzer plotted over delay time between PEM and laser for different wavelengths. The delay times related to the CPs and p polarization are labeled. (Reproduced from Publication A)

11.09 µs to keep the polarization of the light linear p polarized. The plate was then set to a –45° and 45° angle in respect to the horizontal resulting in left and right circularly polarized light. The setup is depicted in left of Figure [12]. The resulting SH spectra (only power corrected) and the calculated anisotropy factor are given at the right of Figure [12]. By comparison to the spectra acquired using the PEM as polarization defining device, the delay time at 5.14 µs can be assigned to left circularly polarized light and 17.03 µs to right circularly polarized light." (Publication A)

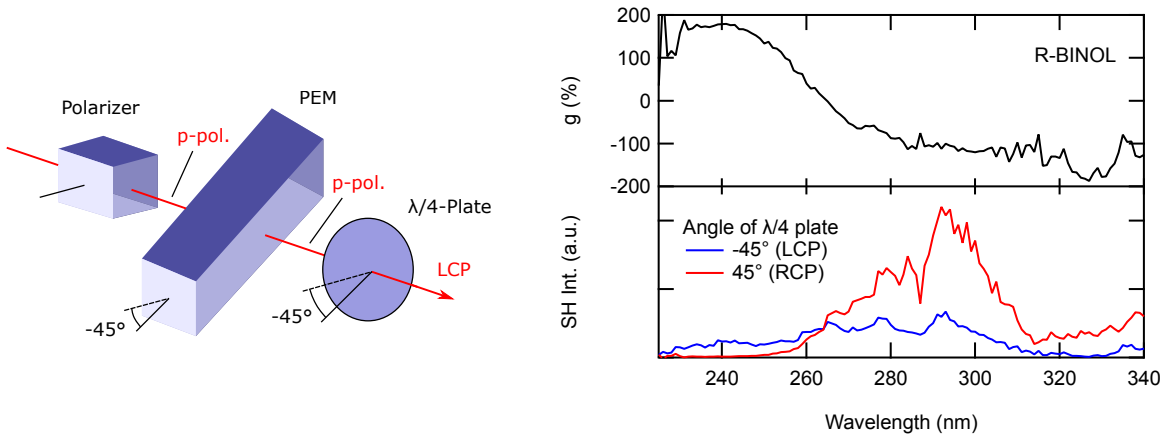

Figure 12 Left: Sequence of optical elements used for absolute assignment between delay times and circular polarization. Right: SH spectra (only power corrected) for both CPs of R-BINOL film and calculated anisotropy factor. (Reproduced from Publication A)

Automation

“The [automation] required for scans over a wide wavelength range is realized by a [new self-written] LabVIEW program which controls all wavelength-dependent parameters and handles the storage of the raw data. The essential connections are depicted in Figure [13]. Outgoing signals from the PC are highlighted in green. With connections to the laser system, trigger box, PEM, prisms, MC and oscilloscope parameters like wavelength, polarization, retardation, prism angles, and number of acquired shots per wavelength and polarization are controlled. The trigger signals are drawn in red and the signal connections of the analog signals between PMT and diode and oscilloscope and the digital signals between oscilloscope and PC are drawn in blue. A screenshot of the LabVIEW program during a typical experiment is given in Figure [14]. Additionally, during the experiment, the program presents a simple evaluation of the data in form of the raw SH and reference signal of each first shot at the top right and the integrated intensity over the wavelength for each delay between PEM and laser (polarization defining).” (Publication A)

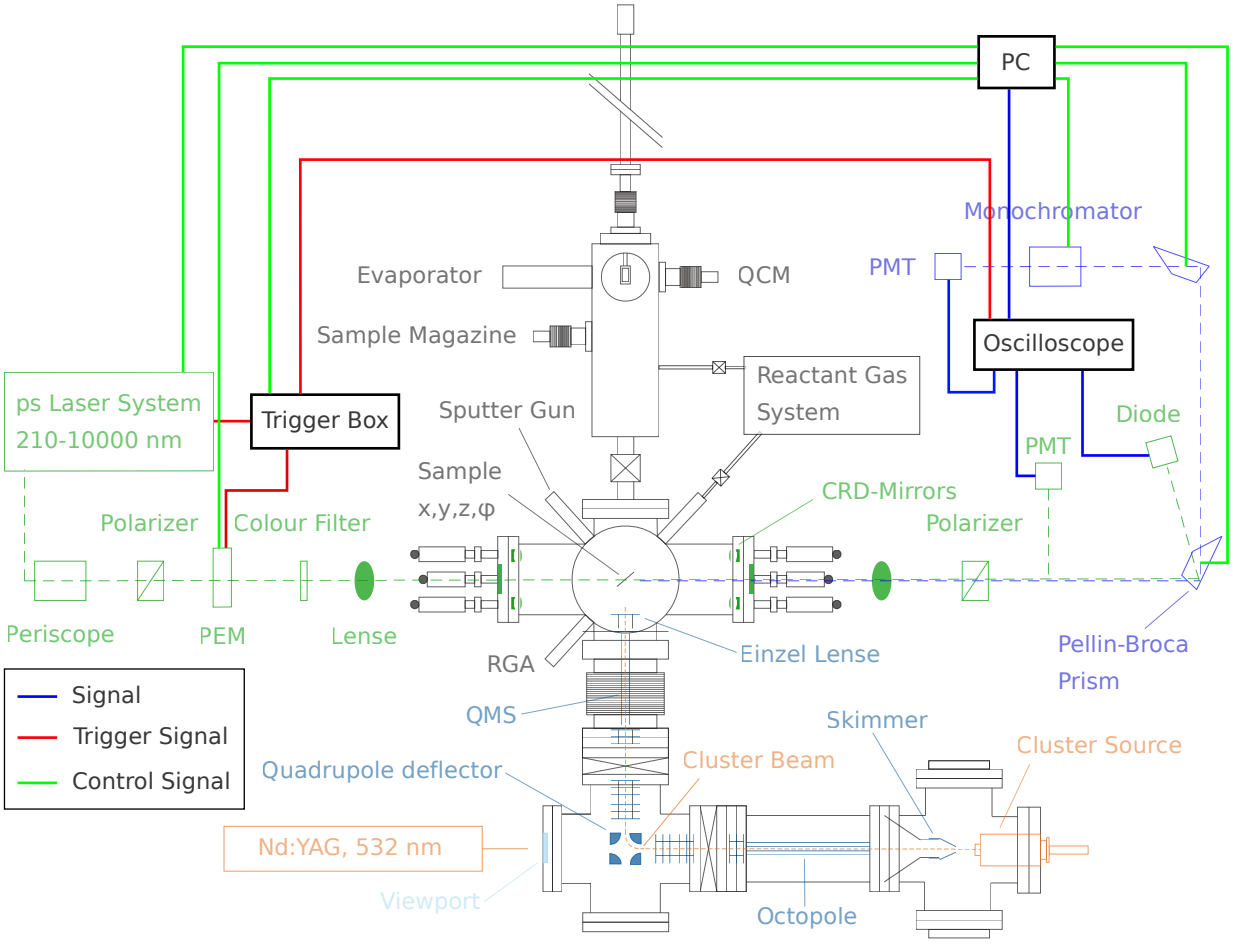

Figure 13 Experimental setup with indication of the electronic connections. Signals are indicated in blue, trigger signals in red and command signals from the LabVIEW program in green. (Reproduced from Publication A)

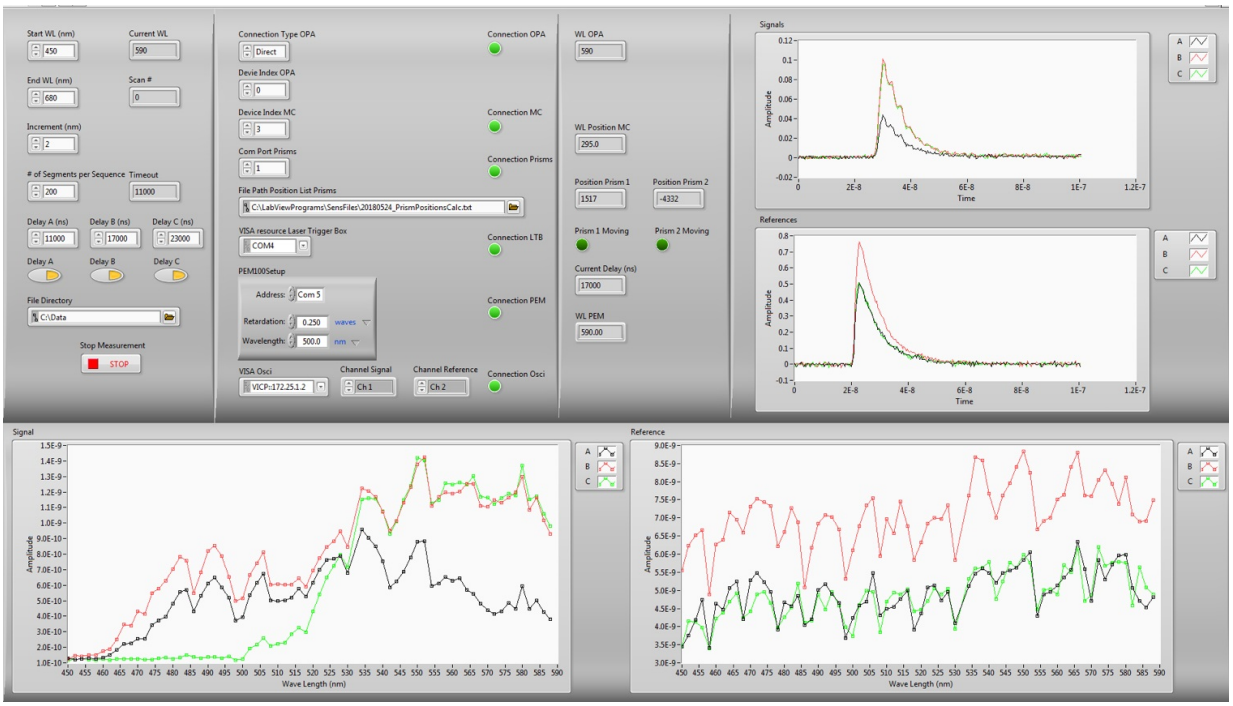

Figure 14 Screenshot of SHG-CD LabVIEW program. (Reproduced from Publication A)

Signal Referencing

"The analog current of the [PMT] recording the SH, and the diode recording the fundamental are shown exemplarily in case of the pristine BK7 substrate and p polarized light at 500 nm in Figure [15]. The first points are averaged and taken as baseline indicated in red which are then subtracted from the signal. In a second step, the baseline corrected signal is integrated (blue area under the curve). Finally, it is averaged over the number of shots, which were recorded for one wavelength and polarization.[...]

[Doing so for multiple wavelengths,] the raw SH spectrum [$I_{SH,raw}$] of [p-polarized] light from a pristine BK7 glass substrate is shown at the top of Figure [16]. The related intensity of the fundamental light [I_{diode}] measured with a diode is given in the middle. Notice that the sensitivity [S_{diode}] of the SI diode is wavelength dependent and [has to be taken into account as well].)

The SH and fundamental light spectrum show an analytical relation because the intensity of SH depends on the intensity of the fundamental light and therefore should be corrected for it. Hence, the SH spectrum was first divided by the square of the wavelength corrected intensity of the fundamental light. [The described power corrections are summarized in following applied formula.]

$$I_{SH,pow} = \frac{I_{SH,raw}}{(I_{diode}/S_{diode})^2} \tag{10}$$

Considering that BK7 has no specific transitions to address, the SH spectrum should not show any spectral features. Accordingly, deviations originate from the wavelength dependent properties of

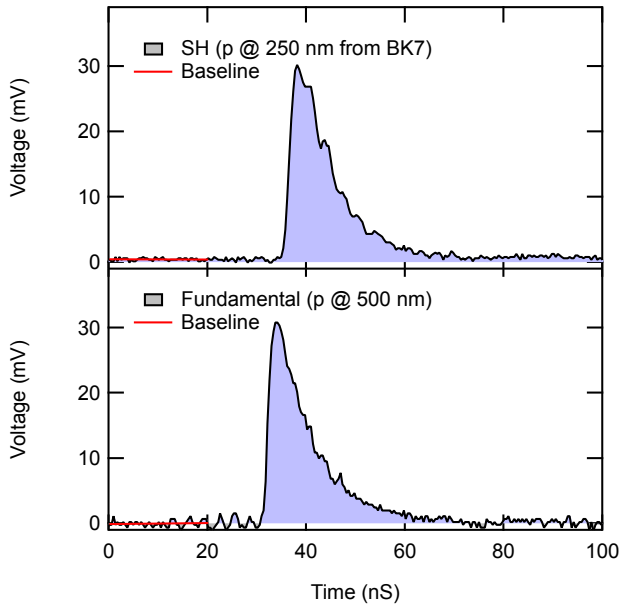

Figure 15 Analog current of diode recording the intensity of the fundamental (bottom) and PMT recording the SH (top) from a pristine BK7 substrate for p-polarized light at 500 nm for the fundamental light over time. (Reproduced from Publication A)

the spectrometer such as transmision of the filters, efficiency of the MC and sensitivity of the PMT. To compensate these influences, the power-corrected SH spectrum is smoothed and defined as a spectrometer function [F_{spec}], which is shown as green curve in Figure [16].[72]" (Publication A)
The spectrometer function is then used to reference SH spectra of other samples than pristine glass substrates where specific transitions are expected. This is done by simple weighting of the power corrected SH spectrum with the spectrometer function.

$$I_{SH,cor} = \frac{I_{SH,pow}}{F_{spec}} \tag{11}$$

The here presented referencing and data processing is done automatically by self-written procedures in Igor which are using the raw data of the oscilloscope as input.

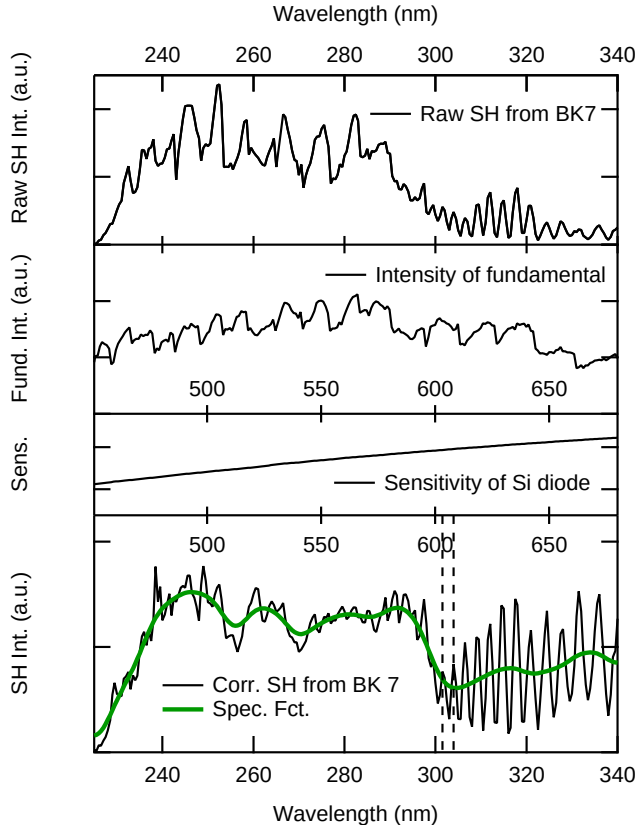

Figure 16 Top: Raw SH spectrum from p polarized light of a BK7 glass substrate. Middle: Intensity of fundamental and sensitivity of silicon diode. Bottom: Respective power corrected SH with spectrometer function as smoothed green curve. (Reproduced from Publication A)

3.2 Molecular Adsorption & Film Preparation by Evaporation

The deposition of molecules on a sample is done by means of a molecular evaporator which is installed in the transfer chamber. Therefore, the evaporation process takes place under high or ultra high vacuum conditions, depending on the momentary base pressure of the newly designed transfer chamber. In order to improve the deposition conditions, the evaporator was extended for a shutter and a shield as well as a self-written LabView program which visualizes the calculated absolute coverage in real time by using a QCM (SL-A1E40 from INFICON). Finally, a new deposition procedure was established which takes advantage of these new upgrades and enable a well-defined and reproducible deposition.

Molecular Evaporator

The evaporator of in-house design is shown in Figure 17. The evaporator holds three crucibles for the molecules of interest which can be heated independently by resistive heating. If necessary, additional cooling of the body of the evaporator by means of cooling water is possible. A new rotatable shutter is used to block the flux of molecules onto the sample if needed. An additional shield, including a mask, is attached to the evaporator and surrounds it. The shield minimizes the deposition of molecules onto the walls of the transfer chamber and, therefore, a contamination for future experiments. It can be easily taken off and cleaned after an experiment.

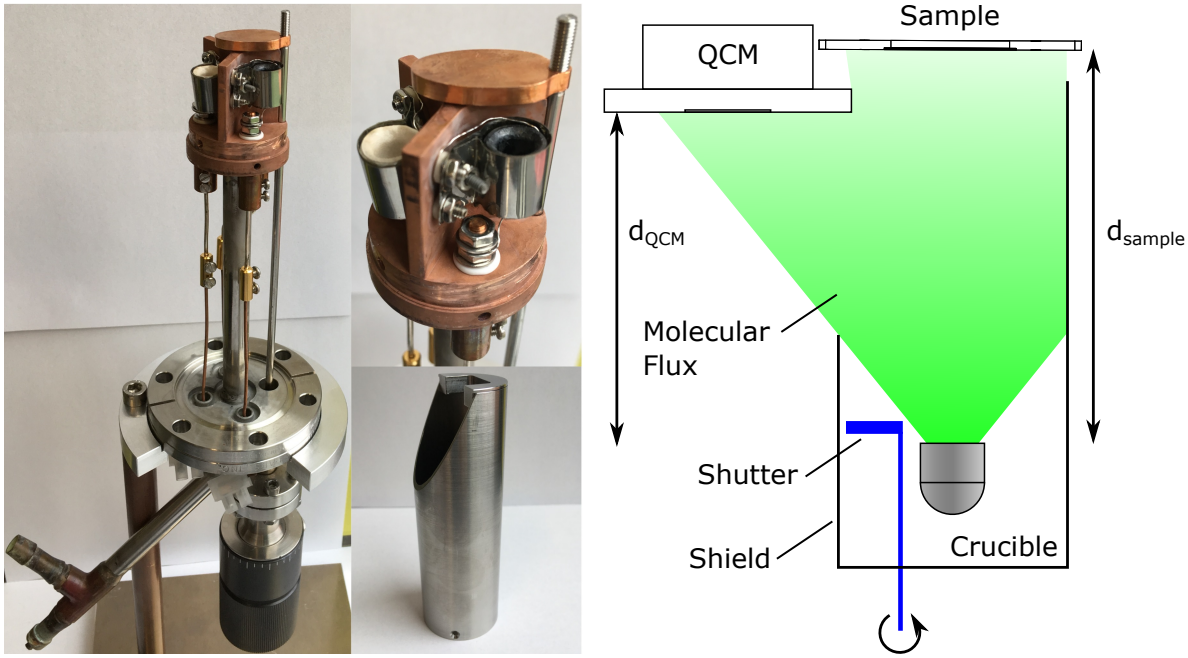

Figure 17 Left: Pictures of evaporator including shutter and shield. Right: Drawing of geometry during evaporation including the lateral and vertical offset between sample and QCM.

Coverage Determination by Quartz Crystal Microbalance

A QCM is commonly used to monitor the coverage during a deposition. Its operation is based on a quartz crystal which is held into the molecular flux. The crystal possesses a certain eigenfrequency which is constantly measured and approx. 6 MHz here. If molecules are deposited onto the crystal they increase its mass by Δm. This yields a decrease of the eigenfrequency by Δf in a linear relation if the frequency is close to the initial eigenfrequency f_0 (within 2 %). The Sauerbrey equation expresses this relation and is defined as follows.[74]

$$\Delta f = -\frac{2\, f_0}{A\sqrt{\rho_q\, \mu_q}}\, \Delta m \tag{12}$$

The equation includes constants related to the crystal like its area A (1.53 cm^2), its density ρ_q (2.648 g/cm^2) and its shear modulus μ_q ($2.947 \cdot 10^{11}$ g/cm^2s). Now, the absolute coverage C can be derived by using the mass of one deposited molecule M_{mol}.

$$C = \frac{\Delta m}{A\, M_{mol}} \tag{13}$$

Because the QCM is placed in a lateral position, including a height offset, in comparison to the sample (see Figure 17) it is expected that the molecular flux onto both is not identical. Therefore, the monitored coverage during the deposition has to be corrected. To compensate for the lateral offset, an evaporation of the same mass of molecules was repeated once with the QCM in its lateral position C_l and once in a vertical line to the evaporator C_v. The ratio between both monitored coverages is defined as $T_l = C_v/C_l$. The effect of the height offset between the QCM and the sample is calculated theoretically. Therefore, it is assumed that the molecular flux density is isotropic on a surface of a hypothetical sphere with a radius of d around the crucible. The ratio between the flux densities is then defined as $T_v = d^3_{sample}/d^3_{QCM}$ with d_{sample} and d_{QCM} as distances to the sample and QCM, respectively. Finally, the correction of the coverage is calculates as follows.

$$C_{cor} = C\, T_l\, T_v = C \cdot 1.033 \tag{14}$$

Further, the film thickness d can be calculated in units of m or monolayers (ML), if the surface area A_{mol} or the volume V_{mol}, one molecule occupies, is known. Note that this is an estimation and depends on factors such as the film structure. It can deviate especially for small coverages where the interaction with the substrate becomes relevant. The film thickness in units of ML calculates as follows.

$$d = C\, A_{mol} = C\, V^{2/3}_{mol} \tag{15}$$

Procedure & Automation

The applied evaporation procedure is the following. While the sample is in the analysis chamber, the crucible which is holding the molecules of interest is heated below the threshold from where the evaporation begins. During this cleaning step water, solvents and other molecules are desorbing which is visible in an increasing background pressure of the transfer chamber. After the pressure returns to its base pressure, the heating power is increased to a set value which depends on the molecule. It is waited till a desired rate is reached. Note that the ideal rate is a compromise. On one hand, the rate should be chosen small enough so that the evaporation on the sample is at least some seconds to ensure a defined coverage. On the other hand, the rate should be large enough to minimize the time in the transfer chamber and possible contamination from residual gas molecules. Then the shutter is rotated above the crucible and the monitored absolute coverage of the program is reset. The sample is brought from the analysis chamber and placed centered above the evaporator. The shutter is rotated again to unblock the molecular flux onto the sample and the deposition starts. When the desired coverage is reached, the shutter is rotated above the crucible again and the sample transferred to the analysis chamber where the spectroscopic experiments are conducted.

As an example, the deposition curve in case of D-tartaric acid with a desired film thickness of 40 ML is shown in Figure 18. The measured eigenfrequency is plotted in top and the corresponding calculated coverage and film thickness in the bottom.

A new self-written LabView program displays the monitored eigenfrequency of the QCM, see Fig-

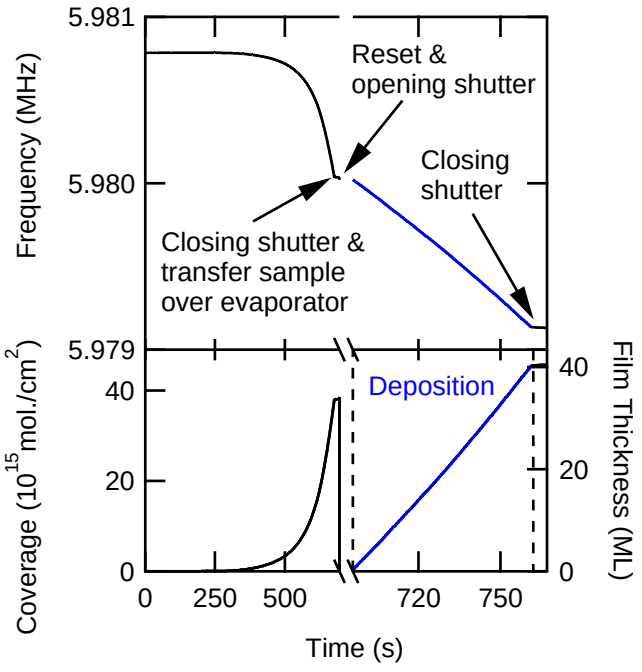

Figure 18 Eigenfrequency of the QCM (top) and calculated coverage and film thickness on the sample (bottom) during a deposition of D-tartaric acid.

ure 19. Further, the program calculates the absolute coverage and film thickness as well as their rates in real time if the required constants of the molecule are given. The percentage of a defined absolute coverage is visualized in a bar graph. All values are saved to a text file afterwards.

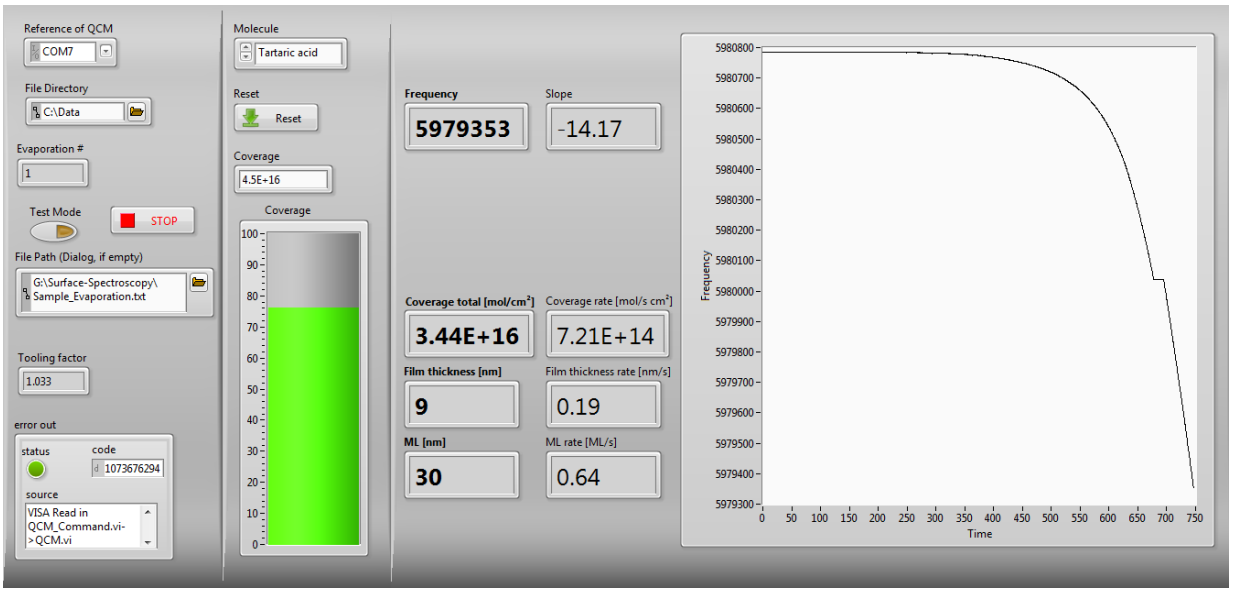

Figure 19 Screenshot of evaporation control LabVIEW program.

3.3 Spin Coating

Spin coating is a widely employed technique for the fabrication of thin films. Thereby it represents an alternative to the molecular evaporation and is favored especially for the preparation of films thicker than 1 µm and chemical compounds which decompose under evaporation. The film thickness can be varied since it is depending on the rotational speed during the coating[75,76] as well as on the viscosity and concentration of the solution.[75] Therefore, a spin coater was developed with a design customized for the studied samples in this thesis. In combination with a newly established coating procedure, a fabrication of films with a high reproducibility and structural uniformity is possible.

Spin Coater

The spin coater with an in-house design is shown in Figure 20. The basis (4) is a aluminum construction with rubber feet which provides a sufficient support and vibrational isolation. Splashing coating solution is blocked by a glass cylinder (1) and collected in a tray (2) & (3). Both, cylinder and tray can easily be taken off for cleaning purposes. The motor (5) is fixed to the basis and its rotational speed is regulated by a potentiostat of a separate power supply. The substrate holder (6) is made from Polyetheretherketon (PEEK) and, therefore, inert to common solvents. The substrate is placed into the centered profile (7) and not additionally fixated. Thus, bending of the substrate is minimized

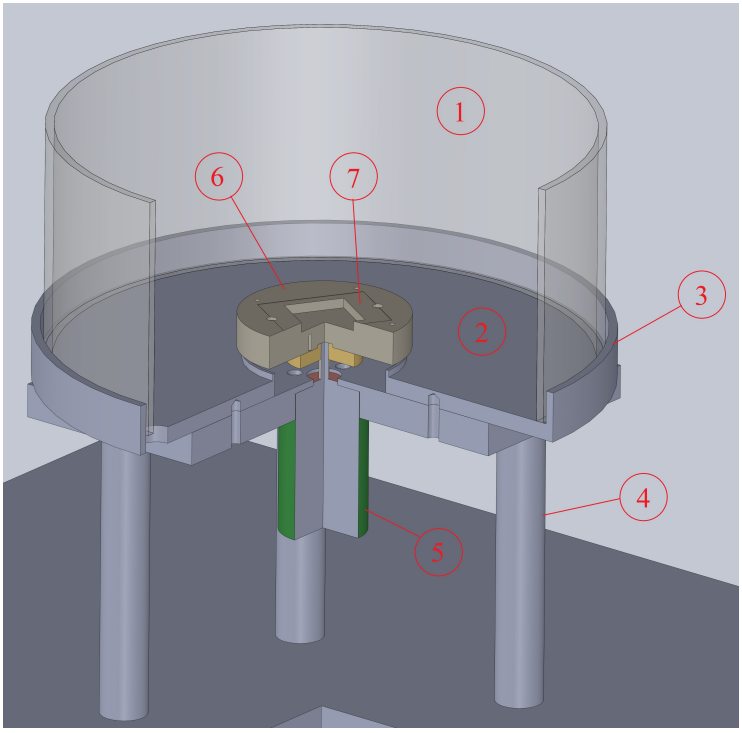

Figure 20 CAD drawing of the used self-made spin coater. (1) Glass cover. (2) & (3) Aluminum tray. (4) Supporting leg. (5) Motor. (6) PEEK substrate holder. (7) Cut out profile for substrate. (Reproduced from Publication G)

and contamination on the backside from, for example, an O-ring of a vacuum-based fixation, which is used in commercial spin coaters, avoided. This is especially from importance since in this study glass substrates of only 150 µm thickness were used and spectroscopy experiments in transmission mode would be sensitive to contamination on the backside of the sample.

"Because the rotational speed of the motor is set by a simple potentiostat, the relation between potentiostat and rotational speed of the self-made spin coater had to be calibrated. Therefore, a piece of reflective aluminum foil was attached to the substrate holder. A helium-neon laser was pointed at the substrate holder and the reflection from the aluminum foil recorded by a diode.[77] The frequency of the diode signal was measured for different potentiostat values and converted into revolutions per minute (rpm) by multiplication with 60." (Publication G) The calculated rotational speed in units of rpm is plotted versus the potentiostat scale in Figure 21. A linear dependency between the potentiostat scale and the rotational speed was found and the according fit shown (red line). From this linear dependency it derives that the rotational speed in rpm is approx. 660 times the potentiostat scale. Therefore, the rotational speed can be fine-tuned to values up to 6600 rpm.

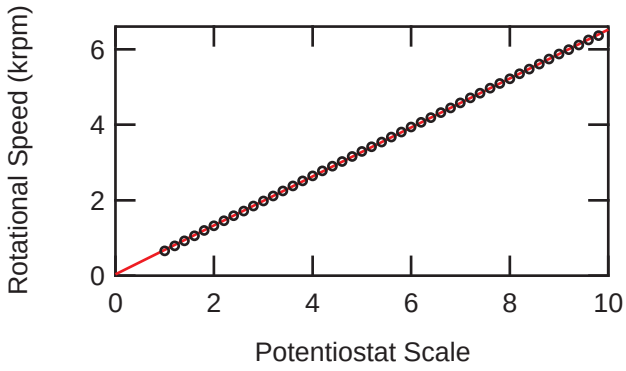

Figure 21 Measured rotational speed of the self-made spin coater plotted vs. potentiostat scale. (Reproduced from Publication G)

Film Thickness Dependencies

As already mentioned, the thickness of the spin coated film depends on several parameters. First, it depends on the viscosity and concentration of the coating solution.[75] Second, it depends on the rotational speed during the coating process.[75,76] In return, the film thickness is controlled through these parameters and can be varied in a defined manner. To demonstrate both effects, two series with the dye Rhodamine 110 solved in ethanol as coating solution were conducted. Absorption spectra of all films were measured and the dipole strength $D_{Rhod.}$ in the visible range calculated. It is assumed that the dipole strength stands in linear relation to the film thickness and can be used instead for this demonstration.

In the first series, the concentration of the dye was varied but the rotaional speed kept at 660 rpm.

The calculated dipole strength is plotted versus the concentration, see Figure 22. A linear behavior is found and shown as fit (red line) which is also known from literature.[75] The film with 1.5 wt% of the dye is estimated to possess three times the thickness of the one with 0.8 wt%.

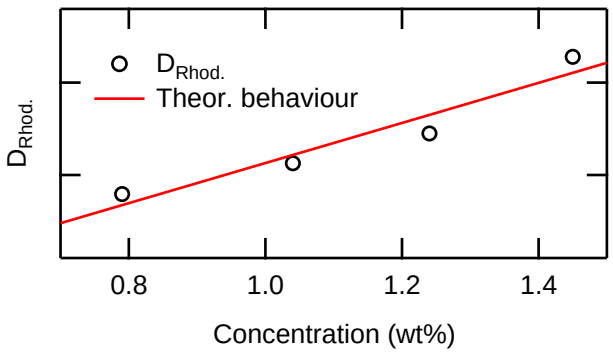

Figure 22 Dipole strength between 420 nm and 700 nm of films with Rhodamine 110 vs. concentration in spin coating solution and theoretical behavior (red curve).

In the second series, the concentration was kept at 1.2 wt% and the rotational speed varied between 960 rpm and 4860 rpm, see Figure 23. An increasing rotational speed yields less absorption, a smaller dipole strength and, therefore, a thinner film, as expected.[75,76] The film thickness follows the theoretical inverse dependency on the square root of the rotational speed $\propto \omega^{-0.5}$, shown as red line.[78,79] The film with 960 rpm is estimated to possess double the thickness of the one with 4860 rpm.

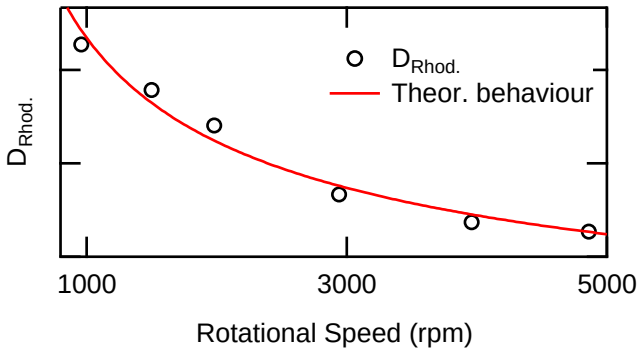

Figure 23 Dipole strength between 420 nm and 700 nm of films with Rhodamine 110 (and R-BINOL with a ratio of 0.67) vs. applied rotational speed during film coating and theoretical behavior (red curve). (Reproduced from Publication G)

Procedure

The following procedure yielded the highest reproducibility and structural uniformity of the films. The concentration of the coating solution is defined by weighting of the compound and solvent. The potentiostat of the spin coater is set to the desired value but the coater is not switched on yet. A volume of 100 µL of the coating solution is dropped onto the static substrate with a pipette so that

the 10 mm x 10 mm center is completely covered. This approach is called static spin coating in comparison to dynamic spin coating where the substrate already rotates while the it is coated. Then, the motor is switched on and run approx. 3 min till all solvent is evaporated and the film dry.

4 Pristine Chiroptical Activity of Films & Surfaces

Picking up the motivation stated in the introduction, the goal is the study of the asymmetrized heterogeneous catalysts. In particular the study of the chiral character by means of the chiroptical properties and the interaction between chiral modifier and achiral heterogeneous catalyst.
But the study of chiroptical properties of films and interfaces comes with two great challenges which are not present in solution-based systems. One is the small amount of molecules and the resulting minute amount of response signal. This is especially the case for functionalized surfaces and asymmetrized heterogeneous catalysts. Great efforts have been made to improve the chiroptical sensitivtiy by developing more sophisticated techniques based on e.g. surface cavity ring-down (s-CRD).[80] Also, nonlinear chiral effects like SHG-CD were shown to be promising in this regard as they are up to 3 orders of magnitude larger than the corresponding linear ones.[52,68,72,81] The other great challenge are isotropy effects which are predominantly present in the solid state. These effects are superimposing with the molecular response and make the interpretation more difficult. Therefore, before studying more complex systems like asymmetrized heterogeneous catalysts, the first steps of this work were to tackle these two fundamental challenges and is the topic of this chapter.

4.1 Probing Chiroptical Activity of Low Coverages

In order to detect small amounts of molecules at an interface, the setup is equipped with s-CRD and SHG spectroscopy. The two complementary spectroscopic methods are inherently sensitive to small amounts of molecules or particularly sensitive to interfaces, respectively. The sensitivity of CRD yields from two facts. First, the measurement of time like the time constant of the optical cavity in case of CRD is far more precise than the measurement of light intensity as in case of a common absorption technique. Second, the effective path length through the sample is enhanced by thousands of times by the cavity.[82,83] Whereas SHG is inherently sensitive to interfaces. This is due to its selection rule which allows it only to be generated in the absence of centrosymmetry which is always the case at interfaces.
To demonstrate their strengths, a combined study including both methods was conducted on the optical response of the laser dye Rhodamine 110 at a vacuum glass interface with a submonolayer coverage.[81]

Optical Properties of Monolayers of bis-pyrenyl with s-CRD

Recently, the high sensitivity of s-CRD was used to study interlayer interactions between the first and second monolayer of 1,4-Di-n-octyloxy-2,5-bis(pyren-1-ylethenyl)benzene (bis-pyrene), see Publication B. Pyrene-containning conjugated materials receive considerable attention for their versatile electronic and optical properties.[84,85] This makes them a promising class for advanced applications in organic field effect transistors, photovoltaic and light emitting diodes.

The bis-pyrene was evaporated onto a glass substrates with different coverages ranging from $1.6 \cdot 10^{13}$ mol./cm^2 to $1.2 \cdot 10^{14}$ mol./cm^2. The optical spectra were acquired by means of s-CRD in a range between 420 and 680 nm. All spectra show a low energy band with a peak at 434 nm which is related to the long-axis polarized transition ^1L_a.[86–88] The spectra show an additional shoulder at 505 nm for coverages higher than $3.1 \cdot 10^{13}$ mol./cm^2. This corresponds approximately to one ML which is confirmed by scanning tunneling microscopy (STM) on bis-pyrene evaporated onto Au(111), as part of the same work. This shoulder saturates for coverages higher than $4.6 \cdot 10^{13}$ mol./cm^2. The normalized s-CRD spectra of this shoulder are shown in Figure 24. It concludes that the additional shoulder at 505 nm originates from interaction of the transition dipole moments of the molecules between the first and the second layer. This phenomenon is called Davydov splitting and is known from organic crystals.[89]

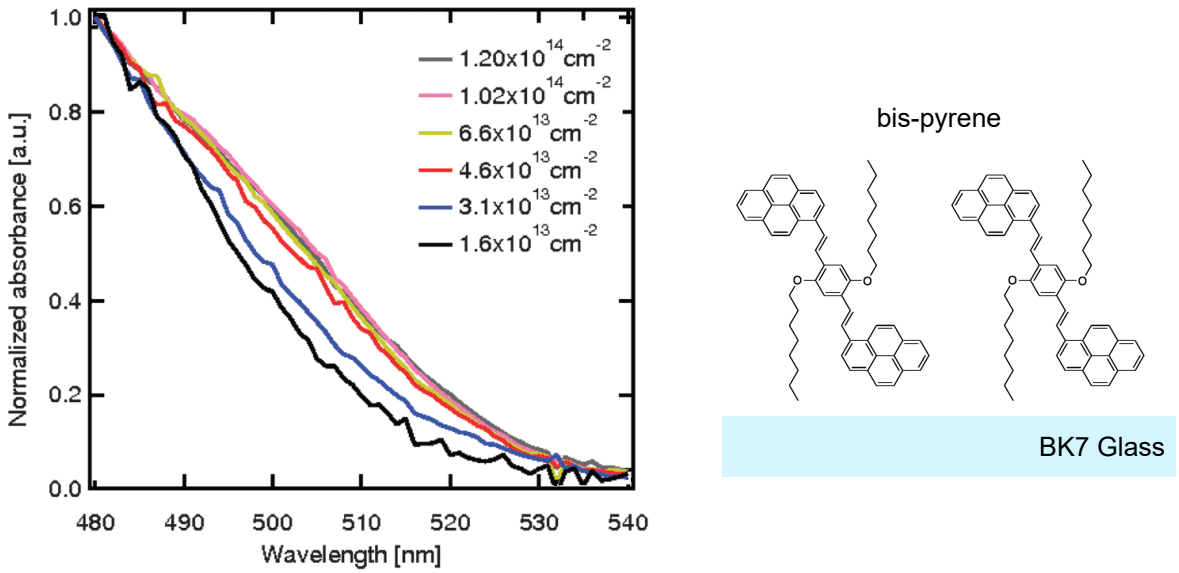

Figure 24 Left: s-CRD spectra recorded for bis-pyrene deposited on BK7 for various coverages and normalized at 480 nm. Right: Chemical structure of the bis-pyrene compound. (Adapted from Publication B)

The study demonstrates the sensitivity of this technique and, therefore, its relevance for the motivation of this work to study asymmetrized heterogeneous catalysts. S-CRD yields information about the optical properties and, thus, the electronic structure of, for example, catalysts and chiral modifiers. Also their interaction can be studied through effects on their optical response. Unfortunately, the devel-

oped s-CRD technique of this setup cannot be used to study the chiroptical properties of a sample. The CP used for this purpose would be converted into the opposite with each reflection within the cavity. This would cancel a difference in absorption between both polarizations and suppress the CD effect. Nevertheless, s-CRD holds additional information compared to nonlinear techniques like SHG because of two reasons. First, it possesses an unambiguous spectral assignment[61,63] and, second, its selection rules concerning the spatial arrangement of the addressed electric dipole moment are different. This makes s-CRD complementary to SHG and a valuable addition to the setup.

Optical Activity of Submonolayer of BINOL with SHG-CD

As mentioned the second technique of our setup to study the optical properties of systems with small coverages is SHG. Its strength has been demonstrated, among others, through studies on supported silver metal clusters.[63] It was shown that their electronic structure strongly depends on their size.[61] Such clusters are well-known for their catalytic activity which often shows similar strong size effects since they are strongly related to their electronic properties. In a further study, their oxidation behavior was studied.[90] In this work, it was presented how the response of the clusters plasmon on the interaction with its surrounding can be used as a probe. This makes it a promising approach for studying the interaction between an asymmetrized heterogeneous catalyst and its chiral modifier. The observed sensitivity of the plasmon response points out the importance to study the systems under well controlled conditions so that contaminations are avoided. This is done by performing the sample preparation and spectroscopic studies in situ under UHV conditions. There, the pure sample can be studied as model system. This is lowering the number of variables and by that reduces the complexity which makes the interpretation of the results easier. Therefore, the higher experimental intricacy related to an UHV part is justified by its benefits and potential of studying samples and systems under controlled conditions. However, the spectroscopic method is not restricted to UHV.

As a next step the SHG technique was extended for SHG-optical rotatory dispersion (SHG-ORD) in order to study the chiroptical properties of a system. There, the angle between the linear polarization of the fundamental light and the polarization of the SH presents optical activity and relates to chiroptical properties. Its potential was proven in a study on the optical activity of enantiopure 1,1'-Bi-2-naphthol (BINOL) films as well as the orders of magnitude larger effects compared to the linear ORD.[68] It could also be concluded from a thickness series that the average orientation of the BINOL molecules change with thickness ranging from a dozen monolayers to thicker films. However, despite its strength SHG-ORD possesses one intrinsic drawback. The fact that SHG-ORD can also occur under nonresonant conditions makes an unambiguous assignment of the observed OA difficult.[55,91] However, this is of great importance in case of an asymmetrized heterogeneous catalyst if the question is weather the OA arises from the chiral modifier alone or if it arises from an induced OA.

Therefore, the SHG technique was extended for SHG-CD which also probes chiroptical properties. SHG-CD is, compared to SHG-ORD, resonant. Thus, it allows an ambiguous spectral assignment. It was shown how SHG-CD can be used to probe in situ the OA of thin films with submonolayer sensitivity, see Publication A. In this work, emphasis was also laid on a detailed description of the experimental aspects including all necessary calibrations which is given in the experimental chapter in Section 3.1 of this thesis. In the following, it is concentrated on the results and interpretation of this work.

For this study, enantiopure and racemic films of BINOL were prepared by means of evaporation onto glass substrates under HV conditions. The coverage was held at approx. $2 \cdot 10^{17}$ mol./cm^2 for the thicker films and at $8(2) \cdot 10^{13}$ mol./cm^2 for the study on low coverages. This corresponds to roughly 2000 ML and 0.4(1) ML which is well below one monolayer.[92] The samples were cooled to 0°C over the period of the experiment in order to suppress self-ordering effects. This has been observed at room temperature and yields additional isotropy effects on the observed OA which were studied in detail in a subsequent work, see Publication D. After the film preparation, the OA was then studied in situ by means of SHG-CD in transmission geometry in the wavelength range between 225 and 340 nm.

The first question is how to reference the measured anisotropy factor. In case of SHG-CD, this is not as trivial as for the linear CD. In the linear case, the sample can be modeled as a stack of films which are all contributing to the total absorption and CD. Consequently, the reference is a sample excluding just the optically active component of interest. Simply applying this approach suggests the pristine glass substrate without the molecular film as reference. But the generation of SH at this glass vacuum interface is not comparable to the SH generated at the glass molecular film and molecular film vacuum interface. Further, the contributions from all interfaces to the total SH signal are difficult to disentangle. Therefore, in case of the nonlinear technique SHG-CD a different approach has to be chosen. In this work, a molecular film of equal thickness and prepared under identical conditions but of racemic mixture is proposed as adequate reference. With that the number and character of interfaces between reference and sample are identical and the OA arising from individual molecules should cancel out in average. The anisotropy factor for such a racemic film of BINOL as reference is shown in top of Figure 25. The smoothed SHG-CD curve (green) and the marks for precise measurements at selected wavelengths are called spectrometer function and are used as reference. The referencing is carried out by a simple subtraction of the spectrometer function from the raw signal of a optically active sample.

The SHG-CD curves of the enantiopure thick films are shown in middle of Figure 25. In case of R-BINOL (red), the anisotropy factor shows a maximum of 178(2) % at 240 nm and is to our knowledge the highest 2nd order anisotropy factor measured so far in a non-plasmonic system. The maximum

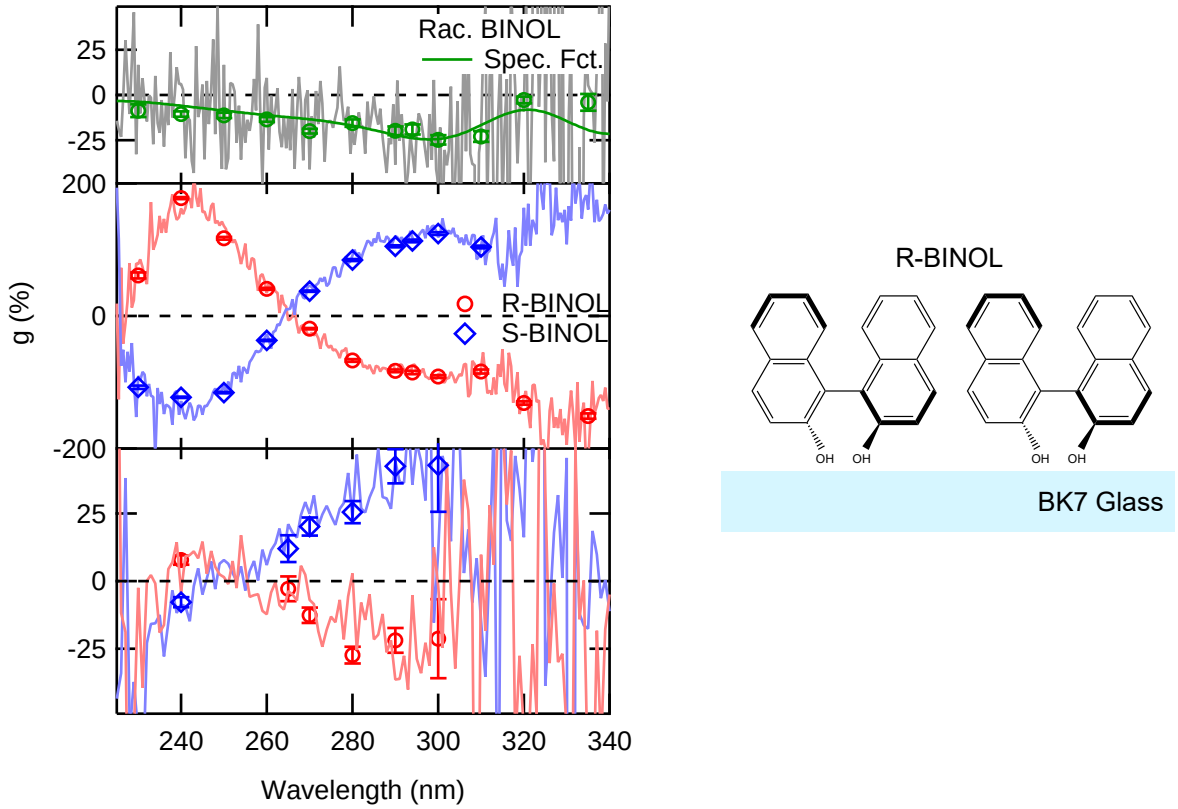

Figure 25 Left: g value for racemate (grey) and spectrometer function (top) and g value for R- (red) and S-BINOL (blue) of a film (middle) and 0.4(1) ML (bottom). Right: Molecular structure of R-/S-BINOL. (Adapted from Publication A)

lies in the region of the high energy band of BINOL which is at wavelengths of 240 nm and below. It originates from a symmetric and antisymmetric coupling between long-axis polarized ^1B_b transitions of 2-naphthol.[52,93,94] At 265 nm, there is a zero crossing and at higher wavelength the anisotropy factor remains negative with –67(2) % at 280 nm and –151(4) % at 335 nm. In this wavelength range, the signal originates from the middle and low energy band which lie between 260 and 300 nm and above 300 nm, respectively. The first is connected to symmetric and antisymmetric coupling between short-axis polarized ^1L_a and the latter between off-axis polarized ^1L_b transitions of 2-naphtol.[52,93,94] The anisotropy factor of S-BINOL (blue) shows the same curve but mirrored and as expected for the opposite enantiomer.

In order to test the sensitivity of the technique, the OA of a submonolayer coverage of 0.4(1) ML was measured, see bottom of Figure 25. The anisotropy factor in case of R-BINOL are 8(2) % and –27(3) % at 240 nm and 280 nm, respectively. A zero crossing lies at 255 nm. Again, S-BINOL shows a mirror behaviour. The anisotropy factor becomes noisy below 240 and above 300 nm because of a low SH intensity. Qualitatively, the anisotropy factors are similar between the thick film and the submonolayer coverage. Quantitatively, they show differences out of three possible reasons. First, in case of the submonolayer coverage, a part of the detected SH is generated at the uncovered and

achiral glass vacuum interface. The measured anisotropy factor is therefore an average over contributions from BINOL and pure glass. Second, the average orientation of the molecules change with film thickness which was already shown in the previous SHG-ORD study.[68] This is of relevance because SHG-CD is sensitive to the orientation of the addressed electric dipole transition moment and, thus, the spatial orientation of the molecule. Third, dipole-dipole interactions between molecules and layers could play a role, such as seen in the previous study, see Publication B. Unfortunately, the three effects cannot be disentangled based on this data.

Nevertheless, the work demonstrates the sensitivity and strength of SHG-CD and shows how the technique can be combined with an in situ UHV sample preparation and spectroscopy. This makes it a promising approach for studying the chiroptical properties of asymmetrized heterogenous model catalysts under controlled UHV conditions.

Optical Activity of Modified Surfaces of Enantiopure Allenes with SHG-CD

The newly implemented technique SHG-CD was employed in a subsequent work to study the chiroptical properties of a self-made and device-compatible functional material, see publication C. The chiroptical properties originate from a monolayer of self-assembled, enantiopure allenes bound to a gold film in a upstanding chiral architecture (UCA). The presented novel class of functional material is intended to be used as, for example, sensor for molecules. The so-called guest molecules would be detected and identified indirectly through a change in the chiroptical response when forming a complex with the chiral host and changing its conformation.[95,96] Particularly chiral spectroscopy techniques like CD are highly sensitive to conformational changes and, therefore, routinely used for the characterization of such complexes where at least one component is chiral.[97,98] In order to prove to chiroptical character of the functionalized surface, the samples were studied by means of SHG-CD. Also linear CD measurements were carried out on the same samples with a commercial J-815 CD spectrometer from JASCO which enables a direct comparison of the two techniques.

The enantiopure allenes were synthesized by the group of Josè Lorenzo Alonso-Gòmez from the university of Vigo and called (M)- and (P)-CF-2. After the synthesis, they were evaporated as film with several multilayers onto a thin gold film on top of a glass substrate. The nonlinear anisotropy factor was measured at 266 nm in transmission geometry for both enantiomeres and the bare substrate. Its linear counterpart was measured on the same samples between 240 and 355 nm, see Figure 26. In case of the enantiomer (M)-CF-2, a linear anisotropy factor of approx. 0.1 % was measured. The corresponding nonlinear anisotropy factor was with 9(1) % three orders of magnitudes larger. In both cases, the opposite enantiomer showed a mirrored behavior and the pure substrates a negligible optical activity. The films were then rinsed with ethanol. Ellipsometry, STM and N K-edge near-edge X-ray absorption fine structure (NEXAFS) data show that one monolayer of allenes remain

in an upstanding position. The molecules are strongly bound with their thiol group to the gold surface which makes the material robust and, thus, device-compatible. The linear anisotropy factor of these monolayers measured with the commercial CD spectrometer is zero and not distinguishable from the pure substrate. On the other hand the nonlinear anisotropy factor proofs the chiroptical activity of the monolayer and shows a value of 12(1) % in case of (M)-CF-2 and a mirrored behavior for the opposite enantiomer.

This work presents a promising novel class of chiroptical, device-compatible functional materials and simultaneously demonstrates the strength of SHG-CD. Especially, it proves the higher sensitivity of SHG-CD towards low coverages compared to linear CD.

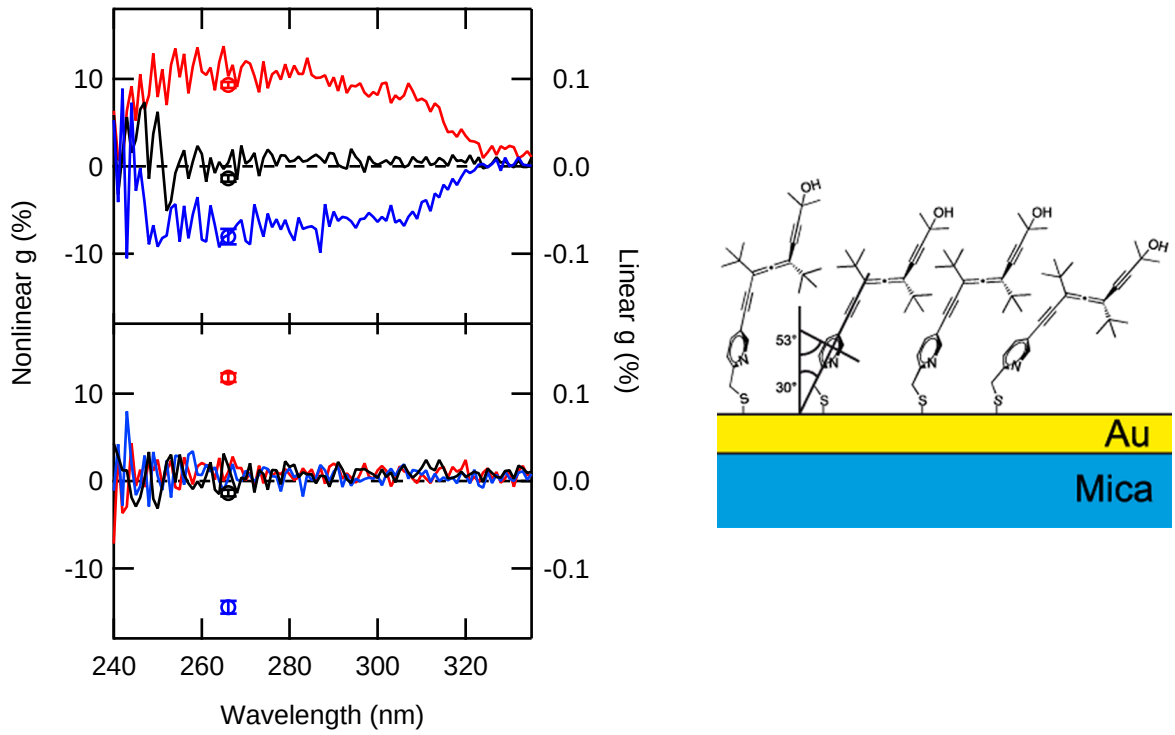

Figure 26 Left: Multilayer (top) and monolayer (bottom) CD (lines, right scales) and SHG-CD (marker, left scales) measurements of (M)-CF-2 (red) and (P)-CF-2 (blue) UCAs on custom-made transparent substrates (black). Right: Scheme showing the proposed, approximate orientation of (M)-CF-2 molecules in the upstanding monolayer architecture. (Adapted from Publication C)

4.2 Isotropy Effects in Chiroptical Activity

So far the work concentrated on the detection of OA of films and interfaces by means of the new implemented nonlinear technique SHG-CD. But as already mentioned, in the solid state, additional effects can contribute to the observed OA. These effects can, for example, arise from interactions between neighboring molecules or isotropy effects due to a long range order in the sample.[99–101] Thus, the observed OA is a superposition of such effects based on superstructures and long range orders and contributions from single elements in the sample like chiral molecules. This makes the interpretation of OA in solid state matter more challenging compared to the solution case. Vice versa information about the structure of a sample can be derived from its OA if their relation is understood. These effects were studied in case of the OA of enantiopure BINOL films measured with CD and SHG-CD, see Publication D.

For this purpose, enantiopure BINOL films were evaporated on glass substrates with a thickness of approx. 1.5 µm. CD measurements were carried out with a commercial CD spectrometer J-815 from JASCO between 300 and 500 nm. The measurements were taken in transmission geometry with the samples surface perpendicular to the light beam and in two possible arrangements. First, with the BINOL film facing the light source of the spectrometer which is referred to as “R/S-BINOL ▷ BK7”. Second, the sample is flipped and the BINOL film faces the detector which is referred to as “BK7 ▷ R/S-BINOL”, see Figure 27.

The BINOL films appear transparent immediately after the evaporation which is reflected in the absence of absorption and OA in the visible range. The low energy band of BINOL shows absorption and OA in the UV range till 360 nm. Both, absorption and CD are identical in either transmission direction. Thus, the absorption and OA is apart from a small Cotton effect at 337 nm comparable to the solution case, see Figure 42 in the appendix.

After some hours at room temperature, the sample changes its appearance as circular shaped whitish domains are growing. Raman measurements show a clear structural difference between the initial transparent film and the new formed domains. This proves that the film undergoes a structural transformation.[102] Further, comparison with Raman measurements on crystalline enantiopure BINOL suggest similarities with the new formed structure within the films. This structural transformation completes after some days and the whole film is covered with domains. A similarly prepared R-BINOL film on a silicon wafer was studied with a optical microscope under cross polarization and dark field conditions, see Figure 27. The picture shows domains of approx. 1 mm in diameter. Further, it shows that the domains posses a radial symmetry which is visible as lines beginning from each domains center. Therefore, the domain structure reminds of a pseudo-focal conic phase which is known from liquid crystals[103] where BINOL derivatives are commonly used as chiral dopant.[104]

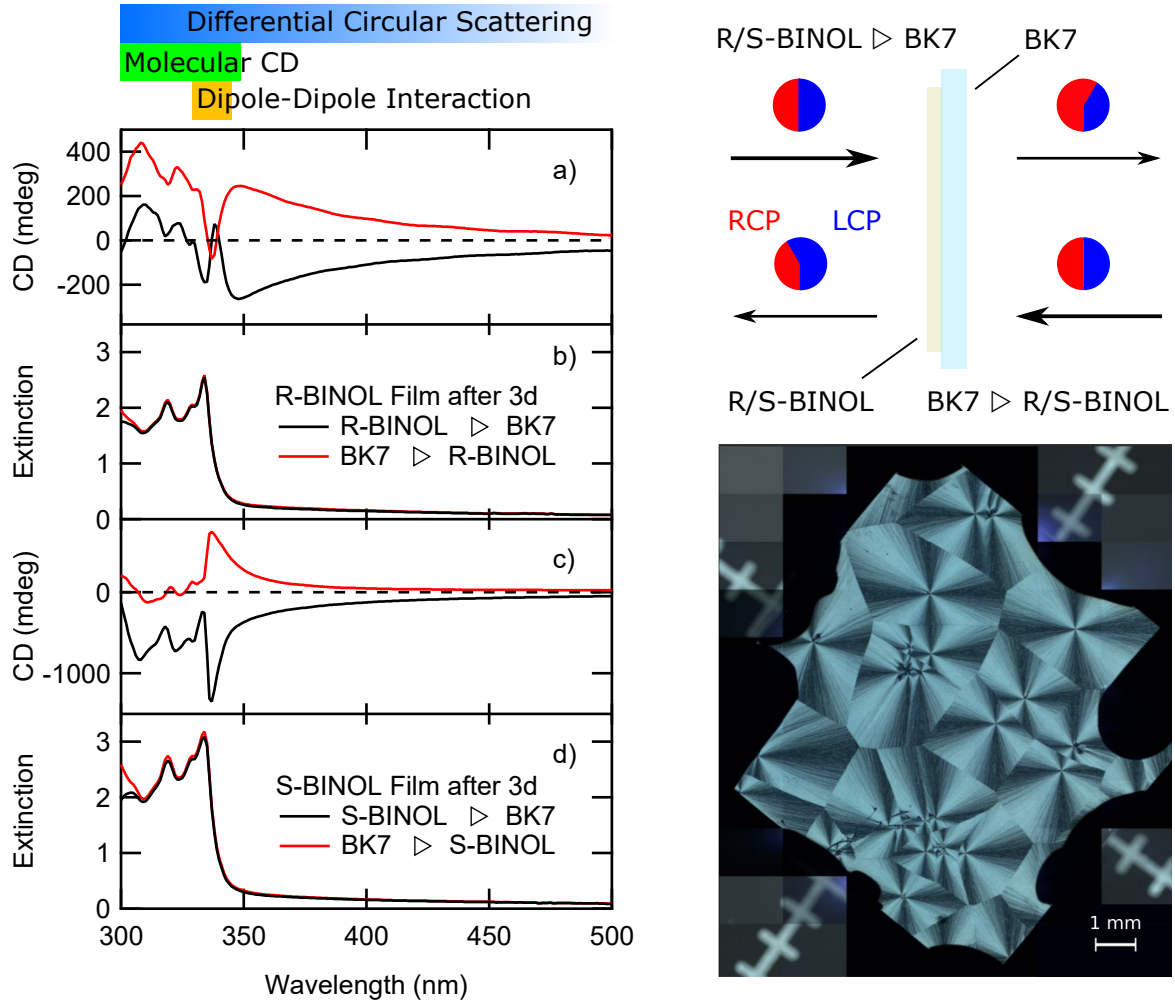

Figure 27 Left: CD (a) and extinction (b) spectrum for both propagation directions of R-BINOL film and S-BINOL (c),(d) 3 days after evaporation. The origins of the observed OA are stated on top and their wavelength regions given with arbitrary colors. Right: Scheme showing the proposed, approximate orientation of (M)-CF-2 molecules in the upstanding monolayer architecture. Right top: Experimental geometry including label for both light propagation direction configurations.Right bottom: Cross polarization picture of a R-BINOL film. (Adapted from Publication C)

These structural transformed films show now optically active extinction in the visible range where there was none before. Additionally, the OA in this region changes sign for the other transmission direction but is unaltered for the opposite enantiomer. The extinction can be assigned as Rayleigh scattering based on its power dependency of the order of 4 on the wavelength and comparison with additional absorption measurements in diffusive transmittance mode in a spectrophotometer, equipped with an Ulbricht sphere, where only absorption is detected. Consequently, the observed OA in the VIS region and part of the one in the UV region originates from circular differential scattering phenomenon which relates to the macroscopic structure of the film and not the individual molecule.[105] Also, the absorption of the low energy band shows a new peak at 328 nm and the CD spectrum a Cotton Effect at 340 nm. Futher, the Cotton effect is changing sign with transmission direction and enantiomer. A phenomena which is known as polarity reversal of ellipticity. In the course of the observed structural change, the molecules are reorientating in general and especially also towards each other. Accord-

ingly, it is proposed that the Cotton effect arises from dipole-dipole coupling between neighboring molecules. This has also been observed in, for example, vitrified liquid crystalline films of chiral polyflourene.[106] Thus, the overall observed OA of the films is a superposition of contributions from CD from the individual molecules, interactions between neighboring molecules and circular differential scattering from the macroscopic structure and isotropy of the film.

The effect of the apparent isotropy on the nonlinear anisotropy factor was studied on the enantiopure R-BINOL film, shown in Figure 28, together with the group of Ventsislav K. Valev from the university of Bath. Therefore, SHG-CD measurements were taken in reflection geometry at the wavelength of 400 nm while the sample was rotated around the surface normal. The laser path is depicted in Figure 28 with the propagation vector $\underline{k}$. During the rotation, the laser spot passes through four different domains. With that the propagation vector also changes its angle to the radial lines of the corresponding domain. Thereby, the related anisotropy factor is varying strongly, see Figure 28. For example in domain III between 50° and 220° it increases from approx. –100 % to 100 %. Keep in mind that the film is from enantiopure R-BINOL. Meanwhile, the propagation vector is changing from being antiparallel to parallel to the radial lines of the domain. This is explained by that the nonlinear anisotropy factor not only depends on the chiroptical property of the molecule but also on its orientation with respect to the propagation vector.[52] Therefore, it concludes that the molecules are aligned in chains, which are spreading in a radial manner from the center of each domain. This supports the previous suggestion of focal conic domains.[107,108]

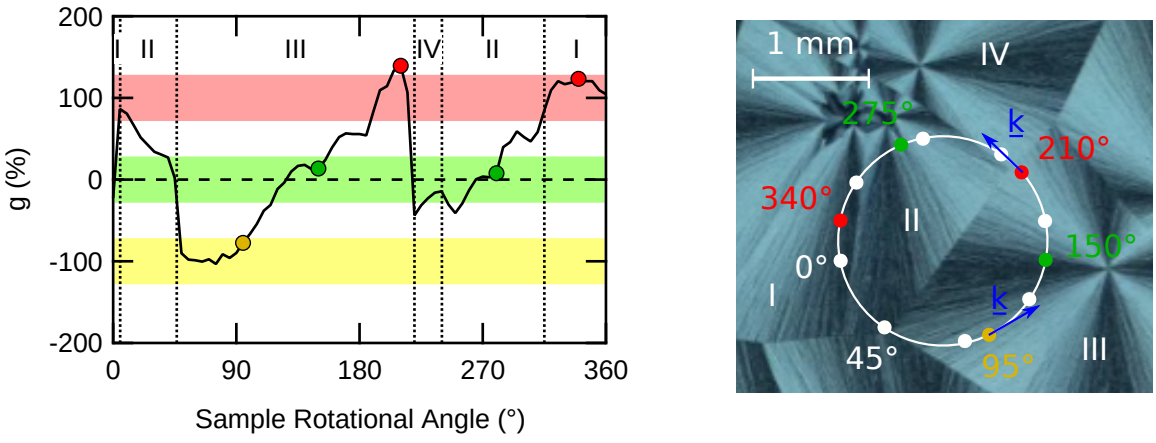

Figure 28 Left: Second order anisotropy factor at 400 nm SH for R-BINOL film at according sample rotational angle. The colored markers refer to positions in the right graph. Right: Cross polarization picture of a R-BINOL film with the laser beam path during anisotropy factor measurements while the sample rotates around surface normal. (Adapted from Publication D)

The findings present how additional effects in solid state matter can influence the observed OA. Thus, the interpretation is more complex than in the solution case. But on the other hand, the work also depicts how additional structural information can be derived from the OA.

However, more work has to be done to fully understand the observed effects like the circular dif-

ferential scattering and in particular the polarity reversal of ellipticity. Experimentally, a study on a comparable isotropic system but different chiral molecule will deliver more data and could yield additional insight. Also, a theoretical description of the film would be interesting in this regard. The model would need to connect a theoretical rotational strength with an average orientation of the transition moments in the film. Additionally, it should include a possible coupling of transition moments from neighboring molecules.

5 Induced Nonlinear Chiroptical Activity of Silver Surface by Chiral Modifier

As already mentioned in the motivation, the final goal is to understand the origin of the enantioselectivity of asymmetrized heterogeneous catalysts.[19–22] In particular the asymmetrization of the catalyst by a chiral modifier itself and their interaction is of great interest. Although the mechanism is generally not known, some possible processes have been suggested.[28–31]

Well-known examples of asymmetrized heterogeneous catalysts are Ni, Cu and Co surfaces which are modified by enantiopure tartaric acid. The catalysts shows a enantioselectivity towards the hydrogenation of β-keto esters.[24,25] These model systems were prepared under UHV conditions with coverages well below one monolayer. Both were essential key points to these studies carried out in situ with UHV compatible techniques like reflection absorption infrared spectroscopy, low-energy electron diffraction, thermal desorption spectroscopy and scanning tunneling microscopy.[109] But so far no optical method was used on such enantioselective, heterogeneous model catalysts to provide further insight into the chirality of such systems. In the following, it will be shown how the nonlinear optical method SHG-CD can be applied for this purpose.

As a prove-of-principle, the OA of a silver surface with different enantiopure adsorbates like BINOL, cysteine and tartaric acid was studied. Further, induced OA in the pristine non-optically active response of the silver SP will be shown where the chiral adsorbate does not posses any transitions. Note that the linear ICD is known to be highly sensitive to the interaction between modifier and achiral component.[32–34] Therefore, it holds the very information which will be of interest to comprehend the asymmetrization of a heterogeneous catalyst by a chiral modifier.

Optical Response of Pristine Silver Surface

A polished polycrystalline silver plate was cleaned by means of Ar^+ sputtering. Then, the SHG-CD measurements were carried out in reflection geometry between 300 and 340 nm and the anisotropy factor was measured with more precision at these limits. An exemplary SHG spectra from both CPs is shown in Figure 29. The spectrum was corrected by simple division by the spectrum from a SiO_2 surface of a Si waver which was measured under identical conditions, see Figure 43 in the appendix. The underlying idea is the same as discussed in the experimental. The spectrum of the SiO_2 surface possesses no characteristic transitions. Therefore, all observed features are related to the setup and the curve can be taken as spectrometer function. The SHG spectra of the sputtered silver surface shows a single peak. A fit with a Gaussian function returns a peak position of 332.9(1) nm and a standard deviation of 8.7(1) nm. The energy calculates to 3.72(9) eV and implies that the observed

peak is connected to a plasmon mode. The question rises whether the plasmon mode is a VP or a SP. Early experiments have shown that the generation of SH through the interaction with the VP mode in silver are unlikely.[110] This is because the inversion symmetry of the VP forbids SHG. Therefore, the observed SH is generated through interaction with the SP which is enhanced through the high surface roughness of the mechanical polished and sputtered surface.[59] This is further supported by the good matching with reported SP energies in case of bulk material of 3.68 eV[57] and in case of films of 3.67 eV.[111] The SP intensity shows sensitivity towards residual gas molecules in the transfer chamber when stored there for 5 min, see Figure 44 in the appendix. It is suggested that water leads to oxidation of the surface and additional advantegeous carbon species to a further damping, see Figure 45 in the appendix. In order to minimize these effects, the transfer chamber was baked and a change of the plasmon intensity was not observed anymore in a subsequent experiment, see Figure 46 in the appendix. Additionally, the depositions times of the chiral molecules were kept as small as possible and generally well below 1 min. The sensitivity of the signal upon surface modifications also supports the observation of the SP and not the VP.

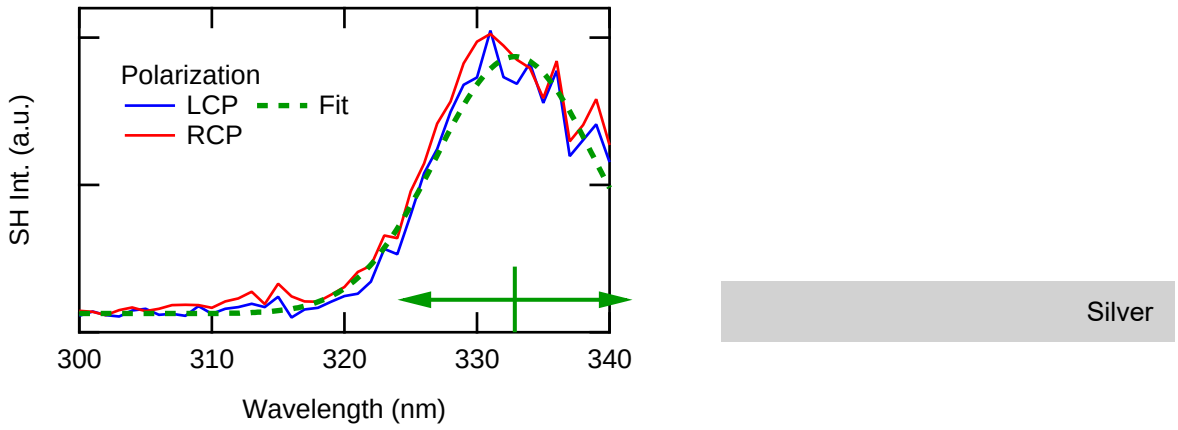

Figure 29 Left: SH spectra from CPs of sputtered silver surface and fit of SH curve from LCP. Right: Sketch of studied system.

Interaction with BINOL

Now, the effect of a chiral adsorbate on the optical response of the silver SP was studied. Therefore, enantiopure BINOL was deposited with subsequent increasing coverage onto the silver surface and SHG spectra were taken at each step, see Figure 46 in the appendix. The plasmon peak position as well as the width were determined in an identical manner as discussed for the pure silver surface and averaged for both enantiomers. Both peak position and width are plotted as a function of the coverage of BINOL which is shown in Figure 30. The plasmon red shifts upon the first monolayer by approx. 0.6 nm. A subsequent deposition yields a further but less strong red shift to a peak position

at 334.8(4) nm in case of 50 ML, which corresponds to an overall shift of approx. 21 meV to smaller energies. Meanwhile, the width does not change during the first monolayers and increases little for high coverages of 50 ML (calculated from $8.7 \cdot 10^{15}$ mol./cm^2 [92]) but not significantly. This indicates that two different processes are responsible for the red shift. It is proposed that the first monolayer physisorbes to the silver surface and oxidizes the surface. Thus, free conduction electrons of the silver are localized around the bonds to the adsorbates and, consequently, their density is decreased. The following layers of BINOL do not interact with the silver surface directly but instead increase the dielectric function of its surrounding. Both effects result in a red shift of the plasmon which is also predicted by the Drude model (see Equation 8). Thus, the deposition of BINOL cannot only be detected through its caused shift of the silver SP but also yields information about the coverage.

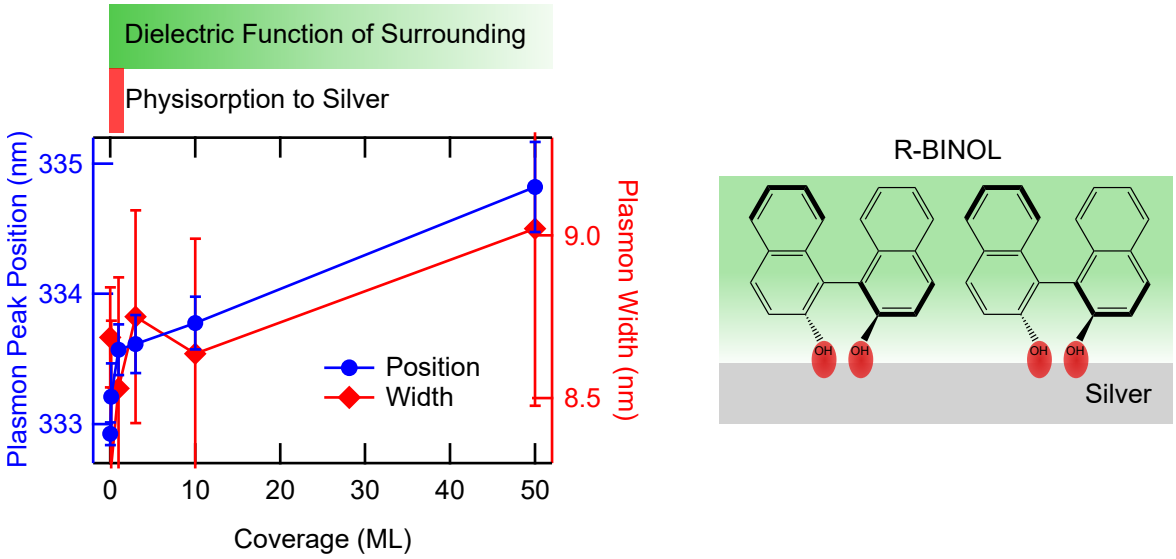

Figure 30 Left: Plasmon position and width of a silver surface with different coverages of enantiopure BINOL. Right: Sketch of studied system.

Anisotropy factors which were measured with a higher precision for each coverage are shown in Figure 31. Note that they were corrected by simple subtraction from the ones taken from the pure silver surface at the beginning of each experiment.

For a small coverage of 0.1 ML, the measured anisotropy factor is zero and no OA is observed. For higher coverages the anisotropy factor at 300 nm is negative in case of R-BINOL and with –15(1) % comparable to pure R-BINOL on glass, see Publication A. The anisotropy factor at 340 nm is nonzero and positive for coverages higher than 10 ML. As expected, S-BINOL shows mirror behavior. This is in strong contrast to the findings for SHG-CD on pure BINOL on glass and for linear CD in solution (see Figure 42 in the appendix) where the anisotropy factors posses the same sign for both wavelengths. There are two possible explanations. First, the BINOL molecules stack differently on glass and silver and, therefore, the average orientation of the transition dipole moments are different for both cases. This would lead to a different observed anisotropy factor. But since it is assumed that the first mono-

layer adsorbes in an upstanding geometry on both surfaces with its OH groups pointing toward the surfaces, this seems unlikely. Second, the measured OA at 300 nm is the one of pure BINOL. On the other hand, the one at 340 nm is a superposition of the former and an induced OA into the plasmon at this wavelength. As discussed before BINOL in consecutive layers are not in direct contact with the silver surface anymore. In this case, the suggested induced OA would originate from a field effect, also called chiral polarization, as seen for gold surfaces before.[31]

Nevertheless, a clear difference in the OA is observed between enantiopure BINOL on glass and on a silver surface. Thus, the interaction between the silver substrate and the chiral adsorbate or modifier is visible in the OA of the system. Also, the findings show that the anisotropy factor shows much larger effects upon the adsorption of enantiopure molecules than the plasmon peak position. Therefore, SHG-CD seems more sensitive towards sensing of adsorbates and presents a promising alternative to the monitoring of the peak position of the plasmon.

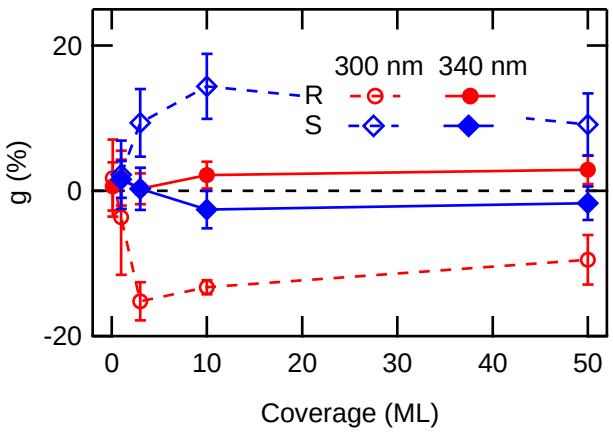

Figure 31 Anisotropy factor of a silver surface with different coverages of R- and S-BINOL.

Interaction with Cysteine

In another experiment, enantiopure cysteine was deposited for different deposition times on the silver surface, see Figure 47 in the appendix. The plasmon peak red shifts rapidly in the first 40 s for approx. 2.8 nm, whereas, the width does not change significantly. It red shifts further for longer deposition times but more slowly up to 337.1(12) nm after 600 s, which corresponds to an overall shift of approx. 46 meV to smaller energies. The width simultaneously increases from 8.7(1) nm to 19.9(19) nm. The interpretation is analog to the case of BINOL. During the first phase, cysteine adsorbes directly to the silver surface, whereas, consecutive layers increase the dielectric function of its surrounding. Both lead to a red shift of the plasmon (see Equation 8). Note that the shift due to the direct adsorption is more than four times bigger than in case of BINOL. This can be explained by the fact that cysteine, like thiols in general, chemisorb to a silver surface, if they impinge from the

gas phase.[112–114] A covalent bond between the sulfur atom and the metal surface is formed under dissociation of the SH bond of the thiol. BINOL in contrast is assumed to physisorb to the surface and, therefore, is less tightly bond and causes a smaller red shift of the plasmon.

Consequently, the shift of the plasmon also holds information about the nature of the interaction between the metal and the adsorbate and here chiral modifier.

The fact that the width remains constant under chemisorption of the first monolayer but increases with increasing dielectric function of the surrounding suggests a causality. In contrast, studies on silver clusters showed a significant chemical interface damping of their plasmon already upon chemisorption of the first monolayer of thiol-ligands, see Publication F. This proves that the predominant damping mechanism is different for both systems.

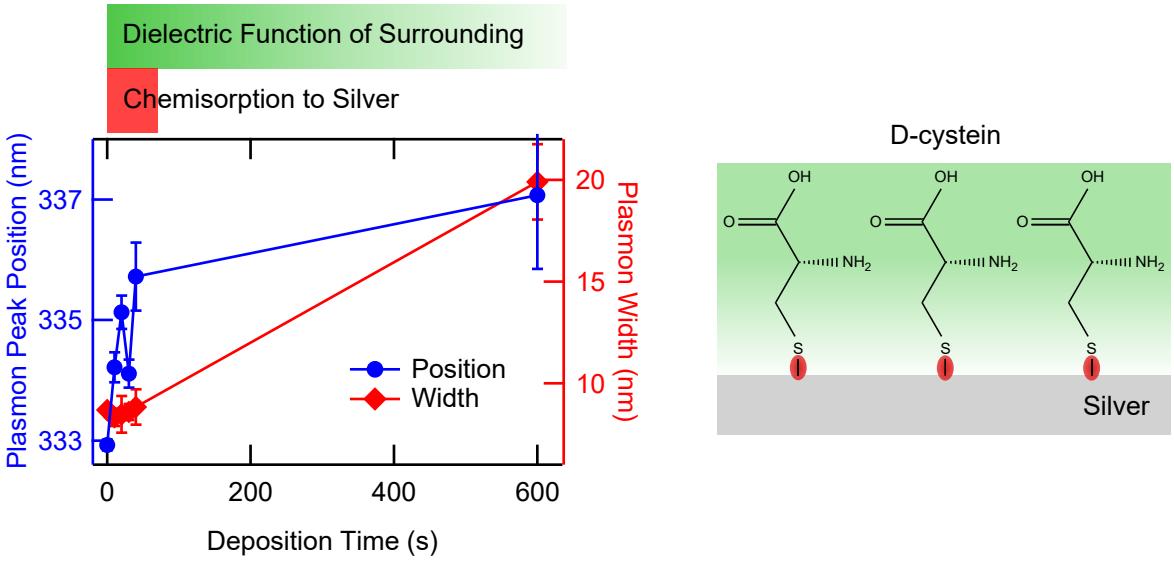

Figure 32 Left: Plasmon position and width of a silver surface with different coverages of enantiopure cysteine. Right: Sketch of studied system.

The anisotropy factors at 300 and 340 nm are both positive or negative in case of D- or L-cysteine respectively and shown in Figure 33. Note that cysteine possesses no optical transitions in this wavelength range, see Figure 48 in the appendix. Therefore, the observed OA cannot originate from the cysteine but is unambiguously induced and brought by the cysteine as chiral modifier. To our knowledge, this is the first time an induced OA is observed in SHG-CD and is called SHG-ICD here. In linear ICD, two possible mechanism could explain the findings. First, the bonding between the chiral modifier and the surface leads to a chiral rearrangement of surface atoms. This effect is called chiral footprint and likely considering the strong chemisorption between cysteine and silver. Second, the cysteine induces optical activity via a field effect. This seems counterintuitive considering that the SHG-ICD does not further increase for longer deposition times. Further, it confirms that only the first monolayer, which chemisorbes to the surface, contribute to the SHG-ICD. It is suggested to measure the anisotropy factor for additional wavelengths in the range of the SP. The shape of curve of the

anisotropy factor could reveal more information on the apparent SHG-ICD mechanism.

The work illustrates how chirality transfer and asymmetrization by enantiopure cysteine, as chiral modifier, into silver, as possible heterogeneous catalyst, can be studied by means of SHG-CD.

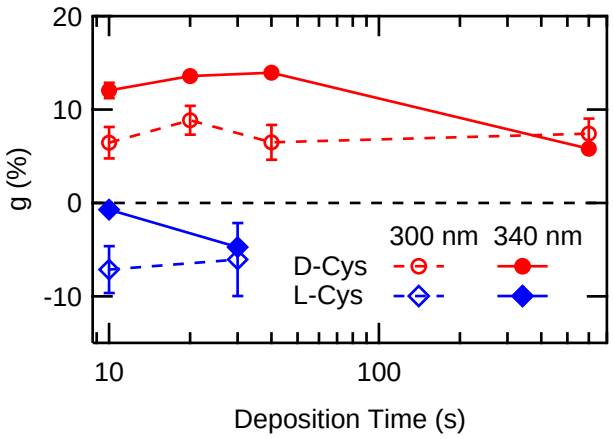

Figure 33 Anisotropy factor of a silver surface for different deposition times of D- and L-cysteine.

Interaction with Tartaric Acid

Tartaric acid was also studied here because of its above-mentioned prominent role as chiral modifier. In an identical manner as in case for BINOL, enantiopure L- and D-tartaric acid or also called (2R,3R)- and (2S,3S)-tartaric acid were deposited on a pristine silver surface with different coverages. The effect on the plasmon peak position and its width are shown in Figure 34. For small coverages of a few layers the plasmon shifts rapidly blue. Based on interpolation the blue shift for the first monolayer is approx. 0.7 nm. Meanwhile, the width stays constant. With subsequent layers the plasmon shifts further blue till 329.9(2) nm in case of a coverage of 50 ML (calculated from $5.6 \cdot 10^{16}$ mol./cm^2 [115]), which corresponds to an overall shift of approx. 34 meV to higher energies. Simultaneously, the width increases significantly.

The observed blue shift of the silver SP is very unexpected. It implies an increase in the density of the conduction electrons and a reduction of the surface upon the adsorption of the first monolayer of tartaric acid (see Equation 8). Also the subsequent blue shift caused by multilayers is inconsistent with the proposed model above. As explained, the multilayers cause an increase of the surrounding dielectric function of the silver plasmon and would theoretically yield a red shift, too. Therefore, the observed blue shift upon adsorption of tartaric acid cannot be explained by this model.

Interestingly, it was shown that tartaric acid adsorbes to a Ni(110) with each carboxylate functionality with its O atoms. The chiral OH groups on the other hand show a repulsive interaction with the metal atoms. This leads to a highly strained adsorption motive and a relaxation of the metal atoms and is called chiral footprint.[51] With that the distances between Ni surface atoms change. Further, it was

shown that the silver SP depends on the crystalline face. Thus, it is possible that the relaxation of the surface due to the adsorption of tartaric acid has an effect on the plasmon energy.
However, the behavior of a rapid shift caused by the first adsorbed monolayer and a subsequent slower shift including an increase in width is similar to the studied cases with BINOL and cysteine. This suggests that the observed plasmon blue shift is here as well caused by two separate mechanism but which are unknown at this point.

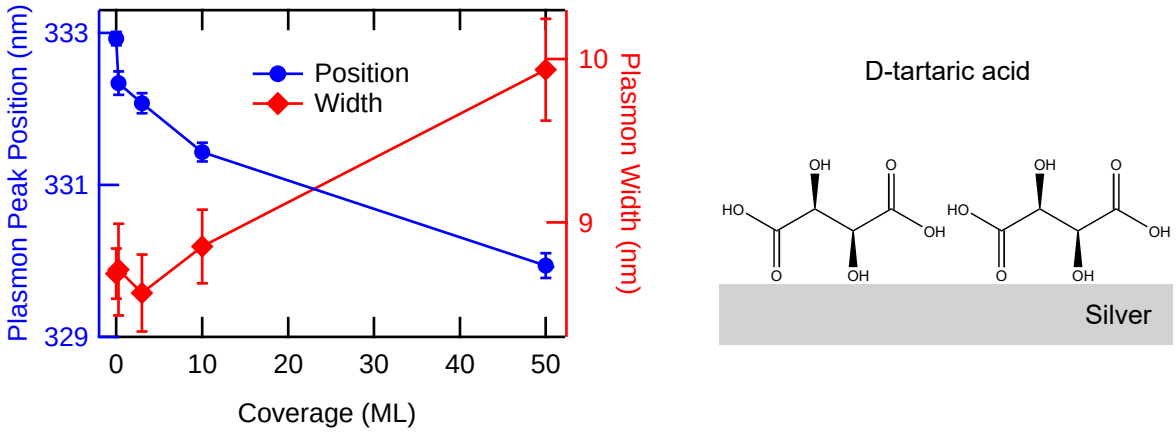

Figure 34 Left: Plasmon position and width of a silver surface with different coverages of enantiopure tartaric acid. Right: Sketch of studied system.

The anisotropy factor for the different coverages of enantiopure tartaric acid is shown in Figure 35. For coverages below 10 ML, the anisotropy factor is close to zero and no OA is apparent. For higher coverages, the anisotropy factor is significantly positive at 300 and negative at 340 nm in case of D-tartaric acid. It increases or respectively decreases even further for higher coverages of 50 ML. Note that tartaric acid possesses no optical transitions in that wavelength region, see Figure 50. Thus, analog to the case of cysteine the observed OA is induced by the tartaric acid into the silver SP. The fact that the induced OA develops for higher coverages suggests that it is brought by a field effect, as suggested for BINOL. The opposite sign of the anisotropy factor at the two wavelengths of 300 and 340 nm hints that its curve undergoes a Cotton effect in the vicinity of the silver plasmon peak.
Surprisingly, the anisotropy factor of the opposite enantiomer possesses the same sign. Studies on tartaric acid adsorbed on Cu(110) revealed the it can undergo an adsorption-induced chiral organization which was studied by means of scanning tunneling microscopy. This results in a global chirality which can stretch over the entire surface and visible in the low-energy electron diffraction pattern.[116] Consequently, the observed OA could be influenced by isotropy effects as already demonstrated for BINOL, see Publication D. In order to test this theory, it is proposed to study the anisotropy factor of the tartaric acid itself. It is particularly of interest if isotropy effects occur as seen for BINOL in Publication D. In a next step, the experiment could be repeated on a Ag(110) single crystal in combination with low-energy electron diffraction. But note that both copper and silver indeed possess a

face-centered cubic crystal structure but different lattice constants. Therefore, it is not certain that the chiral footprint is comparable for silver.

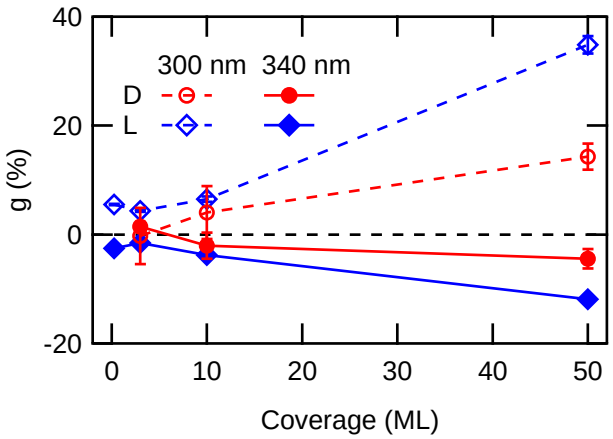

Figure 35 Anisotropy factor of a silver surface with different coverages of D- and L-tartaric acid.

In conclusion it was demonstrated how the adsorption of a chiral molecules onto a silver surface can be sensed and quantified by its effect on the silver SP. For the first time, an induced OA in the signal of the SP could be observed by means of SHG-CD. This illustrates how SHG-CD can be facilitated to study the asymmetrization of heterogeneous catalysts by chiral modifiers.

6 Effect of Achiral & Chiral Modifier on Optical Properties of Coinage Metal Clusters

In the previous section, the interaction of chiral molecules with a silver surface was studied. The silver surface presented the potential catalyst in this system which is aimed to be asymmetrized. But the vast majority of heterogeneous catalysts, which are used in our daily life, come in form of nanoparticles with sizes of a few nanometer. Often they are additionally embedded and stabilized in a matrix which further complicates the system. Consequently, UHV studies on them with common techniques are very arduous. However, the efforts to understand the mechanism of such catalyst and to be able to explain their performance is justified. Particularly, considering that the alternative modus operandi of "cook and look" is costly and inefficient.

Following this argumentation, our group demonstrated in a proof-of-principle work that functionalized Pt nanoparticles can also perform as asymmetric catalysts. In this case, the asymmetrization was brought by enantiopure cysteine bonding to the particles surface and yielding an ee in the hydrogenation of 2-butanone.[23] Recently, such an asymmetrization was studied with optical spectroscopy by means of CD for silver nanoparticles, see Publication E. The dendritic nanoparticles were synthesized in a one-step reduction mediated by thiol-containing biomolecules. A strong induced CD into the optical transitions of the silver proofed a highly efficient transfer of chirality from the chiral modifier to the nanoparticle. The involved mechanism was explained as combination of chiral polarization and chiral footprint. Both studies illustrate a route to synthesize heterogeneous asymmetric catalysts and to study their asymmetrization in order to elucidate their enantioselectivity.

Studying catalysts for the oxidation of carbon monoxide, Haruta et al. found that the most catalytically active species were not nanoparticles but particles even smaller in size.[117] These particles ranging from some atoms up to a few dozen are called cluster. Shortly afterwards, many research groups started studying them with the main focus on their catalytic properties. For most studies, the clusters are prepared under controlled UHV conditions and the experiments carried out in situ. Therefore, the studied systems can be seen as simplified model systems which are used to understand the mechanisms in common catalysts or to even explore entirely new ones. It revealed that their properties change drastic and nonscalable with their size which concluded to the statement "Each atom counts.".[118] Often the characteristic catalytic behavior is explained by the electronic structure, see Publication H.

In our group, we focus on the study of optical properties of metal clusters which holds, among others, this very same information about their electronic structure.[63,82] Recently, the plasmonic behavior of

size-selected silver clusters could be probed by means of SHG.[61] It revealed that the plasmon resonance blue shifts by about 0.2 eV with decreasing size from Ag_{55} to Ag_9. The general trend was superimposed by a nonscalable size-dependence which is known from many catalytic studies. This demonstrates the potential of SHG to bring further insight into the catalytic behavior of clusters.
As a next step, the effects of different adsorbates on the optical response of metal clusters were investigated and are discussed in the following. Particularly, the interaction with chiral molecules was of interest in the background of a possible asymmetrization of such clusters as heterogeneous catalysts.

Probing Interaction of Silver Clusters and Thiol-Ligands with s-CRD

In a first study the plasmonic resonance of size-selected silver clusters was monitored in situ by means of s-CRD while the cluster were exposed to thiol-ligands, see Publication F. Therefore, size-selected silver clusters were deposited on previous Ar^+ sputtered glass substrates. The coverage was kept well below $6 \cdot 10^{12}$ cluster/cm^2. This corresponds to a sub-monolayer coverage[63] and avoided agglomeration and proximity effects.[61] An extinction spectrum was then taken from the bare supported clusters. It can be concluded from a previous study that the observed peak around 3.20 eV (approx. 387 nm) originates from the LSP resonance oriented parallel to the substrate surface.[63] Afterwards, the cluster were alternately exposed to thiol-containing molecules like benzenethiol via background dosing in the transfer chamber and successive extinction spectra were acquired. The derived plasmon peak energy as a function of dosage in Langmuir is given in Figure 36. The peak energy rapidly decreases first which is equivalent to a red shift. After this initial phase, it further decreases but less pronounced to around 2.92 eV (approx. 425 nm) in case of Ag_{20}. A comparison to benzene, which does not possess a thiol group, reveals that the initial rapid red shift of about 0.1 eV can be attributed to a chemisorption of the first monolayer. The successive red shift of approx. 0.2 eV comes from additional physisorbed layers via an increased dielectric constant of the surrounding medium. The width of the plasmon peak is simultaneously increasing from the first dosage on and is caused by chemical interface damping.[64,65] This behavior is different than in case of the polycrystalline silver surface where an increasing width was only observed for the subsequent multilayers of adsorbates. This suggests that different damping mechanism are predominant for both systems. In case of the clusters, also additional size effects become obvious for the initial plasmon energies and their shifts if one compare the shown traces for size-selected Ag_{20}, Ag_{55} and the unselected Ag_x. This is explained by the already stated size-dependent plasmon energy and a difference in surface to volume ratio as well as the perturbation of the local electromagnetic field around metal clusters.
In conclusion, the plasmon shows a characteristic response in form of a two-fold red shift upon adsorption of thiol-ligands. This is similar to the case of the polycrystalline silver surface and cysteine

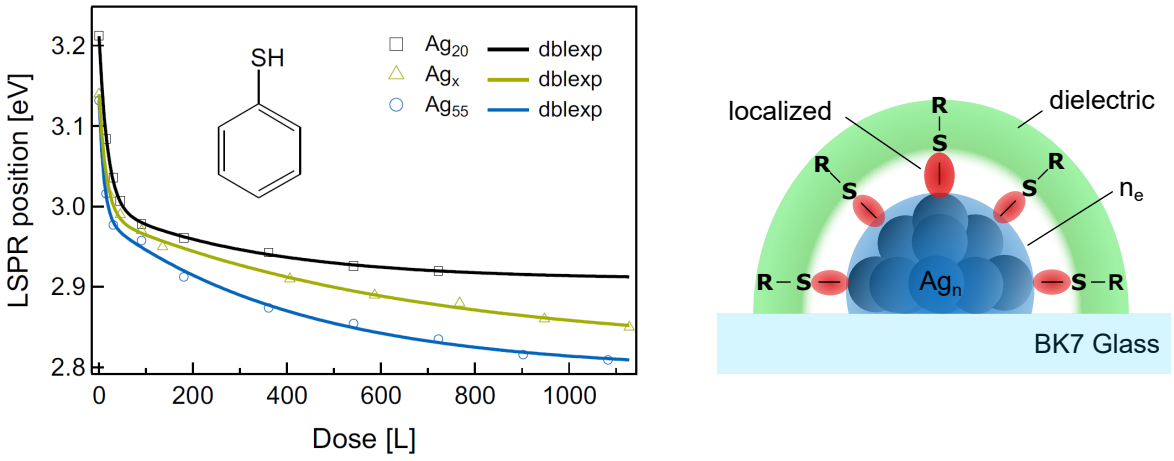

Figure 36 Left: Plasmon position of silver clusters as a function of dosage of benzenethiol. Right: Sketch of studied system. (Adapted from Publication F)

and demonstrates the high sensitivity of their optical response on their chemical state and surrounding.

Probing Interaction of Silver Clusters and Chiral Modifier with SHG

In a next step, the previous demonstrated sensitivity of clusters for adsorbates and their surrounding is used to try to transfer chirality into the clusters. This is done by interaction with enantiopure chiral molecules as modifiers. Meanwhile, the optical response of the LSP is monitored by means of SHG-CD.

Therefore, silver clusters were deposited on previous Ar^+ sputtered BK7 glass substrates. The coverage was with approx. $5 \cdot 10^{13}$ cluster/cm^2 set high to gain more signal. Their mass was not selected prior to the deposition and the size distribution was centered at around 26 atoms, see Figure 51 in the appendix. An exemplary SHG spectra from both CPs is shown in Figure 37 a). The LSP resonance is visible as peak at around 327(1) nm. As expected, it lies at smaller wavelength and corresponding higher energy than the SP of the polycrystalline silver surface.

This peak vanishes if 1.0(5) ML of L-cysteine or 2(1) ML of R-BINOL is evaporated on the silver clusters as shown in Figure 37 b) and c), respectively. Therefore, the interaction with the chiral modifier led to a complete attenuation of the plasmon response in the SHG signal. This is explained by a reduction of the second order polarizability under chemi- and physisorption of the adsorbates and is confirmed by comparable studies in previous works with different thiol containing and non-containing molecules.[119] A comparison to the polycrystalline silver surface prevails that this attenuation is much stronger in case of the silver clusters. Unfortunately, the observed attenuation mechanism caused by adsorbates makes it impossible to observe a chirality transfer based on an induced OA into the plasmon response.

Alternatively, silver clusters were deposited on films of R-BINOL with varying thicknesses of 11(1) ML,

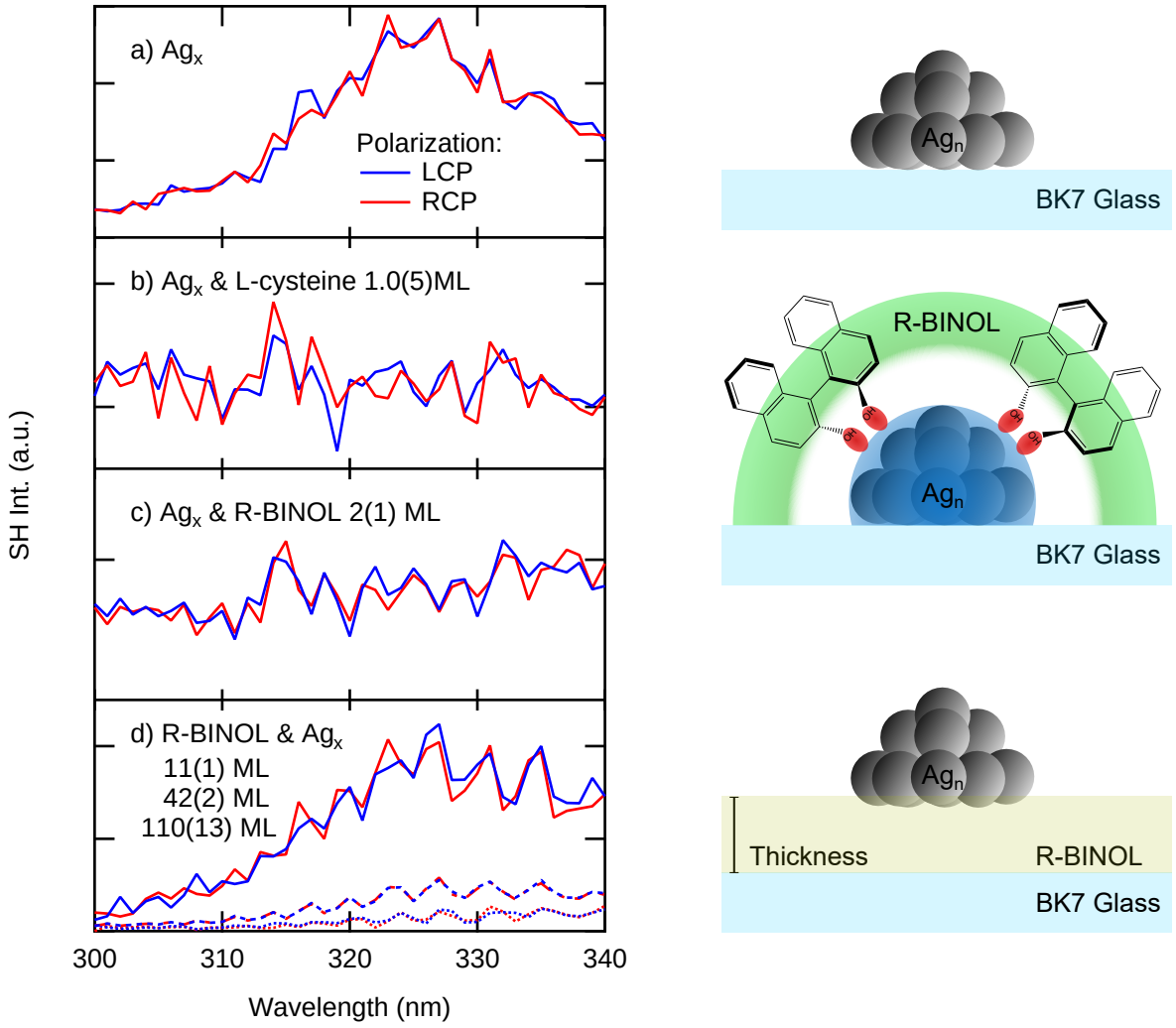

Figure 37 Left: SH spectra from CPs of pristine silver clusters (a) and with L-cysteine (b) and R-BINOL as adsorbates and silver clusters on films of R-BINOL with different thicknesses (c). Right: Sketches of studied systems.

42(2) ML and 110(13) ML. The corresponding SH spectra are given in Figure 37 d). The SH spectra of both CPs in case of a film thickness of 11(1) ML shows a peak at around 329(1) nm. Therefore, the plasmon of the silver clusters is still present but compared to the bare clusters aprrox. five times weaker. Also a small red shift is apparent, possibly due to the higher dielectric function of the surrounding. With increasing film thickness of 42(2) ML and 110(13) ML the intensity of the plasmon further decreases and red shifts to 331(1) and 339(5) nm, respectively. Unfortunately, the anisotropy factor was not measured with high accuracy and, thus, no reliable evaluation on the OA can be done. Nevertheless, the finding proof that the LSP resonance of the clusters can be detected in the vicinity of chiral modifier if the clusters are deposited on top of them. Therefore, this is a promising approach for future studies. However, the impact of the neutralizing slow electrons during the deposition of the cationic clusters on the molecular film has to be investigated in any case. Thereby it should be

proofed that the film still holds chiral information that can be transferred into the cluster.

Because the vicinity of molecules to the cluster led in any case to a damping of the plasmon, an alternative approach is suggested here, too. Instead of molecules as chiral modifier one could think of an inherent chiral substrate on which the clusters are deposited. For example, the group of P. Fischer fabricates such substrates by shadow-growth or glancing-angle deposition.[120] During the process SiO_2 was evaporated in a steep angle onto the here used BK7 substrates while the substrate was constantly rotating and resulting in a deposition with chiral character. This approach holds also the advantage that the clusters would be lying "naked" on the substrate and, thus, would be fully accessible for catalytic reaction.

Probing Interaction of Gold Clusters and Chiral Modifier with SHG

A comparable study was also carried out with gold clusters. This was done in order to check, whether the strong attenuation of the SH signal is universal for clusters or characteristic for silver. The coverage of the gold clusters was with approx. $4 \cdot 10^{14}$ cluster/cm^2 set high to gain more signal and to be able to study them ex situ with a conventional UV-VIS spectrometer. Their size distribution is centered around 18 atoms, see Figure 52 in the appendix. Exemplary SH spectra from both CPs are shown in Figure 38 a) and a peak at approx. 273 nm is apparent.

In a consecutive step, approx. 10 ML of R-BINOL were evaporated on the gold clusters and SH spectra were recorded, see Figure 38 b). The previous observed peak is still visible and no change in intensity or position is observed. Then, the sample was taken out of the UHV and an absorption spectrum was acquired with a conventional UV-VIS spectrometer, see Figure 38 c). The absorption spectrum shows a peak at 559 nm which corresponds to the gold LSP. It is suggested that the peak in the SH spectra also originates from the plasmon but lies in resonance with the fundamental, see Figure 4. No SH signal was observed for wavelengths around 1100 nm. It is suspected that the laser intensity is not high enough in the infrared region to generate sufficient SH. Thus, the peak position derived from the SH spectra is then 546 nm. This is significantly lower compared to the absorption spectrum. An explanation could be a further red shift of the plasmon due to an oxidation of the clusters on air but this remains speculative at this moment.

Evaporation of approx. 50 ML of L-cysteine on gold clusters leads to SH spectra given in 38 d). The same peak is visible and a difference in SH intensity generated from both CPs between 500 and 600 nm suggest OA in the range of the LSP. Note that cysteine itself possesses no optical transitions in this wavelength range which implies an induced OA. However, the anisotropy factors were not measured with high accuracy and before drawing a final conclusions, these experiments must be repeated. The absorption spectrum of the same sample shows a peak at 581 nm. This is 22 nm red shifted compared to the sample with R-BINOL and could be explained by the stronger binding of the

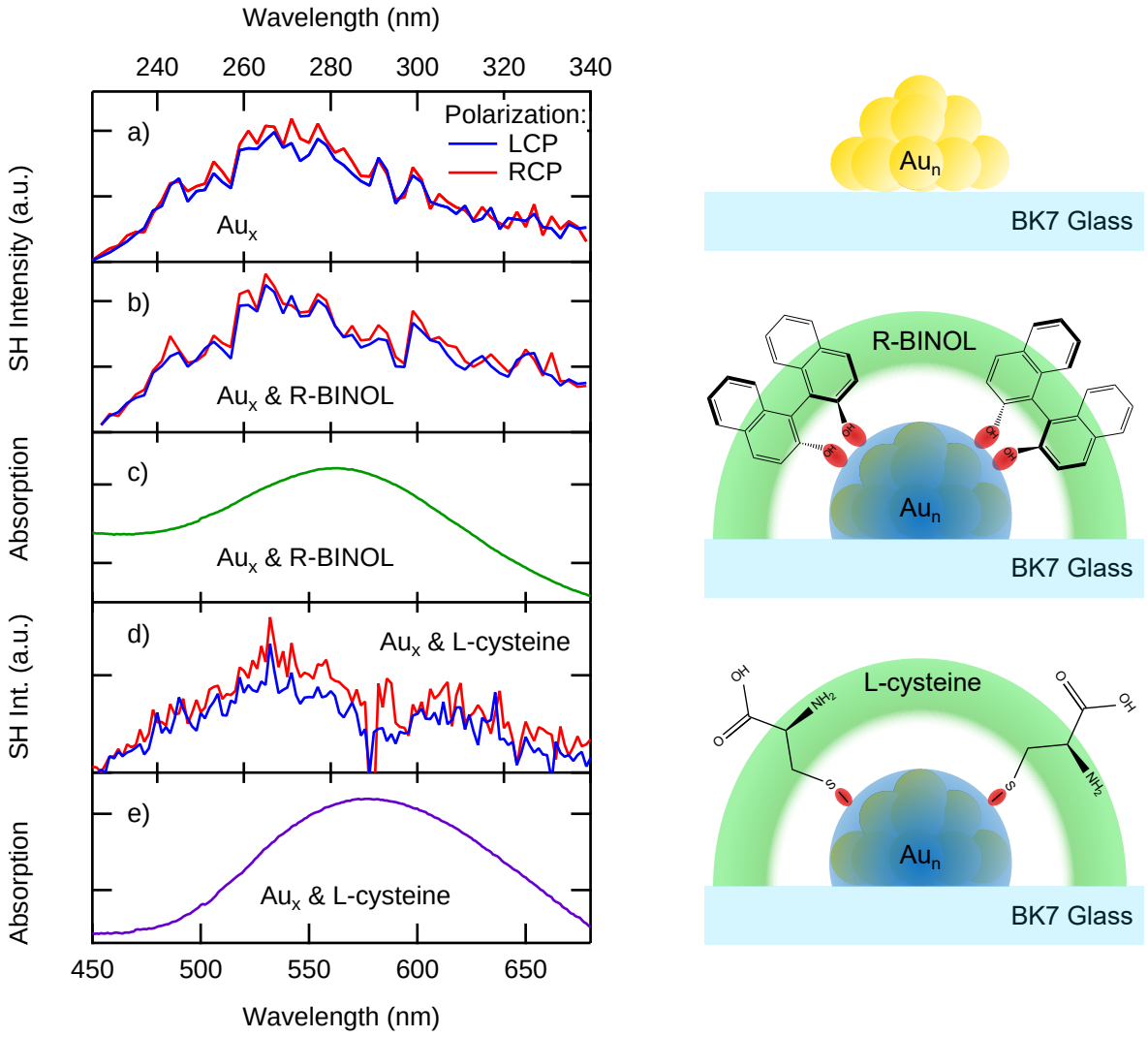

Figure 38 Left: SH spectra from CPs of gold clusters (a) and with R-BINOL (b) and L-cysteine (d). Absorption spectra of gold clusters and R-BINOL (c) and L-cysteine (d) Right: Sketches of studied systems.

cysteine to the gold clusters which causes a larger shift.

The presented comparable studies on gold clusters show that the strong attenuation of the plasmon in case of silver clusters is not universal to all clusters. Therefore, it is suggested to carry out more experiments on gold and copper clusters, as both possess a characteristic plasmon.

7 Induced Linear Chiroptical Activity in Organic Films

As already stated, the final goal of this work is to present a route on how to comprehend the asymmetrization of a heterogeneous catalyst. A key idea of the motivated approach is the study of the chirality transfer from a chiral modifier into the pristine achiral catalyst by means of chiroptical spectroscopy methods. Particularly, the optical effect of ICD is seen as promising tool to investigate the interaction between modifier and catalyst.

In the past, numerous studies with various ICD phenomena were presented and for some even an interpretation and a model have been provided. A prominent example is in the field of biochemistry where the interaction between helix structures like polypeptides or DNA and achiral guest molecules are studied.[44,45] This is, among others, done to probe DNA itself and drug binding sites.[37,46,48] Several different observed ICD effects indicate the interaction between both components which, at the same time, also hold information about its very nature. The involved mechanisms are ranging from structurally induced chirality and off- and resonant excitonic coupling[35,44] to a simply dominating chiral environment[36,46,47].

It becomes obvious that the vast majority of studied systems are in the liquid phase and only a few examples are known so far in solid state. One is a study by the group of Sawada on chiral meta-interfaces between thin films which contain the dye Rhodamine and glucose and show so-termed absorption induced CD.[121] Another example is the new material class of chiral liquid crystals with interesting optical properties originated from ICD.[122–124]

The question rises whether the suggested mechanisms and developed models from the liquid phase can be translated into the solid state. This would simplify the interpretation of ICD effects in the solid state because of the sheer amount of literature in the liquid phase that could be applied. To verify this, a simple solid state system was needed which shows at best multiple ICD effects.

Tunable Induced Circular Dichroism in Organic Films

For the above stated purpose, thin organic films were fabricated by spin coating which show ICD effects in the visible range, see Publication G. The films contain the achiral and pristine optically inactive dye Rhodamine 110 which absorbs in the visible range. The ICD is brought by the chiral, “transparent” modifier BINOL. Therefore, the dye and the enantiopure or racemic BINOL was dissolved in ethanol with various weight ratios of $R = m_{BINOL}/m_{Rhod.}$. This coating solution was then spin coated under static dispense conditions on the already known BK7 glass substrates. The rotational speed of the self-made spin coater was set to 960 rpm which results in a film thickness in the micrometer range. The OA was then studied in the UV and visible range by means of absorption and CD spectroscopy

on a commercial CD spectrometer J-815 from JASCO.

A selection of CD spectra of films with ratios of 0.22, 0.67 and 1.00 as well as the corresponding absorption spectra in case of the films containing R-BINOL are shown in Figure 39.

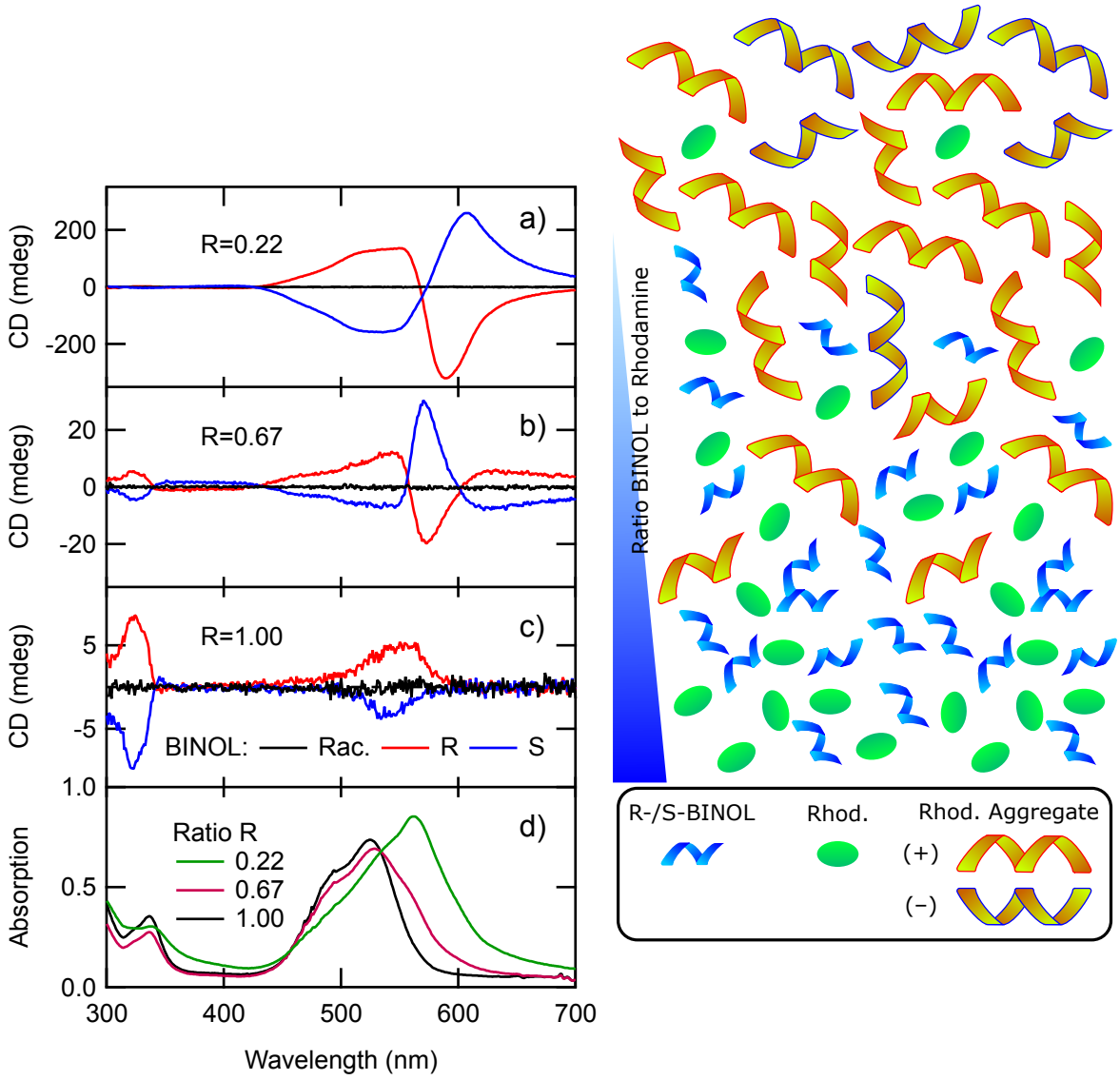

Figure 39 Left: CD spectra of films with R- (red), S- (blue) or racemic BINOL (black) and Rhodamine 110 with a ratio BINOL to Rhodamine of R = 0.22 (a), R = 0.67 (b) and R = 1.00 in the coating solution. d) Diagram of the proposed molecular constellation in a film depending on the ratio between enantiopure BINOL and Rhodamine. (Adapted from Publication G)

In case of a low ratio of 0.22 and R-BINOL as chiral modifier, the CD spectrum possesses a clear OA in the visible range. Note that BINOL is transparent in this range and, therefore, the observed OA is ICD in the absorption of the dye as a consequence of an interaction with the chiral modifier. The CD curve has a bisignate form and shows a positive signal from 430 to approx. 568 nm, a zero crossing at 570 nm and a negative signal at higher wavelengths reaching up to –319 mdeg. The corresponding absorption spectrum (green curve in Figure 39 d) possesses a broad band in the visible range from 400 to 700 nm. Its maximum lies at 560 nm and is related to J-aggregates of the dye which

are commonly known to occur particularly in thin films.[125–129] The ICD curve in case of S-BINOL shows a mirror behavior, as expected for the opposite enantiomer and no OA is observed in case of the racemate. For a higher ratio of 0.67, the CD signals of the films containing enantiopure R- and S-BINOL are approx. one order of magnitude smaller, see Figure 39 b). They also have a different line shape including a second zero crossing at 600 nm. A CD band in the UV region between 300 and 350 nm originates from the enantiopure BINOL itself and indicates the absolute amount of the chiral modifier within the film. The previous maximum at 560 nm, related to dye aggregates, in the absorption spectrum decreased in intensity and is now only observed as shoulder. This is explained by the higher amount of BINOL which is hindering the building of dye aggregates. The new absorption maximum lies at 525 nm and is coming from single isolated dye molecules. The CD signals for films with R- and S-BINOL at higher ratios like 1.0 further decrease and are solely positive and negative, respectively (Figure 39 c). The absorption shoulder of aggregates at 560 nm is not visible anymore and the spectrum is comparable to the one of the pure dye in solution but red shifted for approx. 20 nm.

A quantification was done of the ICD and the aggregate content within the film by calculating the rotational and dipole strength (see Equation 1 and 3) in the visible range and above 600 nm, respectively. It concludes that the ICD increases while the aggregate content remains constant for ratios from 0 to 0.22. The presented model explains as follows. The chiral modifier acts as seed[44] for the building of inherently chiral dye aggregates.[127,130,131] Without modifier the probabilities to form one or the other enantiomer are equal and an OA can only be observed on a microscopic level, whereas it averages out on the macroscopic level.[132,133] Therefore, the chiral modifier leads indirectly to an ee in chiral aggregates and yielding an OA. The measurable IICD is caused by interaction between the transition moments of neighboring dye molecules in the chiral superstructure resulting in bisignate CD curves. With further increasing relative content of the chiral modifier, the rotational strength of the ICD and dipole strength of the aggregates are exponentially decreasing till a ratio of 1. This is caused by the exponential dependency of the aggregates OA and extinction on their size which decreases with increasing BINOL content.[133–135] For ratios higher than 1.0, no aggregates are present in the film anymore and the observed ICD originates from a direct interaction between the chiral modifier and the isolated dye molecules. The different DICD mechanism reflects also in the different line shape of the CD curve compared to the IICD at smaller ratios.

The work proofs not only that well-established concepts from the solution phase can be applied for the studied thin films, it is also the first time that two separate ICD mechanism could be experimentally shown for such a system. The strong dependency of the ICD on the ratio allows excellent tuning of the OA. The reproducible and simple film preparation by spin coating is straightforward and possesses a potential for industrial upscaling. Together this makes it a promising approach for the application as

tunable optically active films, such as filters.

Mechanistic Insights into Induced Circular Dichroism in Organic Films

The previous study demonstrated how the ICD of the films is brought by two different mechanisms. To gain further mechanistic insights into the IICD and DICD, subsequent experiments were carried out where either the chiral modifier was exchanged or the achiral dye, respectively.

Therefore, films were prepared under identical conditions with different enantiopure molecules. To concentrate on the effect of different chiral modifiers on the IICD, a ratio of 0.10 was chosen for all. The CD and absorption spectra for films with Rhodamine 110 and R-BINOL, R-1-phenylethanol (R-1-PE), D-tartaric (D-TA) acid and R-indanol are given in Figure 40. Clear OA is visible in all cases in form of bisignate ICD curves in the visible region. However, the strength and line shape as well as the zero crossing are varying between them. On the other hand the absorption spectra are similar and showing the known broad band with a maximum 560 nm connected to the dye aggregates. This concludes that all modifier are acting as seeds for the building of chiral dye aggregates and that they are all yielding an ee of them. This is in particular astonishing because of the diversity of the used modifiers. For example BINOL possesses an axial chirality, whereas the others possess one or in case of the tartaric acid even two stereocenters. Also their functional groups differ. But what they all share is the ability for hydrogen bonding as Rhodamine 110 does and is, therefore, suggested as key for this IICD mechanism.

The behavior at higher ratio differs strongly between the chiral modifiers and is believed to be dominated by the individual interactions between modifier and dye molecules and between modifier molecules themselves. This is discussed in further detail elsewhere.[136]

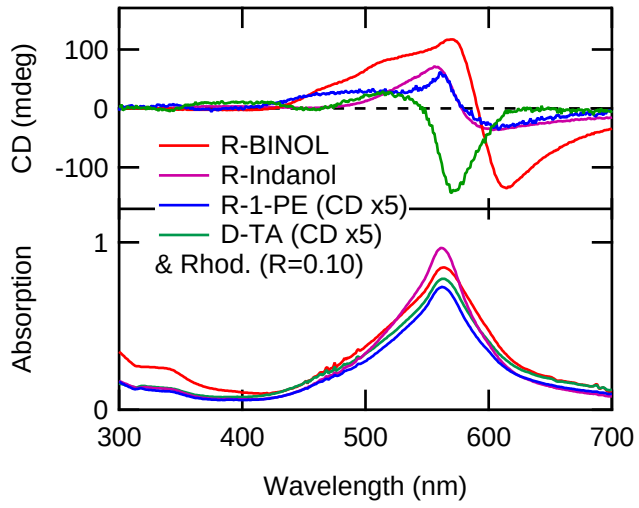

Figure 40 Absorption and CD spectra at a fixed R = 0.10 for Rhodamine and R-BINOL, R-1-phenylethanol (R-1-PE), D-tartaric (D-TA) acid and R-indanol, respectively. For reasons of clarity the CD spectra of R-phenylethanol and D-tartaric acid are scaled x5.

In a second consecutive study, films with R-BINOL but different dyes were fabricated under similar conditions. To solely study the DICD mechanism, a ratio of 5.0 was chosen here. The CD and absorption spectra of films containing Malachite green (MG), Uranine (Uran.) and Rhodamine 110 (Rhod.) are shown in Figure 41. The absorption curves are all comparable to solution and show the already known red shift in case of the films. It concludes that the dye molecules are isolated and no aggregates are present. Therefore, the OA in the visible range, which is observed for all cases, results from DICD mechanism. However, the observed CD feature differ in strength, line shape and wavelength position corresponding to their individual absorption band. For example, the films with Rhodamine 110 and MG show single positive ICD peaks at approx. 530 and 640 nm, respectively. In contrast, Uranine possesses a negative Cotton effect at approx. 490 nm as ICD curve.

The question rises which properties do the dyes share or not share to result in the observed difference in ICD. Comparing the molecular structure of the dyes, Rhodamine and MG possess a different core but are both capable of hydrogen bonding. In contrast, Uranine shares the same core as Rhodamine but cannot establish hydrogen bonds to, for example, BINOL as chiral modifier. Again, the ability to form hydrogen bonds seems to play a key role.

At this point it is suggested to compare the experimental findings with a theoretical model. Such a model with a good assignment of the induced optically active transitions would yield more information about the DICD mechanism and would also allow a precise prediction of the absolute configuration between chiral modifier and dye within the host-guest complex.[36,37]

Analog to the previous study, at lower ratio the systems behave very different. For example, MG and Uranine do not build aggregates in contrast to Rhodamine but possibly merge to dimers. Thus, the observed ICD signals are of very different nature which is discussed in further detail elsewhere.[137]

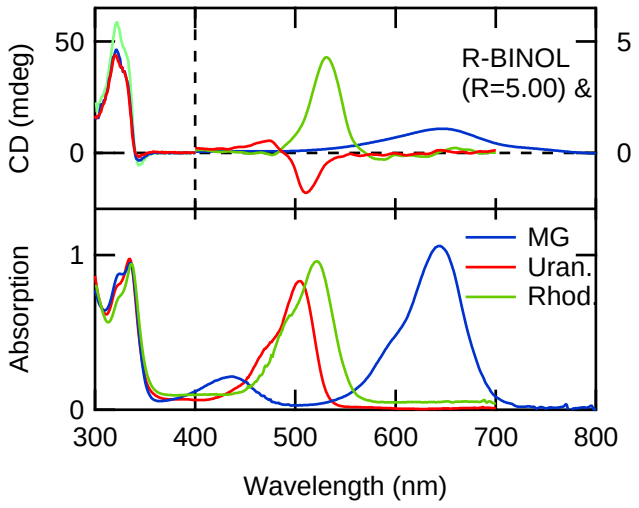

Figure 41 Absorption and CD spectra at a fixed R = 5.00 for R-BINOL and Malachite green (MG), Uranine (Uran.) and Rhodamine 110 (Rhod.), respectively. For reasons of clarity, connected absorption and smoothed CD spectra were scaled and CD spectra are also different scaled for the UV and VIS range.

Together with a theoretical work, the comparing studies are believed to bring further insight into the ICD mechanism and by that take us one step closer in understanding the asymmetrization of heterogeneous catalysts by means of ICD effects. The findings also suggest a possible modular ansatz to create films with custom OA. The basis is choosing a combination of “transparent” chiral modifier and absorbing dye. The choice of the dye defines the wavelength region of the OA, whereas the modifier sets the strength and character of the OA.

8 Conclusion & Outlook

This work presents an approach on how to study the asymmetrization of heterogeneous catalysts by means of chiroptical spectroscopy. In particular the transfer of chirality from the chiral modifier to the pristine achiral catalyst is suggested to be examined based on the induced OA in the optical response of the asymmetrized catalyst. The implemented nonlinear chiroptical method of SHG-CD proved its inherently high sensitivity in multiple in situ studies and ex situ collaboration projects on the OA of enantiomerically pure films with coverages down to the submonolayer range. Therefore, SHG-CD demonstrated to be the ideal tool to probe the chiroptical properties of, for example, chirally functionalized surfaces. Because conventional linear CD spectrometer are often too insensitive, SHG-CD could be used instead in future studies on this new class of materials. It could be also used to study surface reactions in situ and in real time. If either an educt and/or a product is chiral and present in an enantiomeric excess, the reaction can be followed by observing the OA at the surface.

It was shown that SHG-CD is affected by isotropy and thus holds also structural information of a system on the example of a crystallization in a molecular film. Simultaneously, an enantiosensitive polarity reversal of ellipticity effect was observed in the linear CD which can not be explained by the standard model. Future experiments on comparable systems and a theoretical model hopefully yield more insight into this unexplained phenomena.

In order to prove the suggested approach for studying the asymmetrization of heterogeneous catalysts, the adsorption of chiral molecules on a silver surface was investigated by means of SHG-CD. The silver plasmon proved to be very sensitive towards its environment and the capability to measure in situ under controlled UHV conditions necessary. The adsorption mechanism of the chiral modifier can be explained by the observed red or blue shift and simultaneous broadening of the surface plasmon resonance. Therefore, the plasmon acts as probe of the surface and can be, for example, used as this in a surface reaction study where the composition of the adsorbates is changing during the reaction. But most important, an induced OA was observed in the silver plasmon which was brought by the interaction with the chiral adsorbate. This is a proof-of-principle that the asymmetrization of a heterogeneous catalyst can be investigated based on the resulting induced OA measured by means of SHG-CD. The findings clearly motivate further work on different chiral modifier and different coinage metals. A comparison between them is believed to deliver more information about the mechanism of induced OA and how it connects to the asymmetric behavior of the catalyst. Also the plasmons response of coinage metal clusters upon adsorption of molecules was studied. The clusters are known model catalysts and especially famous for their unscalable size-dependent reactivity. Clusters proved to be much more sensitive to adsorbates which results in a partial or complete damping of their plas-

mon and depends strongly on whether the cluster is deposited on top of the chiral modifier or vice versa, respectively. Thus, it is suggested for future experiments to deposit silver clusters on inherently chiral surface and with that avoid a damping of the plasmon. Further, the optical response of gold clusters was found to be much more robust upon adsorption of molecules and, therefore, seems like a promising alternative.

To gain more knowledge about the phenomena of induced OA, it was also explored in thin organic films. There it was proven that well-known concepts from the liquid phase can be applied in the solid state as well to explain the two present an independent mechanism of induced OA. The applied modular approach of a “transparent” chiral modifier and an absorbing dye allows a highly tunable and custom OA. Paired with the simple and straightforward fabrication by spin coating, this makes it a promising approach for optically active films for the application, for example, as filters. Comparing studies with different chiral modifier and dyes suggest that the ability to form hydrogen bonds plays a key role. A theoretical model of a modifier-dye complex could yield valuable insights about the mechanism of the induced OA and also ease the search for more applicable combinations of modifier and dye.

9 Publications

Further information about the publications which were carried out in the course of this dissertation is given in the following. Publications related to the main topic of the dissertation and submitted with the author of the dissertation as the first author are printed in full length.

A In situ Second-Harmonic Generation Circular Dichroism with Submonolayer Sensitivity

Journal ChemPhysChem, 20(1): 134-141, 2019

Authors Alexander von Weber, Matthias Jakob, Eva Kratzer, Aras Kartouzian, and Ueli Heiz

Affiliations Chair of Physical Chemistry, Chemistry Department & Catalysis Research Center, Technical University of Munich

Abstract “In this work, we present an experimental setup for the in situ and ex situ study of the optical activity of samples, which can be prepared under ultra-high vacuum (UHV) conditions by second-harmonic generation circular dichroism (SHG-CD) over a broad spectral range. The use of a racemic mixture as a qualified reference for the anisotropy factor is described and, as an example, the chiroptical properties of 1.5 µm thick (multi- layers) as well as sub-monolayer thin films of the R- and S-enantiomer of 1,1’-Bi-2-naphthol (BINOL) evaporated onto BK7 substrates were investigated.”

ChemPubSoc Europe
DOI: 10.1002/cphc.201800897
CHEMPHYSCHEM Articles

In situ Second-Harmonic Generation Circular Dichroism with Submonolayer Sensitivity

Alexander von Weber,[a] Matthias Jakob,[a] Eva Kratzer,[a] Aras Kartouzian,*[a] and Ueli Heiz[a]

In this work, we present an experimental setup for the in situ and ex situ study of the optical activity of samples, which can be prepared under ultra-high vacuum (UHV) conditions by second-harmonic generation circular dichroism (SHG-CD) over a broad spectral range. The use of a racemic mixture as a qualified reference for the anisotropy factor is described and, as an example, the chiroptical properties of 1.5 μm thick (multilayers) as well as sub-monolayer thin films of the R- and S-enantiomer of 1,1′-Bi-2-naphthol (BINOL) evaporated onto BK7 substrates were investigated.

1. Introduction

In the 19th century, Pasteur was the first who studied chirality by an optical method. He discovered that enantiopure crystals with different shapes show opposite handedness in their optical activity. Later, the concept of chirality proved to be of great importance in biology, which reflects in the predominance for a single enantiomer in most biomaterials. Because natural resources are limited and the demand for enantiomerically pure compounds is increasing, great efforts are made in the field of enantioselective catalysis to synthesize such compounds chemically.[1,2] Until recently, research concentrated on homogeneous asymmetric catalysts, which are already used in industrial applications.[3,4] The heterogeneous counterpart holds intrinsic advantages over homogeneous ones but only a few examples are known at present.[5] Generally, heterogeneous asymmetric catalysts are categorized into two major groups. The first group is based on chiral homogeneous catalysts, which are immobilized by, for example, a support of polymers.[6] The basic concept of the second group are common achiral heterogeneous catalysts like immobilized metal nanoparticles, which are functionalized with enantiomerically pure, organic molecules, so-called chiral modifiers.[7–10] In a proof of principle study, it was shown that Pt nanoparticles functionalized with enantiopure cysteine indeed performed as asymmetric catalyst in the hydrogenation of 2-butanone.[11] Another well-known example is tartaric acid adsorbed on Ni, Cu and Co surfaces. If enantiopure tartaric acid acts as chiral modifier, the catalytic surface enantioselectively hydrogenates β-keto esters.[12,13] Ultra-high vacuum (UHV) studies revealed adsorption-induced chiral organization of the adsorbates, which can even possess a global chirality stretched over the entire surface, as in case of tartaric acid adsorbed on a Cu(110) surface.[14] Of essential importance in these studies was the precise control over the adsorbate coverage, which was generally well below one monolayer. These systems have been studied with common UHV compatible methods, including reflection absorption infrared spectroscopy, low-energy electron diffraction, thermal desorption spectroscopy and scanning tunneling microscopy.[15] Although the mechanism of chirality transfer from the ligands to the metal catalysts is generally not known, the possible processes have been categorized in the past[16,17] and for all of the mechanisms there are reports in the literature.[18–21]

To our knowledge, no optical method was used so far to study the chirality of such enantioselective, heterogeneous catalysts under UHV conditions to provide further mechanistic insight into the chirality transfer and catalytic action. One benefit of UHV sample preparation methods is that contaminations are avoided, and the pure sample can be studied. This reduces the complexity by lowering the number of variables and makes the interpretation of the results easier. Therefore, the higher experimental complexity related to a UHV part is justified by its benefits and potential of studying samples and systems under controlled conditions. We note, however, that the spectroscopic method is not restricted to UHV.

Another experimental challenge is the low coverage of the chiral optically active medium in those systems, which lie often below the sensitivity limit of standard CD-spectrometers. To study the optical activity of low coverages at surfaces and interfaces, Hicks et al. combined the inherently surface-sensitive second-harmonic generation spectroscopy with circular dichroism, called SHG-CD. There, the difference in intensity of generated second harmonic (SH) light expresses the optical activity. Similar to the linear case, a dimensionless anisotropy factor can be defined, where the difference in SH generation by each handedness of circularly polarized (left or right handed) light is weighted by the average of both [Eq. (1)]:[22]

$$\mathrm{SHG-CD} = g = \frac{I_{\mathrm{LCP}} - I_{\mathrm{RCP}}}{1/2\,(I_{\mathrm{LCP}} + I_{\mathrm{RCP}})} \quad (1)$$

with $I_{\mathrm{LCP/RCP}}$ as SH intensity generated by the left circularly polarized (LCP) and right circularly polarized (RCP) fundamental

[a] A. von Weber, M. Jakob, E. Kratzer, Dr. A. Kartouzian, Prof. U. Heiz
Chair of Physical Chemistry
Chemistry Department & Catalysis Research Center
Technical University of Munich
Lichtenbergstr. 4, D-85748 Garching, Germany
E-mail: aras.kartouzian@mytum.de

Supporting information for this article is available on the WWW under https://doi.org/10.1002/cphc.201800897

ChemPubSoc Europe

CHEMPHYSCHEM Articles

light, respectively. The work has been experimentally as well as theoretically carried on by the group of Verbiest, who created a mathematical formalism allowing the determination of the individual elements of the second order susceptibility tensor $\chi^{(2)}$.[23]

A second asymmetry expresses itself in a different response between circularly and linearly polarized light. Toro et al. presented a study on degenerated two- photon absorption circular-linear dichroism (2PA-CLD) of 1,1′-Bi-2-naphthol (BINOL) in solution. There, an enantio-sensitive difference between the simultaneous absorption of two linearly and two circularly polarized photons was demonstrated.[24] Wanapun et al. defined a mathematical expression in analogy to conventional CD to quantify this anisotropy. They demonstrated that the structure-sensitive CLD ratio is purely electric dipole-allowed and depends on conformation.[25] Thus, this technique shares essential properties with SHG-CD. In a similar manner, we adopted this expression for SHG as follows [Eq. (2)]:

$$\mathrm{SHG-CLD} = \frac{I_{\mathrm{CP}} - I_{\mathrm{p}}}{1/2\left(I_{\mathrm{CP}} + I_{\mathrm{p}}\right)} \tag{2}$$

with $I_{\mathrm{CP/p}}$ as the average SH intensity generated from both circular polarized and linearly p-polarized light, respectively. Following Wanapun et al. and in contrast to Toro et al., we define the SHG-CLD using the average over both circular polarizations. Since the signal of individual circular polarizations holds enantio-sensitive contributions from SHG-CD averaging over both CPs enables a deconvolution of the two contributions and a separate study, which is further discussed in the SI.

BINOL and its derivatives possess high relevance in the asymmetric catalysis especially as chiral ligands and chiral modifiers and was therefore chosen as a model molecule.[26,27] This molecule consists of two 2-naphthol units connected through a C–C bond and distorted towards each other, resulting in axial chirality. Its optical spectrum shows three bands in the UV-region, which will be revered as high, middle and low energy bands at wavelengths below 240 nm, between 260 nm and 300 nm and above 300 nm, respectively. The bands originate from symmetric and antisymmetric coupling between long-axis polarized ^1B_b transitions, short-axis polarized ^1L_a and off-axis polarized ^1L_b transitions of 2-naphtol.[28–30] Further, the middle and low energy band show three and respectively two separated transitions. This splitting is due to a coupling between excited states of the naphtols. BINOL is fully transparent throughout the visible range. Its structure, absorption and CD spectrum in solution are shown in Figure S1 in the Supporting Information.

Experimental Setup

Apart from the SHG-CD technique, the setup was described in various studies before. Here we focus on the necessary upgrades and challenges related to SHG-CD accompanied by a brief description of the whole setup. The experimental setup presented in this work is a combination of a UHV system that allows for precise and reproducible sample preparation with a minimum of contamination as well as a laser spectroscopy setup for linear absorption (surface cavity ring down; s-CRD)[31,32] and nonlinear SHG studies.[33,34] A schematic view of the setup is given in Figure 1.

The UHV part of the setup can be divided into three parts. The first part is a UHV analysis chamber with a base pressure of $1\cdot10^{-10}$ mbar armed with a 4-axes manipulator (x, y, z, and θ). Additionally, it is equipped with a sputter gun and an electron shower that emits slow electrons (with a kinetic energy <15 eV) to neutralize a nonconductive substrate during sputtering. The analysis chamber further hosts a sputter gun for UHV surface cleaning. Second, a transfer chamber is connected to the analysis chamber through a UHV gate valve enabling sample transfer without breaking the UHV. The transfer chamber is equipped with a fast entry lock and a sample magazine. It also hosts a molecular evaporator to prepare films while the coverage is monitored by a quartz crystal microbalance (QCM; SL-A1E40 from INFICON). Third, a laser ablation cluster source is connected to the analysis chamber.[35]

The optical part of the setup can be divided into two parts. First is the light source in front of the UHV chamber where monochromatic, coherent light of well-defined polarization is generated and second, the analysis part behind the chamber and sample. The light source consists of an optical parametric amplifier laser system covering the spectral range between 210 nm and 10000 nm with a pulse duration of about 30 ps (PG401 from EKSPLA). The polarization of the laser output is purified by a Glan-Laser calcite polarizer before getting to a photoelastic modulator (PEM; II/FS42A from Hinds Instruments) where its polarization is actively set. Because the timing when the laser pulse is traversing the PEM defines the outcoming polarization, special care has to be taken with regard to the trigger of the laser. The delay between the oscillation of the PEM and one laser shot is handled by a self-made trigger box. A detailed description of the operation mode of the box (Figure S2) and the calibration for both circular polarizations (CPs) and p-polarized light is given in the SI (Figures S3 and S4). After the PEM, a 400 nm long pass filter (FELH0400 from Thorlabs) is used to remove residual SH, that may accompany the output of the laser system, before focusing the laser beam on the sample inside the UHV chamber through a fused silica lens with a focal length of 300 mm. The diameter of the laser spot size at the sample can be varied between 0.5 mm and 4 mm by moving the sample away from the focal point or towards it. The SH generated at the sample and the fundamental light propagate out of the chamber and are recollimated through a second fused silica lens with a 300 nm focal length. Afterwards, the fundamental and SH beams are separated by a combination of two rotatable Pellin-Broca prisms and a monochromator (MC; Omni-λ 150 from LOT). For a 90° deflection of the SH beam at each prism, the angles of the prisms have to be adjusted to the wavelength and are controlled by step motors. The correlation between wavelength and motor positions is calibrated upfront and described in the SI, see Figure S5. A photo diode detects the light intensity of the fundamental light after the first prism for power correction purposes as described later. Finally, the pure SH light is detected by a photomultiplier tube (PMT; H9305-03 from Hamamatsu) and the resulting analog current is taken as signal, see Figure S6. A central LabVIEW program controls the laser, the trigger box, PEM, step motors, MC and oscilloscope and is depicted in Figure S7. This enables full automation and makes it possible to scan over a large wavelength range, while switching between different polarizations for each wavelength or, alternatively, monitor the time evolution in SH at a specific wavelength.

150 μm-thick borosilicate glasses (BK7 cover glass from VWR) were used as substrate and cleaned with spectroscopic grade acetone

ChemPubSoc Europe
CHEMPHYSCHEM Articles

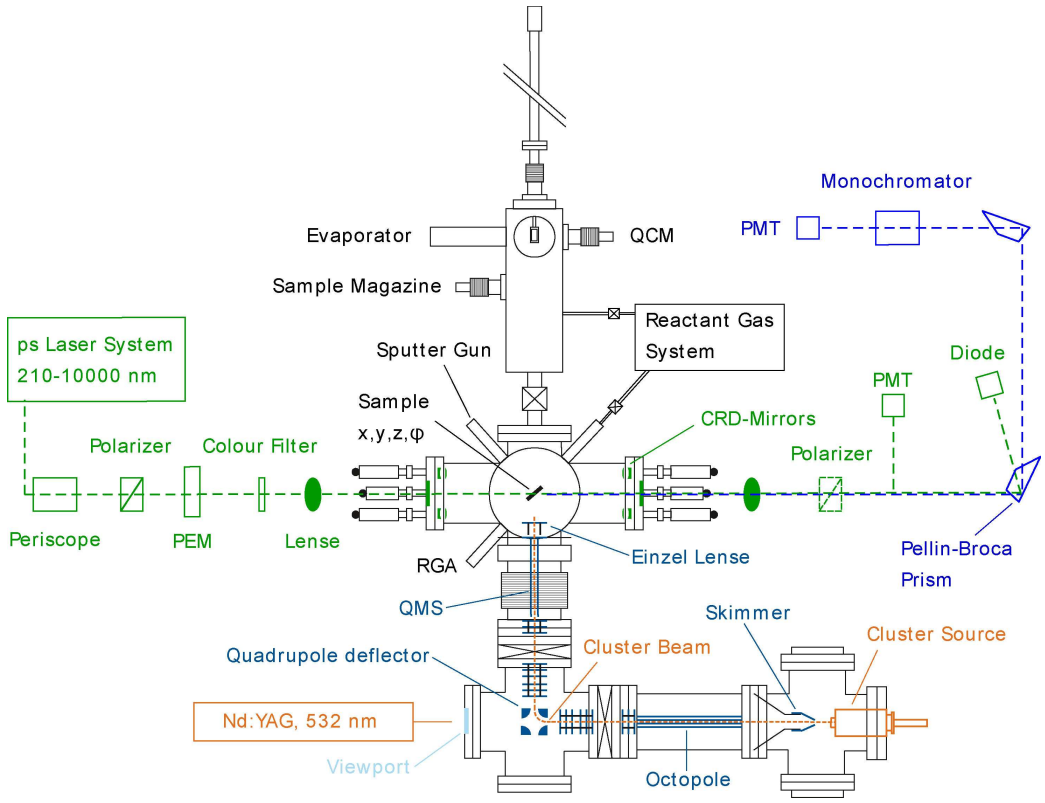

Figure 1. Experimental setup which combines optical spectroscopy methods SHG-CD and sCRD with a UHV setup including a laser ablation cluster source for in situ studies.

beforehand. Samples were prepared by evaporation of BINOL on the glass substrates under HV conditions in the transfer chamber. The coverage was monitored with the QCM and was held at approx. $2{\cdot}10^{17}$ molecules cm^{-2} for the thicker films and at $8(2){\cdot}10^{13}$ molecules cm^{-2} for the study on low coverages. The experiments were performed at 0 C in order to suppress self-ordering effects during the course of the experiment, which have been observed at room temperature for BINOL films.[33,36,37] This is crucial because anisotropy in a system additionally influences the nonlinear optical activity and thus makes it difficult to disentangle the activity due to single molecules and long-range orders.[23]

To study the nonlinear optical activity of BINOL, wavelength scans between 225 nm and 340 nm of the SH (equivalent to 450 nm to 680 nm of the fundamental light) with both CPs and p-polarized fundamental light were recorded for films of the pure enantiomers and the racemate. 100 laser shots per wavelength and polarization were averaged. At selected wavelengths the SH was recorded for at least 10 k shots for each CP. The angle of incidence was set to 70 and the evaporated film faced the detection unit. Thus, the fundamental light transmits through the glass substrate before interacting with the film.

2. Results and Discussion

2.1. SH Spectrometer Function

As with any spectrometer, a standard or reference has to be defined. On the one hand, the wavelength range of the spectrum is dictated by the bandwidth of the laser and resolution power of the prisms and the MC. The SH intensity, on the other hand, needs referencing. For this purpose, a SH spectrum of a pristine BK7 glass substrate was taken with p-polarized light. The raw spectrum and the recorded intensity of the fundamental light are shown in Figure S8. The SH and fundamental light spectrum show an analytical relation because the intensity of SH depends on the intensity of the fundamental light and therefore should be corrected for it. Hence, the SH spectrum was first divided by the square of the wavelength corrected intensity of the fundamental light. These steps are described in further detail in the SI. The power-corrected SH spectrum is shown in Figure 2a). Considering that BK7 has no specific transitions to address, the SH spectrum should not show any spectral features. Accordingly, deviations originate from the wavelength dependent properties of the spectrometer such as transmision of the filters, efficiency of the MC and sensitivity of the PMT. To compensate these influences, the

ChemPubSoc Europe
CHEMPHYSCHEM Articles

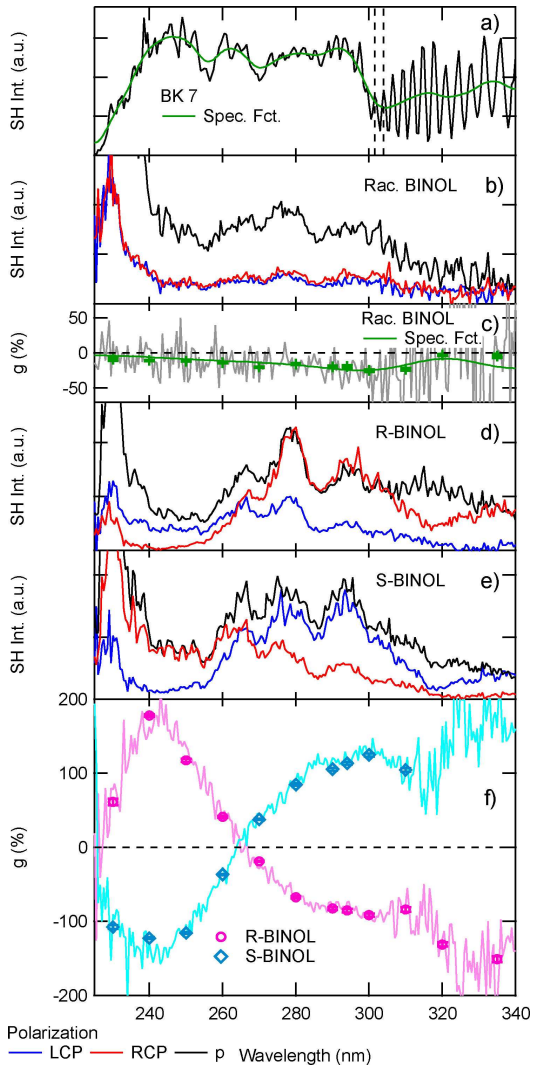

Figure 2. a) SH spectrum from p-polarized light of pristine BK 7 substrate with smoothed curve as spectrometer function. b) SH spectrum from p and CP-polarized light of racemic BINOL film. c) *g* value for racemic BINOL film and spectrometer function. d) and e) SH spectra from p and CP-polarized light of R- and S-BINOL. f) *g* value for R- and S-BINOL.

power-corrected SH spectrum is smoothed and defined as a spectrometer function, which is shown as green curve in Figure 2a). All the spectra shown in the following are power-corrected and divided by this spectrometer function aftwerwards. A more detailed description of these corrections is given elsewhere.[38] An interference pattern is visible above 290 nm, where BK7 becomes transparent and SH generated at the front side interferes with the one generated at the backside. The occurrence of this phenomena also allows for deriving from the distance between two peaks a spectral resolution of 30 meV for the present setup.

2.2. Referencing 2nd Order g Value

As the intensity of the SH spectrum has to be corrected for the spectrometer function, the measured anisotropy factor or *g* value must also be referenced as described in the following. In comparison to linear CD measurements this is not trivial for nonlinear CD measurements, such as SHG-CD. In linear CD, the sample can be seen as a stack of films that contribute to the total absorption and CD in a simple additive manner. Therefore, a sample without the optically active medium component can be used as reference. In the nonlinear case, however, the pristine glass substrate does not qualify as reference because the SH generated at the glass vacuum interface gets suppressed in case of an adsorbed molecular film. Further, individual contributions from all interfaces to the acquired signal are different and difficult to disentangle.

Therefore, we propose to use a racemic film prepared under identical conditions as reference. The SH spectra from p-polarized light (black curve) and both CPs (LCP in blue and RCP in red) of the racemate are shown in Figure 2b). One high energy band above 240 nm and one middle energy band around 280 nm are visible. A difference between the two CPs is negligible or even non-existent. The resulting spectrum of the *g* value based on the SH spectra of both CPs is given in Figure 2c). The markers represent measurements at selected wavelengths where more than 10 k shots have been averaged with the standard deviation representing the experimental error. Assuming that contributions of opposite enantiomers are canceling each other out, the *g* value should be zero. Therefore, a smoothed curve of the anisotropy factors of the racemate (shown as green line) is defined as referencing spectrometer function and subtracted from following spectra. The accurate anisotropy factors at specific wavelengths are separately corrected for the ones of the racemate.

Additionally, both CPs generate significantly less SH than linearly p-polarized light over the whole range. This leads to a negative SHG-CLD. In the range of the middle energy band between 260 nm and 300 nm for instance, the average SHG-CLD becomes −105(7)%.

Surface Coverage

The coverage of approx. $2 \cdot 10^{17}$ molecules cm^{-2} can be calculated from the recorded deposition on the QCM and usage of the Sauerbrey equation.[39] The film thickness can be derived, assuming each BINOL molecules occupies the same volume as in the optically active crystal of 357.8 $Å^3$.[40] Accordingly, the thickness of the film is calculated to be 1.5 µm or roughly 2000 ML.

ChemPubSoc Europe

CHEMPHYSCHEM Articles

2.3. SHG-CD from BINOL

SHG-CD of R-/S-BINOL

The corrected SH spectra from p-polarized light (black) and both CPs (red and blue) of an R-BINOL film are shown in Figure 2d). The spectra show three bands, one below 240 nm, one around 280 nm and one above 330 nm. A significant difference in SH intensity generated by the two CPs is visible. For example, in the region of the high energy band at 240 nm more SH is generated by LCP (blue) than RCP (red). For higher wavelengths, this is reversed coming along with a crossing of the curves at around 265 nm. The resulting anisotropy factor is given in Figure 2f). It shows a maximum of 178(2)% at 240 nm in the region of the high energy band and, as anticipated from the SH spectra, a zero crossing point at 265 nm. The middle energy band shows a value of −67(2)% at 280 nm and the low energy band a value of −151(4)% at 335 nm. The *g* value of 178(2)% is to our knowledge the highest 2nd order anisotropy factor measured so far in a non-plasmonic system. One of the first SHG-CD studies in 1994 by Byers et al. was on BINOL adsorbed on fused silica at monolayer coverages.[41] The spectra were taken in reflection geometry and a spectrum was shown for R-BINOL between 285 nm and 345 nm, including part of the middle energy band and the complete low energy band. Further, the anisotropy factor was measured in two geometries where the molecules were facing upwards and downwards relative to the incident and reflected light by flipping the glass substrate. The anisotropy factor at 294 nm changed sign between both orientations, which demonstrated the sensitivity of the anisotropy factor to the relative orientation of the molecules. The value of −85(2)% at 294 nm for R-BINOL measured here is in good agreement with the comparable down position geometry of the mentioned study, where the light first transmits through the glass and then interacts with the BINOL.

Further, the SH spectra from R-BINOL in Figure 2d) show that the SH intensities generated by one CP is less than generated by linearly p-polarized light at all wavelengths but in the range of the middle energy band between 260 nm and 300 nm in the case of RCP it is close. The average SHG-CLD at these wavelengths is −47(7)%.

The SH and anisotropy factor of the S enantiomer is given in Figure 2e). The SH spectra show similar shape compared to the R enantiomer but are different in their relative intensity. Thus, at wavelengths of the high energy band, more SH is generated by RCP. Again, a crossing of both CPs is observed at 265 nm and for higher wavelengths, more SH is generated by LCP. The anisotropy factor has a minimum of −132(1)% at 240 nm, a crossing at 265 nm and a positive value of 84(2)% at 280 nm and approximately 173% at 335 nm. The anisotropy factors of the opposite enantiomer, plotted in Figure 2f), show mirror like behavior as expected. The SH spectra follow the linear absorption spectrum (see Figure S1) showing the high, middle and low energy bands. The 2nd order anisotropy factor also follows qualitatively the linear counterpart. For example, the high energy band shows an opposite sign of the anisotropy factor compared to the middle and low energy band, going hand in hand with a zero crossing around 270 nm. Notice that the signs of the linear and nonlinear anisotropy factors are inverted for R-BINOL. Hence, the nonlinear factor depends on the orientation of the molecule[33] and according to Hicks et al., it reverses by flipping the molecule with respect to the light propagation.[41] Quantitatively, the nonlinear anisotropy factor is four to five orders of magnitude larger than its linear counterpart. The current understanding is that the nonlinear rotational strength determining the nonlinear optical activity does not necessarily involve the magnetic transition dipole moment and is inherently of a different nature than its linear counterpart.[23] The magnetic transition dipole moment is generally small, thus limiting the linear effect. Also, the relative anisotropy factors of the three bands differ. For example, the relative anisotropy factors for SHG-CD in case of the R-enantiomer are 1:0.5:0.93 for the high (240 nm), middle (280 nm) and low energy band (335 nm). Measured with linear CD for R-BINOL in methanol, the relative factors are 1:0.1:0.08. This could be explained by the same argument about a missing involvement of the magnetic transition dipole moment. Alternatively, the limitation of the second order anisotropy factor to 200% could be responsible. As in case of a homogeneous amplification of the optically active bands in the nonlinear case, the band with the highest optical activity (at 240 nm) will converge against this limit while the anisotropy factors of the other bands are still increasing.

Sign-Defining Step for CD

Interestingly, whereas the nonlinear anisotropy factor from SHG-CD behaves qualitatively equivalent to the linear one, this is not generally the case for nonlinear techniques as seen in case of two-photon absorption circular dichroism (2PA-CD). The degenerate case of 2PA-CD describes the simultaneous absorption of two photons of the same energy and its difference between both photons being left or right circularly polarized.[42] Toro et al. applied this technique on BINOL in solution.[43] The spectrum of both enantiomers are mirror image-like but each one shows the same sign in optical activity throughout the entire spectrum between 200 nm and 350 nm including wavelengths of the high, middle and low energy bands. That is, the spectra do not possess a zero crossing. The linear CD involves a one-photon absorption process between the electronic ground state and an excited state. During 2PA-CD, the same excited state is accessed through simultaneous absorption of two photons each having half of the energy via a virtual level. SHG-CD starts with the two-photon absorption from 2PA-CD followed by a generation of a single photon of the double energy, that is, the same energy as in the linear case. This comparison is summarized in a simplified Jablonski diagram (see Figure 3). What linear CD and SHG-CD have in common and separates them from 2PA-CD is the single photon transition step between the electronic ground and excited state. Additionally, this step obeys an odd-parity selection rule, which is in contrast to the even-parity of the two-photon transition. Although the liquid samples studied by 2PA-CD and the film

ChemPubSoc Europe
CHEMPHYSCHEM Articles

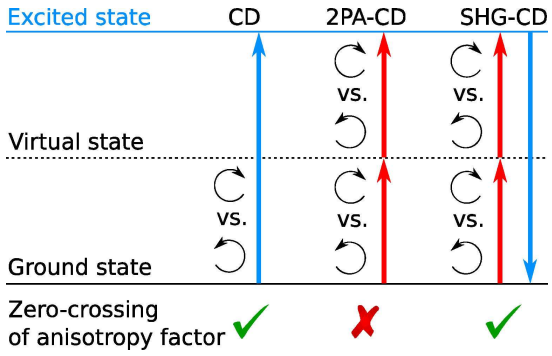

Figure 3. Simplified Jablonski diagram for CD, 2PA-CD and SHG-CD from left to right.

samples studied in this work by SHG-CD represent different nonlinear media, that is, liquid versus thin film, the correlation between the opposite sign in the range of the high-energy band including the zero crossing and the one-photon step in SHG-CD and linear CD indicates a causality.

Additionally, the SH spectra of S-BINOL in Figure 2e) show that, similar to the opposite enantiopure film, SH generated by both CPs is less than generated by linearly p-polarized light. However, in the range of the high energy band and the middle energy band RCP and LCP are close respectively. The SHG-CLD between 260 nm and 300 nm in the range of the middle energy band is approx. −52(13)%. A detailed description of the SHG-CLD curves is given in the SI (see Figure S9) in case of R- and S-BINOL.

Interpreting SHG-CLD

If one compares the average SHG-CLD from the enantiopure films and the racemate at these wavelengths between 260 nm and 300 nm, a significant difference is evident. The signal around this wavelength originates from a coupling between short-axis polarized ^1L_a transitions of the two 2-naphtol units in BINOL. In a simple picture, p- and circular polarizations differ in intensity perpendicular and parallel to the surface and to the addressed transition dipole moment. This difference leads to a weaker or stronger response of a transition dipole moment of a molecule depending on its orientation with respect to the surface normal. Therefore, a difference in SH intensity ratio between the enantiopure film and the racemate can be explained by a difference in average orientation of the transition moment and consequently a different orientation of the molecule. This could result from a different stacking pattern between enantiopure and racemic films. Such differences in stacking patterns are shown for different crystalline optical phases of BINOL with differences in packing density of up to 9.6%.[40] But to the best of our knowledge, this is not known for the optical phase studied here. An alternative explanation is that in case of enantiopure films part of the SH light can also be generated in the non-centrosymmetric bulk of the film. Whereas in case of the racemate, it is assumed that SH is only generated at interfaces. It was shown that the average orientation of the molecules change with each layer and therefore molecules in the bulk show a different orientation than those at the glass/film interface.[33]

2.4. Submonolayer Sensitivity

In contrast to the previously studied film, in many cases the coverages of the optically active compound is very low even reaching below one monolayer. This can be the case, for example, when coupling effects between layers of molecules in a film have to be avoided or in systems where the compound is used as functionalizing chiral ligand or agent. Here, the inherent surface sensitivity of SHG comes into play. In order to demonstrate the capability of the spectrometer, SHG-CD experiments comparable to the previously presented ones were performed on similarly prepared films of the racemic mixture of BINOL as reference and the R and S enantiopure films with a coverage of $8(2)\cdot10^{13}$ molecules cm^{-2}. Considering that the first layer of BINOL molecules binds with its hydroxyl groups in an upstanding motif to the surface, each molecule covers an area of ~0.5 nm^2.[33] This is similar to the assumption before and the coverage can be expressed as 0.4(1) ML meaning that 40(10)% of the glass surface is covered with BINOL.

Referencing 2nd Order g Value

The SH spectra of the racemic film for both CPs are given in Figure 4a). The SH spectra show the highest intensity at around 240 nm. None of the previously seen bands of BINOL are identifiable. Instead, the interference pattern above 300 nm, as known from the pristine glass substrate, is visible. The calculated g value is given in Figure 4b). Again, the smoothed curve is taken as the spectrometer function (green curve) which is subtracted from all following spectra. Below 235 nm and above 305 nm, the g value is dominated by noise due to low SH intensity and is therefore excluded from further evaluation.

SHG-CD of R-/S-BINOL The SH spectra of R-BINOL for both CPs are shown in Figure 4c. These spectra follow the same trend as for the racemate with the only difference that at 240 nm, LCP generates clearly more SH than RCP and vice versa at around 280 nm. The related g values are 8(2)% and −27(3)%, respectively, as plotted in Figure 4e.

The SH spectra of S-BINOL are shown in Figure 4d. Notice that at 240 nm no significant difference between both CPs is visible. Taking the reference correction into account, the g value becomes −8(2)%. At 280 nm, LCP generates more SH than RCP with a g value of 25(4)% which is reversed to the R-BINOL case. Similar to the previous case of thicker films, the g values for low coverages of opposite enantiomers are mirror image like.

That coverage is below one monolayer and part of the glass surface remains uncovered is supported by the appearance of the interference pattern in the SH spectra, which involves the generation of SH at the pristine glass surface. As previously

ChemPubSoc Europe
CHEMPHYSCHEM Articles

described, none of the characteristic bands of BINOL are identifiable in the case of submonolayer films. One explanation is that the signal intensity is simply too low. Alternatively, one can argue that the generation of SH depends on the angle between the addressed transition dipole moment and the surface normal. For example, SH is blind to transition dipole moments parallel to the surface. In this picture, the average orientation of the transition dipole moment and subsequently of the molecule differs between the first layer and following layers of a thicker film. This phenomenon was demonstrated in a study on coverage-dependent SHG-OR of BINOL at the wavelength of the low energy band by Heister et. al.,[33] wherein significant optical activity was observed, which concludes that the SH comes indeed partly from the chiral adsorbent, BINOL.

Comparison to Multilayer

The calculated anisotropy factor qualitatively follows the sample with higher coverage being positive at 240 nm in the region of the high energy band and negative at 280 nm in the region of the middle energy band in the case of R-BINOL. Quantitatively, the anisotropy factors are one order of magnitude smaller, the ratio between both is 0.3:1 compared to 1:0.5 and therefore almost reversed. The crossing point at 255 nm is 10 nm shifted to smaller wavelengths. Three possible effects can be stated here to cause these differences. First, the anisotropy factor is an average over contributions from the achiral glass surface and the molecules. Therefore, the calculated anisotropy factor will be an underestimation of the pure optical activity of the molecule. Furthermore, the relative contributions can be wavelength dependent. Thus, if less SH is generated from the chiral BINOL relative to the achiral glass surface in one wavelength region compared to another, the influence of the achiral glass surface on the anisotropy factor would be stronger in this region. Second, if the average orientation of the molecules and transition dipole moments in multilayer films and films with submonolayer coverage are different, the anisotropy factors will be different since they are connected. Third, dipole-dipole interactions between neighboring molecules in the same layer or between different layers could influence the measured anisotropy factor. These are present in the multi-layer films but absent in the submonolayer samples.

4. Conclusions

The optical activity of UHV-prepared enantiopure and racemic BINOL films were studied with the nonlinear technique SHG-CD. The SH spectrum of the pristine BK7 substrate was used as in-line reference to compensate for the wavelength dependency of the laser power and the spectrometer function. As discussed, this reference is not suitable for the measured optical activity. Instead it was demonstrated how a racemic film serves as a better reference for the nonlinear anisotropy factor. The SHG spectra in the wavelength range between 225 nm and 340 nm of the films show the known high, middle and low energy bands of BINOL. For the enantiopure films the anisotropy factor follows qualitatively the linear one. A comparison between CD, 2PA-CD and SHG-CD suggests a causality between this similar behavior and the one-photon absorption and emission step between the ground and excited state for CD and SHG-CD. The nonlinear anisotropy factor of SHG-CD is four to five orders of magnitude bigger than the linear one and is a mirror image for the two enantiomers. It reaches values up to 178(2) % at 240 nm in the case of R-BINOL, which is to our knowledge the highest measured in a non-plasmonic system, so far. The SH intensity generated from CP is generally less than from linearly p-polarizations, leading to an overall negative SHG-CLD. Additionally, the SHG-CLD in the range of the middle energy band is different for the enantiopure and racemic film. It was proposed that a difference in stacking between both cases and a resulting difference in the average orientation of the molecule and transition dipole moment is responsible.

With the presented SHG-CD setup the optical activity of UHV-prepared samples can be studied in situ over a wide wavelength range in the UV and in the visible range with submonolayer sensitivity. Although SHG-CD is not limited to UHV studies and the combination of a UHV setup and a laser

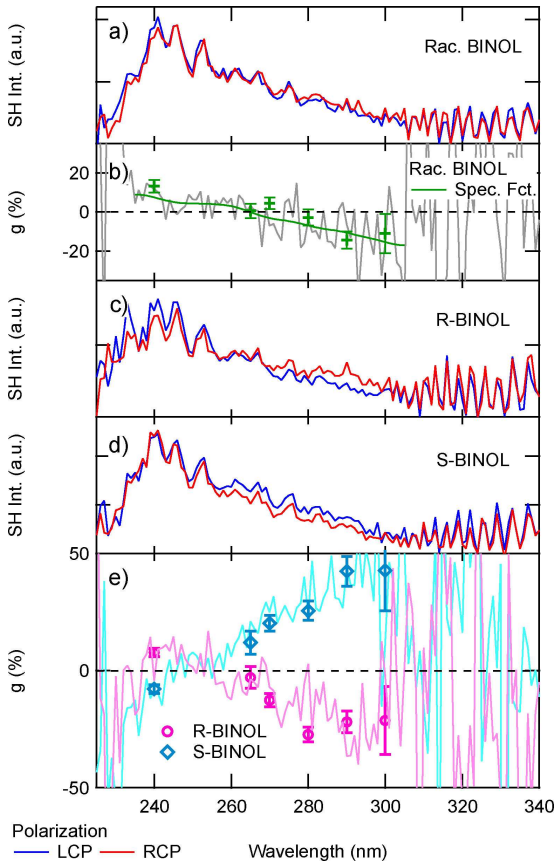

Figure 4. a) SH spectrum from both CPs of racemic BINOL film. b) *g* value for racemic BINOL film and spectrometer function as green curve. c) and d) SH spectra from CPs of R- and S-BINOL. e) *g* value for R- and S-BINOL.

ChemPubSoc Europe

CHEMPHYSCHEM Articles

spectroscopy setup is challenging, it gives the advantage to prepare samples under defined UHV conditions enabling highest control and minimizing contaminations.

We show that SHG-CD can be used to study the optical activity of adsorbates even at coverages well below one monolayer. Qualitatively, the anisotropy factors of the low coverage follow the same trend as in the case of thicker films. Possible reasons for quantitative differences were given.

Acknowledgements

This work has been supported by the DFG through the project HE 3454/21-1.

Conflict of Interest

The authors declare no conflict of interest.

Keywords: circular dichroism · laser spectroscopy · polarized spectroscopy · second-harmonic generation · submonolayer sensitivity

[1] I. Agranat, H. Caner, J. Caldwell, *Nat. Rev. Drug Discovery* **2002**, *1*, 753–768.
[2] S. C. Stinson, *Chem. Eng. News* **2001**, *79*, 79–97.
[3] G. Jannes, V. Dubois, *Chiral Reactions in Heterogeneous Catalysis*, Springer, **1995**.
[4] H.-U. Blaser, B. Pugin, M. Studer, *Chiral Catal. Immobil. Recycl.* **2000**, 1–17.
[5] M. Heitbaum, F. Glorius, I. Escher, *Angew. Chem. Int. Ed.* **2006**, *45*, 4732–4762; *Angew. Chem.* **2006**, *118*, 4850–4881.
[6] S. Chandrasekhar, J. S. Yadav, J. C. Guillemin, P. Lakshmipathi, R. Gree, *Indian J. Chem. Sect. B Org. Med. Chem.* **2002**, *41*, 2116–2128.
[7] M. Studer, H.-U. Blaser, C. Exner, *ChemInform* **2003**, *34*, 45–65.
[8] I. Schrader, S. Neumann, A. Šulce, F. Schmidt, V. Azov, S. Kunz, *ACS Catal.* **2017**, *7*, 3979–3987.
[9] H. Bönnemann, G. A. Braun, *Angew. Chem. Int. Ed. Engl.* **1996**, *35*, 1992–1995.
[10] S. Kunz, *Top. Catal.* **2016**, *59*, 1671–1685.
[11] S. Kunz, P. Schreiber, M. Ludwig, M. M. Maturi, O. Ackermann, M. Tschurl, U. Heiz, *Phys. Chem. Chem. Phys.* **2013**, *15*, 19253–61.
[12] Y. Izumi, *Adv. Catal.* **1983**, *32*, 215–271.
[13] G. Webb, P. B. Wells, *Catal. Today* **1992**, *12*, 319–337.
[14] M. Ortega Lorenzo, C. J. Baddeley, C. Muryn, R. Raval, *Nature* **2000**, *404*, 376.
[15] S. M. Barlow, R. Raval, *Surf. Sci. Rep.* **2003**, *50*, 201–341.
[16] J. Kumar, K. G. Thomas, L. M. Liz-Marzán, *Chem. Commun.* **2016**, *52*, 12555–12569.
[17] C. Gautier, T. Bürgi, *ChemPhysChem* **2009**, *10*, 483–492.
[18] P. D. Jadzinsky, G. Calero, C. J. Ackerson, D. A. Bushnell, R. D. Kornberg, *Science* **2007**, *318*, 430–433.
[19] M. Jakob, A. von Weber, A. Kartouzian, U. Heiz, *Phys. Chem. Chem. Phys.* **2018**, *20*, 20347–20351.
[20] T. G. Schaaff, G. Knight, M. N. Shafigullin, R. F. Borkman, R. L. Whetten, *J. Phys. Chem. B* **1998**, *102*, 10643–10646.
[21] B. M. Maoz, Y. Chaikin, A. B. Tesler, O. Bar Elli, Z. Fan, A. O. Govorov, G. Markovich, *Nano Lett.* **2013**, *13*, 1203–1209.
[22] T. Petralli-Mallow, T. M. Wong, J. D. Byers, H. I. Yee, J. M. Hicks, *J. Phys. Chem.* **1993**, *97*, 1383–1388.
[23] S. Sioncke, T. Verbiest, A. Persoons, *Mater. Sci. Eng. R Reports* **2003**, *42*, 115–155.
[24] C. Toro, L. De Boni, N. Lin, F. Santoro, A. Rizzo, F. E. Hernandez, *Chirality* **2010**, *22*, E202–E210.
[25] D. Wanapun, R. D. Wampler, N. J. Begue, G. J. Simpson, *Chem. Phys. Lett.* **2008**, *455*, 6–12.
[26] Q. L. Zhou, *Privileged Chiral Ligands and Catalysts* **2011**.
[27] J. M. Brunel, *Chem. Rev.* **2007**, *107*, PR1-PR45.
[28] I. Hanazaki, H. Akimoto, *J. Am. Chem. Soc.* **1972**, *94*, 4102–4106.
[29] J. D. Byers, J. M. Hicks, *Chem. Phys. Lett.* **1994**, *231*, 216–224.
[30] S. F. Mason, *Molecular Optical Activity and the Chiral Discriminations*, Cambridge University Press, **1982**.
[31] T. Lünskens, A. Von Weber, M. Jakob, T. Lelaidier, A. Kartouzian, U. Heiz, *J. Phys. Chem. C* **2017**, *121*, 9331–9336.
[32] T. Lelaidier, T. Lunskens, A. von Weber, T. Leoni, A. Ranguis, A. D'Aleo, F. Fages, A. Kartouzian, C. Becker, U. Heiz, *Phys. Chem. Chem. Phys.* **2016**, *18*, 5299–5305.
[33] P. Heister, T. Lunskens, M. Thamer, A. Kartouzian, S. Gerlach, T. Verbiest, U. Heiz, *Phys. Chem. Chem. Phys.* **2014**, *16*, 7299–7306.
[34] T. Lünskens, P. Heister, M. Thämer, C. A. Walenta, A. Kartouzian, U. Heiz, *Phys. Chem. Chem. Phys.* **2015**, *17*, 17541–4.
[35] U. Heiz, F. Vanolli, L. Trento, W. D. Schneider, *Rev. Sci. Instrum.* **1997**, *68*, 1986–1994.
[36] M. Vanbel, S. Vandendriessche, M. A. van der Veen, D. Slavov, P. Heister, R. Paesen, V. K. Valev, M. Ameloot, T. Verbiest, *17th Int. Sch. Quantum Electron. Laser Phys. Appl.* **2013**, *8770*, 87701F.
[37] A. von Weber, D. Hooper, M, Jakob, V. Valev, A. Kartouzian, U. Heiz, *ChemPhysChem* n.d., DOI 10.1002/cphc.201800950.
[38] A. Kartouzian, P. Heister, M. Thämer, S. Gerlach, U. Heiz, *J. Opt. Soc. Am. B* **2013**, *30*, 541–548.
[39] G. Sauerbrey, *Z. Phys.* **1959**, *155*, 206–222.
[40] R. Kuroda, S. F. Mason, *J. Chem. Soc. Perkin Trans. 2* **1981**, 167–170.
[41] J. D. Byers, H. I. Yee, T. Petralli-Mallow, J. M. Hicks, *Phys. Rev. B* **1994**, *49*, 14643–14647.
[42] I. Tinoco, *J. Chem. Phys.* **1975**, *62*, 1006–1009.
[43] C. Toro, L. De Boni, N. Lin, F. Santoro, A. Rizzo, F. E. Hernandez, *Chem. Eur. J.* **2010**, *16*, 3504–3509.

Manuscript received: September 28, 2018
Revised manuscript received: November 5, 2018
Accepted manuscript online: November 7, 2018
Version of record online: November 30, 2018

B Optical and morphological properties of thin films of bis-pyrenyl π-conjugated molecules

Journal Physical Chemistry Chemical Physics, 18(7): 5299-5305, 2016

Authors Tony Lelaidier,[a,b] Tobias Lünskens,[a] Alexander von Weber,[a,b] Thomas Leoni,[b] Alain Ranguis,[b] Anthony D'Aleó,[b] Frédéric Fages,[b] Aras Kartouzian,[a] Conrad Becker[b] and Ulrich Heiz[a]

Affiliations

a Chair of Physical Chemistry, Chemistry Department & Catalysis Research Center, Technical University of Munich

b Aix-Marseille Université, CNRS

Abstract "1,4-Di-n-octyloxy-2,5-bis(pyren-1-ylethenyl)benzene (bis-pyrene) has been studied by the means of surface cavity ring-down (s-CRD) spectroscopy on an amorphous BK7 glass substrate and scanning tunnelling microscopy (STM) on Au(111). Absorption spectra show a modification of the optical properties as a function of coverage, i.e. appearance of a shoulder around 505 nm followed by a saturation of the intensity of this signal observed at higher coverages. We attribute this shoulder to the change of the molecular orientation between the first and the second monolayer and thus to an interfacial effect. These results are confirmed by scanning tunnelling microscopy (STM) measurements where the bis-pyrene molecules have been deposited on Au(111) at room temperature (RT) and onto a cold substrate. Independently of the temperature in the range from 210 K to RT, the first monolayer is always highly organized. At low temperature bis-pyrene molecules constituting the second monolayer are randomly distributed, suggesting that self-organisation is kinetically hindered. Deposited at room temperature, the molecular diffusion is enhanced and the formation of an organized second layer takes place after storing the sample for 150 minutes at room temperature. A HOMO–LUMO gap of 2.85 eV has been determined by scanning tunnelling spectroscopy, which is in very good agreement with the observed optical transition at 434 nm (2.86 eV) in s-CRD spectroscopy."

C Device-Compatible Chiroptical Surfaces through Self-Assembly of Enantiopure Allenes

Journal Langmuir, 34(15): 4548-4553, 2018

Authors A. Ozcelik,[a,#] R. Pereira-Cameselle,[a,#] A. von Weber,[c,#] M. Paszkiewicz,[d,#] M. Carlotti,[e] T. Paintner,[d] L. Zhang,[d] T. Lin,[d] Y.-Q. Zhang,[d] J. V. Barth,[d] T. van den Nobelen,[a] R. C. Chiechi,[e] M. Jakob,[c] U. Heiz,[c] S. Chiussi,[b] A. Kartouzian,[c] F. Klappenberger,[d] and J. L. Alonso-Gòmez[a]

# contributed equally

Affiliations

a Departamento de Química Orgánica and **b** Departamento de Física Aplicada, E. E. Industrial, Universidade de Vigo

c Department of Physical Chemistry, Catalysis Research Center and **d** Physik-Department E20 Technische, Universität München

e Stratingh Institute for Chemistry & Zernike Institute for Advanced Materials, University of Groningen

Abstract "Chiroptical methods have been proven to be superior compared to their achiral counterparts for the structural elucidation of many compounds. To expand the use of chiroptical systems to everyday applications, the development of functional materials exhibiting intense chiroptical responses is essential. Particularly, tailored and robust interfaces compatible with standard device operation conditions are required. Herein, we present the design and synthesis of chiral allenes and their use for the functionalization of gold surfaces. The self-assembly results in a monolayer- thin room-temperature-stable upstanding chiral architecture as ascertained by ellipsometry, X-ray photoelectron spectroscopy, and near-edge X-ray absorption fine structure. Moreover, these nanostructures anchored to device-compatible substrates feature intense chiroptical second harmonic generation. Both straightforward preparation of the device-compatible interfaces along with their chiroptical nature provide major prospects for everyday applications."

LANGMUIR Article
Cite This: Langmuir 2018, 34, 4548−4553 pubs.acs.org/Langmuir

Device-Compatible Chiroptical Surfaces through Self-Assembly of Enantiopure Allenes

A. Ozcelik,[†,#] R. Pereira-Cameselle,[†,#] A. von Weber,[§,#] M. Paszkiewicz,[∥,#] M. Carlotti,[⊥] T. Paintner,[∥] L. Zhang,[∥] T. Lin,[∥] Y.-Q. Zhang,[∥] J. V. Barth,[∥] T. van den Nobelen,[†] R. C. Chiechi,[⊥] M. Jakob,[§] U. Heiz,[§] S. Chiussi,[‡] A. Kartouzian,*[,§] F. Klappenberger,*[,∥] and J. L. Alonso-Gómez*[,†]

[†]Departamento de Química Orgánica and [‡]Departamento de Física Aplicada, E. E. Industrial, Universidade de Vigo, Lagoas-Marcosende s/n, Vigo 36310, Spain

[§]Department of Physical Chemistry, Catalysis Research Center, Technische Universität München, Lichtenbergstr. 4, Garching 85748, Germany

[∥]Physik-Department E20, Technische Universität München, James-Franck-Str. 1, Garching 85748, Germany

[⊥]Stratingh Institute for Chemistry & Zernike Institute for Advanced Materials, University of Groningen, Nijenborgh 4, Groningen 9747 AG, The Netherlands

Supporting Information

ABSTRACT: Chiroptical methods have been proven to be superior compared to their achiral counterparts for the structural elucidation of many compounds. To expand the use of chiroptical systems to everyday applications, the development of functional materials exhibiting intense chiroptical responses is essential. Particularly, tailored and robust interfaces compatible with standard device operation conditions are required. Herein, we present the design and synthesis of chiral allenes and their use for the functionalization of gold surfaces. The self-assembly results in a monolayer-thin room-temperature-stable upstanding chiral architecture as ascertained by ellipsometry, X-ray photoelectron spectroscopy, and near-edge X-ray absorption fine structure. Moreover, these nanostructures anchored to device-compatible substrates feature intense chiroptical second harmonic generation. Both straightforward preparation of the device-compatible interfaces along with their chiroptical nature provide major prospects for everyday applications.

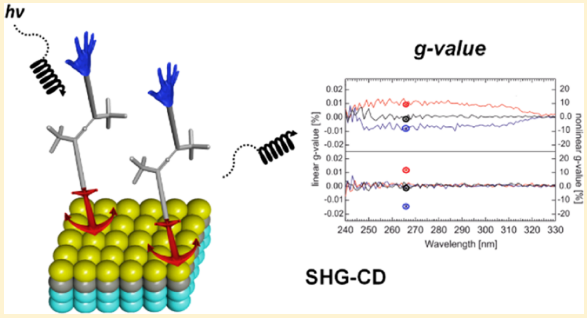

INTRODUCTION

Non-superimposable systems with their mirror images are set to be chiral and may exist in two enantiomeric forms. The two opposite enantiomers of a molecule are indistinguishable when interacting with an achiral entity. However, as in the famous case of thalidomide, when interacting with another chiral entity, they may respond in a different way. Also, light can be chiral, like the case of circularly polarized light. Although a racemic mixture or rac, a 1:1 mixture of two enantiomeric counterparts, is not distinguishable spectroscopically from and achiral system, the opposite response of enantiopure chiral systems when interacting with lights of contrary chirality gives rise to chiroptical spectroscopies.[1,2] These spectroscopies present remarkably high sensitivity to conformational changes and supramolecular interactions. As a consequence, they are routinely used not only for absolute configuration determination[3−5] and conformational assignments[6,7] but also for the characterization of molecular assemblies where at least one of the components is chiral.[8,9] Moreover, a guest molecule may be identified by the characteristic chiroptical responses when forming a complex with a chiral host, a task far from trivial for nonchiral techniques.[1,10] In this regard, there are several studies focused on the design and synthesis of systems presenting enhanced chiroptical responses in the search for applications in solution.[11−15] On the other hand, the construction of chiroptical surfaces is required to develop lab-on-chip devices. However, the limited knowledge regarding the interfacial integration of chiroptical compounds has hampered to date the emergence of chiroptical sensors for everyday use. In that respect, Lakey and co-workers observed folding in a monolayer of a 22 kDa protein domain,[16] and Wälti's group studied the influence of two-dimensional organization on the conformational state in a peptide monolayer using a circular dichroism (CD).[17] Yada and co-workers used the same technique to study the influence of an electric field on oriented films of lipid bilayers.[18] Additionally, Govorov and co-workers have been

Received: January 29, 2018
Revised: March 7, 2018
Published: March 19, 2018

exploring the chiroptical amplification of thick (~10 nm) layers of biomolecules by surface plasmon resonance.[19] However, the complex conformational dynamics and multiple chemical interactions possible for such large molecular systems represent complications with respect to the development of everyday chiroptical applications.

The exploration of chiroptical responses on the surfaces functionalized with a single monolayer of small molecules (<500 Da) for an enhanced conformational control has remained challenging so far. Although the formation of stable interfaces was demonstrated with chiral porphyrins[20] or cyclodextrins,[21] their chiroptical properties remain unexplored.

In contrast to most of the chiral molecules where the chirality comes from chiral centers with notation (*R*) or (*S*) following the Cahn–Ingold–Prelog rules,[22] the chiral axes such as allenes[7,11,15] or spiranes[23,24] with (*P*) of (*M*) configuration have been proven to be useful chiral elements for the construction of systems with remarkable chiroptical responses in solution. With the aim of developing versatile chiroptical surfaces, we have previously investigated the self-assembly of enantiopure (*M*,*M*)-**CF-1** comprising two diethynylallenes on a single crystal surface (Scheme 1a). Under such ideal conditions, we demonstrated the formation of upstanding chiral architectures (UCAs), in which the single chiral molecules are arranged perpendicular to the underlying substrate as two-dimensional nanostructures with the possibilities of postsynthetic modification.[25] However, the weak molecule–substrate interactions hindered the exploration of the chiroptical responses of the formed chiral surfaces at room temperature (RT). Herein, we present the design and synthesis of enantiopure (*P*)-**CF-2** and (*M*)-**CF-2** (Scheme 1) and their use for surface functionalization. The high stability of the formed self-assemblies enabled the construction of monolayer-thin device-compatible interfaces presenting a strong chiroptical second harmonic generation (SHG).

Scheme 1. (a) Structure of (*M*,*M*)-CF-1 Previously Used for Surface Functionalization;[25] (b) Synthesis and Enantiomeric Resolution of (±)-CF-2[a]

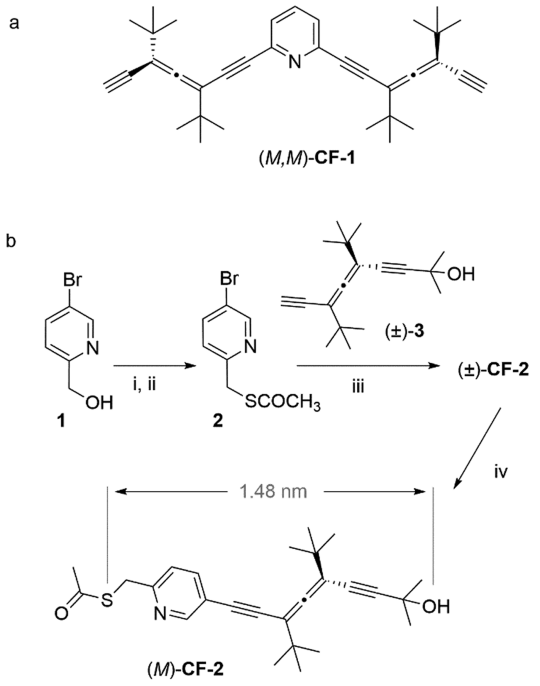

[a]Reagents and conditions: (i) mesyl chloride, Et_3N, CH_2Cl_2, 0–25 °C, 22 h; (ii) CH_3COSK, dimethylformamide, 0–25 °C, 4 h, 80%; (iii) Et_3N, $[Pd(PPh_3)_4]$, tetrahydrofuran, 65 °C, 72 h, 46%; (iv) Chiralpak IA, 96:4 *n*-Hex/i-PrOH, 4.0 mL min^{-1}. The shown length of (*M*)-**CF-2** was predicted at the AM1 level of theory.

RESULTS AND DISCUSSION

The synthesis of (±)-**CF-2** started from alcohol **1**, which was treated with mesyl chloride at 0 °C, and a subsequent treatment with potassium thioacetate in *N*,*N*-dimethylformamide leads to thioacetate pyridine **2** in 80% yield (Scheme 1b). Sonogashira reaction of pyridine **2** with axially chiral diethynylallene (±)-**3** catalyzed by $[Pd(PPh_3)_4]$ with Et_3N in tetrahydrofuran afforded the desired chiral compound (±)-**CF-2**. Enantiomeric resolution was carried out using the chiral stationary phase Chiralpak IA. Assignment of the absolute configuration was performed by comparison of the CD spectrum of (*P*)-**CF-2** synthesized from enantiopure (*P*)-**3** with the two fractions of the enantiomeric resolution. Thermal and photostability of (*M*)-**CF-2** in solution as determined by CD were considered sufficient to employ these chiral molecules for the construction of chiroptical surfaces (for more details, see the Supporting Information (SI)).

Monolayer preparation of enantiopure (*M*)-**CF-2** and (*P*)-**CF-2** and racemate (±)-**CF-2** onto template-stripped Au substrates (AuTS) was performed by immersion in a toluene solution. Ellipsometry data analysis considering a two-layer model showed 1.49 ± 0.12 nm thickness for the monolayer, which is comparable with the predicted length of the molecule plus the Au–S bond (Scheme 1). This supports the fact that the **CF-2** molecules are mostly standing straight up from the substrate at RT as previously proposed for **CF-1** at lower temperatures.

Conductance plots of current–density, *J*, versus potential, *V* are typically used to obtain information regarding the nature and quality of molecular layers. In tunneling junctions, the dependence of *J* on the molecular length, *d*, can be approximated by the equation $J(V) = J_0 e^{-\beta d}$, where J_0 is the injection current and β is the decay coefficient. Because J_0 is defined by the two molecule/electrode interfaces and does not vary significantly between conjugated hydrocarbons, we compared the conductance plots of the self-assembly of (*M*)-**CF-2** with the one of the known self-assembly of *S*,*S*′-(ethyne-1,2-diylbis(4,1-phenylene)) diethanethioate (**OPE2**).[26] Because **OPE2** is a conjugated molecule of comparable length to (*M*)-**CF-2**, the observed overlap between the plots of the two systems is a strong evidence that (*M*)-**CF-2** forms densely packed self-assemblies of upright molecules uniformly bound to the substrate. On the other hand, because allenes may present photoinstability under certain conditions,[27,28] the same measurements were performed during and after light irradiation to evaluate this aspect, with no significant changes observed, suggesting a strong structural stability of the self-assembled (*M*)-**CF-2** monolayers at room temperature (Figure 1, for more information see the SI).

The integrity of the self-assembled **CF-2** molecules after self-assembly was confirmed by the observed C 1s and N 1s X-ray photoelectron spectroscopy (XPS) spectra, each with a single distinguishable peak centered around 285 and 400 eV, respectively (Figure 2a,b). Therefore, no significant degradation

DOI: 10.1021/acs.langmuir.8b00305
Langmuir 2018, 34, 4548–4553

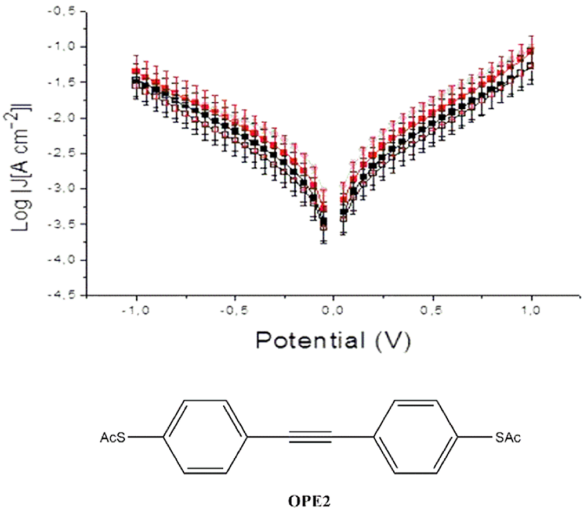

Figure 1. Semilog plot of J vs V for EGaIn/Ga_2O_3//(M)-**CF-2** UCA/AuTS junctions in the dark (black), after illumination in the light (red), and in the dark after illumination step (hollow), and EGaIn/Ga_2O_3//**OPE2**/AuTS junctions (gray). Error bars are per-junction confidence intervals calculated using α = 0.95. The samples were first measured in the dark using a red light source as dim as possible to position the tip on the substrate; they were then irradiated at 256 nm (60 W) for 30 min and measured again in a fully lit environment; finally, the samples were let to rest for 1 h in the dark before being measured again using the initial conditions. UCA stands for upstanding chiral architectures.

to organometallic alkynylic[29,30] or metal−organic pyridinic[31,32] species occurred during preparation (cf. discussion in the SI). The S 2p signature reveals a dominating doublet (green, with S $2p_{3/2}$ component binding energy amounting to 162 eV, Figure 2c) matching nicely with the sulfur reference spectrum of an alkanethiol self-assembled monolayer (SAM) on the same substrate type (C14-S/Au, cf. Figure S11a) and previously reported values,[33−36] thus indicating successful anchoring through thiolate chemisorbed to the Au substrate. The minority species (blue components) is attributed to the presence of an organothiol with a different chemical nature resulting, e.g., from anchoring at step edges or different adsorption configurations. In SAMs constructed from aryl-containing compounds on untreated commercial Au/Mica substrates such features are commonly observed.[37−40] Potentially, the peak could originate from atomic sulfur from cracked molecules or contamination.[41,42] However, this is not likely because the signature of a sample with atomic sulfur is different (see discussion related to Figure S11b in the SI). Noteworthy, the absence of further sulfur peaks, specifically at higher binding energy around 164 eV, indicates the absence of a multilayer formation through the utilized preparation process.[43] Additionally, the O 1s XPS spectrum (Figure 2d) is fitted with one component binding energy of 532 eV, which corresponds to a terminal dimethyl alcohol group.[30] The width of the peak (fwhm = 2.08 eV) is larger than the expected width for a single species (~1.5 eV). We attribute this broadening to the OH groups experiencing different noncovalent interactions with neighboring molecules,[44] consistent with the inhomogeneity of the film indicated by the previous XPS spectra. Overall, these data confirm not only the abstraction of the acetyl moiety and the efficient chemisorption via the thiolate group of (M)-**CF-2** molecules but also the RT stability of the formed UCAs and their persistence under ambient conditions over several days.

For a more structural elucidation, near-edge X-ray absorption fine structure (NEXAFS) N K-edge spectra were taken with three different incident angles θ = 25, 53, and 90° (Figure 2e). The π^*-region (below 404 eV) contains two discernible and differently broadened peaks, thus a richer structure than pure pyridine.[45] The more complex signature is explained by the interaction with the nearby ethynylene π-system and packing effects inducing splitting of resonances and intensity redistribution.[46−48] The spectra exhibit no discernible angular dependence of the first two π^* resonances centered at 399 and 401 eV. A fitting of the leading edge of the experimental spectra with Voigt peaks (Figure S12a) and comparison of the peak intensities to theoretical curves[49] indicate an average adsorption angle α of the pyridine moiety between 50 and 60° (between the normal of the ring plane and the surface normal, Figure S12b), clearly ruling out a flat adsorption geometry as the dominant configuration. On the other hand, the consistent anchoring via the thiol groups rules out a random orientation of the pyridine rings.[50] Thus, even though the quality of the film is inferior to what has been achieved with simple alkene SAMs, the combined X-ray spectroscopic data evidence the formation of a monolayer-thin **CF-2** upstanding chiral architecture and indicate a preferential average inclination of the molecular backbone of approximately 30° (Figure 2f, for more detail see the SI), in accordance with the ellipsometry experiments.

The exploration of chiroptical properties of interfaces is greatly hindered by the small amount of molecules as compared to solution-based setups, rendering the analysis challenging due to the minute amount of the response signal. To improve chiroptical sensitivity, extensive efforts have been made in the development of more sophisticated techniques.[51] In this regard, nonlinear chiral effects have been shown to be up to 3 orders of magnitude larger than the corresponding linear ones.[52−55] To evaluate the chiroptical properties of the **CF-2** self-assemblies, we measure the second harmonic generation circular dichroism (SHG-CD).[52−54,56−58] The corresponding g-values were then calculated according to the following equation (LCP and RCP stand for left and right circularly polarized light, respectively)

$$g_{\mathrm{SHG}} = \frac{\mathrm{SHG_{LCP}} - \mathrm{SHG_{RCP}}}{\left(\frac{\mathrm{SHG_{LCP}} + \mathrm{SHG_{RCP}}}{2}\right)}$$

We observed a 1000-fold magnification of the SHG-CD g-values for monolayer-thin films of (P)-**CF-2** and (M)-**CF-2** molecules compared to the linear CD g-values of **CF-2** in a multilayer or solution. These results enabled the clear observation of the chiroptical response for the developed device-compatible surfaces (Figure 3, see also Figure S2 in the SI).

■ CONCLUSIONS

In conclusion, we have designed and synthesized enantiopure (P)-**CF-2** and (M)-**CF-2** and successfully anchored them to Au surfaces to construct stable upstanding chiral architectures. The self-assembly was verified by means of ellipsometry, XPS, and NEXAFS. More importantly, SHG-CD measurements proved that the afforded molecule-thin sheets possess chiroptical activity. These interfaces were successfully integrated in electronic circuitry, thus demonstrating suitability for optoelectronic devices. The higher accuracy and reliability offered by chiroptical sensing techniques along with the more character-

DOI: 10.1021/acs.langmuir.8b00305
Langmuir 2018, 34, 4548−4553

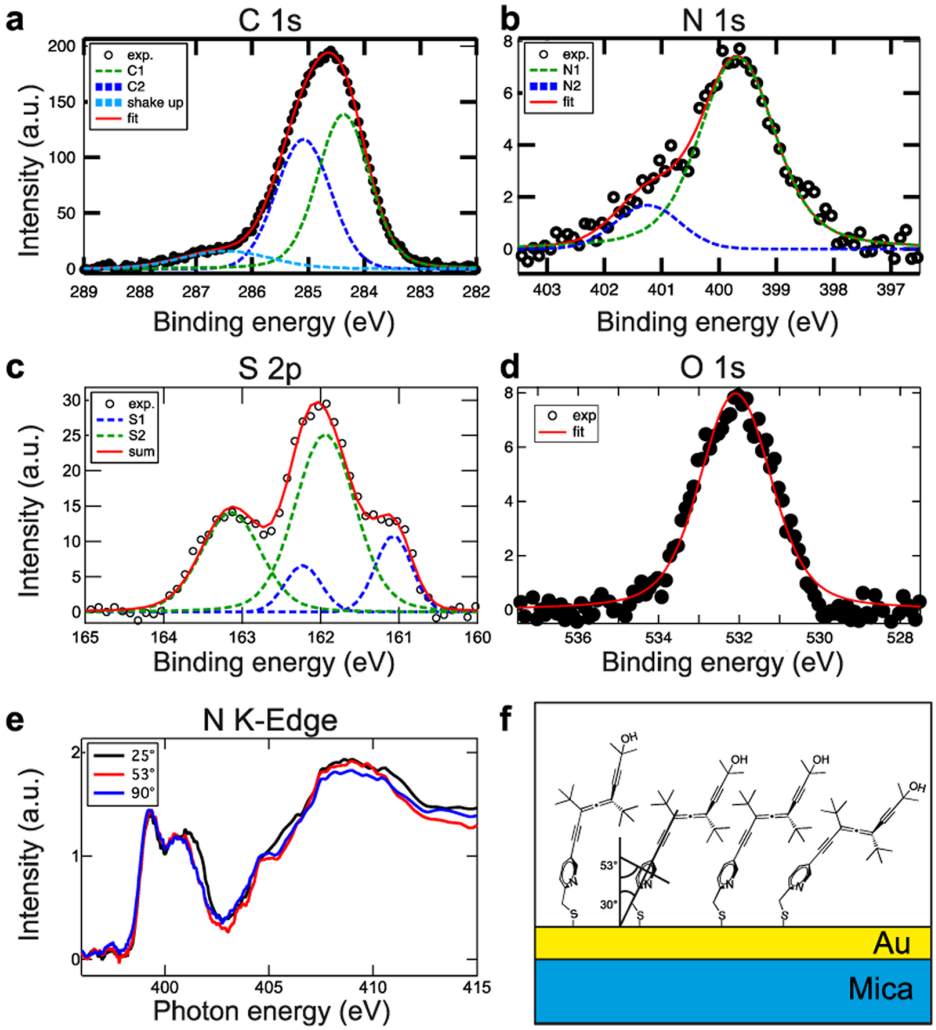

Figure 2. (a–d) XPS spectra of (*M*)-**CF-2** framework on Au/Mica substrate the C 1s, N 1d, S 2p, and O 1s regions are depicted in (a), (b), (c), and (d), respectively. (e) The N K-edge near-edge X-ray absorption fine structure (NEXAFS) signatures recorded with three different incidence angles (25, 53, and 90°). (f) Scheme showing the proposed, approximate orientation of (*M*)-**CF-2** molecules in the upstanding monolayer architecture.

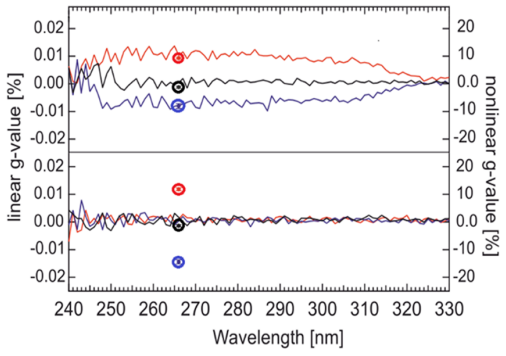

Figure 3. Multilayer (top), as obtained from sublimation of **CF-2** by heating up to 230 °C at 10^{-8} kPa, and monolayer (bottom) circular dichroism (lines, left scales) and second harmonic generation (dots, right scales) measurements of (*M*)-**CF-2** (red) and (*P*)-**CF-2** (blue) upstanding architectures on custom-made transparent substrates (black).

istic signatures related to varying target compounds render upstanding chiral architectures as a promising novel class of robust chiroptical materials. We are currently pursuing nanoparticle stabilization and electric isolation of metal surfaces to develop chiroptical sensing with plasmonic nanoparticles, as well as to control and inhibit corrosion on artworks.

■ ASSOCIATED CONTENT

Supporting Information

The Supporting Information is available free of charge on the ACS Publications website at DOI: 10.1021/acs.langmuir.8b00305.

Experimental procedures, spectral data, and computational study results (PDF)

■ AUTHOR INFORMATION

Corresponding Authors

*E-mail: aras.kartouzian@mytum.de (A.K.).

*E-mail: florian.klappenberger@tum.de (F.K.).

DOI: 10.1021/acs.langmuir.8b00305
Langmuir 2018, 34, 4548–4553

*E-mail: lorenzo@uvigo.es (J.L.A.-G.).

ORCID

M. Carlotti: 0000-0001-8086-7613
R. C. Chiechi: 0000-0002-0895-2095
M. Jakob: 0000-0002-4312-4500
F. Klappenberger: 0000-0002-2877-6105
J. L. Alonso-Gómez: 0000-0002-6107-0120

Author Contributions

#A.O., R.P.-C, A.v.W, and M.P. contributed equally.

Notes

The authors declare no competing financial interest.

■ ACKNOWLEDGMENTS

A. Guerrero-Martínez and J. P. Coelho are acknowledged for the preliminary studies on colloidal nanoparticles. C. Pérez and X. R. Nóvoa are acknowledged for the preliminary studies on corrosion. L. M. Salonen (INL, Portugal) is acknowledged for fruitful discussions. J.L.A.-G. thanks the Spanish Ministerio de Economía y Competitividad for a "Ramón y Cajal" research contract. All the authors are thankful to the Supercomputing Center of Galicia (CESGA) for generous allocation of computer time. This work has been funded by the Spanish Ministerio de Economía y Competitividad (CTQ2013-50575-EXP, CTQ2014-58629-R, and CTQ2015-71924-REDT) and Xunta de Galicia (ED431F 2016/005). The German Research Foundation (DFG) via F.K. (2294/3-1), and via A.K. (HE 3454/21-1) and the Munich-Center for Advanced Photonics (MAP) is gratefully acknowledged. L.Z. was supported by the International Max Planck Research School of Advanced Photon Science (IMPRS-APS). We thank the Helmholtz-Zentrum Berlin for the allocation of synchrotron radiation beamtime and for financial support.

■ REFERENCES

(1) Pescitelli, G.; Di Bari, L.; Berova, N. Application of Electronic Circular Dichroism in the Study of Supramolecular Systems. *Chem. Soc. Rev.* **2014**, *43*, 5211−5233.
(2) Petrovic, A. G.; Navarro-Vázquez, A.; Alonso-Gómez, J. L. From Relative to Absolute Configuration of Complex Natural Products: Interplay Between NMR , ECD , VCD , and ORD Assisted by Ab Initio Calculations. *Curr. Org. Chem.* **2010**, 1612−1628.
(3) Giorgio, E.; Roje, M.; Tanaka, K.; Hamersak, Z.; Sunjic, V.; Nakanishi, K.; Rosini, C.; Berova, N. Determination of the Absolute Configuration of Flexible Molecules by Ab Initio ORD Calculations: A Case Study with Cytoxazones and Isocytoxazones. *J. Org. Chem.* **2005**, *70*, 6557−6563.
(4) Nakanishi, K.; Berova, N.; Polavarapu, P. L.; Woody, R. W. *Comprehensive Chiroptical Spectroscopy*; Instrumentation, Methodologies, and Theoretical Simulations; Wiley-VCH Verlag, 2013; Vol. *1*.
(5) Petrovic, A. G.; Berova, N.; Alonso-Gómez, J. L. *Structure Elucidation in Organic Chemistry*; Cid, M.-M., Bravo, J., Eds.; Wiley-VCH Verlag GmbH & Co. KGaA: Weinheim, Germany, 2015.
(6) Alonso-Gómez, J. L.; Petrovic, A. G.; Harada, N.; Rivera-Fuentes, P.; Berova, N.; Diederich, F. Chiral Induction from Allenes into Twisted 1,1,4,4-Tetracyanobuta-1,3-Dienes (TCBDs): Conformational Assignment by Circular Dichroism Spectroscopy. *Chem. - Eur. J.* **2009**, *15*, 8396−8400.
(7) Rivera-Fuentes, P.; Alonso-Gómez, J. L.; Petrovic, A. G.; Santoro, F.; Harada, N.; Berova, N.; Diederich, F. Amplification of Chirality in Monodisperse, Enantiopure Alleno-Acetylenic Oligomers. *Angew. Chem., Int. Ed.* **2010**, *49*, 2247−2250.
(8) Gropp, C.; Trapp, N.; Diederich, F. Alleno-Acetylenic Cage (AAC) Receptors: Chiroptical Switching and Enantioselective Complexation of Trans-1,2-Dimethylcyclohexane in a Diaxial Conformation. *Angew. Chem., Int. Ed.* **2016**, *55*, 14444−14449.
(9) Gidron, O.; Ebert, M.-O. O.; Trapp, N.; Diederich, F. Chiroptical Detection of Nonchromophoric, Achiral Guests by Enantiopure Alleno-Acetylenic Helicages. *Angew. Chem., Int. Ed.* **2014**, *53*, 13614−13618.
(10) Mineo, P.; Micali, N.; Villari, V.; Donato, M. G.; Scamporrino, E. Reading of Protein Surfaces in the Native State at Micromolar Concentrations by a Chirogenetic Porphyrin Probe. *Chem. - Eur. J.* **2012**, *18*, 12452−12457.
(11) Alonso-Gómez, J. L.; Rivera-Fuentes, P.; Harada, N.; Berova, N.; Diederich, F. An Enantiomerically Pure Alleno-Acetylenic Macrocycle: Synthesis and Rationalization of Its Outstanding Chiroptical Response. *Angew. Chem., Int. Ed.* **2009**, *48*, 5545−5548.
(12) Míguez-Lago, S.; Cid, M. M.; Alonso-Gómez, J. L. Covalent Organic Helical Cages as Sandwich Compound Containers. *Eur. J. Org. Chem.* **2016**, *2016*, 5716−5721.
(13) Walters, R. S.; Kraml, C. M.; Byrne, N.; Ho, D. M.; Qin, Q.; Coughlin, F. J.; Bernhard, S.; Pascal, R. A. Configurationally Stable Longitudinally Twisted Polycyclic Aromatic Compounds. *J. Am. Chem. Soc.* **2008**, *130*, 16435−16441.
(14) Dougherty, K. J.; Kraml, C. M.; Byrne, N.; Porras, J. A.; Bernhard, S.; Mague, J. T.; Pascal, R. A. Helical Mesobenzanthrones: A Class of Highly Luminescent Helicenes. *Tetrahedron* **2015**, *71*, 1694−1699.
(15) Míguez-Lago, S.; Llamas-Saiz, A. L.; Magdalena Cid, M.; Alonso-Gómez, J. L. A Covalent Organic Helical Cage with Remarkable Chiroptical Amplification. *Chem. - Eur. J.* **2015**, *21*, 18085−18088.
(16) Keegan, N.; Wright, N. G.; Lakey, J. H. Circular Dichroism Spectroscopy of Folding in a Protein Monolayer. *Angew. Chem., Int. Ed.* **2005**, *44*, 4801−4804.
(17) White, S. J.; Johnson, S. D.; Sellick, M. A.; Bronowska, A.; Stockley, P. G.; Wälti, C. The Influence of Two-Dimensional Organization on Peptide Conformation. *Angew. Chem., Int. Ed.* **2015**, *54*, 974−978.
(18) Fiche, J. B.; Laredo, T.; Tanchak, O.; Lipkowski, J.; Dutcher, J. R.; Yada, R. Y. Influence of an Electric Field on Oriented Films of DMPC/gramicidin Bilayers: A Circular Dichroism Study. *Langmuir* **2010**, *26*, 1057−1066.
(19) Maoz, B. M.; Chaikin, Y.; Tesler, A. B.; Elli, O. B.; Fan, Z.; Govorov, A. O.; Markovich, G. Amplification of Chiroptical Activity of Chiral Biomolecules by Surface Plasmons. *Nano Lett.* **2013**, *13*, 1203−1209.
(20) Paolesse, R.; Monti, D.; La Monica, L.; Venanzi, M.; Froiio, A.; Nardis, S.; Di Natale, C.; Martinelli, E.; D'Amico, A. Preparation and Self-Assembly of Chiral Porphyrin Diads on the Gold Electrodes of Quartz Crystal Microbalances: A Novel Potential Approach to the Development of Enantioselective Chemical Sensors. *Chem. - Eur. J.* **2002**, *8*, 2476−2483.
(21) Luo, M. L.; Zhang, W. G.; Zhang, S.; Fan, J.; Su, W. C.; Yin, X. Self-Assembly and Chiral Recognition of Quartz Crystal Microbalance Chiral Sensor. *Chirality* **2010**, *22*, 411−415.
(22) Cahn, R. S.; Ingold, C.; Prelog, V. Specification of Molecular Chirality. *Angew. Chem., Int. Ed. Engl.* **1966**, *5*, 385−415.
(23) Castro-Fernández, S.; Cid, M. M.; Alonso-Gómez, J. L.; Silva López, C.; et al. Opening Access to New Chiral Macrocycles: From Allenes to Spiranes. *J. Phys. Chem. A* **2015**, 1747−1753.
(24) Castro-Fernández, S.; Yang, R.; García, A. P.; Garzón, I. L.; Xu, H.; Petrovic, A. G.; Alonso-Gómez, J. L. Diverse Chiral Scaffolds from Diethynylspiranes: All-Carbon Double Helices and Flexible Shape-Persistent Macrocycles. *Chem. - Eur. J.* **2017**, *23*, 11747−11751.
(25) Zhang, Y.-Q.; Oner, M. A.; Cirera, B.; Palma, C.-A.; Castro-Fernández, S.; Míguez-Lago, S.; Cid, M. M.; Barth, J. V.; Alonso-Gómez, J. L.; Klappenberger, F.; et al. Morphological Self-Assembly of Enantiopure Allenes for Upstanding Chiral Architectures at Interfaces. *Chem. Commun.* **2014**, *50*, 15022−15025.
(26) Valkenier, H.; Huisman, E. H.; van Hal, P. A.; de Leeuw, D. M.; Chiechi, R. C.; Hummelen, J. C. Formation of High-Quality Self-

DOI: 10.1021/acs.langmuir.8b00305
Langmuir 2018, 34, 4548−4553

Assembled Monolayers of Conjugated Dithiols on Gold: Base Matters. *J. Am. Chem. Soc.* **2011**, *133*, 4930−4939.
(27) Odermatt, S.; Alonso-Gómez, J. L.; Seiler, P.; Cid, M. M.; Diederich, F. Shape-Persistent Chiral Alleno-Acetylenic Macrocycles and Cyclophanes by Acetylenic Scaffolding with 1,3-Diethynylallenes. *Angew. Chem. Int. Ed.* **2005**, *44*, 5074−5078.
(28) Alonso-Gómez, J. L.; Schanen, P.; Rivera-Fuentes, P.; Seiler, P.; Diederich, F. 1,3-Diethynylallenes (DEAs): Enantioselective Synthesis, Absolute Configuration, and Chiral Induction in 1,1,4,4-Tetracyanobuta-1,3-Dienes (TCBDs). *Chem. - Eur. J.* **2008**, *14*, 10564−10568.
(29) Zhang, Y.-Q.; Kepčija, N.; Kleinschrodt, M.; Diller, K.; Fischer, S.; Papageorgiou, A. C.; Allegretti, F.; Björk, J.; Klyatskaya, S.; Klappenberger, F.; Ruben, M.; Barth, J. V. Homo-Coupling of Terminal Alkynes on a Noble Metal Surface. *Nat. Commun.* **2012**, *3*, No. 1286.
(30) Gleason, N.; Guevremont, J.; Zaera, F. Thermal Chemistry of 2-Propanol and 2-Propyl Iodide on Clean and Oxygen-Pretreated Ni(100) Single-Crystal Surfaces. *J. Phys. Chem. B* **2003**, *107*, 11133−11141.
(31) Klappenberger, F.; Weber-Bargioni, A.; Auwärter, W.; Marschall, M.; Schiffrin, A.; Barth, J. V. Temperature Dependence of Conformation, Chemical State, and Metal-Directed Assembly of Tetrapyridyl-Porphyrin on Cu(111). *J. Chem. Phys.* **2008**, *129*, No. 214702.
(32) Li, Y.; Xiao, J.; Shubina, T. E.; Chen, M.; Shi, Z.; Schmid, M.; Steinrück, H.-P.; Gottfried, J. M.; Lin, N. Coordination and Metalation Bifunctionality of Cu with 5,10,15,20-Tetra(4-Pyridyl)porphyrin: Toward a Mixed-Valence Two-Dimensional Coordination Network. *J. Am. Chem. Soc.* **2012**, *134*, 6401−6408.
(33) Cavalleri, O.; Gonella, G.; Terreni, S.; Vignolo, M.; Floreano, L.; Morgante, A.; Canepa, M.; Rolandi, R. High Resolution X-Ray Photoelectron Spectroscopy of L-Cysteine Self-Assembled Films. *Phys. Chem. Chem. Phys.* **2004**, *6*, 4042−4046.
(34) Fischer, S.; Papageorgiou, A. C.; Marschall, M.; Reichert, J.; Diller, K.; Klappenberger, F.; Allegretti, F.; Nefedov, A.; Wöll, C.; Barth, J. V. L -Cysteine on Ag(111): A Combined STM and X-Ray Spectroscopy Study of Anchorage and Deprotonation. *J. Phys. Chem. C* **2012**, *116*, 20356−20362.
(35) Zharnikov, M.; Grunze, M. Spectroscopic Characterization of Thiol-Derived Self-Assembling Monolayers. *J. Phys.: Condens. Matter* **2001**, *13*, 11333−11365.
(36) Cyganik, P.; Buck, M.; Strunskus, T.; Shaporenko, A.; Wilton-Ely, J. D. E. T.; Zharnikov, M.; Wöll, C. Competition as a Design Concept: Polymorphism in Self-Assembled Monolayers of Biphenyl-Based Thiols. *J. Am. Chem. Soc.* **2006**, *128*, 13868−13878.
(37) Luo, Y.; Bernien, M.; Krüger, A.; Hermanns, C. F.; Miguel, J.; Chang, Y.-M.; Jaekel, S.; Kuch, W.; Haag, R. In Situ Hydrolysis of Imine Derivatives on Au(111) for the Formation of Aromatic Mixed Self-Assembled Monolayers: Multitechnique Analysis of This Tunable Surface Modification. *Langmuir* **2012**, *28*, 358−366.
(38) Shaporenko, A.; Terfort, A.; Grunze, M.; Zharnikov, M. A Detailed Analysis of the Photoemission Spectra of Basic Thioaromatic Monolayers on Noble Metal Substrates. *J. Electron Spectrosc. Relat. Phenom.* **2006**, *151*, 45−51.
(39) Weidner, T.; Krämer, A.; Bruhn, C.; Zharnikov, M.; Shaporenko, A.; Siemeling, U.; Träger, F. Novel Tripod Ligands for Prickly Self-Assembled Monolayers. *Dalton Trans.* **2006**, 2767−2777.
(40) Chesneau, F.; Zhao, J.; Shen, C.; Buck, M.; Zharnikov, M. Adsorption of Long-Chain Alkanethiols on Au(111): A Look from the Substrate by High Resolution X-Ray Photoelectron Spectroscopy. *J. Phys. Chem. C* **2010**, *114*, 7112−7119.
(41) Buckley, A. N.; Hamilton, I. C.; Woods, R. An Investigation of the sulphur(-II)/sulphur(0) System on Bold Electrodes. *J. Electroanal. Chem. Interfacial Electrochem.* **1987**, *216*, 213−227.
(42) Yang, Y. W.; Fan, L. J. High-Resolution XPS Study of Decanethiol on Au(111): Single Sulfur-Gold Bonding Interaction. *Langmuir* **2002**, *18*, 1157−1164.
(43) Weckenmann, U.; Mittler, S.; Naumann, K.; Fischer, R. A. Ordered Self-Assembled Monolayers of 4,4′-Biphenyldithiol on Polycrystalline Silver: Suppression of Multilayer Formation by Addition of Tri-N-Butylphosphine. *Langmuir* **2002**, *18*, 5479−5486.
(44) Cossaro, A.; Puppin, M.; Cvetko, D.; Kladnik, G.; Verdini, A.; Coreno, M.; de Simone, M.; Floreano, L.; Morgante, A. Tailoring SAM-on-SAM Formation. *J. Phys. Chem. Lett.* **2011**, *2*, 3124−3129.
(45) Kolczewski, C.; Püttner, R.; Plashkevych, O.; Ågren, H.; Staemmler, V.; Martins, M.; Snell, G.; Schlachter, A. S.; Sant'Anna, M.; Kaindl, G.; Pettersson, L. G. M. Detailed Study of Pyridine at the C1 *S* and N1 *S* Ionization Thresholds: The Influence of the Vibrational Fine Structure. *J. Chem. Phys.* **2001**, *115*, 6426−6437.
(46) Carniato, S.; Ilakovac, V.; Gallet, J.-J.; Kukk, E.; Luo, Y. Hybrid Density-Functional Theory Calculations of near-Edge X-Ray Absorption Fine-Structure Spectra: Applications on Benzonitrile in Gas Phase. *Phys. Rev. A* **2005**, *71*, No. 22511.
(47) Liu, J.; Schüpbach, B.; Bashir, A.; Shekhah, O.; Nefedov, A.; Kind, M.; Terfort, A.; Wöll, C. Structural Characterization of Self-Assembled Monolayers of Pyridine-Terminated Thiolates on Gold. *Phys. Chem. Chem. Phys.* **2010**, *12*, 4459.
(48) Zhang, Y.-Q.; Björk, J.; Weber, P.; Hellwig, R.; Diller, K.; Papageorgiou, A. C.; Oh, S. C.; Fischer, S.; Allegretti, F.; Klyatskaya, S.; Ruben, M.; Barth, J. V.; Klappenberger, F. Unusual Deprotonated Alkynyl Hydrogen Bonding in Metal-Supported Hydrocarbon Assembly. *J. Phys. Chem. C* **2015**, *119*, 9669−9679.
(49) Stöhr, J.; Outka, D. A. Determination of Molecular Orientations on Surfaces from the Angular Dependence of near-Edge X-Ray-Absorption Fine-Structure Spectra. *Phys. Rev. B* **1987**, *36*, 7891−7905.
(50) Klappenberger, F.; Kühne, D.; Marschall, M.; Neppl, S.; Krenner, W.; Nefedov, A.; Strunskus, T.; Fink, K.; Wöll, C.; Klyatskaya, S.; Fuhr, O.; Ruben, M.; Barth, J. V. Uniform π-System Alignment in Thin Films of Template-Grown Dicarbonitrile-Oligophenyls. *Adv. Funct. Mater.* **2011**, *21*, 1631−1642.
(51) Sofikitis, D.; Bougas, L.; Katsoprinakis, G. E.; Spiliotis, A. K.; Loppinet, B.; Rakitzis, T. P. Evanescent-Wave and Ambient Chiral Sensing by Signal-Reversing Cavity Ringdown Polarimetry. *Nature* **2014**, *514*, 76−79.
(52) Heister, P.; Lünskens, T.; Thämer, M.; Kartouzian, A.; Gerlach, S.; Verbiest, T.; Heiz, U. Orientational Changes of Supported Chiral 2,2′-Dihydroxy-1,1′binaphthyl Molecules. *Phys. Chem. Chem. Phys.* **2014**, *16*, 7299−7306.
(53) Thämer, M.; Kartouzian, A.; Heister, P.; Gerlach, S.; Tschurl, M.; Boesl, U.; Heiz, U. Linear and Nonlinear Laser Spectroscopy of Surface Adsorbates with Sub-Monolayer Sensitivity. *J. Phys. Chem. C* **2012**, *116*, 8642−8648.
(54) Kartouzian, A.; Heister, P.; Thämer, M.; Gerlach, S.; Heiz, U. In-Line Reference Measurement for Surface Second Harmonic Generation Spectroscopy. *J. Opt. Soc. Am. B* **2013**, *30*, 541−548.
(55) Byers, J. D.; Yee, H. I.; Petralli-Mallow, T.; Hicks, J. M. Second-Harmonic Generation Circular-Dichroism Spectroscopy from Chiral Monolayers. *Phys. Rev. B* **1994**, *49*, 14643−14647.
(56) Thämer, M.; Kartouzian, A.; Heister, P.; Lünskens, T.; Gerlach, S.; Heiz, U. Small Supported Plasmonic Silver Clusters. *Small* **2014**, *10*, 2340−2344.
(57) Lünskens, T.; Heister, P.; Thämer, M.; Walenta, C. A.; Kartouzian, A.; Heiz, U. Plasmons in Supported Size-Selected Silver Nanoclusters. *Phys. Chem. Chem. Phys.* **2015**, *17*, 17541−17544.
(58) Lünskens, T.; Walenta, C. A.; Heister, P.; Kartouzian, A.; Heiz, U. Surface Oxidation of Supported, Size-Selected Silver Clusters. *J. Cluster Sci.* **2017**, 3185−3192.

DOI: 10.1021/acs.langmuir.8b00305
Langmuir 2018, 34, 4548−4553

D Circular Dichroism and Isotropy - Polarity Reversal of Ellipticity in Molecular Films of 1,1′-Bi-2-Naphtol

Journal ChemPhysChem, 20(1): 62-69, 2019

Authors Alexander von Weber,[a] David C. Hooper,[b,c] Matthias Jakob,[a] Ventsislav K. Valev,[b,c] Aras Kartouzian,[a] and Ueli Heiz[a]

Affiliations

a Chair of Physical Chemistry, Chemistry Department & Catalysis Research Center, Technical University of Munich

b Centre for Photonics and Photonic Materials and **c** Centre for Nanoscience and Nanotechnology, Department of Physics, University of Bath

Abstract "We have studied the circular dichroism (CD), in the ultraviolet and visible regions, of the transparent, chiral molecule 1,1'-Bi-2-naphtol (BINOL) in 1.5 µm thick films. The initial transparent film shows an additional negative cotton effect in the CD compared to solution. With time under room temperature the film undergoes a structural phase transition. This goes hand in hand with a cotton effect at the low energy absorption band which inverts with opposite propagation direction of light through the film which is revealed as a polarity reversal of ellipticity (PRE). After completion of the phase transition the film exhibits circular differential scattering throughout the visible range which also shows PRE. The structure change was studied with Raman, microscopy under cross polarization conditions and nonlinear second-harmonic generation circular dichroism (SHG-CD). The superposition of the optical activity of individual molecules and isotropy effects makes an interpretation challenging. Yet overcoming this challenge by finding a suitable model structural information can be derived from CD measurements."

ChemPubSoc Europe
DOI: 10.1002/cphc.201800950
CHEMPHYSCHEM Articles

Circular Dichroism and Isotropy – Polarity Reversal of Ellipticity in Molecular Films of 1,1′-Bi-2-Naphtol

Alexander von Weber,[a] David C. Hooper,[b, c] Matthias Jakob,[a] Ventsislav K. Valev,[b, c] Aras Kartouzian,*[a] and Ueli Heiz[a]

We have studied the circular dichroism (CD), in the ultraviolet and visible regions, of the transparent, chiral molecule 1,1′-Bi-2-naphtol (BINOL) in 1.5 μm thick films. The initial transparent film shows an additional negative cotton effect in the CD compared to solution. With time under room temperature the film undergoes a structural phase transition. This goes hand in hand with a cotton effect at the low energy absorption band which inverts with opposite propagation direction of light through the film which is revealed as a polarity reversal of ellipticity (PRE). After completion of the phase transition the film exhibits circular differential scattering throughout the visible range which also shows PRE. The structure change was studied with Raman, microscopy under cross polarization conditions and nonlinear second-harmonic generation circular dichroism (SHG-CD). The superposition of the optical activity of individual molecules and isotropy effects makes an interpretation challenging. Yet overcoming this challenge by finding a suitable model structural information can be derived from CD measurements.

1. Introduction

If light travels through optically active media, its linearly polarized plane rotates, which is called optical rotatory dispersion (ORD). This is described by a difference between the real parts of the indices of refraction for left-/right-handed circularly polarized light. In an adsorptive, chiral medium this is accompanied by a difference in absorption of left and right circularly polarized light, which is known as circular dichroism (CD).[1] The optical activity is caused by chiral molecules within the medium and additionally it can also originate from structural properties. This superposition makes an interpretation more challenging in comparison to solution. However, if the individual contributions can be assigned and understood, additional information about the structure can be derived. Within this work, correlations between optical activity and structural properties are studied to bring further insight to this topic.

One effect related to structural properties is called polarity reversal of ellipticity (PRE). It describes the inversion in sign of the optical activity when light propagates in the opposite direction through the medium. This antisymmetric behavior breaks time reversal symmetry and the Lorentz reciprocity and is commonly known from magneto-optical effects like the Faraday effect. There an external magnetic field results in a magnetization direction within the medium which determines the ellipticity.

Recently metamaterials were presented where PRE was observed through enantiomerically sensitive plasmonic excitations in the absence of an external magnetic field and described as asymmetric transmission.[2] PRE was also studied in chiral double-layer meta-interfaces of chiral, transparent molecules and nonchiral, absorptive molecules. The effect was explained by a virtual magnetic field connected to a different index of refraction for both propagation directions.[3]

Within this work two independent PRE effects of enantiopure 1,1′-Bi-2-naphtol (BINOL) films are observed. BINOL consists of two 2-naphthol units connected through a C–C bond. The planes of the two 2-naphtol units are angled towards each other resulting in an overall axial chirality, see Figure 1. BINOL and its derivatives possess a high relevance as chiral ligands and modifiers and was therefore chosen as a model molecule.[4,5] The system neither possesses a meta-interface nor a plasmonic character and therefore presents an alternative material exhibiting PRE. The effects' nature as well as the connected film structure is investigated.

Experimental Section

The samples were prepared by evaporation of enantiopure (R)-/(S)-BINOL on BK7 substrates or on silicon wafer with an artificial oxide layer in the case of the SHG-CD and cross polarization measurement. The 150 μm thick substrates were cleaned with spectroscopic clean acetone and then sputtered with Ar^+ under ultra-high vacuum (UHV) conditions. Afterwards the BINOL was evaporated on the glass substrate under high vacuum conditions. The substrate was kept at room temperature during the evaporation and the

[a] A. von Weber, M. Jakob, Dr. A. Kartouzian, Prof. U. Heiz
Chair of Physical Chemistry, Chemistry Department & Catalysis Research Center, Technical University of Munich, Lichtenbergstr. 4, D-85748 Garching, Germany
E-mail: aras.kartouzian@mytum.de
[b] D. C. Hooper, Dr. V. K. Valev
Centre for Photonics and Photonic Materials, Department of Physics, University of Bath, Claverton Down, Bath, BA2 7AY, United Kingdom
[c] D. C. Hooper, Dr. V. K. Valev
Centre for Nanoscience and Nanotechnology, Department of Physics, University of Bath, Claverton Down, Bath, BA2 7AY, United Kingdom

Supporting information for this article is available on the WWW under https://doi.org/10.1002/cphc.201800950

ChemPubSoc Europe
CHEMPHYSCHEM Articles

experiments. The details of the used vacuum setup are described elsewhere.[6]

A J-815 CD-spectrometer was used to acquire the extinction and CD spectra between 300 nm and 500 nm with the sample surface plane perpendicular to the light path. The spectra were taken in two geometries. In the first, light enters the BINOL film and then the glass substrate. Which is referred to as "R/S-BINOL ▷ BK7". In the second case the sample is flipped 180 and light hits the glass first which is labeled as "BK7 ▷ R/S-BINOL". For a better understanding the geometric configuration is sketched in Figure 1. It was taken care that the same circular region with a diameter of ca. 13 mm of the sample was probed in both directions.

The SHG-CD experiments were done in reflection mode with a 45 angle of incidence. Left and right circularly polarized light of a fs laser system at 800 nm was focused on the sample while the sample was rotated around the surface normal. Light intensity of the second harmonic (SH) with a wavelength of 400 nm, which was generated at the sample, was detected by a photomultiplier tube. A detailed description of the setup is given elsewhere.[7]

Raman spectra were obtained with an inVia Qontor Raman microscope from Renishaw where an excitation wavelength of 633 nm was chosen.

Darkfield and cross polarization measurements were carried out with a Zeiss Axio Imager M2 microscope and additional absorption measurements in diffusive transmittance with a Lambda 650 spectrophotometer from BerkinElmer equipped with an Ulbricht sphere.

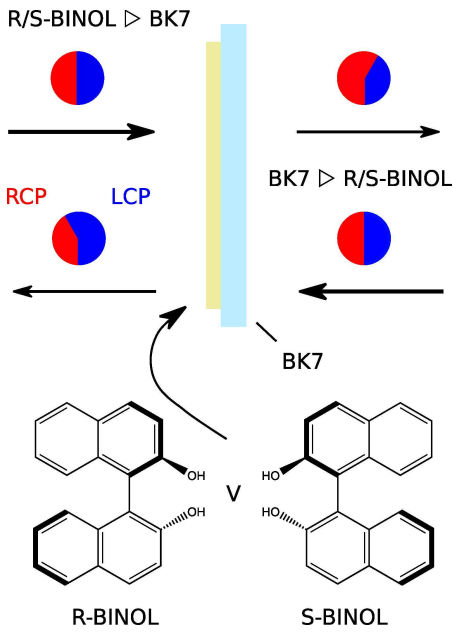

Figure 1. Experimental geometry including label for both light propagation direction configurations.

2. Results and Discussion

2.1. Linear Optical Activity

As a starting point and for comparison the extinction and CD of R-BINOL dissolved in ethanol were measured and are shown in Figure 2a. The extinction shows the low energy band (LEB) of

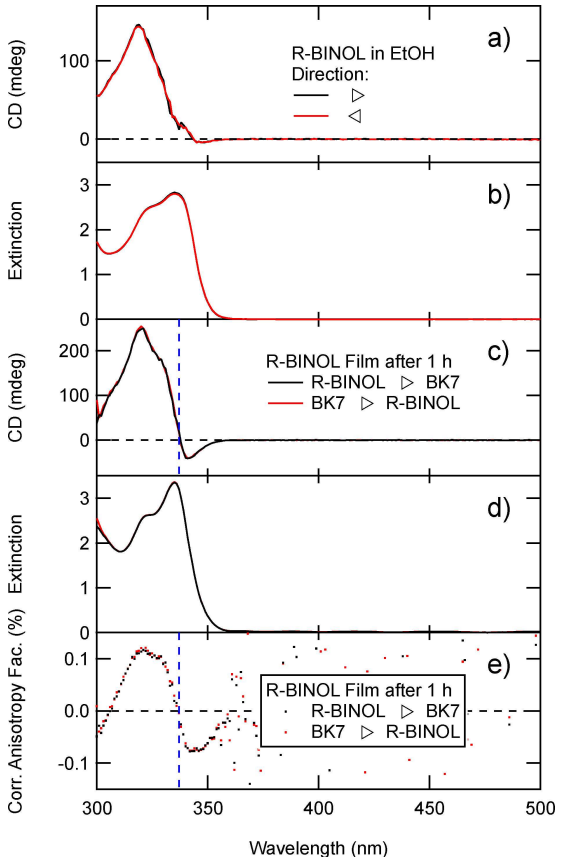

Figure 2. CD (a) and extinction (b) spectrum for both propagation directions of R-BINOL in EtOH and as film 1 h after evaporation (c), (d). Difference in anisotropy factor (e).

the long-axis polarization of both naphtol molecules as building block of BINOL. Due to coupling of the excited states of both naphtols an exciton-split state is formed resulting in two transitions from a common ground state.[8,9] This low energy band shows a positive band in the CD spectrum for the R enantiomer. Above ca. 360 nm the solution is fully transparent and shows no extinction nor optical activity. Both extinction and CD are invariant under sample rotation. The extinction and CD spectra of both enantiomers at smaller wavelength in solution is shown in Figure S1. A comparison to previously reported spectra proves their optical purity.[10]

Immediately after the evaporation the samples were taken out of the UHV system. They were fully transparent by eye (see

ChemPubSoc Europe
CHEMPHYSCHEM Articles

Figure S2a). The extinction and CD were measured 1 h after the evaporation for the first time and are shown in Figure 2b. The extinction shows the known LEB with a positive band in the CD spectrum and no activity above 360 nm. Additionally, the CD spectrum shows a negative feature at the flank of the band in the range between 325 nm and 360 nm. To isolate the effect the anisotropy factor of the solution is subtracted from one of the evaporated samples (Figure 2c). The anisotropy factor is equal the difference in absorption between left and right handed circularly polarized light weighted with the absorption resulting in a dimensionless quantity which is independent of concentration.[1] It reveals that this feature is a negative cotton effect with its crossing point at 337 nm. Again, the extinction and the CD of the initial, transparent film are invariant under sample rotation.

The film thickness was estimated to be 1.5 μm based on the interference pattern in the extinction spectrum (Figure S3) near the absorption edge and independently the measured loading on a quartz crystal microbalance (Figure S4).

Several effects are likely to cause the difference in optical activity between solution and film, appearing as cotton effect in the latter case. First, a solvent effect that is absent in the film. Second, an interaction between neighboring molecules in the means of e.g. dipole-dipole interactions. Third, the dihedral angel between the naphtol monomers is different and known to influence the optical activity.[11] In solution it is about 90 .[12] In crystalline form depending on the crystal structure, it can adopt values between 68.6 [13] (racemic, flat, diamond shaped) and 103.1 [14] (chiral, tetragonal bipyramidal). Because the films were prepared from enantiopure BINOL, only the latter would be possible.

After 6 hours at room temperature small white spots were visible by eye in the film (see Figure S2b). The appearance of white spots is an indication of a restructuring within the film beginning from multiple seeds. The extinction and the CD at this state is given in Figure 3a. Compared to the 1 h old sample the extinction has not changed. However, the CD spectrum shows a new feature in the region of the absorption bands flank between 335 nm and 360 nm. To focus on this effect, the CD of the 1 h old sample is subtracted (Figure 3b) and smoothed curves are shown as solid line. The difference in CD shows a negative cotton effect with an asymmetry in width and magnitude left and right from the crossing point at 340 nm in the "R/S-BINOL ▷ BK7" geometry. While the body of the CD band stays invariant under sample rotation the feature changes into a positive cotton effect when the light first hits the glass, i.e. PRE.

The appearance is unambiguously connected to a restructuring within the film. Decomposition or other effects can be excluded because both absorption and CD were unchanged except the new feature and furthermore BINOL is known to be stable in air and at room temperature. Therefore, the new feature at 340 nm is likely related to the observed beginning of a restructuring. In the course of such a structural change the molecules are reorientating in general and especially also towards each other. Accordingly, it is proposed that the effect is caused by interactions between neighboring molecules via

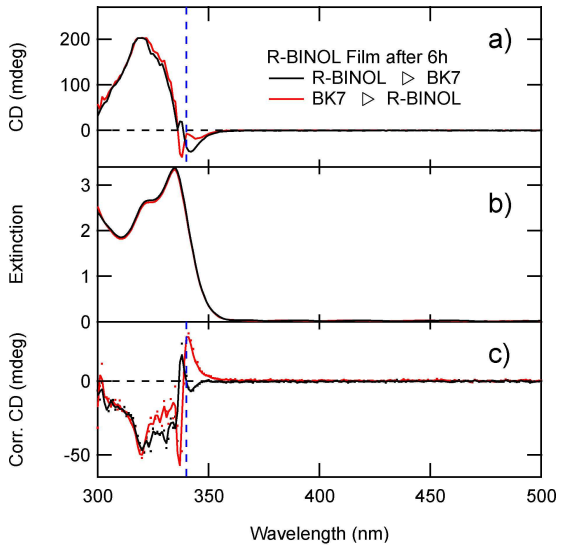

Figure 3. CD (a) and extinction (b) spectrum for both propagation directions of R-BINOL film 6 h after evaporation and difference in CD between 6 h and 1 h (c).

dipole-dipole interactions. This cotton effect has also been observed in vitrified liquid crystalline films of chiral polyfluorene.[15] But it has not been investigated in the sense of PRE but circular differential scattering which will also play a role later. Compared to the above-mentioned systems, which showed PRE the system presented here does not possess a double-layer meta-interface nor an enantiomerically sensitive plasmon. We do not have any different explanation for it. We believe therefore that PRE is not limited to such systems. In contrast the optical activity of the main CD band is a property of individual molecules and consequently not influenced by propagation direction of the light through the sample.

When left for 3 days the samples looked milky, white by eye (see Figure S2c). The structure of the LEB changed including a new peak at 328 nm (Figure 4a). Additionally, the film showed extinction at higher wavelengths throughout the visible range. The structure of the CD band at the low energy absorption band changed too. The previous observed feature at 340 nm increased in intensity and the sample showed optical activity throughout the whole range including the visible range where it was inactive before. The optical activity underwent PRE under sample rotation in the visible range as well as the previous described feature at 340 nm whereas the optical activity at wavelengths of the LEB are offset.

A film of the opposite S enantiomer shows the same extinction as anticipated (Figure 4b). The structure of the CD band at the LEB is similar but opposite in sign as expected for normal systems. However, the feature at 340 nm is reversed comparing the same direction and inverts under sample rotation as seen before. In contrast, the optical activity in the visible range does not change in sign with change of the

ChemPubSoc Europe
CHEMPHYSCHEM Articles

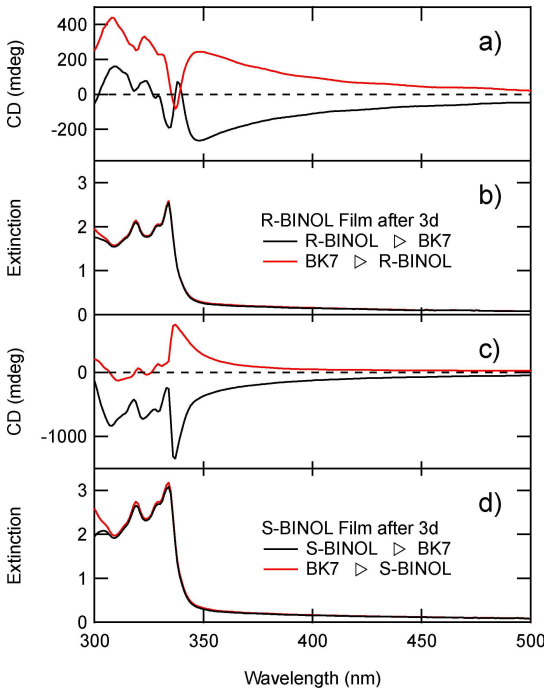

Figure 4. CD (a) and extinction (b) spectrum for both propagation directions of R-BINOL film and S-BINOL (c),(d) 3 d after evaporation.

enantiomer but again reverses in the opposite sample alignment.

By the appearance of the sample the restructuring process went on and seemed completed at this point by an overall milky, white appearance. The fact that the feature at 340 nm simultaneously increased in optical activity with the ongoing restructuring affirms the proposed connection. Another question is whether the measured extinction in the visible range is indeed absorption or scattering, which cannot be distinguished with the CD spectrometer. If the onset in extinction in this region is fitted with a power function, an inverse dependency of the order of 4 on the wavelength is evaluated (Table S1 and Figure S5). This is the dependency of Rayleigh scattering. To prove this point further an absorption spectrum of the R-BINOL film was measured in diffusive transmittance mode in a spectrophotometer equipped with an Ulbricht sphere where clearly only absorption is detected (Figure S6). The spectrum shows no absorption in the visible range and is qualitatively comparable to the 1 h and 6 h old film. This is final evidence that the film does not absorb in the visible region but scatters. Consequently, the optical activity in the visible region is a circular differential scattering phenomenon[16] and related to the macroscopic structure of the film and not the molecules itself. The clear dominance of scattering also rules out circular differential reflection as mechanism which has been concluded in case of differential scattering of vitrified liquid crystalline films of chiral polyflourene too.[15] That the macroscopic structure and not individual molecules are related to the circular differential scattering is supported by the fact that the sign of the optical activity at these wavelengths is independent of the enantiomer but alters with the direction of light through the sample.

A similar prepared film with R-BINOL and ca. half the coverage shows the same characteristics, see Figure S7. As expected the initial extinction and CD is cut in half but the same PRE effect at 340 nm and circular differential scattering develop along with the structural change of the film. Thus, the effects can be observed in a wider thickness range.

A measurement artifact as the potential origin for the presented phenomena can be excluded because of the following reasons. The extinction and CD spectrum of the pristine BK7 substrate show now specific transitions or spectral features, see Figure S8. Particularly, the CD is zero for all wavelengths and both propagation directions of the light. An influence from the substrate or substrate holder can therefore be excluded. From an instrumental standpoint, the measured extinction and CD values are within the specifications of the manufacturer. A coverage series was carried out in order to prove this experimentally and to rule out anomalous behavior at higher coverage and extinction. As expected, the measured extinction and CD depend linearly on the coverage and film thickness throughout the whole range and especially no deviation from this relation is seen for high coverages, see Figure S9. Further, no curves show signs of saturation, e.g. flattening or an increased noise level. Finally, similar behavior has been seen on films of different molecules measured with a different CD-spectrometer before.[15]

2.2. Structural Analysis and Nonlinear Optical Activity

Because the phase transition within the film correlates with both PRE effects the question about the structure rises.

The white spots in the film which were seen 6 h after the evaporation reveal to be circular shaped domains with a diameter of ca. 400 μm (see Figure 5a) if investigated under the microscope with 50× magnification (3 h after the evaporation). A black spot is visible in the center of the domain. This was likely a dust particle which could function as seed from where the restructuring began. Raman spectra in a range between 200 cm^{-1} and 1100 cm^{-1} were obtained inside the domain and outside the domain (which is indicated by the crosses) and compared to each other and crysalline powder. It has been shown that the intensity ratios of pairs of bands at 460, 520 and 1025 cm^{-1} are sensitive to the crystal structure.[12] Therefore, these regions are separately graphed in Figure 5c,d. The intensity ratio of the band pair at 1025 cm^{-1} is different for the transparent film outside and inside the domain. This provides further evidence of a structural change inside the film. Compared to the crystalline powder, which presents the chiral, crystalline form of R-BINOL, the intensity ratio for the the bands within the domain matches well. This is not clearly the case for the band pairs at 460 cm^{-1} and 520 cm^{-1}. However, the Raman spectrum of the domain shows more similarities with the one of the crystalline form than the transparent, initial structure. This

ChemPubSoc Europe
CHEMPHYSCHEM Articles

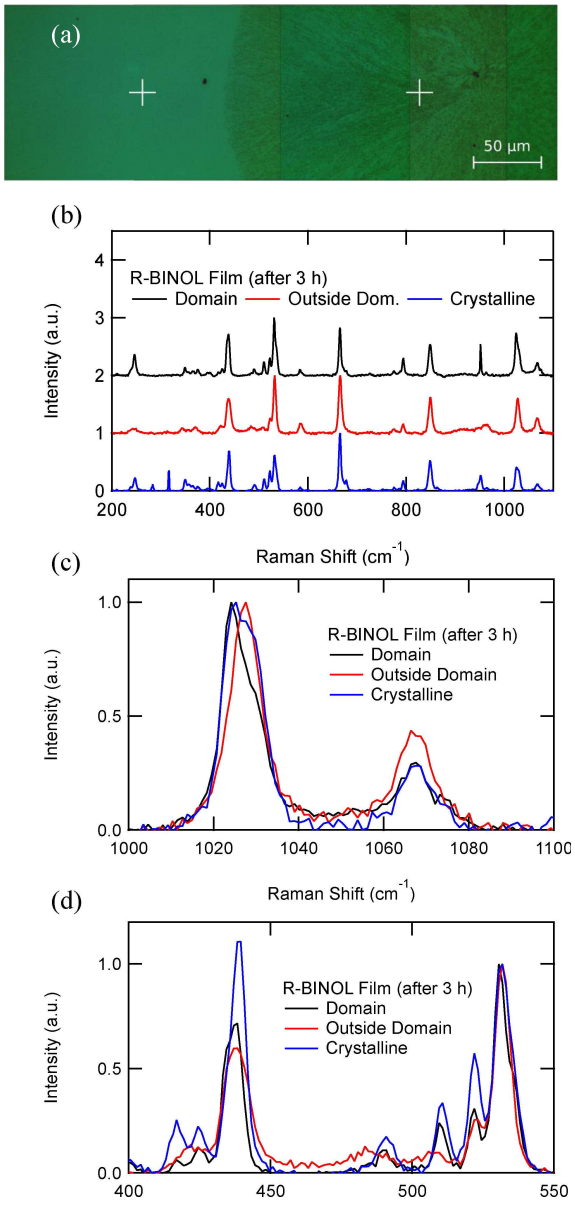

Figure 5. (a) Microscope picture of R-BINOL film 3 h after evaporation. Crosses indicate the positions where Raman spectra were obtained inside and outside the circular domain. (b) Raman spectra of the film and crystalline powder and normalized parts of the spectra are shown in (c) and (d). The excitation wavelength was 633 nm.

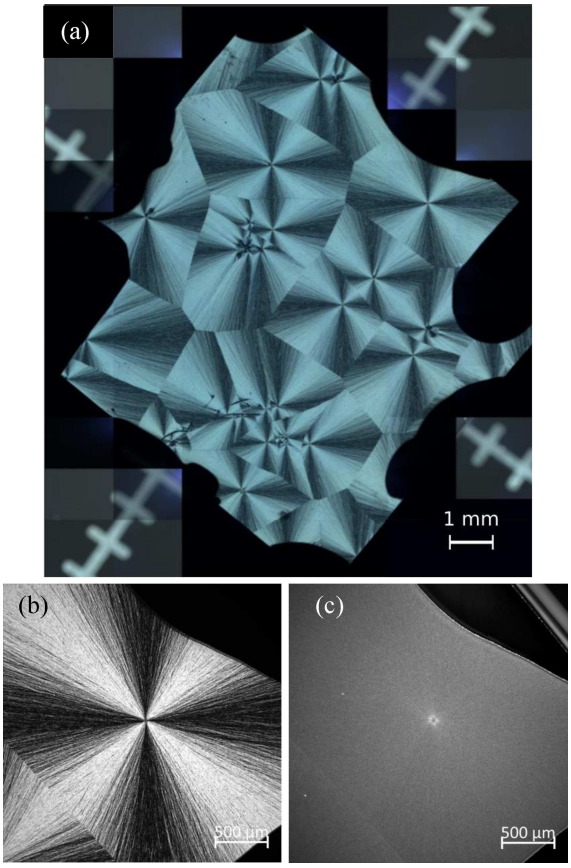

Figure 6. (a) Cross polarization picture of a R-BINOL film and zoom into top right part (b) and dark field picture of the zoom (c).

indicates that the structure of the film is getting closer to the crystalline, chiral form during the process of the restructuring.

A similarly prepared R-BINOL film on a silicon wafer was investigated with a microscope under cross polarization (Figure 6a,b) and dark field conditions (Figure 6c). Under cross polarization the film shows domains of about 1 mm in diameter. All domains show dark crosses (isogyres), which are similarly aligned as a consequence of the cross polarization. Since the microscope was working with visible light this is direct proof of polarization effect in this wavelength range and the relation to the evolved structure. As reference, the picture shows dark shadows in the corners and edges of the sample, which come from the pure substrate (shadow of the clamp during evaporation) and glue and look dark since they are not optically active. The domain structure appears similar to a pseudo-focal conic phase, which is known from liquid crystals[17] where BINOL derivatives are also used as chiral dopant.[18] Figure 6b shows a zoom on the top right domain. Besides the isogyres, fine radial lines beginning from one center point can be seen. When switched to dark field a bright spot is visible where the melatope (crossing of the isogyres) in the cross polarization picture lies. Because this finding is exemplary for all other domains, it confirms the hypothesis that the phase transition is seeded from imperfections.

SHG-CD measurements were performed on this sample to gain further knowledge about the optical activity and orientation of the molecules[19] within a domain, since the two are connected in the nonlinear regime. A circularly polarized laser beam, with a wavelength of 800 nm, was focused onto the sample while the sample was rotated around the surface

ChemPubSoc Europe
CHEMPHYSCHEM Articles

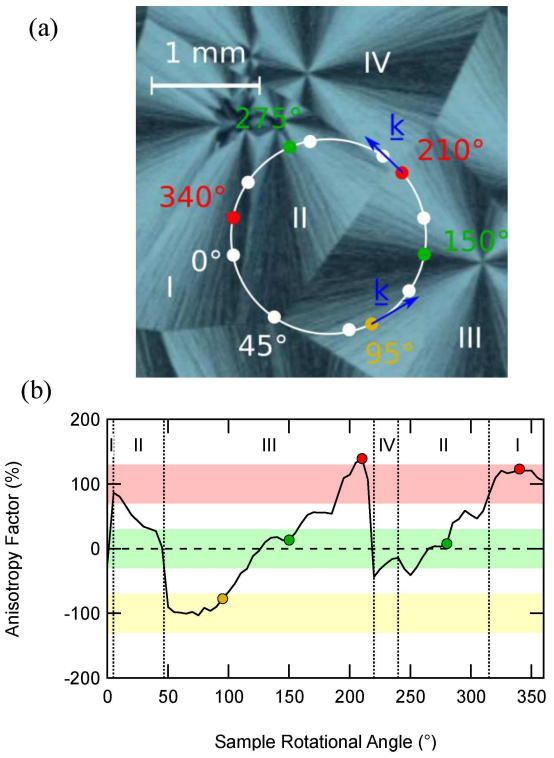

Figure 7. (a) Cross polarization picture of a R-BINOL film with the laser beam path during anisotropy factor measurements while the sample rotates around surface normal. (b) Related second order anisotropy factor at 400 nm SH for R-BINOL film at according sample rotational angle.

normal. The laser path is depicted in Figure 7a and crosses several domains in the center (see Figure 6a). The propagation vector $\underline{k}$ of the light is shown as an arrow for several angles. As the sample is rotated the intensity of the SH at 400 nm (in the scattering region and beyond the low energy absorption band) is detected. The difference between the SH intensities $I_{LCP/RCP}$ generated by the left circularly polarized (LCP) and right circularly polarized (RCP) fundamental light is weighted by the average resulting in the commonly defined second order anisotropy factor[20]

$$g = \frac{I_{LCP} - I_{RCP}}{1/2\ (I_{LCP} + I_{RCP})}$$

This anisotropy factor is plotted against the sample rotation angle in Figure 7b.

As one can see the anisotropy factor varies strongly with the sample orientation and, therefore, the position of the laser spot on the sample. If concentrating on the path inside domain III between 50 and 220 the anisotropy factor increases from roughly −100% to 100%. At 100 the propagation vector $\underline{k}$ is parallel to the radial lines pointing to the center spot in the cross-polarization picture whereas at 210 it is pointing away. The anisotropy factor is about the same in absolute at the two angles but show the opposite sign. In the nonlinear regime, the optical activity does not only depend on the activity of individual molecules but also on their orientation and long-range order in the sample. Thus, the anisotropy factor can reveal information about the average orientation of the molecules at the laser spot.[19] It follows that on average the molecules are orientated opposite to the propagation vector at the two mentioned sample angles. This is the case, if for example, the molecules are aligned in chains, which are spreading in a radial matter from the center point of each domain. Finally, a structure of focal conic domains in smectic films is proposed based on the available knowledge.[21,22]

If the domain size gets smaller than the laser spot size, the recorded anisotropy factor would be an average of multiple domains as in case of the linear CD studies. An S-BINOL film with domain sizes smaller than the laser spot (see Figure S10a) was investigated. The anisotropy factor was constant at a value of −26(2)%, independent of the sample rotation angle (Figure S10b).

2.3. Theoretical Description

So far, the optical activity is assumed to originate from pure circular dichroism. However, other effects such as linear birefringence (LB) and linear dichroism (LD) cannot be ruled out yet. Both are based on the interaction of linearly polarized light with the sample and a difference between polarizations perpendicular to each other. The superposition of CD, LD and LB can be derived for a general sample using the Mueller matrix approach.[23] The signal of the CD spectrometer is expressed as

$$S = A\ [CD + 1/2\ (LD'\ LB - LD\ LB')] + B\ [LB'\ \sin(2\theta) - LB\ \cos(2\theta)]$$

where A and B are apparatus constants, which are described in detail in the SI. LD is linear dichroism and LD' is linear dichroism for a sample rotated at 45 around the surface normal. θ is the rotational angle of the sample around the surface normal.[24] It follows that contributions from LB and LB' can be isolated by comparing signals at different sample angles. This has been done with one S-BINOL film in both propagation directions and the results are plotted in Figure 8. Neither the extinction nor the optical activity alters significantly under rotation, but they are affected by flipping the sample. Thus, the second term including LB and LB' is negligible or zero. To show that the apparatus dependent factor B is nonzero, a baseline without sample was acquired. As shown in Figure S11, the baseline is nonzero and changes with wavelength. Therefore, it is concluded that LB and LB' are negligible or zero.

Furthermore, the difference in optical activity between opposite propagation direction of the light can be expressed as:[23]

$$\Delta S = A\ \left(LD'\ LB - LB'\ LD\right) + 2\ B\ LB'\ \sin(2\theta)$$

with transformations $LB = LB$ and $LB' = -LB'$ (analog for LD).

ChemPubSoc Europe
CHEMPHYSCHEM Articles

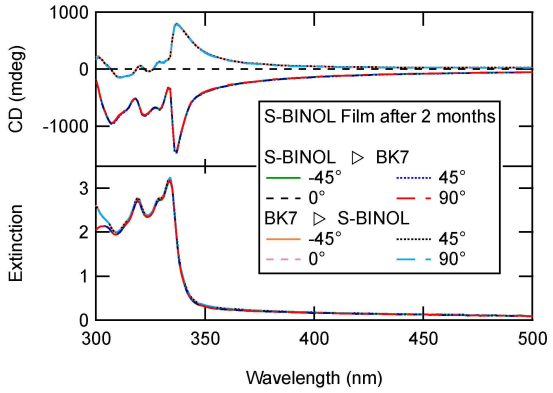

Figure 8. Extinction and CD of S-BINOL film for different rotational angles around the surface normal 2 months after evaporation. Note that curves of same propagation direction overlay.

Thus, the model predicts that the reversal of ellipticity is caused by a combination of LB and LD. Note that contributions from CD are subtracted out here. The latter term is only dependent on LB' and therefore neglected. The PRE is then defined as the product of LB and LD.

There are two possible interpretations. First, LD is the dominant effect present. Even multiplied with negligible contributions from LB it is strong enough to explain the observed PRE. The latter is rather unlikely as the radial symmetry of each domain by definition cannot cause LB and LD. Thus, this holds even if the applied theoretical model is incorrect. In case of LB, this is experimentally proven and unlikely to be different for LD. The second interpretation is that the model is simply inadequate or incomplete. For example, the model does not consider domain boundaries and interfaces between neighboring domains. In addition, the three dimensionality of the sample is ignored.

For the sake of completeness, several important studies should be discussed regarding their relevance for the interpretation of the observations in this work. A vibrational CD (VCD) study on solid polymer films and effects of the sample orientation by Merten *et al.* should be mentioned.[25] In this work, films of achiral polymers were rotated around the surface normal and flipped with respect to the propagation direction of the light in a similar manner as done here. The VCD signal shifted strongly upon sample rotation, and even led to opposite signs of the recorded VCD. Whereas, sample flipping led to inversion of 'artificial' VCD bands, which was also seen in another study from Buffeteau *et al.* by again simple rotation of the sample.[26] A theoretical description of the effects based on the Mueller matrix approach was also provided. However, there are important differences between these findings and the effects observed here. First, in comparison to the works of Merten and Buffeteau, the CD of the BINOL film does not change with sample rotation. Second, the CD feature showing PRE is unambiguously related to transitions of BINOL and are not of artificial nature. Third, the proposed formalism in these works cannot explain the enantiosensitivity of the effect observed in the present work. Another work, which should be mentioned at this point is the microscopy study on chiroptical artifacts by the group of Bart Kahr. The team demonstrated how LB causes artificial "CB" and "CD" signals in thick polycrystalline spherulites of D-sorbitol and developed a theoretical description.[27] Interestingly, the formalism considers several key properties of the system studied here like e.g. the rotational symmetry of a single domain, the three-dimensional character of the film and the interface between neighboring domains. However, the experimental and theoretical findings are described on a local level. The LB, as it is proposed to be generated at interfaces between neighboring domains would average to zero, upon averaging over a large number of domains, as it is the case in our work. Also, the proposed formalism would ignore the correlation between the PRE effect in the CD signal and transitions of BINOL. Equally importantly, it cannot explain the enantiosensitivity of this effect as already correctly stated by the same group.[28]

Summarizing it is proposed that the observed PRE cannot be explained by LB and LD in connection with the standard model and it is indeed an effect of CD, which is not considered in this model.

Note that the spectra in Figure 8 were taken 2 months after the evaporation and are identical to the spectra shown previously. The samples were stored in air and at room temperature. Thus, once the film changes into the crystalline phase it stays stable over an extended period of time.

3. Conclusion

In conclusion, BINOL films with a thickness of 1.5 μm were prepared by evaporation. The initial transparent films showed an additional negative cotton effect at 337 nm the wavelength of the low energy absorption band compared to the solution phase. 6 h after the evaporation the sample showed circular shaped white domains which was assigned as the beginning of a structural phase transformation within the film. At this stage the CD spectrum showed an additional cotton effect at 340 nm which showed PRE when the sample was flipped with respect to the light path as well as with change of the enantiomer. This PRE was related to dipole-dipole interactions between neighboring molecules in the new structural phase. Raman spectroscopy confirmed this structural change and showed similarities between the crystalline, chiral form of BINOL and the final film structure. The phase transition at room temperature was finished after 3 d and the sample showed a white appearance, which was proven as Rayleigh scattering beyond the absorption of BINOL throughout the visible range and showed optical activity. The circular differential scattering underwent PRE when the sample was flipped but not with change of the enantiomer in contrast to the previous mentioned effect in the absorption region. This underlined that both effects showing PRE are of fundamentally different origin.

A combined study of microscopy under cross polarization settings and SHG-CD revealed the structure and orientation of

ChemPubSoc Europe

CHEMPHYSCHEM Articles

the molecules and a structure of focal conic domains with radial symmetry in smectic film is proposed. Furthermore, the SHG-CD experiments showed that the films are also optically active in the nonlinear regime.

A theoretical description through the Mueller matrix approach and comparison to the results was made. It is argued that the effects LB and LD are negligible and that the enantioselective PRE is caused by CD but indescribable with the standard model.

Compared to systems which showed PRE the one presented here does not possess a double-layer meta-interface nor an enantiomerically sensitive plasmon and is simpler in sense of preparation and material composition. We believe therefore that PRE is not limited to such systems.

In summary, CD of solid-state samples with isotropy are more complicated than in solution. Due to the superposition of the optical activity of individual molecules and effects caused by long-range order the interpretation is more challenging. However, vice versa if a sufficient model can be found, describing all contributions, additional structural information can be derived from CD measurements.

Acknowledgements

This work has been supported by the DFG through the project (HE 3454/21-1) and through the projects Alberta/Technische Universität München Graduate School for Functional Hybrid Materials ATUMS (IRTG2022). VKV acknowledges support from the Royal Society through the University Research Fellowships and through Grant Nos. CHG\R1\170067, PEF1\170015, and RGF\EA\180228, as well as from the STFC Grant No. ST/R005842/1. DCH acknowledges funding and support from the Engineering and Physical Sciences Research Council (EPSRC) Centre for Doctoral Training in Condensed Matter Physics (CDTCMP), Grant No. EP/L015544/1.

Conflict of Interest

The authors declare no conflict of interest.

Keywords: circular dichroism · ellipticity · films · isotropy · second-harmonic generation

[1] N. Berova, K. Nakanishi, R. Woody, *Circular Dichroism: Principles and Applications*, Wiley, **2000**.
[2] V. A. Fedotov, A. S. Schwanecke, N. I. Zheludev, V. V. Khardikov, S. L. Prosvirnin, *Nano Lett.* **2007**, *7*, 1996–1999.
[3] S. Tomita, Y. Kosaka, H. Yanagi, K. Sawada, *Phys. Rev. B – Condens. Matter Mater. Phys.* **2013**, *87*, 041404.
[4] Q. L. Zhou, *Privileged Chiral Ligands and Catalysts*, **2011**.
[5] J. M. Brunel, *Chem. Rev.* **2007**, *107*, PR1-PR45.
[6] P. Heister, T. Lunskens, M. Thamer, A. Kartouzian, S. Gerlach, T. Verbiest, U. Heiz, *Phys. Chem. Chem. Phys.* **2014**, *16*, 7299–7306.
[7] D. C. Hooper, A. G. Mark, C. Kuppe, J. T. Collins, P. Fischer, V. K. Valev, *Adv. Mater.* **2017**, *29*, 1605110.
[8] Y. R. Shen, *Fundamentals of Sum-Frequency Spectroscopy*, Cambridge University Press, **2016**.
[9] S. H. Han, N. Ji, M. A. Belkin, Y. R. Shen, *Phys. Rev. B* **2002**, *66*, 165415.
[10] B. Suchod, A. Renault, J. Lajzerowicz, G. P. Spada, *J. Chem. Soc. Perkin Trans. 2* **1992**, 1839–1844.
[11] S. F. Mason, *Molecular Optical Activity and the Chiral Discriminations*, Cambridge University Press, **1982**.
[12] A. R. Lacey, F. J. Craven, *Chem. Phys. Lett.* **1986**, *126*, 588–592.
[13] K. A. Kerr, J. M. Robertson, *J. Chem. Soc. B* **1969**, 1146–1149.
[14] R. B. Kress, E. N. Duesler, M. C. Etter, I. C. Paul, D. Y. Curtin, *J. Am. Chem. Soc.* **1980**, *102*, 7709–7714.
[15] G. Lakhwani, S. C. J. Meskers, R. A. J. Janssen, *J. Phys. Chem. B* **2007**, *111*, 5124–5131.
[16] C. Bustamante, I. Tinoco, M. F. Maestre, *Proc. Natl. Acad. Sci. USA* **1983**, *80*, 3568–3572.
[17] T. Frizon, Dal-Bó, Lopez, D. Silva Paula, D. Silva, *Liq. Cryst.* **2014**, *41*, 1162–1172.
[18] H. Goto, K. Akagi, *Macromolecules* **2005**, *38*, 1091–1098.
[19] J. D. Byers, H. I. Yee, T. Petralli-Mallow, J. M. Hicks, *Phys. Rev. B* **1994**, *49*, 14643–14647.
[20] T. Petralli-Mallow, T. M. Wong, J. D. Byers, H. I. Yee, J. M. Hicks, *J. Phys. Chem.* **1993**, *97*, 1383–1388.
[21] W. Guo, C. Bahr, *Phys. Rev. E* **2009**, *79*, 61701.
[22] V. Designolle, S. Herminghaus, T. Pfohl, C. Bahr, *Langmuir* **2006**, *22*, 363–368.
[23] Y. Shindo, *Opt. Eng.* **1995**, *34*, 3369–3384.
[24] R. Kuroda, T. Harada, Y. Shindo, *Rev. Sci. Instrum.* **2001**, *72*, 3802–3810.
[25] C. Merten, T. Kowalik, A. Hartwig, *Appl. Spectrosc.* **2008**, *62*, 901–905.
[26] T. Buffeteau, F. Lagugné-Labarthet, C. Sourisseau, *Appl. Spectrosc.* **2005**, *59*, 732–745.
[27] J. H. Freudenthal, E. Hollis, B. Kahr, *Chirality* **2010**, *21*, E20–E27.
[28] H.-M. Ye, J. Xu, J. Freudenthal, B. Kahr, *J. Am. Chem. Soc.* **2011**, *133*, 13848–13851.

Manuscript received: October 11, 2018
Revised manuscript received: November 15, 2018
Accepted manuscript online: November 16, 2018
Version of record online: December 4, 2018

E Chirality transfer from organic ligands to silver nanostructures *via* chiral polarisation of the electric field

Journal Physical Chemistry Chemical Physics 20(31): 20347-20351, 2018

Authors Matthias Jakob, Alexander von Weber, Aras Kartouzian and Ulrich Heiz

Affiliations Chair of Physical Chemistry, Technical University of Munich

Abstract "Water-soluble ligand protected optically active silver nanostructures were synthesised in a one-step reduction and capping process mediated by thiol-containing biomolecules. The synthesis was performed successfully with D-and L-cysteine and L-glutathione. The chiroptical properties of the obtained nanostructures were investigated by circular dichroism spectroscopy in the ultraviolet and visible wavelength range. They exhibit a g-value of up to 0.7%, which is about one order of magnitude larger compared to particles prepared by citrate reduction followed by a ligand exchange reaction. The structure and composition of the prepared materials were characterised by transmission electron microscopy, energy-dispersive X-ray and X-ray photoelectron spectroscopy. Although these structures do not have a chiral geometry, they show mirror image g-values when capped with D- and L-cysteine. This indicates that the underlying chirality transfer mechanism is based on an electric field polarisation process."

F Effect of Thiol-Ligands on the Optical Response of Supported Silver Clusters

Journal The Journal of Physical Chemistry C, 121(17): 9331-9336, 2017

Authors Tobias Lünskens,[a] Alexander von Weber,[a] Matthias Jakob,[a] Tony Lelaidier,[b] Aras Kartouzian,[a] and Ueli Heiz[a]

Affiliations

a Chair of Physical Chemistry, Chemistry Department & Catalysis Research Center, Technical University of Munich

b Aix-Marseille Université, CNRS

Abstract "The extinction spectra of size-selected, supported Ag_{20} and Ag_{55} clusters have been measured with surface cavity ring- down (s-CRD) spectroscopy under ultrahigh vacuum (UHV) conditions. A single plasmonic resonance around 3.2 eV is observed. The reaction with benzenethiol shifts the localized surface plasmon resonance (LSPR) by ≈0.3 eV to lower energies, which is attributed to an increased dielectric function of the surrounding medium as well as to a reduction of the free-electron density inside the silver clusters. The time dependence of the LSPR redshift under exposure to benzenethiol has a double exponential behavior. A rapid redshift is caused by chemisorption of benzenethiol from the gas phase via the formation of a sulfur-silver bond, whereas a slow redshift is caused by additional physisorption of benzenethiol. Comparative studies with benzene, which do not show any chemisorption but show physisorption character on silver, reveal that ≈0.2 eV of the overall redshift can be attributed to an increased dielectric constant of the surrounding medium, whereas a reduction of the free-electron density accounts for ≈0.1 eV of the observed redshift."

G Tunable Induced Circular Dichroism in Thin Organic Films

Journal The Journal of Physical Chemistry C, 123(14): 9255–9261, 2019

Authors Alexander von Weber, Philip Stanley, Matthias Jakob, Aras Kartouzian, and Ueli Heiz

Affiliations Chair of Physical Chemistry, Chemistry Department & Catalysis Research Center, Technical University of Munich

Abstract "In this work, we study the induced optical activity (OA) of spin-coated molecular films made of a pristine optically inactive laser dye (Rhodamine 110) in the visible range. The OA is brought about by a "transparent" chiral modifier (1,1'-Bi-2-naphthol). For the first time, it was experimentally shown how two separate mechanisms yield induced circular dichroism (ICD) in such a film and how they are describable through a model. In one, ICD occurs via a direct interaction between dye and modifier molecules. In the other, ICD takes place in optical transitions of present dye aggregates. It is proposed that this is caused by a chiral bias through an enantiomeric excess in inherently chiral and optically active dye aggregates promoted by the chiral modifier in a sergeant-soldier manner. Further, the strength of ICD strongly depends on the ratio between the modifier and the dye as well as on the preparation conditions. The resulting high tunability of the OA paired with a straightforward film preparation opens up a route for fabrication of homogeneous thin films with customized OA."

THE JOURNAL OF PHYSICAL CHEMISTRY C
Article
Cite This: J. Phys. Chem. C 2019, 123, 9255−9261
pubs.acs.org/JPCC

Tunable Induced Circular Dichroism in Thin Organic Films

Alexander von Weber, Philip Stanley, Matthias Jakob, Aras Kartouzian,* and Ueli Heiz

Chair of Physical Chemistry, Chemistry Department & Catalysis Research Center, Technical University of Munich, Lichtenbergstr. 4, D-85748 Garching, Germany

Supporting Information

ABSTRACT: In this work, we study the induced optical activity (OA) of spin-coated molecular films made of a pristine optically inactive laser dye (Rhodamine 110) in the visible range. The OA is brought about by a "transparent" chiral modifier (1,1′-Bi-2-naphthol). For the first time, it was experimentally shown how two separate mechanisms yield induced circular dichroism (ICD) in such a film and how they are describable through a model. In one, ICD occurs via a direct interaction between dye and modifier molecules. In the other, ICD takes place in optical transitions of present dye aggregates. It is proposed that this is caused by a chiral bias through an enantiomeric excess in inherently chiral and optically active dye aggregates promoted by the chiral modifier in a sergeant-soldier manner. Further, the strength of ICD strongly depends on the ratio between the modifier and the dye as well as on the preparation conditions. The resulting high tunability of the OA paired with a straightforward film preparation opens up a route for fabrication of homogeneous thin films with customized OA.

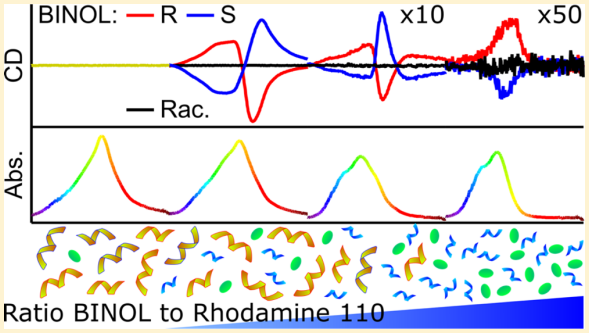

INTRODUCTION

The concept of chirality possesses great importance in biology and manifests itself in the predominance for a single enantiomer in most biomaterials. Therefore, the study of these enantiopure compounds in purified and isolated form as well as their demand for medical usage has become a rapidly increasing research field.[1,2] Circular dichroism (CD), among others, is a popular tool used for their study and is described as the difference in absorption between left and right circularly polarized light.[3] This so-called OA is strongly related to the chiral character of the molecule and holds, for example, structural information.[3]

Because natural resources are limited and the demand for enantiomerically pure compounds was further increasing, great efforts were made in the field of enantioselective catalysis to synthesize such compounds chemically. Until recently, research concentrated on homogeneous asymmetric catalysts, which are already used in industrial applications.[4,5] The heterogeneous counterpart holds intrinsic advantages over homogeneous ones, but only a few examples are known at present.[6] One basic approach for the design of such a catalyst is the usage of a common achiral heterogeneous catalyst, which is then asymmetrized. This can be done by functionalization with, for example, an enantiomerically pure, organic molecule, a so-called chiral modifier.[7−11] To fully comprehend how chirality is transferred to heterogeneous catalysts, it is important to understand how a chiral molecule interacts with its environment and how it induces chirality.

Induced CD (ICD) is an effect that answers these questions because the molecular interactions between chiral (host) and achiral (guest) compounds can give rise to an ICD in the pristine nonoptically active response of the achiral counterpart. This expresses itself in a CD signal within the absorption bands of the achiral substance.[12−14]

Generally, all ICD mechanisms can be classified into two different categories, namely, direct ICD (DICD),[15,16] in which the structure of the guest molecule remains untouched, and indirect ICD (IICD). The former (DICD) follows the original definition of ICD, in which the chiral host and achiral guest are in vicinity of each other, yielding an ICD in the absorption of the achiral guest.[17,18] In this case, the induced OA can arise from two mechanisms. One is known as coupled oscillator effect which is dominant if the electronic transition moments of the achiral chromophore and the chiral counterpart are close in energy. The other is called one-electron effect, in which the chiral compound possesses a strong asymmetric static field, which perturbs the molecular orbitals of the achiral chromophore.[12] Every mechanism which does not fulfill these requirements falls under the second category, that is, IICD. This includes, for example, a structural perturbation of the achiral guest because of strong binding between host and guest or the induction of a chiral superstructure. In such a superstructure, the achiral guests are arranged in a chiral manner and exciton coupling between their identical chromophores would lead to bisignate CD curves because of the split Cotton effect.[19,20] Therefore, the chiral host would

Received: February 10, 2019
Revised: March 12, 2019
Published: March 12, 2019

indirectly induce CD. The concept of ICD and the given classification are illustrated in a simplified diagram in Figure 1.[16]

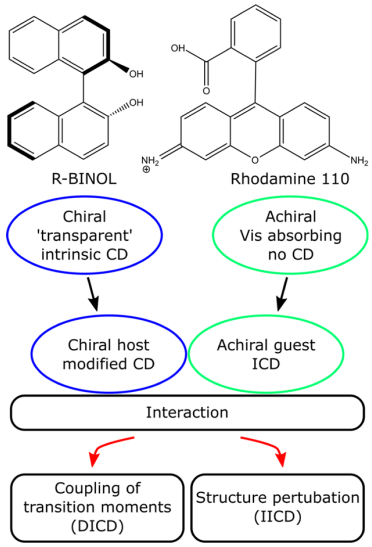

Figure 1. Diagram of the interaction between the chiral and achiral compound, yielding an ICD effect.

Over numerous years of research, several ICD phenomena, models, and interpretations have been provided, and a selected overview is given in the following. In particular in the field of biochemistry, the interaction between helix structures, for example, polypeptides or DNA and an achiral guest molecule leads to a variety of different ICD effects. These were used to discriminate between chemical binding modes, including intercalation or groove binding to DNA and various interaction possibilities between a dye and a polypeptide helix.[21,22] The proposed mechanisms lead to induced OA, ranging from structurally induced chirality to off- and resonant excitonic coupling.[19,21] Another frequent result is that no chemical bond between the two molecule types occurs, but rather strong electrostatic effects, hydrogen bonds, van der Waals interactions, decrease of strain energy, or even simply a dominating chiral environment are the cause for an observable ICD.[15,23,24] Also, ICD has been applied to establish the absolute configuration of a transparent chiral molecule with the aid of an achiral, chromophoric guest or to determine the orientation of the respective molecules within a host−guest complex.[15,16] ICD can hold unique information about supramolecular events.[16] Furthermore, cases have been published where DNA and drug binding sites were probed, intrinsic chirality was amplified, and ion pair structure was studied.[16,23,25]

However, a key aspect shared by all examples mentioned above is that they are in a liquid phase. The question is whether and how the presented ICD effects and their proposed mechanisms transfer into solid state. This is especially crucial for systems including chirally functionalized asymmetric heterogeneous catalysts. In this sense, the group of Sawada studied ICD phenomena in solid films, indicating that a chiral metainterface and thin films of the dye Rhodamine with glucose show so-termed absorption-induced CD.[26] Also, chirally modified liquid crystals were studied as a new material for their promising OA related to ICD.[27−29]

Here, we chose 1,1′-Bi-2-naphthol (BINOL) as the chiral modifier and the laser dye Rhodamine 110 as the achiral guest for our model system and prepared thin films by spin-coating. Rhodamine and BINOL were chosen because their spectroscopic properties match the given scheme of ICD perfectly and are as follows. For the optically inactive Rhodamine 110, two main bands are expected. The derivatized three-ring xanthene group serves as the visible chromophore, with an intense broad band $S_1 \leftarrow S_0$ transition between 500 and 510 nm depending on experimental conditions.[30−33] Additionally, a second smaller absorption peak occurs in the ultraviolet (UV) region at 334 nm stemming from the $S_2 \leftarrow S_0$ transition in the dye.[30] The optically active BINOL is a twisted dimer of two coupled naphthol monomers, yielding an axial chirality. It is transparent in the visible range but possesses optically active absorption bands in the UV region, for example, the low energy band between 310 and 350 nm of the long-axis polarization with two transitions because of splitting from coupling between the excited states of the monomers.[34,35] Both studied substances are shown in Figure 1 with their respective molecular structures.

RESULTS AND DISCUSSION

Individual Compounds. As described above, the ICD effects originate from an interplay between a "transparent" chiral modifier and an absorbing achiral guest. To experimentally show these properties and exclude any intrinsic OA, which could be mistaken for ICD, the CD and absorption of the individual compounds were measured separately. The CD (top) and absorption (bottom) spectra of Rhodamine 110 dissolved in EtOH (green) and of Rhodamine 110 (yellow) and R-BINOL (blue) as a spin-coated film, respectively, are shown in Figure 2.

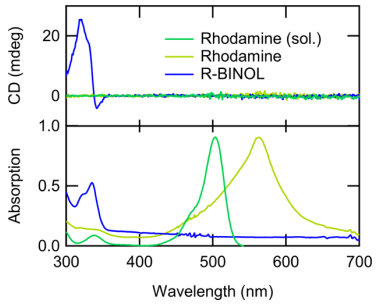

Figure 2. CD (top) and absorption (bottom) spectra of Rhodamine 110 dissolved in EtOH (green) and of Rhodamine 110 (yellow) and R-BINOL (blue) as a spin-coated film.

Starting with the CD spectra of the compounds, it can be seen that only an OA is observable for BINOL. For example, R-BINOL shows here, between 300 and 350 nm, in the wavelength region of its low energy band, a CD signal reaching +25 mdeg at 321 nm, whereas S-BINOL shows an inverted CD signal. The two inverted CD spectra of the opposite enantiomers are often described as resembling mirror images. Rhodamine 110 exhibits a zero line in solution and as a film. In terms of absorption, R-BINOL has a single band in the UV region with two peaks at 321 and 338 nm, as observed previously.[34,36,37] For the dye in solution, two bands occur, one

DOI: 10.1021/acs.jpcc.9b01323
J. Phys. Chem. C 2019, 123, 9255−9261

with low intensity from 300 to 350 nm and the other strong one in the visible region from 450 to 550 nm with a peak at 500 nm and a shoulder at approx. 470 nm, which is in good agreement with the literature.[30,31,38] The absorption of the dye film is different from the case in solution. The absorption band in the visible range is broadened from 400 to 700 nm and shows a maximum at approx. 560 nm with a flank to smaller and higher wavelengths.

This peak at 560 nm can be assigned to J-aggregates built from dye molecules, which is common and known to occur particularly in thin films.[39−43] The J-aggregates imply a head-to-tail arrangement of transition dipole moments characterized by an intense red-shifted transition compared to the solvated monomer. The absorption flank to higher wavelengths originates from bigger aggregates, whose transitions are more red-shifted.[44] Also, the transition of the single isolated dye molecules in the film is red-shifted compared to the solution case and lies at approx. 490 and 525 nm. They resemble a flank at smaller wavelengths with respect to the peak maximum. Note that the assignments of the transitions will be supported by experimental findings later.

ICD Effects and Ratio Dependency. Now, in order to probe possible ICD effects, the chiral, "transparent" BINOL and the achiral, absorbing Rhodamine dye were mixed together in the coating solution and the weight ratio $R = m_{BINOL}/m_{Rhod.}$ between them was systematically varied.

First, it is of interest whether the discussed effects occur in solution, which has been seen for other systems.[21] Thus, solutions with ratios between 0.1 and 4.0 were studied. ICD was not present in any case (see Figure S1). It is therefore apparent that the ICD effect does not occur in solution for the system studied here and is a unique property of thin films, as it will be demonstrated. The absence of an ICD in solution suggests a weak bonding motif between the chiral modifier and the dye. Thus, in the case of covalent bonding, this effect is expected to be present in solution as well.

Then films were fabricated by spin-coating. Figure 3 shows the obtained CD spectra for different weight ratios of 0.22 (a), 0.67 (b), and 1.00 (c) with R-BINOL (red), S-BINOL (blue), and the racemate (black). The absorption spectra of the films with R-BINOL for the respective weight ratios are presented in (d).

Starting with the case of a low ratio of 0.22 and R-BINOL as a chiral modifier, the CD signal is positive from 430 nm to approx. 568 nm. A zero crossing occurs at 570 nm, and subsequently, the signal becomes negative and reaches −319 mdeg. At higher wavelengths, the signal increases and converges against zero until the cutoff wavelength of 700 nm. This is mirrored in the case of S-BINOL, and the signal for the racemic mixture is zero. The absorption spectrum (green curve in Figure 3d) shows a broad band in the visible range from 400 to 700 nm with a maximum at 560 nm.

The CD spectrum for a larger weight ratio of 0.67 shows a positive signal from 300 to 350 nm and from 430 to 560 nm when applying R-BINOL. At the latter value, a zero crossing occurs, and subsequently, the signal becomes negative and reaches −20 mdeg. At 600 nm, a second zero crossing is visible, followed by a positive CD signal until the cutoff wavelength of 700 nm. Again, the curves of the opposite enantiomers are mirror images of each other, and no OA is apparent for the racemic mixture. The absorption spectrum (red curve in Figure 3d) shows two regions with higher absorption. A small band is present in the UV region from 300 to 350 nm, with peaks at 321 and 338 nm. Then, a broad and intense band was observed in the visible region. Here, the band maximum lies at 525 nm, and the transition at 560 nm only occurs as shoulders at higher wavelengths. A second shoulder at smaller wavelengths lies approximately at 490 nm.

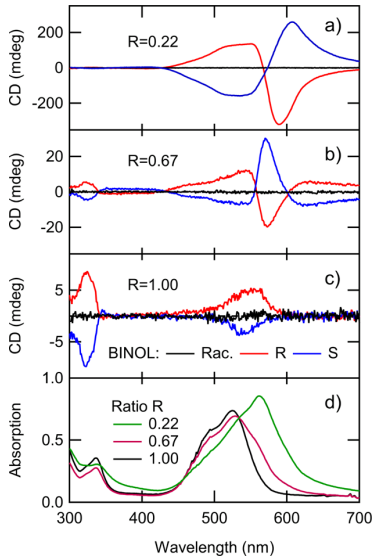

Figure 3. CD spectra of films with R-BINOL (red), S-BINOL (blue), or racemic BINOL (black) and Rhodamine 110 with a ratio BINOL to Rhodamine of R = 0.22 (a), R = 0.67 (b), and R = 1.00 in the coating solution. (d) Absorption spectra of films including R-BINOL. Note the different scale of the CD spectra in (a−c).

In the case of a weight ratio of 1.0, the film with R-BINOL displays a positive CD signal up to approx. +10 mdeg from 300 to 350 nm. This is followed by a positive band from 450 to 600 nm without a zero crossing. The S enantiomer (blue curve) mirrors this behavior. Additionally, the racemic mixture (black curve) does not show any OA. Regarding the absorption spectra (black curve in Figure 3d), two bands are apparent once again. The first is in the UV region and the broad band in the visible region with a maximum at 525 nm and a shoulder at 490 nm. Note that the shoulder at 560 nm, seen in the previous case, is not observed here.

The ICD effect is clearly present, as the samples with R- or S-BINOL display a considerable OA between 430 and 700 nm where BINOL does not have any optical transitions. This behavior is mirrored by the enantiomers and nonexistent for the racemic mixture. Furthermore, ICD is very sensitive to the ratio between the chiral modifier and dye. The ICD profiles of the sample with a ratio of 0.67 in comparison with other samples shown in Figure 3 suggest that a superposition of multiple CD bands is present. If complemented with reliable theoretical assignment of the CD bands to specific transitions, configurational information of the aggregates and their binding to BINOL would be obtained. The absolute content of enantiopure BINOL can be taken from the CD band between 300 and 350 nm as it solely originates from the chiral modifier.

Two additional experimental observations have to be mentioned here. First, by increasing the rotational speed during the coating procedure of a film with a ratio of 0.67, the absorption-independent-induced anisotropy factor g_{ICD} decreases until it remains constant (see Figures S2 and S4). Simultaneously, the absorption peak at 560 nm decreases

DOI: 10.1021/acs.jpcc.9b01323
J. Phys. Chem. C 2019, 123, 9255−9261

The Journal of Physical Chemistry C Article

relative to the other peaks of the $S_1 \leftarrow S_0$ transition. Second, a film with a ratio between 0.22 and 0.67 prepared by molecular evaporation instead of spin coating shows no peak at 560 nm in the absorption spectrum (see Figure S5). The CD spectrum of the film shows clear ICD but is not of bisignate nature. In the case of R-BINOL, ICD remains strictly positive. Therefore, the absorption and ICD can be compared with those of a spin-coated film and a ratio of 1.0.

The presence of bisignate CD bands, in the case of weight ratios $R < 1.0$, seems correlated to the transition at 560 nm and absorption at higher wavelengths. This transition is known from optically inactive pure dye films (see Figure 2) and related to aggregates from dye molecules.[39−43] Thus, ICD originates from dye aggregates, which show OA only in the presence of a chiral modifier. ICD for high ratios $R \geq 1.0$ shows no such Cotton effects, and the transition at 560 nm in the absorption spectrum is absent. Moreover, the remaining transitions at 490 and 525 nm can be connected to transitions of individual, separated dye molecules, which are approx. 20 nm red-shifted with respect to the solution (see Figure 2). Hence, the induced OA is coming from single, isolated dye molecules via perturbation of transition dipole moments by the chiral modifier, which makes the effect DICD (see Figure 2). A structural perturbation due to the binding between BINOL and Rhodamine, which would be IICD, is excluded. This is because the bonding is expected to be of weak hydrogen bonding nature and a structural change of the dye molecule seems implausible in this picture. A random twisting of the dye molecule for simple steric reasons within the film cannot explain the enantiosensitivity of ICD and can hence be excluded as well. Analogously, both arguments hold for ICD observed for the transitions of the aggregates. Additional CD and absorption spectra of ratios between 0.04 and 5 are given in the Supporting Information (see Figure S6).

In order to support the proposed hypothesis about different ICD effects, the spectra are further analyzed, and a model is derived. To quantify the tendency of a film to produce an ICD effect, the dipole strength of the aggregates $D_{\mathrm{Aggr.}}$ and the rotational strength of ICD R_{ICD} were calculated for all films. These two values are defined as follows[45,46]

$$D_{\mathrm{Aggr.}}[\mathrm{erg\ cm^3}] = \left(\frac{6909hc}{8\pi^3 N_0}\right)\int_{600\ \mathrm{nm}}^{700\ \mathrm{nm}} \frac{\varepsilon}{\lambda}\mathrm{d}\lambda$$

$$R_{\mathrm{ICD}}[\mathrm{erg\ cm^3}] = \left(\frac{6909hc}{32\pi^3 N_0}\right)\int_{430\ \mathrm{nm}}^{700\ \mathrm{nm}} \left|\frac{\Delta\varepsilon}{\lambda}\right|\mathrm{d}\lambda$$

with h as the Planck constant, c as the speed of light, N_0 as the Avogadro constant, and ε as the extinction. The dipole strength was calculated between 600 and 700 nm, where isolated dye molecules show no absorption and only contributions from the aggregates are taken into account (see Figure 3). Thus, the defined dipole strength $D_{\mathrm{Aggr.}}$ quantifies the extinction of the dye aggregates present in the film. The observed ICD is quantified via an induced rotational strength R_{ICD}, which is defined in analogy to the dipole strength but with $\Delta\varepsilon$ as the difference in extinction between left and right circularly polarized light. The integration region was carried out in the visible region between 420 and 700 nm, where only ICD contributes to the recorded signal.

The induced rotational strength R_{ICD} and the dipole strength $D_{\mathrm{Aggr.}}$ are plotted against the weight ratio of enantiopure BINOL to Rhodamine 110 in Figure 4. Note that the logarithm is plotted from both strengths. As presented, the pure dye film shows dipole strength of aggregates but negligible rotational strength. Starting from 0, the rotational strength increases with increasing relative concentration of the chiral modifier until a ratio of approx. 0.2. Meanwhile, the dipole strength remains constant. In the region between 0.2 and 1.0, the logarithm of both the dipole and the rotational strength declines linearly. Thus, the actual strengths decrease exponentially with an increasing ratio in this region. The linear fits to the data points that are shown support this exponential dependency. At higher ratios >1.0, the rotational strength remains constant.

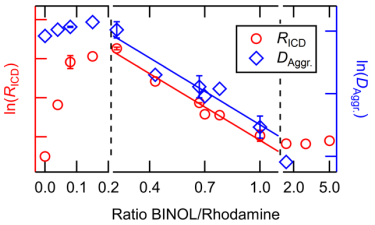

Figure 4. Logarithm of rotational strength R_{ICD} between 420 and 700 nm of films with enantiopure BINOL and Rhodamine 110 and dipole strength $D_{\mathrm{Aggr.}}$ between 600 and 700 nm plotted vs their weight ratio in the coating solution.

Interpretation and Model. The explanation is as follows: the pure dye film contains aggregates of dye molecules, but no OA is measurable in the absence of a chiral modifier. Now, by adding a chiral modifier, an ICD occurs and increases in strength, whereas the aggregate content remains unaltered. This can be explained as follows. The pure dye film contains inherently chiral aggregates, which has been proposed in multiple works before.[47−49] The identical chromophores of neighboring dye molecules couple via exciton coupling in this chiral superstructure, leading to bisignate CD curves. In fact, Spitz and De Rossi et al. found that on a microscopic level, such spontaneously built aggregates can show an OA in the form of CD. However, because of the equal chances to form one or the other enantiomer, the overall OA vanishes on a macroscopic scale as is observed by the wide focus used in this study.[50,51] In this picture, the chiral additive increases the probability to generate one enantiomeric aggregate over the opposite one by acting as chiral seed for the aggregation process as Stryer and Blout propose for cationic dyes.[21] This chiral bias leads to an enantiomeric excess in chiral aggregates and to measurable OA in the transitions of the aggregates, while their total number remains constant. Because the chiral modifier causes ICD via a structure perturbation, this effect is IICD. The flattening of the R_{ICD} curve in this region until a ratio of 0.2 suggests that this effect is limited. The theoretical overall limit would be reached at an induced enantiomeric excess of 100%, but it cannot be verified if this is the case here. An alternative interpretation would be if BINOL actively affects the structure of the aggregates, transforming them from, for example, linear, achiral to twisted, chiral. This could originate from a twisting of the aggregates themselves or by inducing a helical twist between layers of aggregates, which has been seen for helical polyacetylene and liquid crystal N*−LC phases.[27] However, it has also been shown that the transition energy of the chiral superstructures in the presence of the chiral modifier is shifted compared to its achiral counterpart.[28] This is an unlikely scenario as the observed peak position at

DOI: 10.1021/acs.jpcc.9b01323
J. Phys. Chem. C 2019, 123, 9255−9261

560 nm, which is related to the aggregates, is insensitive to the BINOL content here at these concentrations. Also, microscopy images were taken from films containing only Rhodamine and mixtures with R-BINOL with ratios of 0.22, 0.67, and 1.00 (see Figure S7). No characteristic textures known from chiral liquid crystal N*−LC phases, including domains and so-called Grandjean-Cano lines, were seen in the films.[28] Thus, the role of chiroptical active liquid crystals was excluded as a mechanism for the observed ICD. A second alternative interpretation would be that the chiral modifier perturbs the angle between the electric and magnetic dipole transition moments of the dye aggregate, leading to a change in rotational strength.[3] In this alternative scenario, ICD would be of direct nature and therefore DICD. However, this explanation is less likely compared to the first one because it does not predict the bisignate nature of the CD curves.

In the intermediate regime at ratios between 0.2 and 1.0, both ICD and dipole strength of the aggregates decrease exponentially. Similar exponential behavior was found for the OA of the chiral polymer and polysilane helices depending on their size.[44,52,53] Note that in these studies, the CD originated from the intrinsic helical structure and was therefore not induced. It was demonstrated how the nonlinear dependency of CD relates to the chain length in such systems. In fact, Fujiki found an exact exponential relation of both the extinction of the aggregate and its OA in $\Delta\varepsilon$ and the length of the helical rod.[44] Taking this as a model, the chiral modifier actively disturbs here the formation of the dye aggregates during the coating process. Thus, the aggregates are shrinking in size with increasing BINOL content. Consequently, the dipole and rotational strength related to them decrease with the presented exponential manner. It is therefore apparent that the magnitude of the Cotton effect in the CD spectra declines. Analogously, an increasing rotational speed during the coating process hinders the building of aggregates. This leads to a decrease in their dipole strength and a comparable exponential decrease in g_{ICD} with rotational speed. However, in both cases, ICD remains of bisignate nature. This signalizes that the previously described effect is still the dominant mechanism in this ratio regime.

Finally, at high weight ratios >1.0, the dipole strength related to the aggregates is reduced to a minimum, which is also seen by the absence of the transition at 560 nm in the absorption spectra. This concludes that the aggregate content in the film is very small to zero and only the isolated dye molecule contributes to the absorption in the visible region. Nevertheless, the CD spectra still show ICD. As mentioned above, evaporated films show comparable absorption and ICD. Here, the formation of aggregates is extremely hampered because of a poor surface mobility of the molecules. Thus, in both cases, the observed ICD comes from the interaction between the chiral modifier and the individual, achiral dye molecule via perturbation of the dye transition dipole moments. Compared to the former ICD mechanism, this makes it unambiguously of a direct nature—DICD. Two observations support the different origin of this mechanism. First, the CD curves are not bisignate anymore, and second, the rotational strength remains constant with an increasing ratio in this regime.

Figure 5 depicts a scheme of the proposed molecular constellation in the film depending on the ratio between enantiopure BINOL and Rhodamine.

The question arises if linear birefringence (LB) and linear dichroism (LD) effects are responsible for the observable ICD.

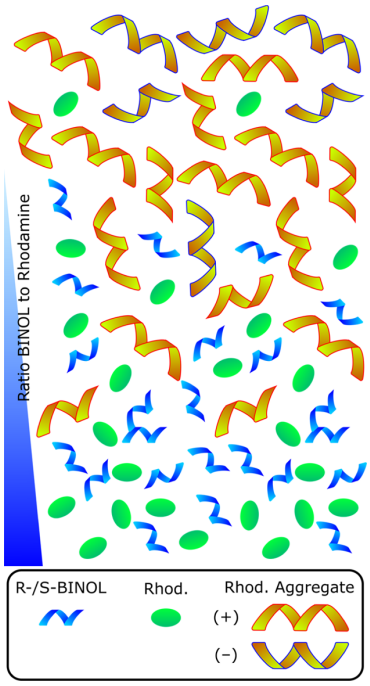

Figure 5. Diagram of the proposed molecular constellation in a film depending on the ratio between enantiopure BINOL and Rhodamine.

Even though this seems unlikely, considering that no anisotropic, macroscopic structures were seen in the films and LD/LB are not enantiosensitive in contrast to the effect observed here, this was additionally examined experimentally. For this purpose, the sample was once rotated 90° around the surface normal and once flipped around with respect to the light path, and CD spectra were recorded and compared to the original geometry. According to the general Mueller matrix description, LB and LD should cause a difference in CD signal in both cases, which is described in more detail in the Supporting Information.[54] However, the studied films do not show such an effect (see Figure S8). Also, no polarity reversal of ellipticity effects occurs when flipping the sample. Such isotropy effects were, for example, observed previously for crystalline enantiopure BINOL films[37] and metainterfaces between Rhodamine and enantiopure glucose-containing layers.[26] Therefore, the observed CD can unambiguously be assigned to ICD. Note that these spectra were performed 6 months later than the first one on the same sample as shown in Figure 3. The fact that the CD and absorption curves are identical demonstrates the long-term stability of the films.

CONCLUSIONS

In short, the system of Rhodamine 110 as the achiral, absorbing component and BINOL as the chiral, "transparent" modifier has been thoroughly examined to provide further insights into ICD mechanisms in such optically active films. This was determined by the systematic variation of the relative concentration of the chiral modifier. It was found that ICD differs strongly and nonlinearly in strength upon changing the rotational speed during the coating process and the relative concentration of the chiral modifier. Additionally, ICD also differs in character for the latter. Three regimes were identified, and a quantitative analysis, combined with a provided model,

DOI: 10.1021/acs.jpcc.9b01323
J. Phys. Chem. C 2019, 123, 9255−9261

describes how two different mechanisms contribute to the observed ICD in the films. The first mechanism is the direct interaction between the chiral modifier and the isolated dye molecule via a perturbation of the dipole transition moments of the dye. This effect was also observed in the compared evaporated films, making it independent of the film preparation method and universal. ICD from a second mechanism is apparent when part of the dye molecules combine to aggregates. It is proposed that the chiral modifier yields a chiral bias through an enantiomeric excess in inherently chiral and optically active dye aggregates.

The findings demonstrate that ICD concepts known from the liquid phase can also be applied in the solid state. Further, these concepts could be used in the future to understand induced chirality in other systems like asymmetrized heterogeneous catalysts.

The high sensitivity of ICD upon varying the relative concentration of the chiral modifier and preparation settings enables excellent tuning of the OA. This makes it a promising approach for the application as tunable optically active films. Our ansatz lies on a modular basis by choosing a combination of "transparent" chiral modifier and absorbing dye. We suggest that the defined OA within these films via ICD can be tuned not only by a variation of the ratio of the dye and the modifier but also by selecting a different modifier or dye. This would further allow us to shift ICD anywhere in the spectral range and still be able to tune its strength. Finally, this approach holds potential for industrial upscaling because of the straightforward and reproducible spin-coating film preparation.

MATERIALS AND METHODS

All studied films were fabricated by spin-coating using a self-made spin-coater with a rotational speed range from 660 to 6360 rpm, as described in detail in the Supporting Information (Figures S9 and S10). To this end, a coating solution of Rhodamine 110 (from Radiant Dyes) with a concentration of 1.2 wt % and enantiopure or racemic BINOL (99% from Sigma-Aldrich) dissolved in ethanol (EtOH; ≥99.5 from Carl Roth) was prepared. The concentration of BINOL was systematically varied and is given proportionally to the weight $m_{\mathrm{Rhod.}}$ of the laser dye in the form of a weight ratio $R = m_{\mathrm{BINOL}}/m_{\mathrm{Rhod.}}$. The coating solution was spin-coated under static dispense conditions, providing highly homogeneous films (see Figure S11). The coating material was first applied to the center of the stagnant 150 μm thick borosilicate glass substrates (BK7 cover glass from VWR), which were cleaned with optically clean acetone beforehand. Unless otherwise stated, a rotational speed of 960 rpm was applied.

Alternatively, films were evaporated under high vacuum conditions using a self-made molecular evaporator.[36] Both components, R-BINOL and Rhodamine 110, were evaporated simultaneously onto the substrate, which was at room temperature, however.

CD and absorption measurements were performed in a wavelength range between 300 and 700 nm on a J-815 CD spectrometer from JASCO.

ASSOCIATED CONTENT

Supporting Information

The Supporting Information is available free of charge on the ACS Publications website at DOI: 10.1021/acs.jpcc.9b01323.

Absorption and CD spectra of solutions, with rotational speed dependency, of molecular evaporated films, of rotated and flipped samples and for every not shown weight ratio; pictures and microscopy study of films; and characterization of the spin-coater (PDF)

AUTHOR INFORMATION

Corresponding Author

*E-mail: aras.kartouzian@tum.de.

ORCID

Alexander von Weber: 0000-0001-6570-3207

Matthias Jakob: 0000-0002-4312-4500

Aras Kartouzian: 0000-0002-2193-2902

Ueli Heiz: 0000-0002-9403-1486

Notes

The authors declare no competing financial interest.

ACKNOWLEDGMENTS

This work was supported by the DFG through project HE 3454/21-1. We are very grateful to E. Keil and W. Feng for their contributions.

REFERENCES

(1) Agranat, I.; Caner, H.; Caldwell, J. Putting Chirality to Work: The Strategy of Chiral Switches. *Nat. Rev. Drug Discovery* **2002**, *1*, 753−768.

(2) Stinson, S. C.; Chiral, S. Chiral Pharmaceuticals. *Chem. Eng. News* **2001**, *79*, 79−97.

(3) Berova, N.; Nakanishi, K.; Woody, R. *Circular Dichroism: Principles and Applications*; Wiley, 2000.

(4) Jannes, G.; Dubois, V. *Chiral Reactions in Heterogeneous Catalysis*; Springer, 1995.

(5) Blaser, H.-U.; Pugin, B.; Studer, M. Enantioselective Heterogeneous Catalysis: Academic and Industrial Challenges. *Chiral Catal. Immobilization Recycl.* **2007**, 1−17.

(6) Heitbaum, M.; Glorius, F.; Escher, I. Asymmetric Heterogeneous Catalysis. *Angew. Chem., Int. Ed.* **2006**, *45*, 4732−4762.

(7) Studer, M.; Blaser, H.-U.; Exner, C. Enantioselective Hydrogenation Using Heterogeneous Modified Catalysts: An Update. *Adv. Synth. Catal.* **2003**, *345*, 45−65.

(8) Schrader, I.; Neumann, S.; Šulce, A.; Schmidt, F.; Azov, V.; Kunz, S. Asymmetric Heterogeneous Catalysis: Transfer of Molecular Principles to Nanoparticles by Ligand Functionalization. *ACS Catal.* **2017**, *7*, 3979−3987.

(9) Bönnemann, H.; Braun, G. A. Enantioselective Hydrogenations on Platinum Colloids. *Angew. Chem., Int. Ed. Engl.* **1996**, *35*, 1992−1995.

(10) Kunz, S. Supported, Ligand-Functionalized Nanoparticles: An Attempt to Rationalize the Application and Potential of Ligands in Heterogeneous Catalysis. *Top. Catal.* **2016**, *59*, 1671−1685.

(11) Jakob, M.; Von Weber, A.; Kartouzian, A.; Heiz, U. Chirality Transfer from Organic Ligands to Silver Nanostructures: Via Chiral Polarisation of the Electric Field. *Phys. Chem. Chem. Phys.* **2018**, *20*, 20347−20351.

(12) Inskeep, W. H.; Miles, D. W.; Eyring, H. Circular Dichroism of Nucleoside Derivatives. VIII. Coupled Oscillator Calculations of Molecules with Fixed Structure. *J. Am. Chem. Soc.* **1970**, *92*, 3866−3872.

(13) Craig, D. P.; Power, E. A.; Thirunamachandran, T. Induced Circular Dichroism: A Theoretical Description. *Chem. Phys. Lett.* **1974**, *27*, 149−153.

(14) Mason, S. F. Induced Circular Dichroism. *Chem. Phys. Lett.* **1975**, *32*, 201−203.

(15) Gawroński, J.; Grajewski, J. The Significance of Induced Circular Dichroism. *Org. Lett.* **2003**, *5*, 3301−3303.

DOI: 10.1021/acs.jpcc.9b01323
J. Phys. Chem. C 2019, 123, 9255−9261

(16) Allenmark, S. Induced Circular Dichroism by Chiral Molecular Interaction. *Chirality* **2003**, *15*, 409−422.
(17) Tinoco, I. Theoretical Aspects of Optical Activity Part Two: Polymers. *Adv. Chem. Phys.* **2007**, *4*, 113−160.
(18) Schellman, J. A. Symmetry Rules for Optical Rotation. *Acc. Chem. Res.* **1968**, *1*, 144−151.
(19) List, N. H.; Knoops, J.; Rubio-Magnieto, J.; Idé, J.; Beljonne, D.; Norman, P.; Surin, M.; Linares, M. Origin of DNA-Induced Circular Dichroism in a Minor-Groove Binder. *J. Am. Chem. Soc.* **2017**, *139*, 14947−14953.
(20) Harada, N.; Nakanishi, K. *Circular Dichroic Spectroscopy: Exciton Coupling in Organic Stereochemistry*; Univ Science Books, 1983.
(21) Stryer, L.; Blout, E. R. Optical Rotatory Dispersion of Dyes Bound to Macromolecules. Cationic Dyes: Polyglutamic Acid Complexes. *J. Am. Chem. Soc.* **1961**, *83*, 1411−1418.
(22) Ardhammer, M.; Nordén, B.; Kurucsev, T. *DNA-Drug Interactions*, 2nd ed.; Berova, N., Woody, R. W., Nakanishi, K., Eds.; Wiley-VCH: New York, Chichester, 2000.
(23) Shimizu, H.; Kaito, A.; Hatano, M. Induced Circular Dichroism of β-Cyclodextrin Complexes with Substituted Benzenes. *Bull. Chem. Soc. Jpn.* **1979**, *52*, 2678−2684.
(24) Ikeda, S.; Nezu, T.; Ebert, G. Induced CD and Interaction of Some Porphyrin Derivatives with α-Helical Polypeptides in Aqueous Solutions. *Biopolymers* **1991**, *31*, 1257−1263.
(25) Zsila, F.; Iwao, Y. The Drug Binding Site of Human Alpha1-Acid Glycoprotein: Insight from Induced Circular Dichroism and Electronic Absorption Spectra. *Biochim. Biophys. Acta* **2007**, *1770*, 797−809.
(26) Tomita, S.; Kosaka, Y.; Yanagi, H.; Sawada, K. Chiral Meta-Interface: Polarity Reversal of Ellipticity through Double Layers Consisting of Transparent Chiral and Absorptive Achiral Media. *Phys. Rev. B: Condens. Matter Mater. Phys.* **2013**, *87*, 041404.
(27) Akagi, K. Helical Polyacetylene: Asymmetric Polymerization in a Chiral Liquid-Crystal Field. *Chem. Rev.* **2009**, *109*, 5354−5401.
(28) Li, X.; Li, Q.; Wang, Y.; Quan, Y.; Chen, D.; Cheng, Y. Strong Aggregation-Induced CPL Response Promoted by Chiral Emissive Nematic Liquid Crystals (N*-LCs). *Chem.—Eur. J.* **2018**, *24*, 12607−12612.
(29) Shopsowitz, K. E.; Qi, H.; Hamad, W. Y.; MacLachlan, M. J. Free-Standing Mesoporous Silica Films with Tunable Chiral Nematic Structures. *Nature* **2010**, *468*, 422.
(30) Thämer, M.; Kartouzian, A.; Heister, P.; Gerlach, S.; Tschurl, M.; Boesl, U.; Heiz, U. Linear and Nonlinear Laser Spectroscopy of Surface Adsorbates with Sub-Monolayer Sensitivity. *J. Phys. Chem. C* **2012**, *116*, 8642−8648.
(31) Wellman, S. M. J.; Jockusch, R. A. Moving in on the Action: An Experimental Comparison of Fluorescence Excitation and Photodissociation Action Spectroscopy. *J. Phys. Chem. A* **2015**, *119*, 6333−6338.
(32) Rangełowa-Jankowska, S.; Jankowski, D.; Bogdanowicz, R.; Grobelna, B.; Bojarski, P. Surface Plasmon-Coupled Emission of Rhodamine 110 Aggregates in a Silica Nanolayer. *J. Phys. Chem. Lett.* **2012**, *3*, 3626−3631.
(33) Dobryakov, A. L.; Kovalenko, S. A.; Ernsting, N. P. Coherent and Sequential Contributions to Femtosecond Transient Absorption Spectra of a Rhodamine Dye in Solution. *J. Chem. Phys.* **2005**, *123*, 044502.
(34) Shen, Y. R. *Fundamentals of Sum-Frequency Spectroscopy*; Cambridge Molecular Science; Cambridge University Press, 2016.
(35) Han, S. H.; Ji, N.; Belkin, M. A.; Shen, Y. R. Sum-Frequency Spectroscopy of Electronic Resonances on a Chiral Surface Monolayer of Bi-Naphthol. *Phys. Rev. B* **2002**, *66*, 165415.
(36) Heister, P.; Lünskens, T.; Thämer, M.; Kartouzian, A.; Gerlach, S.; Verbiest, T.; Heiz, U. Orientational Changes of Supported Chiral 2,2'-Dihydroxy-1,1'binaphthyl Molecules. *Phys. Chem. Chem. Phys.* **2014**, *16*, 7299−7306.
(37) von Weber, A.; Hooper, D. C.; Jakob, M.; Valev, V. K.; Kartouzian, A.; Heiz, U. Circular Dichroism and Isotropy − Polarity Reversal of Ellipticity in Molecular Films of 1,1'-Bi-2-Naphthol. *ChemPhysChem* **2019**, *20*, 62−69.
(38) Brackmann, U. *Lambdachrome Laser Dyes*; Lambda Physik, 1986.
(39) Buncel, E.; McKerrow, A. J.; Kazmaier, P. M. Solvent-Controlled Aggregation of a Photoconductive Dye. *J. Chem. Soc., Chem. Commun.* **1992**, *17*, 1242−1243.
(40) Bird, G. R.; Debuch, G.; Moebius, D. Preparation of a Totally Ordered Monolayer of a Chromophore by Rapid Epitaxial Attachment. *J. Phys. Chem.* **1977**, *81*, 2657−2663.
(41) Jyothish, K.; Hariharan, M.; Ramaiah, D. Chiral Supramolecular Assemblies of a Squaraine Dye in Solution and Thin Films: Concentration-, Temperature-, and Solvent-Induced Chirality Inversion. *Chem.—Eur. J.* **2007**, *13*, 5944−5951.
(42) Song, X.; Perlstein, J.; Whitten, D. G. Supramolecular Aggregates of Azobenzene Phospholipids and Related Compounds in Bilayer Assemblies and Other Microheterogeneous Media: Structure, Properties, and Photoreactivity1. *J. Am. Chem. Soc.* **1997**, *119*, 9144−9159.
(43) Egorov, V. V. Nature of the Optical Band Shapes in Polymethine Dyes and H-Aggregates: Dozy Chaos and Excitons. Comparison with Dimers, H*- and J-Aggregates. *R. Soc. Open Sci.* **2017**, *4*, 160550.
(44) Fujiki, M. Effect of Main Chain Length in the Exciton Spectra of Helical-Rod Polysilanes as a Model of a 5 Å Wide Quantum Wire. *Appl. Phys. Lett.* **1994**, *65*, 3251−3253.
(45) Fasman, G. D. *Circular Dichroism and the Conformational Analysis of Biomolecules*; Plenum Press: New York, 1996.
(46) Sathyanarayana, D. N. *Electronic Absorption Spectroscopy and Related Techniques*; Universities Press: Hyderabad, India, 2001.
(47) Maurus, J. K.; Bird, G. R. Circular Dichroism of Sensitizing Dye Aggregates. *J. Phys. Chem.* **1972**, *76*, 2982−2986.
(48) von Berlepsch, H.; Böttcher, C.; Dähne, L. Structure of J-Aggregates of Pseudoisocyanine Dye in Aqueous Solution. *J. Phys. Chem. B* **2000**, *104*, 8792−8799.
(49) Jyothish, K.; Hariharan, M.; Ramaiah, D. Chiral Supramolecular Assemblies of a Squaraine Dye in Solution and Thin Films: Concentration-, Temperature-, and Solvent-Induced Chirality Inversion. *Chemistry* **2007**, *13*, 5944−5951.
(50) De Rossi, U.; Dähne, S.; Meskers, S. C. J.; Dekkers, H. P. J. M. Spontane Bildung von Optischer Aktivität in J-Aggregaten Mit Davydov-Aufspaltung. *Angew. Chem.* **1996**, *108*, 827−830.
(51) Spitz, C.; Dähne, S.; Ouart, A.; Abraham, H.-W. Proof of Chirality of J-Aggregates Spontaneously and Enantioselectively Generated from Achiral Dyes. *J. Phys. Chem. B* **2000**, *104*, 8664−8669.
(52) Green, M. M.; Peterson, N. C.; Sato, T.; Teramoto, A.; Cook, R.; Lifson, S. A Helical Polymer with a Cooperative Response to Chiral Information. *Science* **1995**, *268*, 1860−1866.
(53) Trefonas, P.; West, R.; Miller, R. D.; Hofer, D. Organosilane high polymers: Electronic spectra and photodegradation. *J. Polym. Sci., Polym. Lett. Ed.* **1983**, *21*, 823−829.
(54) Kuroda, R.; Harada, T.; Shindo, Y. A Solid-State Dedicated Circular Dichroism Spectrophotometer: Development and Application. *Rev. Sci. Instrum.* **2001**, *72*, 3802−3810.

DOI: 10.1021/acs.jpcc.9b01323
J. Phys. Chem. C 2019, 123, 9255−9261

10 Other Publications

Publications which are not directly related to the dissertation are given in the following for completeness.

H Size-dependent electronic structure controls activity for ethanol electro-oxidation at Pt_n/indium tin oxide (n = 1 to 14)

Journal Physical Chemistry Chemical Physics, 17(27): 17601-17610, 2015

Authors Alexander von Weber, Eric T. Baxter, Sebastian Proch, Matthew D. Kane, Michael Rosenfelder, Henry S. White and Scott L. Anderson

Affiliations Department of Chemistry, University of Utah

Abstract "Understanding the factors that control electrochemical catalysis is essential to improving performance. We report a study of electrocatalytic ethanol oxidation – a process important for direct ethanol fuel cells – over size-selected Pt centers ranging from single atoms to Pt_{14}. Model electrodes were prepared by soft-landing of mass-selected Pt_n^+ on indium tin oxide (ITO) supports in ultrahigh vacuum, and transferred to an in situ electrochemical cell without exposure to air. Each electrode had identical Pt coverage, and differed only in the size of Pt clusters deposited. The small Pt_n have activities that vary strongly, and non-monotonically with deposited size. Activity per gram Pt ranges up to ten times higher than that of 5 to 10 nm Pt particles dispersed on ITO. Activity is anti-correlated with the Pt 4d core orbital binding energy, indicating that electron rich clusters are essential for high activity."

I Cluster Size Controls Branching between Water and Hydrogen Peroxide Production in Electrochemical Oxygen Reduction at Pt_n/ITO

Journal The Journal of Physical Chemistry C, 119(20): 11160-11170, 2015

Authors Alexander von Weber, Eric T. Baxter, Henry S. White, and Scott L. Anderson

Affiliations Department of Chemistry, University of Utah

Abstract "Deposition of size-selected Pt_n clusters on indium tin oxide (ITO) films in ultra-high vacuum was used to create electrodes with catalytic sites of controlled size. We report a study of the oxygen reduction reaction (ORR) in 0.1 M $HClO_4$ at size-selected Pt_n/ITO electrodes that were prepared and characterized without exposure to laboratory air. It was found that the ORR onset potential was size-dependent, varying from $\sim$0.66 V vs NHE for Pt_1/ITO to $\sim$0.78 V vs NHE for Pt_n ($n \geq 10$). The maximum ORR currents per gram of Pt were found to be about an order of magnitude higher than that for ITO with 5 nm Pt particles. The branching ratio between the production of water and hydrogen peroxide in ORR was found to be strongly size-dependent. For 5 nm Pt particles on ITO or for polycrystalline Pt, little H2O2 was produced, but as cluster size was decreased, the H_2O_2 branching became large, suggesting that small Pt clusters could be useful selective catalysts for H_2O_2 electrosynthesis. Because there was no obvious correlation of ORR activity with Pt_n electronic properties, as probed by photoemission, the effect of size on branching is tentatively attributed to size of the available oxygen binding sites."

J Electrocatalysis by Mass-Selected Pt_n Clusters

Journal Accounts of chemical research, 49(11): 2632-2639, 2016

Authors Alexander von Weber[a] and Scott L. Anderson[b]

Affiliations

a Chair of Physical Chemistry, Chemistry Department & Catalysis Research Center, Technical University of Munich

b Department of Chemistry, University of Utah

Abstract "Mass-selected Pt_n^+ ion deposition in ultrahigh vacuum (UHV) was used to prepare a series of size-selected electrodes with Pt_n ($n \leq 14$) clusters supported on either glassy carbon (GC) or indium tin oxide (ITO). After characterization of the physical properties of the electrodes in UHV, an in situ method was used to study electrocatalytic activity for the oxygen reduction and ethanol oxidation reactions, without significant air exposure. For each reaction studied, there are similarities between the catalytic properties of Pt_n-containing electrodes and those of nanoparticulate or bulk Pt electrodes, but there are also important differences that provide mechanistic insights. For all systems, strong cluster size effects were observed. For comparison, select experiments were done under identical conditions but with the Pt_n electrodes exposed to air prior to electrochemical studies, resulting in strong modification/ suppression of catalytic activity due to adventitious contaminants.

For ethanol oxidation at Pt_n/ITO, activity varies with size nonmonotonically, by more than an order of magnitude. The sharp size dependence persists during at least 30 to 40 cycles through the Pt redox potential, indicating that processes that would tend to broaden the size distribution are not efficient. All but the least active sizes are substantially more active per mass of Pt, than Pt nanoparticles under the same conditions. The oscillatory dependence of activity on size is anticorrelated with the binding energy of the Pt 4d core level, demonstrating that activity is controlled by the electronic structure of the supported clusters."

Abstract “For oxygen reduction at Pt_n/ITO, the branching between water and hydrogen peroxide production is strongly dependent on cluster size, with small clusters selectively producing peroxide with high activity. The selectivity appears to be related to the size of the active site, with no obvious correlation to Pt electronic properties. The most unusual effect seen was for Pt_n/GC, studied under acid conditions appropriate to oxygen reduction. Pt7 and a few other cluster sizes show “normal”oxygen reduction activity, similar to what is measured for Pt nanoparticles on GC under the same conditions. Many of the small clusters, however, are found to catalyze highly efficient oxidation, by water, of the glassy carbon support, with essentially no overpotential. The high activity for carbon oxidation for many Pt_n/GC electrodes and the absence of significant carbon oxidation for a GC electrode with Pt nanoparticles raise the question of whether small Pt clusters may be responsible for much of the corrosion observed in Pt/carbon electrodes. This system provides another example where activity for oxidation catalysis is anticorrelated with the Pt core level binding energies, indicating that it is electronic, rather than geometric, structure that limits activity.”

K Suppression of Deactivation Processes in Photocatalytic Reduction of CO_2 Using Pulsed Light

Journal ChemCatChem, 8(16): 2688-2695, 2016

Authors Markus Pschenitza,[a] Simon Meister,[a] Alexander von Weber,[b] Aras Kartouzian,[b] Ueli Heiz,[b] and Bernhard Rieger[a]

Affiliations **a** Wacker-Chair of Macromolecular Chemistry and **b** Chair of Physical Chemistry, Chemistry Department & Catalysis Research Center, Technical University of Munich

Abstract "The one-electron-reduced (OER) species of rhenium-based catalysts in the homogeneous photocatalytic reduction of CO_2 represents the starting point of light-induced deactivation processes, which lead to low catalyst activity and productivity. Herein, we report the suppression of these processes using pulsed light. Experimental parameters to avoid the irradiation of the OER species were estimated, leading us to conclude that pulse lengths shorter than 1 ns and repetition rates lower than 33 Hz should be employed. [Re(bpy)$(CO)_3$X] (bpy=2,2'-bipyridine;X=Cl (**1**), Br (**3**)) catalysts were employed in pulsed irradiation experiments using different light sources,pulse lengths and repetition rates. Pulsed irradiation experiments using LEDs revealed that a minimum average photon flux is necessary to enable CO_2 conversion. Furthermore, pulsed laser light with a 10 ns pulse length partially prevented light-induced deactivation processes, whereas efficient suppression was achieved using a 30 ps pulse length."

Appendix with Supporting Information & Print Permissions

Supporting Information

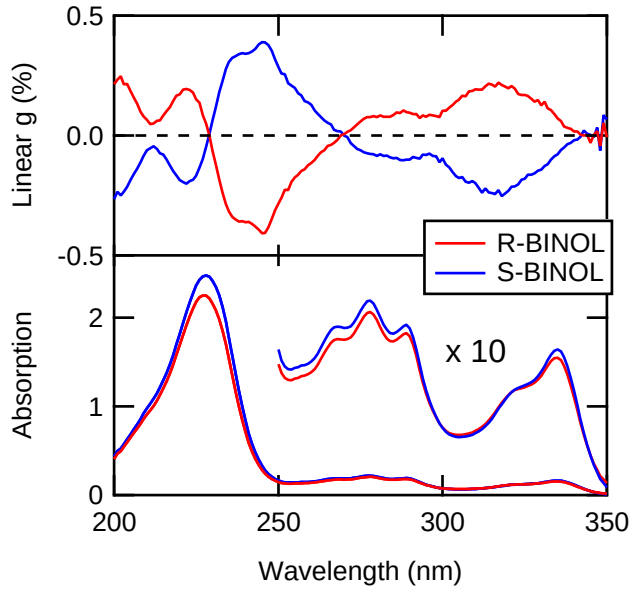

Figure 42 Linear anisotropy factor (top) and absorption (bottom) spectrum of R- and S-BINOL in MeOH. (Adapted from publication D)

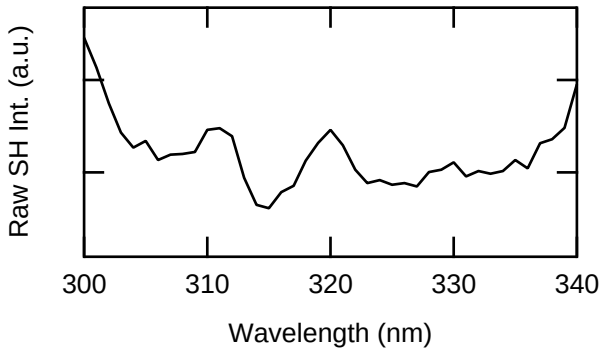

Figure 43 Raw SH spectrum from p-polarized light of a SiO_2 surface of a Si waver.

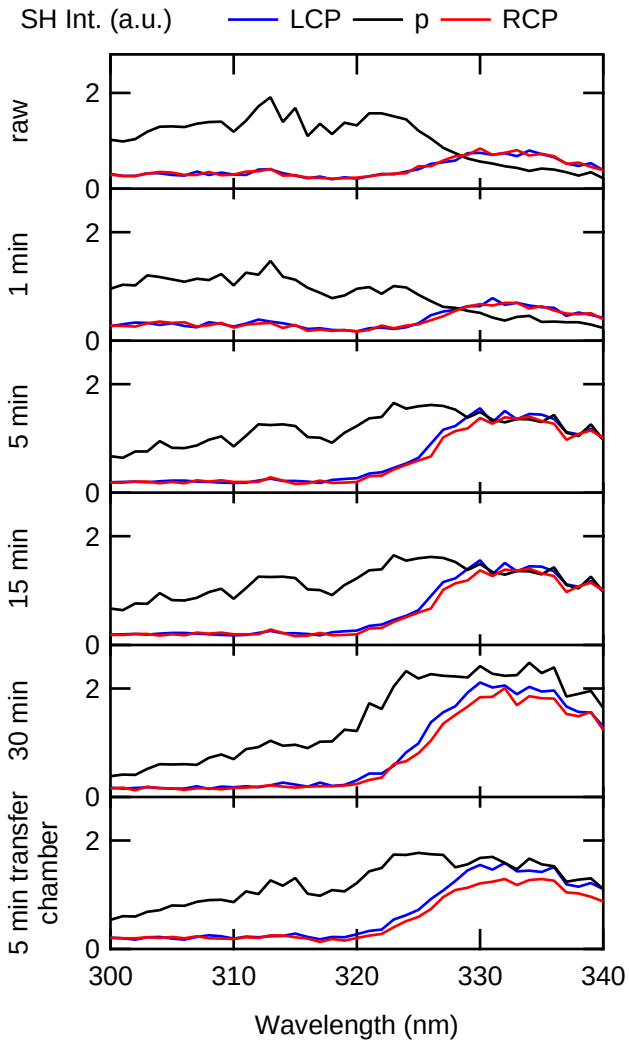

Figure 44 SH spectra from p- and circularly polarized light of a silver surface after different times of Ar^+ sputtering and storing time of 5 min in the transfer chamber at $1 \cdot 10^{-8}$ mbar background pressure.

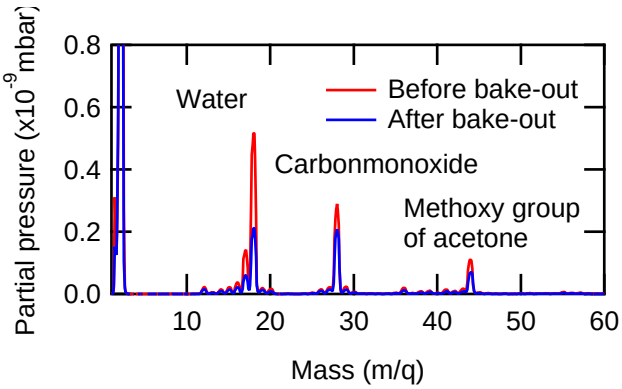

Figure 45 Residual gas mass spectrum of transfer chamber before and after beak-out with a pressure of $1 \cdot 10^{-8}$ mbar and $1 \cdot 10^{-9}$ mbar respectively.

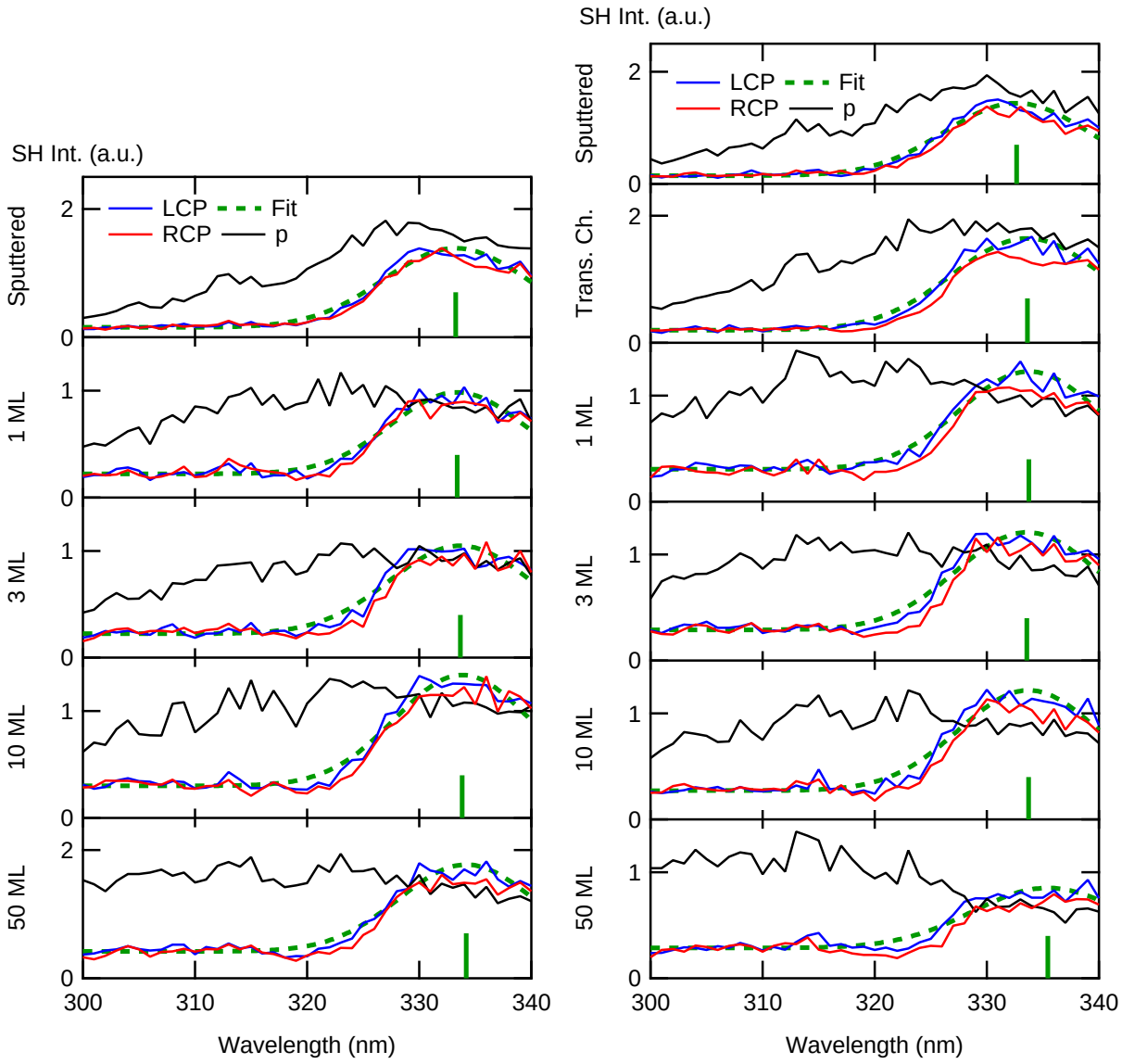

Figure 46 SH spectra from p- and circularly polarized light of a silver surface width different coverages of S- (left) and R-BINOL (right).

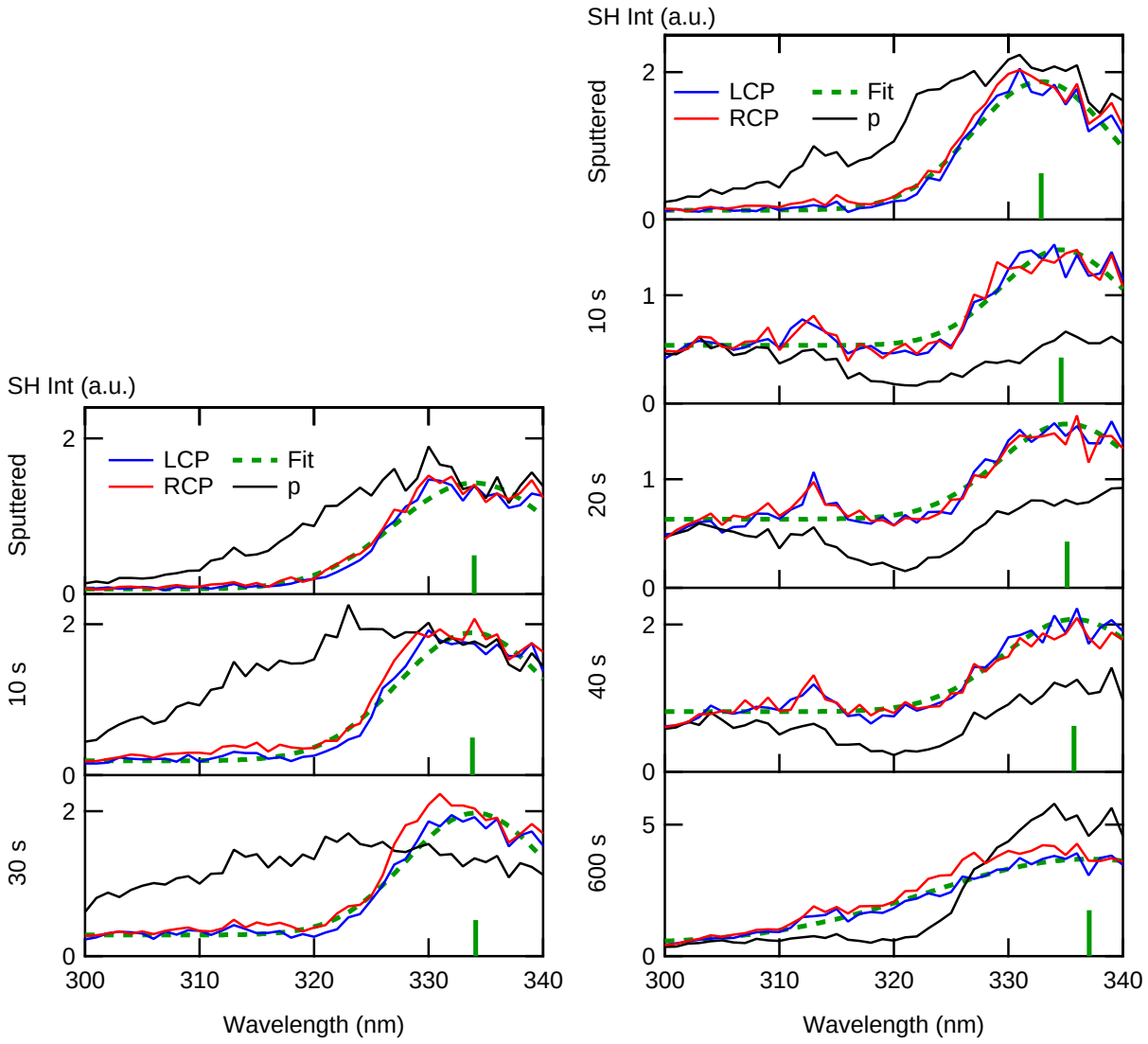

Figure 47 SH spectra from p- and circularly polarized light of a silver surface width different deposition times of L- (left) and D-cystein (right).

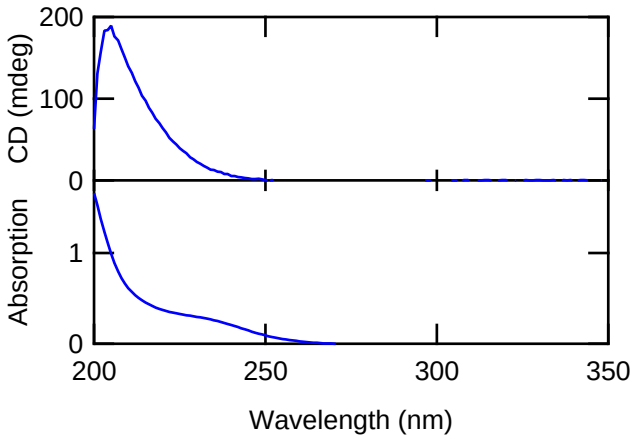

Figure 48 CD (top) and absorption (bottom) spectrum of L-cystein in water.

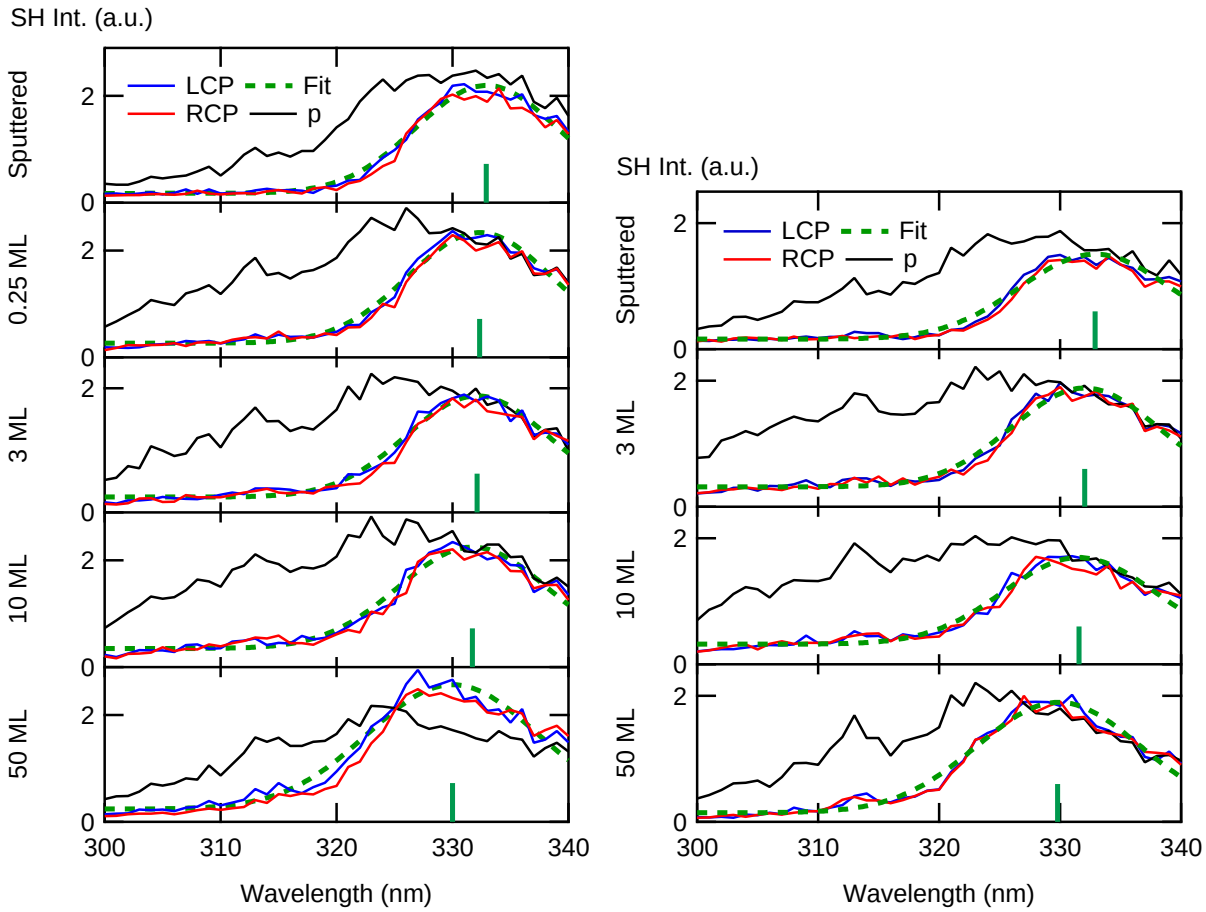

Figure 49 SH spectra from p- and circularly polarized light of a silver surface width different coverages of L- (left) and D-tartaric acid (right).

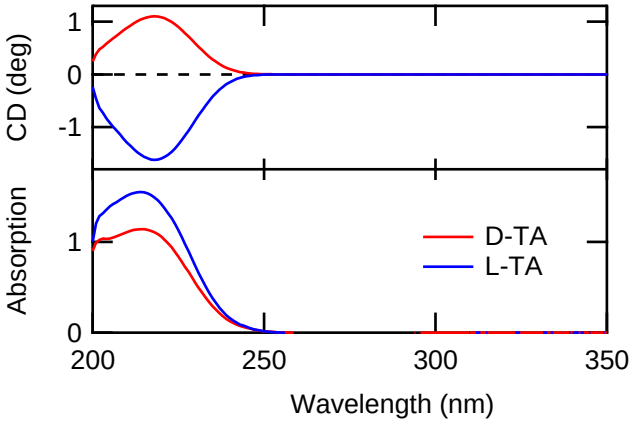

Figure 50 CD (top) and absorption (bottom) spectrum of D- and L-tartaric acid in EtOH.

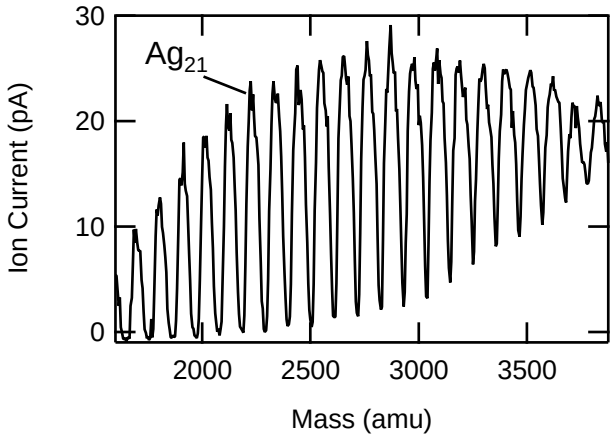

Figure 51 Mass spectrum of silver clusters.

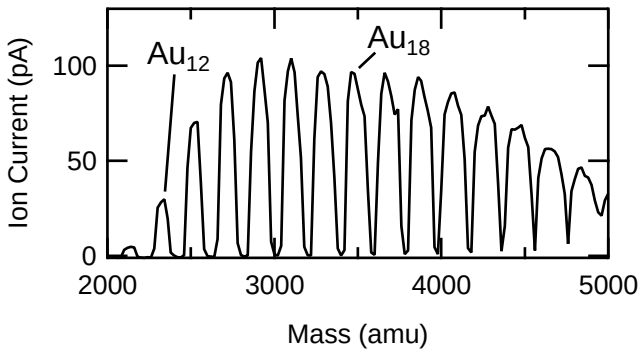

Figure 52 Mass spectrum of gold clusters.

Print Permissions

Optical and morphological properties of thin films of bis-pyrenyl π-conjugated molecules

T. Lelaidier, T. Lünskens, A. von Weber, T. Leoni, A. Ranguis, A. D'Aléo, F. Fages, A. Kartouzian, C. Becker and U. Heiz, *Phys. Chem. Chem. Phys.*, 2016, **18**, 5299
DOI: 10.1039/C5CP06011G

Copyright Clearance Center RightsLink® Home | Account Info | Help

ACS Publications Most Trusted. Most Cited. Most Read.

Title:	Effect of Thiol-Ligands on the Optical Response of Supported Silver Clusters
Author:	Tobias Lünskens, Alexander von Weber, Matthias Jakob, et al
Publication:	The Journal of Physical Chemistry C
Publisher:	American Chemical Society
Date:	May 1, 2017

Logged in as:
Alexander von Weber
Technical University of Munich
Account #:
3001390240
LOGOUT

PERMISSION/LICENSE IS GRANTED FOR YOUR ORDER AT NO CHARGE

This type of permission/license, instead of the standard Terms & Conditions, is sent to you because no fee is being charged for your order. Please note the following:

- Permission is granted for your request in both print and electronic formats, and translations.
- If figures and/or tables were requested, they may be adapted or used in part.
- Please print this page for your records and send a copy of it to your publisher/graduate school.
- Appropriate credit for the requested material should be given as follows: "Reprinted (adapted) with permission from (COMPLETE REFERENCE CITATION). Copyright (YEAR) American Chemical Society." Insert appropriate information in place of the capitalized words.
- One-time permission is granted only for the use specified in your request. No additional uses are granted (such as derivative works or other editions). For any other uses, please submit a new request.

BACK CLOSE WINDOW

Copyright Clearance Center RightsLink® Home | Account Info | Help

ACS Publications Most Trusted. Most Cited. Most Read.

Title:	Device-Compatible Chiroptical Surfaces through Self-Assembly of Enantiopure Allenes
Author:	A. Ozcelik, R. Pereira-Cameselle, A. von Weber, et al
Publication:	Langmuir
Publisher:	American Chemical Society
Date:	Apr 1, 2018

Logged in as:
Alexander von Weber
Technical University of Munich
Account #:
3001390240
LOGOUT

PERMISSION/LICENSE IS GRANTED FOR YOUR ORDER AT NO CHARGE

This type of permission/license, instead of the standard Terms & Conditions, is sent to you because no fee is being charged for your order. Please note the following:

- Permission is granted for your request in both print and electronic formats, and translations.
- If figures and/or tables were requested, they may be adapted or used in part.
- Please print this page for your records and send a copy of it to your publisher/graduate school.
- Appropriate credit for the requested material should be given as follows: "Reprinted (adapted) with permission from (COMPLETE REFERENCE CITATION). Copyright (YEAR) American Chemical Society." Insert appropriate information in place of the capitalized words.
- One-time permission is granted only for the use specified in your request. No additional uses are granted (such as derivative works or other editions). For any other uses, please submit a new request.

BACK CLOSE WINDOW

Copyright Clearance Center RightsLink® Home | Account Info | Help

ACS Publications Most Trusted. Most Cited. Most Read.

Title:	Cluster Size Controls Branching between Water and Hydrogen Peroxide Production in Electrochemical Oxygen Reduction at Pt/n/ITO
Author:	Alexander von Weber, Eric T. Baxter, Henry S. White, et al
Publication:	The Journal of Physical Chemistry C
Publisher:	American Chemical Society
Date:	May 1, 2015

Logged in as:
Alexander von Weber
Technical University of Munich
Account #:
3001390240
LOGOUT

PERMISSION/LICENSE IS GRANTED FOR YOUR ORDER AT NO CHARGE

This type of permission/license, instead of the standard Terms & Conditions, is sent to you because no fee is being charged for your order. Please note the following:

- Permission is granted for your request in both print and electronic formats, and translations.
- If figures and/or tables were requested, they may be adapted or used in part.
- Please print this page for your records and send a copy of it to your publisher/graduate school.
- Appropriate credit for the requested material should be given as follows: "Reprinted (adapted) with permission from (COMPLETE REFERENCE CITATION). Copyright (YEAR) American Chemical Society." Insert appropriate information in place of the capitalized words.
- One-time permission is granted only for the use specified in your request. No additional uses are granted (such as derivative works or other editions). For any other uses, please submit a new request.

Size-dependent electronic structure controls activity for ethanol electro-oxidation at Pt_x/indium tin oxide (n = 1 to 14)

A. von Weber, E. T. Baxter, S. Proch, M. D. Kane, M. Rosenfelder, H. S. White and S. L. Anderson, *Phys. Chem. Chem. Phys.*, 2015, **17**, 17601
DOI: 10.1039/C5CP01824B

JOHN WILEY AND SONS LICENSE TERMS AND CONDITIONS

Apr 09, 2019

This Agreement between Technical University of Munich -- Alexander von Weber ("You") and John Wiley and Sons ("John Wiley and Sons") consists of your license details and the terms and conditions provided by John Wiley and Sons and Copyright Clearance Center.

License Number	4564780319730
License date	Apr 09, 2019
Licensed Content Publisher	John Wiley and Sons
Licensed Content Publication	ChemPhysChem
Licensed Content Title	In situ Second-Harmonic Generation Circular Dichroism with Submonolayer Sensitivity
Licensed Content Author	Alexander von Weber, Matthias Jakob, Eva Kratzer, et al
Licensed Content Date	Nov 30, 2018
Licensed Content Volume	20
Licensed Content Issue	1
Licensed Content Pages	8
Type of use	Dissertation/Thesis
Requestor type	Author of this Wiley article
Format	Print and electronic
Portion	Full article
Will you be translating?	No
Title of your thesis / dissertation	Pristine and Induced Linear and Nonlinear Chiroptical Activity in Films and at Surfaces
Expected completion date	Jun 2019
Expected size (number of pages)	140
Requestor Location	Technical University of Munich Lichtenbergstr. 4 Garching b. München, Bavaria 85748 Germany Attn: Technical University of Munich
Publisher Tax ID	EU826007151
Total	0.00 EUR

Chirality transfer from organic ligands to silver nanostructures *via* chiral polarisation of the electric field

M. Jakob, A. von Weber, A. Kartouzian and U. Heiz, *Phys. Chem. Chem. Phys.*, 2018, **20**, 20347
DOI: 10.1039/C8CP02970A

JOHN WILEY AND SONS LICENSE TERMS AND CONDITIONS

Apr 09, 2019

This Agreement between Technical University of Munich -- Alexander von Weber ("You") and John Wiley and Sons ("John Wiley and Sons") consists of your license details and the terms and conditions provided by John Wiley and Sons and Copyright Clearance Center.

License Number	4564780717982
License date	Apr 09, 2019
Licensed Content Publisher	John Wiley and Sons
Licensed Content Publication	ChemPhysChem
Licensed Content Title	Circular Dichroism and Isotropy – Polarity Reversal of Ellipticity in Molecular Films of 1,1'-Bi-2-Naphtol
Licensed Content Author	Alexander von Weber, David C. Hooper, Matthias Jakob, et al
Licensed Content Date	Dec 4, 2018
Licensed Content Volume	20
Licensed Content Issue	1
Licensed Content Pages	8
Type of use	Dissertation/Thesis
Requestor type	Author of this Wiley article
Format	Print and electronic
Portion	Full article
Will you be translating?	No
Title of your thesis / dissertation	Pristine and Induced Linear and Nonlinear Chiroptical Activity in Films and at Surfaces
Expected completion date	Jun 2019
Expected size (number of pages)	140
Requestor Location	Technical University of Munich Lichtenbergstr. 4 Garching b. München, Bavaria 85748 Germany Attn: Technical University of Munich
Publisher Tax ID	EU826007151
Total	0.00 EUR

9.1.2019 Rightslink® by Copyright Clearance Center

Copyright Clearance Center RightsLink® Home Account Info Help

ACS Publications Most Trusted. Most Cited. Most Read.

Title: Electrocatalysis by Mass-Selected Ptn Clusters
Author: Alexander von Weber, Scott L. Anderson
Publication: Accounts of Chemical Research
Publisher: American Chemical Society
Date: Nov 1, 2016

Logged in as:
Alexander von Weber
Technical University of Munich
Account #: 3001390240
LOGOUT

PERMISSION/LICENSE IS GRANTED FOR YOUR ORDER AT NO CHARGE

This type of permission/license, instead of the standard Terms & Conditions, is sent to you because no fee is being charged for your order. Please note the following:

- Permission is granted for your request in both print and electronic formats, and translations.
- If figures and/or tables were requested, they may be adapted or used in part.
- Please print this page for your records and send a copy of it to your publisher/graduate school.
- Appropriate credit for the requested material should be given as follows: "Reprinted (adapted) with permission from (COMPLETE REFERENCE CITATION). Copyright (YEAR) American Chemical Society." Insert appropriate information in place of the capitalized words.
- One-time permission is granted only for the use specified in your request. No additional uses are granted (such as derivative works or other editions). For any other uses, please submit a new request.

BACK CLOSE WINDOW

3.4.2019 Rightslink® by Copyright Clearance Center

Copyright Clearance Center RightsLink® Home Account Info Help

ACS Publications Most Trusted. Most Cited. Most Read.

Title: Tunable Induced Circular Dichroism in Thin Organic Films
Author: Alexander von Weber, Philip Stanley, Matthias Jakob, et al
Publication: The Journal of Physical Chemistry C
Publisher: American Chemical Society
Date: Mar 1, 2019

Logged in as:
Alexander von Weber
Technical University of Munich
Account #: 3001390240
LOGOUT

PERMISSION/LICENSE IS GRANTED FOR YOUR ORDER AT NO CHARGE

This type of permission/license, instead of the standard Terms & Conditions, is sent to you because no fee is being charged for your order. Please note the following:

- Permission is granted for your request in both print and electronic formats, and translations.
- If figures and/or tables were requested, they may be adapted or used in part.
- Please print this page for your records and send a copy of it to your publisher/graduate school.
- Appropriate credit for the requested material should be given as follows: "Reprinted (adapted) with permission from (COMPLETE REFERENCE CITATION). Copyright (YEAR) American Chemical Society." Insert appropriate information in place of the capitalized words.
- One-time permission is granted only for the use specified in your request. No additional uses are granted (such as derivative works or other editions). For any other uses, please submit a new request.

BACK CLOSE WINDOW

JOHN WILEY AND SONS LICENSE TERMS AND CONDITIONS

Apr 09, 2019

This Agreement between Technical University of Munich -- Alexander von Weber ("You") and John Wiley and Sons ("John Wiley and Sons") consists of your license details and the terms and conditions provided by John Wiley and Sons and Copyright Clearance Center.

License Number	4564780897855
License date	Apr 09, 2019
Licensed Content Publisher	John Wiley and Sons
Licensed Content Publication	ChemCatChem
Licensed Content Title	Suppression of Deactivation Processes in Photocatalytic Reduction of CO2 Using Pulsed Light
Licensed Content Author	Markus Pschenitza, Simon Meister, Alexander von Weber, et al
Licensed Content Date	Jul 21, 2016
Licensed Content Volume	8
Licensed Content Issue	16
Licensed Content Pages	8
Type of use	Dissertation/Thesis
Requestor type	Author of this Wiley article
Format	Print and electronic
Portion	Full article
Will you be translating?	No
Title of your thesis / dissertation	Pristine and Induced Linear and Nonlinear Chiroptical Activity in Films and at Surfaces
Expected completion date	Jun 2019
Expected size (number of pages)	140
Requestor Location	Technical University of Munich Lichtenbergstr. 4 Garching b. München, Bavaria 85748 Germany Attn: Technical University of Munich
Publisher Tax ID	EU826007151
Total	0.00 EUR

Glossary

CD	Circular Dichroism
CP	Circular Polarization
CRD	Cavity Ring-Down
DICD	Direct Induced Circular Dichroism
ee	Enantiomeric Excess
g	Anisotropy Factor or g Value
ICD	Induced Circular Dichroism
IICD	Indirect Induced Circular Dichroism
LSP	Localized Surface Plasmon
ML	Monolayer
OA	Optical Activity
SH	Second-Harmonic
SHG	Second-Harmonic Generation
SHG-CD	Second-Harmonic Generation Circular Dichroism
SP	Surface Plasmon
UHV	Ultra-High Vacuum
UV	Ultraviolet
VIS	Visible
VP	Volume Plasmon

References

1 A. Beil, D. Luckhaus, R. Marquardt, and M. Quack. Intramolecular energy transfer and vibrational redistribution in chiral molecules: experiment and theory. *Faraday Discuss.*, 99:49–76, 1994.

2 M. Quack. How Important is Parity Violation for Molecular and Biomolecular Chirality? *Angew. Chemie Int. Ed.*, 41(24):4618–4630, 2002.

3 C. Fábri, L. Horný, and M. Quack. Tunneling and Parity Violation in Trisulfane (HSSSH): An Almost Ideal Molecule for Detecting Parity Violation in Chiral Molecules. *ChemPhysChem*, 16(17):3584–3589, 2015.

4 M. Senami and K. Ito. Asymmetry of electron chirality between enantiomeric pair molecules and the origin of homochirality in nature. *Phys. Rev. A*, 99(1):12509, 2019.

5 P. Cintas and C. Viedma. On the Physical Basis of Asymmetry and Homochirality. *Chirality*, 24(11):894–908, 2012.

6 J. Bailey, A. Chrysostomou, J. H. Hough, T. M. Gledhill, A. McCall, S. Clark, F. Ménard, and M. Tamura. Circular polarization in star-formation regions: Implications for biomolecular homochirality. *Science*, 281(5377):672–674, 1998.

7 U. Meierhenrich, W. H.-P. Thiemann, and H. Rosenbauer. Molecular parity violation via comets? *Chirality*, 11(7):575–582, 1999.

8 M. Laska and P. Teubner. Olfactory Discrimination Ability of Human Subjects for Ten Pairs of Enantiomers. *Chem. Senses*, 24(2):161–170, 1999.

9 W. Lenz, R. A. Pfeiffer, W. Kosenow, and D. J. Hayman. Thalidomide and Congenital Abnormalities. *Lancet*, 279(7219):45–46, 1962.

10 T. Eriksson, S. Björkman, B. Roth, and P. Höglund. Intravenous Formulations of the Enantiomers of Thalidomide: Pharmacokinetic and Initial Pharmacodynamic Characterization in Man. *J. Pharm. Pharmacol.*, 52(7):807–817, 2000.

11 N. Berova, K. Nakanishi, and R. Woody. Circular Dichroism: Principles and Applications. *Wiley*, 2000.

12 I. Agranat, H. Caner, and J. Caldwell. Putting chirality to work: The strategy of chiral switches. *Nat. Rev. Drug Discov.*, 1(10):753–768, 2002.

13 S. C. Stinson. Chiral pharmaceuticals. *Chem. Eng. News*, 79(40):79–97, 2001.

14 F. Rost. Die Entstehung der optischen Asymmetrie. *Angew. Chemie*, 48(4):73–75, 1935.

15 G. Jannes and V. Dubois. Chiral reactions in heterogeneous catalysis. *Springer*, 1995.

16 H.-U. Blaser, B. Pugin, and M. Studer. Enantioselective Heterogeneous Catalysis: Academic and Industrial Challenges. *Chiral Catal. Immobil. Recycl.*, pages 1–17, 2000.

17 M. Heitbaum, F. Glorius, and I. Escher. Asymmetric heterogeneous catalysis. *Angew. Chemie - Int. Ed.*, 45(29):4732–4762, 2006.

18 S. Chandrasekhar, J. S. Yadav, J. C. Guillemin, P. Lakshmipathi, and R. Gree. Soluble polymer supported asymmetric synthesis (SPSAS). *Indian J. Chem. - Sect. B Org. Med. Chem.*, 41(10):2116–2128, 2002.

19 M. Studer, H.-U. Blaser, and C. Exner. Enantioselective Hydrogenation Using Heterogeneous Modified Catalysts: An Update. *ChemInform*, 34(18):45–65, 2003.

20 I. Schrader, S. Neumann, A. Šulce, F. Schmidt, V. Azov, and S. Kunz. Asymmetric Heterogeneous Catalysis: Transfer of Molecular Principles to Nanoparticles by Ligand Functionalization. *ACS Catal.*, 7(6):3979–3987, 2017.

21 H. Bönnemann and G. A. Braun. Enantioselective hydrogenations on platinum colloids. *Angew. Chemie (International Ed. English)*, 35(17):1992–1995, 1996.

22 S. Kunz. Supported, Ligand-Functionalized Nanoparticles: An Attempt to Rationalize the Application and Potential of Ligands in Heterogeneous Catalysis. *Top. Catal.*, 59(19):1671–1685, 2016.

23 S. Kunz, P. Schreiber, M. Ludwig, M. M. Maturi, O. Ackermann, M. Tschurl, and U. Heiz. Rational Design, Characterization and Catalytic Application of Metal Clusters Functionalized with Hydrophilic, Chiral Ligands: A Proof of Principle Study. *Phys. Chem. Chem. Phys.*, 15(44):19253–61, 2013.

24 Y. Izumi. Modified Raney Nickel (MRNi) Catalyst: Heterogeneous Enantio-Differentiating (Asymmetric) Catalyst. *Adv. Catal.*, 32:215–271, 1983.

25 G. Webb and P. B. Wells. Asymmetric hydrogenation. *Catal. Today*, 12(2):319–337, 1992.

26 J. Kumar, K. G. Thomas, and L. M. Liz-Marzán. Nanoscale chirality in metal and semiconductor nanoparticles. *Chem. Commun.*, 52(85):12555–12569, 2016.

27 C. Gautier and T. Bürgi. Chiral gold nanoparticles. *ChemPhysChem*, 10(3):483–492, 2009.

28 P. D. Jadzinsky, G. Calero, C. J. Ackerson, D. A. Bushnell, and R. D. Kornberg. Structure of a thiol monolayer-protected gold nanoparticle at 1.1 Å resolution. *Science*, 318(5849):430–433, 2007.

29 M. Jakob, A. Von Weber, A. Kartouzian, and U. Heiz. Chirality transfer from organic ligands to silver nanostructures: Via chiral polarisation of the electric field. *Phys. Chem. Chem. Phys.*, 20(31):20347–20351, 2018.

30 T. G. Schaaff, G. Knight, M. N. Shafigullin, R. F. Borkman, and R. L. Whetten. Isolation and Selected Properties of a 10.4 kDa Gold:Glutathione Cluster Compound. *J. Phys. Chem. B*, 102(52):10643–10646, 1998.

31 B. M. Maoz, Y. Chaikin, A. B. Tesler, O. Bar Elli, Z. Fan, A. O. Govorov, and G. Markovich. Amplification of chiroptical activity of chiral biomolecules by surface plasmons. *Nano Lett.*, 13(3):1203–1209, 2013.

32 W. H. Inskeep, D. W. Miles, and H. Eyring. Circular dichroism of nucleoside derivatives. VIII. Coupled oscillator calculations of molecules with fixed structure. *J. Am. Chem. Soc.*, 92(13):3866–3872, 1970.

33 D. P. Craig, E. A. Power, and T. Thirunamachandran. Induced circular dichroism: A theoretical description. *Chem. Phys. Lett.*, 27(2):149–153, 1974.

34 S. F. Mason. Induced circular dichroism. *Chem. Phys. Lett.*, 32(2):201–203, 1975.

35 N. Holmgaard List, J. Knoops, J. Rubio-Magnieto, J. Idé, D. Beljonne, P. Norman, M. Surin, and M. Linares. Origin of DNA-Induced Circular Dichroism in a Minor-Groove Binder. *J. Am. Chem. Soc.*, 139(42):14947–14953, 2017.

36 J. Gawroński and J. Grajewski. The significance of induced circular dichroism. *Org. Lett.*, 5(18):3301–3303, 2003.

37 S. Allenmark. Induced circular dichroism by chiral molecular interaction. *Chirality*, 15(5):409–422, 2003.

38 T. Petralli-Mallow, T. M. Wong, J. D. Byers, H. I. Yee, and J. M. Hicks. Circular dichroism spectroscopy at interfaces: a surface second harmonic generation study. *J. Phys. Chem.*, 97(7):1383–1388, 1993.

39 G. D. Fasman. Circular dichroism and the conformational analysis of biomolecules. *Plenum Press*, New York, 1996.

40 W. Kuhn. The physical significance of optical rotatory power. *Trans. Faraday Soc.*, 26:293–308, 1930.

41 I. Tinoco. Theoretical Aspects of Optical Activity Part Two: Polymers. *Adv. Chem. Phys.*, 4:113–160, 1962.

42 J. A. Schellman. Symmetry rules for optical rotation. *Acc. Chem. Res.*, 1(5):144–151, 1968.

43 N. Harada and K. Nakanishi. Circular dichroic spectroscopy: exciton coupling in organic stereochemistry. *Univ Science Books*, 1983.

44 L. Stryer and E. R. Blout. Optical Rotatory Dispersion of Dyes Bound to Macromolecules. Cationic Dyes: Polyglutamic Acid Complexes. *J. Am. Chem. Soc.*, 83(6):1411–1418, 1961.

45 M. Ardhammer, B. Nordén, and T. Kurucsev. DNA-Drug interactions. *Wiley-VCH*, New York; Chichester, 2nd ed. edition, 2000.

46 H. Shimizu, A. Kaito, and M. Hatano. Induced Circular Dichroism of β-Cyclodextrin Complexes with Substituted Benzenes. *Bull. Chem. Soc. Jpn.*, 52(9):2678–2684, 1979.

47 S. Ikeda, T. Nezu, and G. Ebert. Induced CD and interaction of some porphyrin derivatives with α-helical polypeptides in aqueous solutions. *Biopolymers*, 31(11):1257–1263, 1991.

48 F. Zsila and Y. Iwao. The drug binding site of human alpha1-acid glycoprotein: insight from induced circular dichroism and electronic absorption spectra. *Biochim. Biophys. Acta*, 1770(5):797–809, 2007.

49 M.-R. Goldsmith, C. B. George, G. Zuber, R. Naaman, D. H. Waldeck, P. Wipf, and D. N. Beratan. The chiroptical signature of achiral metal clusters induced by dissymmetric adsorbates. *Phys. Chem. Chem. Phys.*, 8(1):63–67, 2006.

50 T. G. Schaaff and R. L. Whetten. Giant Gold-Glutathione Cluster Compounds: Intense Optical Activity in Metal-Based Transitions. *J. Phys. Chem. B*, 104(12):2630–2641, 2000.

51 V. Humblot, S. Haq, C. Muryn, W. A. Hofer, and R. Raval. From local adsorption stresses to chiral surfaces: (R,R)-tartaric acid on Ni(110). *J. Am. Chem. Soc.*, 124(3):503–510, 2002.

52 J. D. Byers, H. I. Yee, T. Petralli-Mallow, and J. M. Hicks. Second-harmonic generation circular-dichroism spectroscopy from chiral monolayers. *Phys. Rev. B*, 49(20):14643–14647, 1994.

53 M. M. Kauranen, T. Verbiest, A. Persoons, E. W. Meijer, M. N. Teerenstra, A. J. Schouten, R. J. M. Nolte, and E. E. Havinga. Chiral effects in the second-order optical nonlinearity of a poly(isocyanide) monolayer. *Adv. Mater.*, 7(7):641–644, 1995.

54 M. Kauranen, J. J. Maki, T. Verbiest, S. Van Elshocht, and A. Persoons. Quantitative determination of electric and magnetic second-order susceptibility tensors of chiral surfaces. *Phys. Rev. B*, 55(4):R1985–R1988, 1997.

55 S. Sioncke, T. Verbiest, and A. Persoons. Second-order nonlinear optical properties of chiral materials. *Mater. Sci. Eng. R Reports*, 42(5-6):115–155, 2003.

56 C. Kittel. Introduction to solid state physics, volume 8. *Wiley New York*, 1976.

57 E. D. Palik. Handbook of optical constants of solids, volume 3. *Academic press*, 1998.

58 S. A. Maier. Plasmonics: fundamentals and applications. *Springer Science & Business Media*, 2007.

59 H. Raether. Surface plasmons on smooth and rough surfaces and on gratings. *Springer-Verlag Berlin An*, 2013.

60 C. Sönnichsen, T. Franzl, T. Wilk, G. von Plessen, and J. Feldmann. Plasmon resonances in large noble-metal clusters. *New J. Phys.*, 4:93, 2002.

61 T. Lünskens, P. Heister, M. Thämer, C. A. Walenta, A. Kartouzian, and U. Heiz. Plasmons in supported size-selected silver nanoclusters. *Phys. Chem. Chem. Phys.*, 17(27):17541–4, 2015.

62 J. J. Mock, M. Barbic, D. R. Smith, D. A. Schultz, and S. Schultz. Shape effects in plasmon resonance of individual colloidal silver nanoparticles. *J. Chem. Phys.*, 116(15):6755–6759, 2002.

63 M. Thämer, A. Kartouzian, P. Heister, T. Lünskens, S. Gerlach, and U. Heiz. Small supported plasmonic silver clusters. *Small*, 10(12):2340–2344, 2014.

64 H. Hövel, S. Fritz, A. Hilger, U. Kreibig, and M. Vollmer. Width of cluster plasmon resonances: Bulk dielectric functions and chemical interface damping. *Phys. Rev. B*, 48(24):18178–18188, 1993.

65 C. Hendrich, J. Bosbach, F. Stietz, F. Hubenthal, T. Vartanyan, and F. Träger. Chemical interface damping of surface plasmon excitation in metal nanoparticles: a study by persistent spectral hole burning. *Appl. Phys. B*, 76(8):869–875, 2003.

66 T. Lelaidier, T. Lünskens, A. von Weber, T. Leoni, A. Ranguis, A. D'Aleo, F. Fages, A. Kartouzian, C. Becker, and U. Heiz. Optical and morphological properties of thin films of bis-pyrenyl [small pi]-conjugated molecules. *Phys. Chem. Chem. Phys.*, 18(7):5299–5305, 2016.

67 T. Lünskens, A. Von Weber, M. Jakob, T. Lelaidier, A. Kartouzian, and U. Heiz. Effect of Thiol-Ligands on the Optical Response of Supported Silver Clusters. *J. Phys. Chem. C*, 121(17):9331–9336, 2017.

68 P. Heister, T. Lünskens, M. Thämer, A. Kartouzian, S. Gerlach, T. Verbiest, and U. Heiz. Orientational changes of supported chiral 2,2'-dihydroxy-1,1'binaphthyl molecules. *Phys. Chem. Chem. Phys.*, 16(16):7299–7306, 2014.

69 M. Vanbel, S. Vandendriessche, M. A. van der Veen, D. Slavov, P. Heister, R. Paesen, V. K. Valev, M. Ameloot, and T. Verbiest. Second-harmonic generation from complex chiral samples. *17th Int. Sch. Quantum Electron. Laser Phys. Appl.*, 8770:87701F, 2013.

70 A. von Weber, D. C. Hooper, M. Jakob, V. K. Valev, A. Kartouzian, and U. Heiz. Circular Dichroism and Isotropy – Polarity Reversal of Ellipticity in Molecular Films of 1,1'-Bi-2-Naphtol. *ChemPhysChem*, 20(1):62–69, 2019.

71 U. Heiz, F. Vanolli, L. Trento, and W. D. Schneider. Chemical reactivity of size-selected supported clusters: An experimental setup. *Rev. Sci. Instrum.*, 68(5):1986–1994, 1997.

72 A. Kartouzian, P. Heister, M. Thämer, S. Gerlach, and U. Heiz. In-line reference measurement for surface second harmonic generation spectroscopy. *J. Opt. Soc. Am. B*, 30(3):541–548, 2013.

73 I. Hinds Instruments. PEM-100 Photoelastic Modulator User Manual. 2013.

74 G. Sauerbrey. Verwendung von Schwingquarzen zur Wägung dünner Schichten und zur Mikrowägung. *Zeitschrift für Phys.*, 155(2):206–222, 1959.

75 L. E. Scriven. Physics and Applications of DIP Coating and Spin Coating. *MRS Proc.*, 121:717, 1988.

76 D. W. Schubert and T. Dunkel. Spin coating from a molecular point of view. *Mater. Res. Innov.*, 7(5):314–321, 2003.

77 P. M. Stanley. Absorption-Induced Circular Dichroism in Optically Active Thin Films: Study

on 1,1'-Bi-2-naphthol and Rhodamine 110. *Internship report*, Technical University of Munich, 2018.

78 K. Norrman, A. Ghanbari-Siahkali, and N. B. Larsen. 6 Studies of spin-coated polymer films. *Annu. Reports Sect. "C" (Physical Chem.*, 101(0):174–201, 2005.

79 D. Meyerhofer. Characteristics of resist films produced by spinning. *J. Appl. Phys.*, 49(7):3993–3997, 1978.

80 D. Sofikitis, L. Bougas, G. E. Katsoprinakis, A. K. Spiliotis, B. Loppinet, and T. P. Rakitzis. Evanescent-wave and ambient chiral sensing by signal-reversing cavity ringdown polarimetry. *Nature*, 514(7520):76, 2014.

81 M. Thämer, A. Kartouzian, P. Heister, S. Gerlach, M. Tschurl, U. Boesl, and U. Heiz. Linear and nonlinear laser spectroscopy of surface adsorbates with sub-monolayer sensitivity. *J. Phys. Chem. C*, 116(15):8642–8648, 2012.

82 A. Kartouzian, M. Thämer, T. Soini, J. Peter, P. Pitschi, S. Gilb, and U. Heiz. Cavity ringdown spectrometer for measuring the optical response of supported size-selected clusters and surface defects in ultrahigh vacuum. *J. Appl. Phys.*, 104(12):124313, 2008.

83 S. Gilb, K. Hartl, A. Kartouzian, J. Peter, U. Heiz, H.-G. Boyen, and P. Ziemann. Cavity ringdown spectroscopy of metallic gold nanoparticles. *Eur. Phys. J. D*, 45(3):501–506, 2007.

84 T. M. Figueira-Duarte and K. Müllen. Pyrene-Based Materials for Organic Electronics. *Chem. Rev.*, 111(11):7260–7314, 2011.

85 F. Moggia, C. Videlot-Ackermann, J. Ackermann, P. Raynal, H. Brisset, and F. Fages. Synthesis and thin film electronic properties of two pyrene-substituted oligothiophene derivatives. *J. Mater. Chem.*, 16(24):2380–2386, 2006.

86 S. Leroy-Lhez, M. Allain, J. Oberlé, and F. Fages. Synthesis and zinc(ii) complexation modulated fluorescence emission properties of two pyrene-oligo(phenylene vinylene)-2,2'-bipyridine conjugated molecular rods. *New J. Chem.*, 31(6):1013–1021, 2007.

87 H. Li, D. R. Powell, R. K. Hayashi, and R. West. Poly((2,5-dialkoxy-p-phenylene)ethynylene-p-phenyleneethynylene)s and Their Model Compounds. *Macromolecules*, 31(1):52–58, 1998.

88 S. Leroy-Lhez, A. Parker, P. Lapouyade, C. Belin, L. Ducasse, J. Oberlé, and

F. Fages. Tunable fluorescence emission in pyrene–(2,2'-bipyridine) dyads containing phenylene–ethynylene bridges. *Photochem. Photobiol. Sci.*, 3(10):949–959, 2004.

89 A. S. Davydov. Theory of absorption spectra of molecular crystals. 1949.

90 T. Lünskens, C. A. Walenta, P. Heister, A. Kartouzian, and U. Heiz. Surface Oxidation of Supported, Size-Selected Silver Clusters. *J. Clust. Sci.*, 28(6):3185–3192, 2017.

91 T. Verbiest, K. Clays, and V. Rodriguez. Second-order Nonlinear Optical Characterization Techniques: An Introduction. *CRC press*, 2009.

92 R. Kuroda and S. F. Mason. The crystal and molecular structure of R-(-)-1,1'-binaphthyl: the conformational isomerism and a comparison of the chiral with the racemic packing mode. *J. Chem. Soc., Perkin Trans. 2*, (1):167–170, 1981.

93 I. Hanazaki and H. Akimoto. Optical rotatory power of 2,2'-dihydroxy-1,1'-binaphthyl and related compounds. *J. Am. Chem. Soc.*, 94(12):4102–4106, 1972.

94 S. F. Mason. Molecular Optical Activity and the Chiral Discriminations. *Cambridge University Press*, 1982.

95 C. Gropp, N. Trapp, and F. Diederich. Alleno-Acetylenic Cage (AAC) Receptors: Chiroptical Switching and Enantioselective Complexation of trans-1,2-Dimethylcyclohexane in a Diaxial Conformation. *Angew. Chemie Int. Ed.*, 55(46):14444–14449, 2016.

96 O. Gidron, M.-O. Ebert, N. Trapp, and F. Diederich. Chiroptical Detection of Nonchromophoric, Achiral Guests by Enantiopure Alleno-Acetylenic Helicages. *Angew. Chemie Int. Ed.*, 53(49):13614–13618, 2014.

97 G. Pescitelli, L. Di Bari, and N. Berova. Application of electronic circular dichroism in the study of supramolecular systems. *Chem. Soc. Rev.*, 43(15):5211–5233, 2014.

98 P. Mineo, N. Micali, V. Villari, M. G. Donato, and E. Scamporrino. Reading of Protein Surfaces in the Native State at Micromolar Concentrations by a Chirogenetic Porphyrin Probe. *Chem. – A Eur. J.*, 18(39):12452–12457, 2012.

99 R. Kuroda, T. Harada, and Y. Shindo. A solid-state dedicated circular dichroism spectrophotometer: Development and application. *Rev. Sci. Instrum.*, 72(10):3802–3810, 2001.

100 J. H. Freudenthal, E. Hollis, and B. Kahr. Imaging chiroptical artifacts. *Chirality*, 21(1E):E20–E27, 2010.

101 H.-M. Ye, J. Xu, J. Freudenthal, and B. Kahr. On the Circular Birefringence of Polycrystalline Polymers: Polylactide. *J. Am. Chem. Soc.*, 133(35):13848–13851, 2011.

102 A. R. Lacey and F. J. Craven. A preliminary study of the conformation of 1,1'-binaphthyl in solution by Raman spectroscopy. *Chem. Phys. Lett.*, 126(6):588–592, 1986.

103 T. Frizon, Dal-Bó, Lopez, D. Silva Paula, and D. Silva. Synthesis of luminescent liquid crystals derived from gallic acid containing heterocyclic 1,3,4-oxadiazole. *Liq. Cryst.*, 41(8):1162–1172, 2014.

104 H. Goto and K. Akagi. Asymmetric Electrochemical Polymerization: Preparation of Polybithiophene in a Chiral Nematic Liquid Crystal Field and Optically Active Electrochromism. *Macromolecules*, 38(4):1091–1098, 2005.

105 C. Bustamante, I. Tinoco, and M. F. Maestre. Circular differential scattering can be an important part of the circular dichroism of macromolecules. *Proc. Natl. Acad. Sci. U. S. A.*, 80(12):3568–3572, 1983.

106 G. Lakhwani, S. C. J. Meskers, and R. A. J. Janssen. Circular Differential Scattering of Light in Films of Chiral Polyfluorene. *J. Phys. Chem. B*, 111(19):5124–5131, 2007.

107 W. Guo and C. Bahr. Influence of phase sequence on focal conic domains in smectic films. *Phys. Rev. E*, 79(6):61701, 2009.

108 V. Designolle, S. Herminghaus, T. Pfohl, and C. Bahr. AFM Study of Defect-Induced Depressions of the Smectic-A/Air Interface. *Langmuir*, 22(1):363–368, 2006.

109 S. M. Barlow and R. Raval. Complex organic molecules at metal surfaces: bonding, organisation and chirality. *Surf. Sci. Rep.*, 50(6-8):201–341, 2003.

110 N. Bloembergen, R. K. Chang, and C. H. Lee. Second-Harmonic Generation of Light in Reflection from Media with Inversion Symmetry. *Phys. Rev. Lett.*, 16(22):986–989, 1966.

111 J. Gong, R. Dai, Z. Wang, and Z. Zhang. Thickness Dispersion of Surface Plasmon of Ag Nano-thin Films: Determination by Ellipsometry Iterated with Transmittance Method. *Sci. Rep.*, 5, 2015.

112 R. L. Aggarwal, L. W. Farrar, and S. K. Saikin. Increase of SERS Signal upon Heating or Exposure to a High-Intensity Laser Field: Benzenethiol on an AgFON Substrate. *J. Phys. Chem. C*, 116(31):16656–16659, 2012.

113 K. B. Biggs, J. P. Camden, J. N. Anker, and R. P. V. Duyne. Surface-Enhanced Raman Spec-

troscopy of Benzenethiol Adsorbed from the Gas Phase onto Silver Film over Nanosphere Surfaces: Determination of the Sticking Probability and Detection Limit Time. *J. Phys. Chem. A*, 113(16):4581–4586, 2009.

114 J. C. Love, L. A. Estroff, J. K. Kriebel, R. G. Nuzzo, and G. M. Whitesides. Self-Assembled Monolayers of Thiolates on Metals as a Form of Nanotechnology. *Chem. Rev.*, 105(4):1103–1170, 2005.

115 W. T. Astbury. The Crystalline Structure and Properties of Tartaric Acid. *Proc. R. Soc. A Math. Phys. Eng. Sci.*, 102(718):506–528, 2006.

116 M. Ortega Lorenzo, C. J. Baddeley, C. Muryn, and R. Raval. Extended surface chirality from supramolecular assemblies of adsorbed chiral molecules. *Nature*, 404(6776):376, 2000.

117 M. Okumura, T. Fujitani, J. Huang, and T. Ishida. A Career in Catalysis: Masatake Haruta. *ACS Catal.*, 5(8):4699–4707, 2015.

118 U. Heiz, A. Sanchez, S. Abbet, and W.-D. Schneider. Catalytic Oxidation of Carbon Monoxide on Monodispersed Platinum Clusters: Each Atom Counts. *J. Am. Chem. Soc.*, 121(13):3214–3217, 1999.

119 T. Lünskens. Size-dependent Plasmonic Properties of Supported Silver Clusters and Cluster-Molecule Complexes. *PhD thesis*, Technical University of Munich, 2016.

120 A. G. Mark, J. G. Gibbs, T.-C. Lee, and P. Fischer. Hybrid nanocolloids with programmed three-dimensional shape and material composition. *Nat. Mater.*, 12(9):802–7, 2013.

121 S. Tomita, Y. Kosaka, H. Yanagi, and K. Sawada. Chiral meta-interface: Polarity reversal of ellipticity through double layers consisting of transparent chiral and absorptive achiral media. *Phys. Rev. B - Condens. Matter Mater. Phys.*, 87(4):041404, 2013.

122 K. Akagi. Helical polyacetylene: asymmetric polymerization in a chiral liquid-crystal field. *Chem. Rev.*, 109(11):5354–5401, 2009.

123 X. Li, Q. Li, Y. Wang, Y. Quan, D. Chen, and Y. Cheng. Strong Aggregation-Induced CPL Response Promoted by Chiral Emissive Nematic Liquid Crystals (N*-LCs). *Chem. – A Eur. J.*, 24(48):12607–12612, 2018.

124 K. E. Shopsowitz, H. Qi, W. Y. Hamad, and M. J. MacLachlan. Free-standing mesoporous silica films with tunable chiral nematic structures. *Nature*, 468(7322):422, 2010.

125 E. Buncel, A. J. McKerrow, and P. M. Kazmaier. Solvent-controlled aggregation of a photoconductive dye. *J. Chem. Soc. Chem. Commun.*, (17):1242–1243, 1992.

126 G. R. Bird, G. Debuch, and D. Moebius. Preparation of a totally ordered monolayer of a chromophore by rapid epitaxial attachment. *J. Phys. Chem.*, 81(26):2657–2663, 1977.

127 K. Jyothish, M. Hariharan, and D. Ramaiah. Chiral supramolecular assemblies of a squaraine dye in solution and thin films: concentration-, temperature-, and solvent-induced chirality inversion. *Chem. - A Eur. J.*, 13(20):5944–5951, 2007.

128 X. Song, J. Perlstein, and D. G. Whitten. Supramolecular Aggregates of Azobenzene Phospholipids and Related Compounds in Bilayer Assemblies and Other Microheterogeneous Media: Structure, Properties, and Photoreactivity1. *J. Am. Chem. Soc.*, 119(39):9144–9159, 1997.

129 V. V. Egorov. Nature of the optical band shapes in polymethine dyes and H-aggregates: dozy chaos and excitons. Comparison with dimers, H*- and J-aggregates. *R. Soc. Open Sci.*, 4(5):160550, 2017.

130 J. K. Maurus and G. R. Bird. Circular dichroism of sensitizing dye aggregates. *J. Phys. Chem.*, 76(21):2982–2986, 1972.

131 H. von Berlepsch, C. Böttcher, and L. Dähne. Structure of J-Aggregates of Pseudoisocyanine Dye in Aqueous Solution. *J. Phys. Chem. B*, 104(37):8792–8799, 2000.

132 U. De Rossi, S. Dähne, S. C. J. Meskers, and H. P. J. M. Dekkers. Spontane Bildung von optischer Aktivität in J-Aggregaten mit Davydov-Aufspaltung. *Angew. Chemie*, 108(7):827–830, 1996.

133 C. Spitz, S. Dähne, A. Ouart, and H.-W. Abraham. Proof of Chirality of J-Aggregates Spontaneously and Enantioselectively Generated from Achiral Dyes. *J. Phys. Chem. B*, 104(36):8664–8669, 2000.

134 M. Fujiki. Effect of main chain length in the exciton spectra of helical-rod polysilanes as a model of a 5 Å wide quantum wire. *Appl. Phys. Lett.*, 65(25):3251–3253, 1994.

135 P. Trefonas, R. West, R. D. Miller, and D. Hofer. Organosilane high polymers. *J. Polym. Sci. Polym. Lett. Ed.*, 21(10):823–829, 1983.

136 P. M. Stanley. Tunable Induced Circular Dichroism in Spin Coated Molecular Films. *Internship report*, Technical University of Munich, 2018.

137 E. Keil. Mechanistic Insights in Induced Circular Dichroism in Organic Films. *Internship report*, Technical University of Munich, 2019.